Bromine complexing agents for use in vanadium bromide (V/Br) redox flow cell

Author:
Poon, Grace

Publication Date:
2008

DOI:
https://doi.org/10.26190/unsworks/17824

“Bromine Complexing Agents For Use in Vanadium Bromide (V/Br) Redox Flow Cell”

A thesis submitted as part of the requirements for the degree of

Master of Science

by

Grace Poon

School of Chemical Sciences and Engineering

The University of New South Wales

AUSTRALIA

January 2008

Acknowledgements

I sincerely thank Professor Maria Skyllas-Kazacos for her guidance and supervision during the course of this project. I respectfully thank Dr. Nick Milne for his invaluable assistance in the voltammetry studies. Ms Helen Prifti whose invaluable assistance is most appreciated. I would also like to thank all my fellow postgraduates and staff of the Laboratory, especially M. Risbud, R. Holmes, A. Chau and K. Nasev.

Also, many thanks to all my friends for their constant encouragement. And above all, thanks to my parents and my sister for their love, and support.

Abstract

The Vanadium bromide (V/Br) flow cell employs the Br_3^-/Br^- couple in the positive and the V(II)/V(III) couple in the negative half cell. One major issue of this flow cell is bromine gas formation in the positive half cell during charging which results from the low solubility of bromine in aqueous solutions.

Bromine complexing agents previously used in the zinc-bromine fuel cell were evaluated for their applicability in V/Br flow cell electrolytes. Three quaternary ammonium bromides: N-ethyl-N-methyl-morpholinium bromide (MEM), N-ethyl-N-methyl-pyrrolidinium bromide (MEP) and Tetra-butyl ammonium bromide (TBA) were studied. It is known that aqueous bromine reacts with quaternary ammonium bromides to form an immiscible organic phase. Depending on the number of quaternary ammonium bromides used and the environmental temperature, the second phase formed will either be solid or liquid. As any solid formation would interrupt the flow cell operation, potential formation of such kind has to be eliminated.

Stability tests of simulated V/Br electrolyte with added quaternary ammonium bromides were carried out at 11, 25 and 40 ^oC. In the absence of bromine, the addition of MEM, MEP and TBA were found to be stable in V/Br electrolytes. However, in the presence of bromine, solid formation was observed in the bromine rich organic phase when the V/Br electrolyte contained a single quaternary ammonium bromide (QBr) compound. For V/Br electrolytes with binary or ternary QBr mixtures containing TBA, the presence of bromine caused a viscous polybromide phase to form at room temperature and the

release of bromine gas at higher temperature. Only a binary mixture of MEM and MEP formed a stable liquid organic phase between 11 – 40 ^{o}C. In this study it was found that V/Br electrolytes containing a binary QBr mixture (0.75M) of MEM and MEP gave the best combination that formed an orange oily layer in the presence of bromine without solidification between 11 – 40^{o}C. Furthermore, it was found that samples of V/Br electrolytes containing a ternary QBr mixture, are less effective in bromine capturing if the total QBr concentration was less than 1 M at 40^{o}C, where bromine gas evolution was observed.

From electrochemical studies of V^{3+}/V^{2+}, it was found that the addition of MEM and MEP had a minimal effect on the formal potential of the V^{3+}/V^{2+} couple, the V^{2+}/V^{3+} transfer coefficient and the diffusion coefficient of V^{3+}. Therefore, MEM and MEP can be added to the negative half-cell of a V/Br flow cell without major interference

From linear sweep voltammetry, the kinetics of the Br^{-}/Br_3^{-} redox couple was found to be mass transfer controlled. After the addition of MEM and MEP mixture, the exchange current density was found to decrease from 0.013 Acm^{-2} to 0.01 Acm^{-2}. On the other hand the transfer coefficient before and after MEM and MEP addition was found to be 0.5 and 0.44 respectively. Since the kinetic parameters were not significantly affected by the addition of MEM and MEP mixture, they can be added to the positive half-cell of the V/Br flow cell as bromine complexing agents. The electrochemical studies of both V^{3+}/V^{2+} and Br^{-}/Br_3^{-} showed the addition of MEM and MEP has minimal interference with the redox reactions of the vanadium bromide flow cell.

This thesis also investigated the effect of MEM and MEP addition on the cell performance of a lab scale V/Br flow cell using two different membranes (ChiNaf and

VF11). Flow cell performance for 2 M $V^{3.7+}$ + 0.19 M MEM + 0.56 M MEP electrolytes utilising ChiNaf membrane at 10 $mAcm^{-2}$ produced an energy efficiency of 59%, and this decreased to 43% after 15 cycles. For the static cell utilising VF11 membrane, the addition of MEM and MEP reduced the energy efficiency from 59.7% to 43.4%. It is believed that this is caused by the mass transfer controlled Br^-/Br_3^- couple in the complexed positive half-cell solution. Therefore, uniformity between the organic and aqueous phase is important for flow cells utilising electrolytes with MEM and MEP.

Finally, the polarization resistance of a lab scale V/Br flow cell utilising ChiNaf membrane and 2 M $V^{3.7+}$ electrolytes was found to be slightly higher during cell charging (3.9 Ω cm^2) than during the discharge process (3.6 Ωcm^2), which is opposed to that in the all-vanadium redox cell.

Table of Contents

List of Figures

List of Tables

List of Symbols and Abbreviations

Symbol	Meaning	Units
A	Area	cm^2
C_A	Concentration of species A	M, mol/cm^3
C^o	Concentration of bulk solution	M, mol/cm^3
D	Diffusion coefficient	cm^2/s
$E^{o'}$	Formal electrode potential	V
E_p	Peak potential	V
ΔE_p	Peak potential separation	V
E_{pa}	Anodic peak potential	V
E_{pc}	Cathodic peak potential	V
F	Faraday's constant = 96500	C/mol e
I	Current	A
i_{pa}	Anodic peak current	A
i_{pc}	Cathodic peak current	A
i_p	Peak current	A
K	Equilibrium constant of reaction	none
k^o	Heterogeneous rate constant	cm/s
N_A	number of moles of species A	moles
n	number of electrons	none
O	Oxidised from standard system O + ne --> R	none
R	a) Reduced from standard system O + ne --> R	none
	b) ideal gas constant = 8.314	$J\ mol^{-1}K^{-1}$
	c) resistance	Ohms
T	Temperature	^oC, K
T	Time	Seconds
α	Transfer coefficient	None
ν	Potential sweep rate	Vs^{-1}
ηc	Coulombic Efficiency (C.E.)	%
ηv	Voltaic Efficiency (V.E.)	%
ηe	Energy Efficiency (E.E.)	%

Abbreviations	Meaning
MEM	N-ethyl-N-methyl-morpholinium bromide
MEP	N-ethyl-N-methyl-pyrrolidinium bromide
TBA	Tetra-butyl ammonium bromide
QBr	Quaternary ammonium bromides

Chapter 1 Introduction

Fossil fuel combustion is causing an accumulation of carbon dioxide in the atmosphere that leads to global warming and possibly the major cause of climate change. Scientists had made huge efforts on the investigation of different alternate energy sources. However, to date no such alternate energy can provide as much power and energy efficiency as the combustion engine. As believed by many researches, before the novel engine is developed it would be wise to develop a method to store the harvested energy.

In the past, energy storage tended to focus on large scale devices such as pumped-hydro facilities and compressed air storage. In recent years the concept of the redox cell has attracted more attention due to its simple design and long cycle life. This included the development of Iron-Chromium (Fe/Cr), zinc-bromine (Zn/Br_2), polysulfide-bromine (S_{x+1}^{2-}/Br_2) and all vanadium redox flow cell. Redox flow cells allow the storage of energy during off-peak hours and supply energy during peak usage at a lower cost, which is a major economical advantage.

In a redox flow cell the electro-active species are stored in two separate electrolyte tanks. When the system is charged, the electro-active species change to a different oxidation state and allow the storage of energy. Major issues in early redox flow cells

included membrane failure and cross contamination of electrolytes when different chemicals were used in each half-cell.

The All-Vanadium Redox Battery (VRB) developed at The University of New South Wales [1-4] was the only exception, as the same electrolyte is employed in both half-cells. Therefore, even if ions diffuse across the membrane they will not cause cross contamination. However, due to solubility limits of V(II) and V(III) in sulphuric acid, the maximum vanadium ion concentration is usually 2 M [5]. A more recent study showed the use of hydrochloric acid as supporting electrolyte allows vanadium electrolytes up to 4M to be prepared. This led to the development of Generation 2 Vanadium Redox Flow Battery (G2 VRB) – or the vanadium bromide redox flow cell (V/Br).

The vanadium bromide redox flow cell (V/Br) employs Br_3^-/Br^- and V(II)/V(III) couples in the positive and negative half cells respectively. The design of the V/Br is similar to a conventional redox flow cell. Feed solution stored in the reservoirs comprises a 50:50 mixture of V(III) and V(IV) in a supporting electrolyte of 7.5 M HBr plus 1.5 M HCl. This electrolyte is referred as $V^{3.5+}$. The two half cells are separated by an ion exchange membrane and are assembled in a cell stack arrangement. In each half-cell, electrochemical reactions take place on the inert carbon felt electrodes from which current may be used to charge or discharge the flow cell. The major challenge is the formation of bromine vapour in the positive half cell during normal operation. Therefore, the search of an adequate bromine complexing agent to capture bromine gases became the major task.

This thesis aims to study the suitability of three quaternary ammonium bromides, N-ethyl-N-methyl morpholinium bromide (MEM) N-ethyl-N-methyl pyrrolidinium bromide (MEP) Tetra-butyl ammonium bromide (TBA), as the bromine complexing agents for the novel vanadium bromide flow cell electrolyte.

Firstly, a stability test was conducted by observing physical changes in test electrolytes after quaternary ammonium bromides (QBr) are added. Different concentrations and combinations of the ammonium bromides were tested at simulated cell operating temperatures.

Secondly, the electrochemical properties in each half-cell were studied separately by voltammetry techniques. This included cyclic voltametric studies of the V(III)/V(II) couple and linear voltametric studies of Br^-/Br_3^-. The effects of QBr addition on the electrochemical parameters in each half cell were also investigated.

Finally, V/Br redox cell performance before and after QBr addition were investigated. Lab scale static and flow cells were charge-discharge cycled at controlled temperatures. Cell performance such as cell efficiencies and polarisation resistance were examined, both with and without the bromine complexing agents to establish the practical viability of a complexed electrolyte in V/Br redox cell for energy storage applications.

Chapter 2 Literature Review

2.0 Overview

Over the years, different redox flow cells have been developed. However to date, researchers are still investigating the development of a redox flow cell that can deliver higher efficiency with higher specific energy and energy density. This section includes theory and techniques used in the process of redox flow cell development. This section also reviews the few commercialised redox flow cell techniques together with some newly developed systems. Furthermore, the literature of bromine complexing agents used in the zinc bromine battery is also reviewed for potential application in the novel V/Br redox flow cell.

2.1 Principle of Redox Flow Cell

Redox flow cells use two soluble redox couples as electroactive materials (electrolytes) that store and deliver energy via oxidation and reduction reactions. In a single cell configuration (Figure 2.1) the power conversion section is separated into two half cells by an ion exchange membrane. As series cell connection would be most efficient in a bipolar electrode arrangement, in reality the power conversion section is a stack of 50 or more cells [6].

In each half cell, electrochemical reactions take place on the electrodes from which current may be used to charge or discharge the flow cell. Electrolytes are circulated through the power conversion section by pumps.

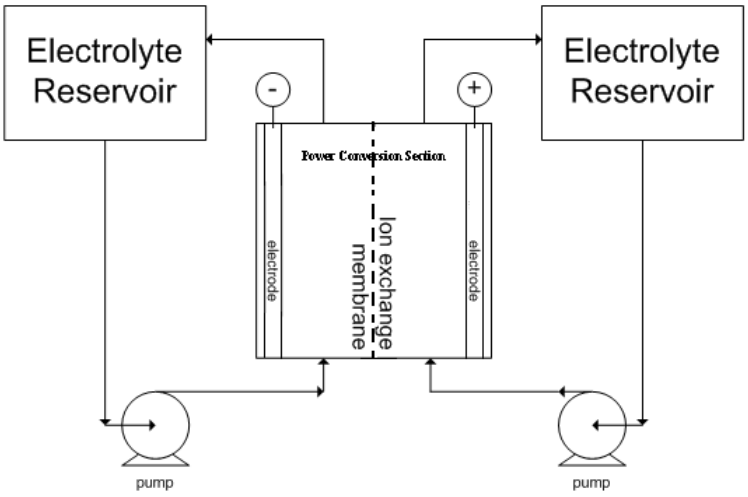

Figure 2.1 schematic diagram of redox flow cell

Redox flow cells normally have relatively low energy density due to solubility limits of the electroactive materials. They also have high life cycles because all active materials remain in solution and are not lost or degraded.

2.2 Types of Redox Flow Cells

There are many types of flow batteries using aqueous electrolytes, these include the early developed iron chromium cell, as well as polysulfide bromine, zinc bromine and all vanadium redox flow cells. All flow cells have a similar design as mentioned above but use different electrolytes in the positive and negative half cells. Each cell varies in open circuit potential, coulombic efficiency, energy efficiency and cycle life, but they share similar challenges such as electrolyte management and membrane failure.

2.2.1 Iron –Chromium Redox Cell

Iron-Chromium (Fe/Cr) was one of the first redox cell studied and expanded in the early 1970s [7]. In this system the electrolytes involved $CrCl_3$ and $FeCl_2$ in the negative and positive half cell respectively, with HCl as the supporting electrolyte. In the charging step of the cell Cr^{3+} is reduced to Cr^{2+} in the negative half cell (2.1) [8], while Fe^{2+} is oxidised to Fe^{3+} in the positive half cell (2.2). Both reactions are reversed during the discharge process [9]. The two half cells are separated by an ion exchange membrane with carbon felts acting as electrodes and graphite plates used as current collectors [9].

The chromic ion and chromous ion redox reaction occurs in negative half cell as follows:

$$Cr^{2+} \underset{charge}{\overset{discharge}{\rightleftharpoons}} Cr^{3+} + e \qquad E^o = -0.41V \text{ (vs SHE)} \qquad (2.1)$$

The ferrous ion and ferric ion redox reaction occurrs in positive half cell according to:

$$Fe^{3+} + e \underset{charge}{\overset{discharge}{\rightleftharpoons}} Fe^{2+} \qquad E^o = 0.77V \text{ (vs SHE)} \qquad (2.2)$$

2.2.1.1 Electrolytes composition and performance in iron chromium flow cell

In early studies, the positive and negative half-cell electrolytes contained 2 N HCl, 1 M $FeCl_2$ and 1 M $CrCl_3$ respectively [10]. However, cross mixing of the two solutions across the membrane, has caused problems in cell performance and lead to the use of identical electrolytes (named as mixed reactant mode) [9]. Therefore, in later studies fully discharged electrolytes would contained 1 M $FeCl_2$, 1 M $CrCl_3$ and 2 – 3 N HCl in

both half cells. An optimisation study by Lopez-Atalaya and co-workers [11] showed that the system would be in optimal condition when the electrolyte is a mixture of 2.3 M HCl, 1.25 M $FeCl_2$ and 1.25 M $CrCl_3$. When this system utilised a Nafion 117 and operated at 44^oC with a charging current destiny of 40mAcm^{-2} it achieved 97% coulombic efficiency, 73% energy efficiency and delivered a maximum discharge power of 73 mW/cm^2.

2.2.1.2 Methods to resolve electrolyte unbalance in iron chromium flow cell

In the Fe/Cr redox flow cell, hydrogen evolution was a major problem. This occurred in the negative half cell during cell charging. This is because the hydrogen ion reduction potential in acidic solution is similar to the reduction potential of the Cr^{3+} ion. As shown in the cyclic voltammogram (Figure 2.2) the Cr^{3+} reduction peak occurs at about -0.65 V (vs SCE) while H^+ reduction begins at about -0.8 V (vs SCE) [12]. With hydrogen evolution as a competitive reaction against Cr^{3+} reduction, this could result the decrease in coulombic efficiency of the cell and the imbalance of electroactive species between the two half-cells. Hydrogen evolution was mainly overcome by the addition of $PbCl_2$ that inhibits hydrogen ion reduction [11] or by using a rebalance cell to solve the system imbalance internally.

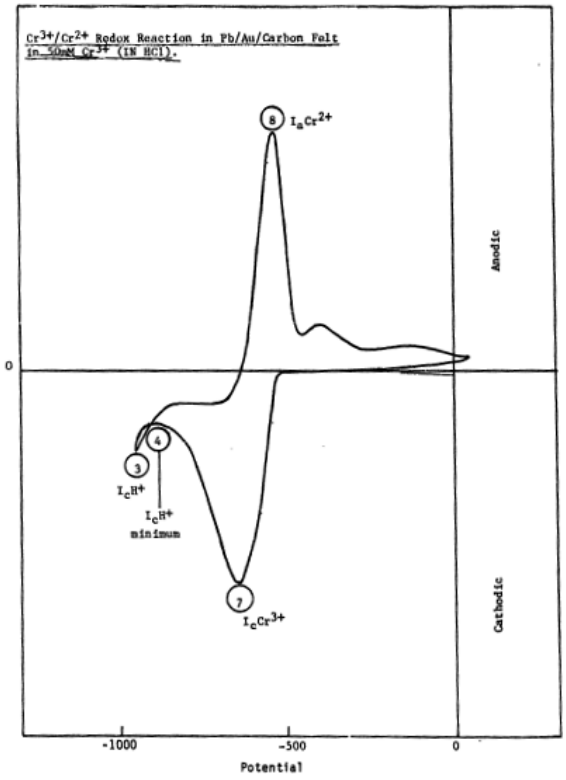

Figure 2.2 Cyclic voltammetry of Cr^{3+}/Cr^{2+} in 1 N HCl showed hydrogen evolution (or H^+ reduction) on carbon electrode begins at -0.8 V vs SCE [12]

2.2.2 Polysulfide Bromine Flow Cell

This system was first evaluated by Innogy Technologies Ltd the former owner of the Regenesys project. A demonstration storage plant was planned to be built in Little Barford UK that expected to provide 15 MW power output and store 120 MWh electricity [13]. However, due to funding issues the project was abandoned in the late 2003 [14]. Since then the Canadian company VRB power system Inc. obtained the intellectual property of the Regenesys system. They plan to commercialise the system to provide 10 – 100 MW power with duration of 8 – 12 hours [15].

In the polysulfide / bromine (PSB) fuel cell NaBr and Na_2S_x are used as positive and negative electrolytes respectively [8, 16, 17]. During cell discharge, bromine is converted to bromide ion in the positive chamber (2.6) while sulphide is converted to

sulphur on the negative side (2.3). Both reactions only represent the changing of overall reactive species in the system. Practically, the bisulfide ion also exists due to the basicity of the electrolyte, and the presence of sulphide ion lead to the formation of polysulfide (2.4 and 2.5). Meanwhile sodium ions move from the positive to the negative half cell to carry the current and complete the circuit. During the cell charging process bromide ions are converted to bromine in the positive chamber whilst polysulfide (S_{x+1}^{2-}) is converted to sulphide ions in the negative half cell. The circuit is completed by the migration of sodium ions from the negative to the positive side.

Negative half cell reactions:

$$S^{2-} \underset{charge}{\overset{discharge}{\rightleftharpoons}} S + 2e \qquad (2.3)$$

$$S^{2-} + xS \rightleftharpoons S_{x+1}^{2-} \qquad (2.4)$$

$$S^{2-} \underset{charge}{\overset{discharge}{\rightleftharpoons}} S_{x+1}^{2-} \qquad (2.5)$$

Positive half cell reaction:

$$Br_2 + 2e \underset{charge}{\overset{discharge}{\rightleftharpoons}} 2Br^- \qquad (2.6)$$

2.2.2.1 Issues occurring in polysulfide bromine flow cell

This system uses a cation exchange membrane to separate the two electrolytes and prevent the electroactive anions from mixing. However over extended cycling, S^{2-} and

HS^- ions will migrate from the negative to the positive half cell that causes an imbalance in the system. This unwanted diffusion affects different reactions in each side of the system.

The migrated sulphide ions (HS^- or S_{x+1}^{2-}) are oxidised by bromine in the positive chamber to form sulphate ions. This reaction consumes more bromine than the normal one bromine molecule per sulphide ion depending on the migrated sulphide ions (4 Br_2: HS^-, $(3x+4)Br_2$: S_{x+1}^{2-}). Therefore, the positive half cell discharges to a greater extent than the sulphide/polysulphide half cell. When the unbalanced system is discharging the bromine present would be insufficient to react with all the sulphide ions, and causing the discharge cycle to be incomplete. This leads to the generated voltage to decline earlier in the discharge process compare to a balanced system [17].

For those sulphide ions that are migrated to the positive side they cannot be fully recovered in the negative chamber when the cell is discharged. When this process is repeated for a several cycles, the concentration of polysulfide ions is further reduced. Then this leads to insufficient polysulphide ion to accept charge during charging process, and causes the reduction of water and hydrogen gas evolution [17].

2.2.2.2 Methods to overcome problems in polysulfide bromine flow cell

Zito and co-workers [16] evaluated an apparatus to restore the imbalance electrolytes. The apparatus adds a buffer section separating the positive and the negative section by two ion exchange membranes. The idle electrolyte that flows though the buffer section normally contain a mixture of NaBr and Na_2S_x. Over extended cycles sulphide ions migrating from the negative half cell to the buffer section are oxidised by bromine migrating from the positive half cell that formed sulphur and NaBr. Sulphur precipitates

are filtered out and redissolved in the system as polysulfide. The ideal electrolyte would pass through an external electrochemical cell to oxidised excess HS^- and S^{2-} ion electrochemically by passing a DC current.

2.2.2.3 Polysulfide bromine flow cell prototype

A lab scale PSB fuel cell evaluated by Innogy Technologies Ltd contained 300 ml electrolytes in each half cell. In the positive side was 5 M NaBr while the negative side contained a mixture of 1.3 M Na_2S_5 and 1 M NaBr [18]. The constructed cell had an electrode area of 173 cm^2 and used polyethylene impregnated activated carbon (AC) as the electrode material and Nafion 115^{TM} as the cation exchange membrane. With a constant charge and discharge current of 60 $mAcm^{-2}$ this cell showed an average energy efficiency of 56%. The low cell efficiency was caused by the deterioration of electrode performance as sulphur is trapped inside the micropores and blocked the pores of the AC electrode during cell discharge [19].

2.2.2.4 Electrode material development in polysulfide bromine cell

Current research focuses on new electrode material development for the PSB fuel cell to improve cell energy efficiency.

Table 2.1 Energy efficiency with different electrodes in PSB fuel cell [19, 20]

Negative Electrode	Positive Electrode	Energy Efficiency (%)
NF	PAN – CF	77.2
Co – ACE	ACE	66.1
ACE	ACE	64.7
PAN – CF	PAN – CF	64.3
Co – GF	PAN – GF	81.0

NF: Nickel Foam PAN – CF: Polyacrylonitrile based carbon felt, Co – ACE: Cobalt coated activated carbon electrode, ACE: Activated Carbon Electrode, Co – GF: Cobalt coated Graphite Felt, PAN – GF: Polyacrylonitrile based Graphite Felt

Zhao and co-workers [20] studied the use of nickel foam in the negative electrode and polyacrylonitrile based carbon felt as the positive electrode. This cell used 4 M NaBr in the positive side and a mixture of 1.3 M Na_2S_4 and 1 M NaOH in the negative side. When charged at 40 $mAcm^{-2}$ it has an energy efficiency of 77.2%. In another study using electrolytes with the same composition as Zhao [20], Zhou et al. [19] showed that a cell using cobalt coated graphite felt as negative electrode and a polyacrylonitrile based graphite felt as positive electrode can provide an energy efficiency of 81.0%. Table 2.1 compare the energy efficiency of PSB cells that used different electrodes.

2.2.3 Zinc – Bromine Redox Flow Cell

The concept of zinc / bromine couple for a battery system has been patented since 1885 [21]. Early studies focused in small scale non-flowing electric storage [22]. A flow cell system of this kind was not commercialised until Exxon and Gould technology developed a design in 1980s that solved the problems of dendritic zinc deposition and bromine diffusion. A large number of companies were involved in this research area since Exxon started to license out the zinc / bromine technology in the mid-1980s. The main companies involved were, Johnson Controls, Inc. (JCI), Studiengesellschaft fur Energiespeicher und Antriebssysteme (SEA), Toyota Motor Coporation and Meidensha Corporation, Sherwood Industries, ZBB Energy Cooperation and Powercell Corporation [23]. The major reason of attracting such a huge interest as zinc bromine flow cell has a high theoretical specific energy density of 429 Wh/kg [24] which in practice is as high as 65 – 75 Wh/kg [25].

2.2.3.1 Zinc bromine flow cell design

The design of a zinc bromine redox flow cell is similar to a conventional flow cell. Positive and negative electrolytes containing aqueous $ZnBr_2$ and other salts are stored in two separate external storage tanks. Electrolytes are circulated by pumps and passed through the power conversion section in two different streams where a separator is used to prevent bulk solution mixing.

The initial electrolyte compositions in both the positive and negative sides are the same. Since the development of the zinc bromine battery from 1970s, the electrolyte composition has changed slightly over the years (Table 2.2). Bipolar electrodes made from extruded carbon filled polyethylene [25] were used for the zinc bromine flow cell. One side of the bipolar electrode has a smooth carbon plastic face acting as the negative electrode. It allows zinc metal to deposit uniformly on the smooth surface during cell charging. The other side has a porous carbon layer (carbon felt) serving as positive electrode. The addition of a carbon felt increases the surface area and allows it to be more active for the bromine oxidation and reduction reactions [26]. The terminal electrodes are made from carbon with embedded expanded metal mesh for current collection, while a microporous polyethylene (MPPE) separator is normally used to separate the positive and negative electrolytes.

In some designs an ion exchange membrane is used because it is more efficient in blocking the transport of species other than zinc and bromide ions. Although a higher coulombic efficiency can be reached [27], trade-offs of high cost, less durability and water balance problems were the main factors that hinder its usage [23]. During cell charging, aqueous zinc bromide is reduced to zinc and deposited on the negative

electrode (2.7). At the positive electrode (2.8) oxidation of Br^- to Br_2 occurs [28]. Both reactions are reversed when the cell is discharged.

Negative half cell reaction:

$$Zn \underset{charge}{\overset{discharge}{\rightleftharpoons}} Zn^{2+} + 2e \qquad E^o = 0.763\ V \qquad (2.7)$$

Positive half cell reaction:

$$Br_2 + 2e \underset{charge}{\overset{discharge}{\rightleftharpoons}} 2Br^- \qquad E^o = 1.087\ V \qquad (2.8)$$

In reality chemical species present in the electrolytes are more complex. In the positive electrolyte, elemental bromine formed during cell charging is in equilibrium with Br^- and forms polybromides (Br_n^- , n = 3,5,7), while aqueous zinc bromide solution is ionised with zinc existing as different complexes or ion pairs [23]. The electrolytes also contained complexing agents to reduce the amount of bromine in the aqueous phase. The most commonly used complexing agents are N-ethyl-N-methyl morpholinium bromide (MEM) and N-ethyl-N-methyl pyrrolidinium bromide (MEP). The complexing agents coupled with polybromide ions and bromine to form a second liquid phase (see section 2.7 for further discussion).

The life time of a zinc bromine cell is not sensitive to the depth of discharge [25]. However, a periodic complete discharge is sometimes necessary to maintain a uniform zinc deposit on the anode.

Table 2.2 Electrolyte composition of zinc bromine flow cell as storage system

Year	Research Institute	$ZnBr_2$ (M)	MEM (M)	MEP (M)	$ZnSO_4$ (M)	ZnCl 2 (M)	Dendrite inhibitor
1978	Exxon [29]	3	0	1	0.2	0	0
1983	Meidensha [30]	3	0.5	0.5	0	0	Sn^{2+}/Pb^{2+}
1985	Exxon [31]	2	0.5	0.5	0	1	0
1989	JCI [25]	3	0.25	0.75	0	0	0
1995	ZBB [32]	2.25	0	0.8	0	0.55	0
1999	SNL [33]	2.25	0.8 (50/50)		0	0.55	0

2.2.3.2 Issues in Zinc bromine flow cell

The problems occur in the zinc bromine flow cell system are similar to the other flow cells described. Besides the common problems in electrolyte cross contamination and hydrogen evolution on the negative side, however, it also has to overcome bromine diffusion from the positive side and zinc dendrite deposition on the anode. These issues can lead to cell self discharge and a drop in cell efficiency.

Hydrogen evolution in the Zn/Br flow cell is relatively low compared to other flow cells, however, it only occurs when water reacts with zinc. This is because the hydrogen overpotential on zinc metal is relatively larger than that on platinum, so that hydrogen evolution is a slow reaction on zinc. Therefore, in the absence of contaminated metal that has low hydrogen overpotential, hydrogen generation is minimal in Zn/Br flow cells [23].

In the case of bromine diffusion, it is believed that two chemical reactions occur (2.9 and 2.10) when dissolved bromine reacts with zinc metal on the anode and causes self discharge of the cell [34].

$$Br_2 + H_2O \longrightarrow HBr + HBrO \qquad (2.9)$$

$$2HBr + Zn \longrightarrow ZnBr_2 + H_2 \qquad (2.10)$$

2.2.3.3 Common methods to overcome bromine transport and zinc dendrites

Bromine transport and vapour formation is mainly solved by the addition of MEM and MEP that forms a dense second phase which is removed from the cell until the discharge stage. Due to changes in operating temperature, however, further studies in different composition of complexing agents were in the research scope of Cathro [35], Cedzynska [36] and co workers (see section 2.6). In another study, Kantner [31] tried to reduce the free aqueous bromine in the electrolyte by increasing chloride concentration in addition to the use of complexing agent. The study claimed the addition of 1 M $ZnCl_2$ will reduce free bromine in the electrolyte and increase the coulombic efficiency of an 8-cell system (Table 2.3), this is similar to the findings of Bellow et al. [37].

Table 2.3 Improvement in coulombic efficiency by $ZnCl_2$ addition [31, 37]

Electrolyte	Electrode Area (cm^2)	Charge Current (Amp)	C. Eff (%)
3 M $ZnBr_2$ 0.5 M MEM 0.5 M MEP	600	12	75
	1200	24	71
2 M $ZnBr_2$ 1 M $ZnCl_2$ 0.5 M MEM 0.5 M MEP	600	12	81
	1200	24	80

Zinc dendrite deposition was usually overcome by the circulation of electrolyte and the use of a smooth carbon plastic electrode as the anode that allowed a uniform deposit of zinc [25, 38]. The addition of Sn^{2+} and Pb^{2+} as dendrites inhibitors was also studied by Ando et al [30].

2.2.3.4 Zinc bromine flow cell applications

Electric vehicles (EV) and load management (LM) were the major research focus for application of the zinc bromine flow cell since its development by Exxon Technology. In Johnson Controls INC. (JCI) an 8-cell zinc bromine flow cell containing complexing agent was built to power up a Ford ETX-II van. It provided a sustained power of 35 kW with an energy efficiency of 69.4% and a specific energy density of 67.3 Wh/kg [25]. To reduce the electrolyte resistance NH_4Cl was added to the cell, and this provided a higher energy density (Table 2.4).

Table 2.4 Efficiency comparisons with different electrolyte composition [25]

Electrolyte for EV studied in JCI	Energy Efficiency (%)	Energy Density (Wh/kg)
3 M $ZnBr_2$ 0.25 M MEM 0.75 M MEP	69.4	67.3
3 M $ZnBr_2$ 3 M NH_4Cl 0.25 M MEM 0.75 M MEP	62.7	71.9

The feasibility of using a zinc bromine flow cell as a load management battery module with a capacity between 20 – 50 kWh was demonstrated by various research groups (Table 2.5) A difference in electrolyte composition, cell design or electrode area, would have affected the cell performance. When a number of modules are connected in series and / or parallel configuration a total capacity of 400 kWh – 4 MWh could be achieved [23, 39].

2.2.3.5 Bromine/Propionitrile positive electrolytes

By using propionitrile (PN) solvent in the positive electrolyte Singh et al. [40] used a totally different approach to lower the rate of self discharge. Instead of using the same initial electrolyte in the discharged stage, the negative side consisted of 4 M $ZnBr_2$ and 3 M NaCl, while the positive electrolyte contained 2 M $ZnBr_2$, 2 M Br_2 which was

dissolved in water saturated propionitrile. The performance was tested with a single cell using 20 cm^2 graphite carbon electrodes and polypropylene separator. The cell achieved a coulombic efficiency of 85% and voltaic efficiency of 76%.

Table 2.5 Results of $ZnBr_2$ load management module properties and performance from various research companies [25, 41, 42]

Cell Properties	Exxon [41]	Exxon [41]	JCI Z design	JCI V design	ZBB V design	MITI [42]
Electrolyte	A	A	B	B	C	NA
Membrane	M1	M1	M1	M1	M1	M2
Capacity (kWh)	20	30	20	20	50	50
Bipolar Cell	80 – 100	124	78	78	60	30
Stack	2	2	2	2	3	24 x 2 series
Electrode Area (cm^2)	NA	NA	1170	1270	2500 [39]	1600
Coulombic Eff. (%)	86.7	81.8	80	85 – 90	NA	92.4
Energy Eff. (%)	67.4	52.7	60	70 – 75	77	81.1

A: 2 M $ZnBr_2$ 0.5 M $ZnCl_2$ 0.5 M MEM 0.5 M MEP [31]

B: 3 M $ZnBr_2$ 0.25 M MEM 0.75 M MEP [25]

C: 2.25 M $ZnBr_2$ 0.5 M $ZnCl_2$ 0.8 M QBr (MEM: MEP 50:50) [33]

M1: Microporous MPPE separator [25, 39]

M2: Perforated membrane of polyolefin type or ion exchange membrane [43]

2.2.4 All Vanadium Redox Flow Battery

The all vanadium redox flow battery is an electrical energy storage system developed and patented by the School of Chemical Engineering and Industrial Chemistry since 1984 [1, 2, 4, 44-48]. Based on the principle of converting chemical energy stored in solutions to electrical energy, this system has been successfully commercialised by

Sumitomo Electric Industries, Ltd. (SEI) [49] and VRB Power Systems Incorporated in Canada [50].

2.2.4.1 All vanadium flow cell design

The all vanadium redox flow battery utilises different ionic forms of vanadium in 1 M to 3 M sulphuric acid which is stored in two separate electrolyte tanks. The V(V)/V(IV) redox couple acts as the positive electrolyte whereas the V(II)/V(III) redox couple reacts in the negative electrolyte. The electrolytes are pumped through the battery, where V(V) is reduced and V(II) is oxidised during the discharge of the cell [1, 2, 44, 45]. The reversibility of the vanadium redox reaction allows this type of battery to be rechargeable. Porous carbon felt is used as the flow through electrode, because of its range of characteristics, that provides excellent mass transfer and increased surface for the oxidation and reduction reactions [51].

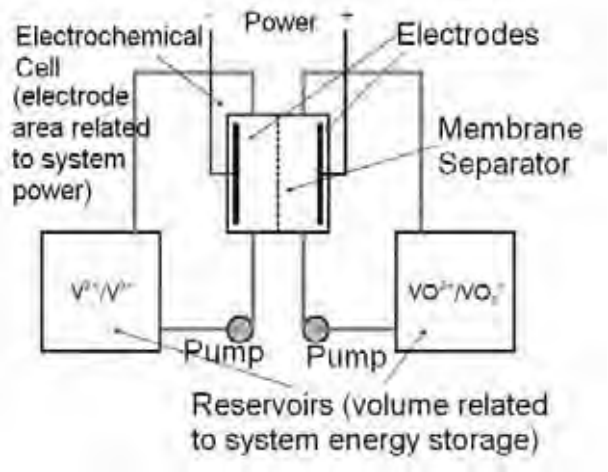

Figure 2.3 Schematic Diagram of the Vanadium Redox Flow Cell [52]

The half-cell reactions involved and their respective standard potentials during charge-discharge of the vanadium redox flow cell are summarised and tabulated below (Table 2.6). When the cell is charging V(III) is reduced to V(II) at the negative electrode (2.11) meanwhile V(IV) is oxidised to V(V) (2.12). These reactions are reversed during cell

discharge. The standard half-cell potentials are reported to be -0.255 V and 1.000 V at the negative and positive electrode respectively [50]. This provides a theoretical standard cell potential E^0_{cell} = 1.26 V at standard conditions. The open circuit cell voltage observed under typical cell conditions is 1.4 V at 50% state of charge and over 1.6 V for a fully charged cell [51]. This is much higher than that of the theoretical values mainly due to the high concentration of vanadium ions and sulphuric acid used [50].

Negative half cell reaction:

$$V^{2+} \underset{charge}{\overset{discharge}{\rightleftharpoons}} V^{3+} + e \qquad (2.11)$$

Positive half cell reaction:

$$VO_2^{+} + 2H^{+} + e \underset{charge}{\overset{discharge}{\rightleftharpoons}} VO^{2+} + H_2O \qquad (2.12)$$

Table 2.6 Summary of the half cell reactions involved and the corresponding standard potential of the vanadium redox flow battery during charge or discharge [50], [51]

	Half Cell Reaction	**E^o (vs NHE)**	**E^o (in different [H_2SO_4])**
Negative Electrode	V^{3+} / V^{2+}	-0.255 V [50] or -0.26 V [51]	-0.258 V (0.5 M H_2SO_4) -0.291 V (3.0 M H_2SO_4)
Positive Electrode	VO^{2+} / VO_2^{+}	1.000 V or 1.004 V	1.008 V (1.0 M H_2SO_4) 1.103 V (3.0 M H_2SO_4)

2.2.4.2 Advantages of all vanadium flow cell

The major advantage of utilising vanadium ions in both half-cell electrolytes in the vanadium redox fuel cell is that electrolyte contamination resulting from cross mixing has no major influence on the battery capacity [53]. Moreover, as active materials are kept in solution and are not degraded by battery cycling, a higher cycle life is achieved. Furthermore, the energy storage capacity is determined by the electrolyte concentration and volume. As with cell redox flow cells, additional storage capacity can be added by increasing electrolyte volume. This makes the flow battery design flexible, cost effective and highly adaptive for remote operation [52].

2.2.4.3 All vanadium flow cell applications

The vanadium redox flow battery development to date has mainly focused on large stationary storage applications due to the limited solubility of the redox species in the electrolyte that causes low volumetric and specific energy densities (about 25 Wh/kg for 2 M V(II) electrolyte) [50]. The following list summarises the targeted market sectors of the vanadium redox flow battery [50]:

- Commercial Buildings and production facility can use the battery as a uninterrupted power supply system or generator system
- Electricity Market trading may use the battery as energy storage and charge up during off peak prices time and discharge during peak price periods
- Remote area power supply
- Reversible energy storage for large wind and solar farms

2.2.5 Vanadium bromide flow cell

Described as the Generation 2 Vanadium redox flow cell – The Vanadium bromide Redox Flow Cell (G2 V/Br) employs the Br_3^-/Br^- and the V(II)/V(III) couples in the positive and negative half cell respectively. The G2 V/Br design is similar to that of an all-vanadium redox flow cell. The feed solution is made up of a 50:50 mixture of V(III) and V(IV) bromides, which is referred as $V^{3.5+}$ from here onwards [54].

2.2.5.1 Vanadium bromide flow cell reaction

The initial charging of the V/Br redox fuel cell reduces the feed electrolyte $V^{3.5+}$ to V(III) state in the negative half-cell (2.13) and oxidised it to V(IV) state in the positive half cell (2.16). For the subsequent charging, VBr_3^- is further reduced to VBr_2 in the negative half-cell (2.15) while the corresponding oxidation reaction of Br^- to Br_3^- takes place in the positive half cell (2.18). Due to the multiple ionic equilibria of bromide ions in aqueous solution, the possibility of bromine emission during cell charging exists [55].

Negative Half Cell Reactions:

Initial Charging:

$$V^{3+} + VO^{2+} + 2H^+ + e \rightarrow 2V^{3+} + H_2O \qquad (2.13)$$

$$2V^{3+} + 2e \rightarrow 2V^{2+} \qquad (2.14)$$

Subsequent Charge-Discharge:

$$VBr_2 + Br^- \underset{charge}{\overset{discharge}{\rightleftharpoons}} VBr_3 + e \qquad (2.15)$$

Positive Half Cell Reactions:

Initial Charging:

$$V^{3+} + VO^{2+} + H_2O \rightarrow 2VO^{2+} + 2H^{+} + e \quad (2.16)$$

$$3Br^{-} \rightarrow Br_3^{-} + 2e \quad (2.17)$$

Subsequent Charge-Discharge:

$$Br_3^{-} + 2e \underset{charge}{\overset{discharge}{\rightleftharpoons}} 3Br^{-} \quad (2.18)$$

A G2 V/Br Flow Cell with a 3 M to 4 M $V^{3.5+}$ electrolyte would potentially have an energy density of 30 – 50 Wh/kg (1Wh watt hour = 3600 J), which is twice that of an all – vanadium redox flow battery described earlier. The performance of various common energy storage systems are compared and tabulated below (Table 2.7). The G2 V/Br flow cell potentially has an energy density much higher than that of a lead-acid battery but lower than that of a zinc-bromine battery.

Table 2.7 Comparison of Cell Performance in various aqueous rechargeable batteries

Battery Type	Energy Density (Wh/kg)	Energy Density [24] (Wh/L)	Cycle Life
Lead – Acid	30 – 50 [53]	80	600 – 1500 [53]
Zinc Bromine	60 – 75 [53]	60	500 [53]
All Vanadium Redox	10 – 25 [24, 51]	12 -33	> 1000 [51]
Vanadium Bromide flow cell (3 – 4 M) [54]	35 – 40	35 - 60	400

2.2.5.2 Advantage of vanadium bromide flow cell

By using the same electrolyte on both side of the half-cell V/Br cell has no problem of cross-contamination. It has a low self-discharge rate compared to a zinc-bromine battery and allows a high coulombic efficiency of about 92% depending on the membrane in use [5]. Therefore, the V/Br redox flow cell should attract major research awareness, even though the energy density is lower than that of the zinc bromine battery.

2.2.5.3 Vanadium bromide flow cell applications

The applications for the V/Br flow cell are similar to those motioned for an all – vanadium redox flow cell listed earlier. Further, due to the possibility of a compact cell design by the use of a concentrated electrolyte, mobile applications also become feasible.

2.2.5.4 Issues and development focus for vanadium bromide flow cell

Electrolyte leakage or vapour pressure build up in the reservoir might lead to the escape of bromine vapour during operation of the V/Br cell. A critical issue for the development of the V/Br cell is therefore the reduction of bromine vapour in the positive half cell.

2.2.6 Other recent research on redox flow battery technologies

In the quest for a redox cell with higher open circuit potential (OCP), some recent research has started to study new systems such as an iron – complex / bromine (Fe/Br) [56, 57] and a cerium / vanadium redox cell (Ce/V) [58, 59]. Both redox cells have a theoretical OCP higher than that of an all vanadium redox battery, which is 1.9 V (Fe/Br) and 1.45 – 1.96 V (Ce/V) respectively.

Wen and co – workers [56] studied the Fe/Br system that used 0.4 M Fe(III)-triethanolamine (TEA, ~0.6 M) complex in 3 M NaOH as the negative half cell and 2 M NaBr as the positive half cell. When fully charged at 20 $mAcm^{-2}$ it was shown to have an OCP of 1.98 which delivered an 82.4 % coulombic efficiency and 83.9 % voltage efficiency [56]. In an attempt to lower the price by using EDTA as the ligand, Wen et al. [57] studied the Fe – EDTA / bromine system and showed an OCP of 1.1 V that provided a 80% energy efficiency when charged at 10 mA cm^{-2} [57].

B. Fang and co-workers [59] studied the Ce/V system, that used 0.5 M Ce^{3+}/Ce^{4+} in the positive and 0.5 M V^{3+}/V^{2+} in negative half cell, 1 M H_2SO_4 is used as the supporting electrolyte in both halves. This system showed an OCP of 1.87 V when fully charged at 22 $mAcm^{-2}$. For constant current charge-discharge cycles, the coulombic and the voltaic efficiencies were 87.1%, 82.3% respectively. In another study by Xia et al [58] reported otherwise. This system used 0.3 M Ce^{3+} + 0.5 M H_2SO_4 as positive and 0.3 M V^{3+} + 1.25 M H_2SO_4 as negative half cell. A constant charge-discharge current of 2 mA cm^{-2} delivered a coulombic efficiency of 90.228% and an energy efficiency of 55.267% with an OCP of about 1.7 V when fully charged.

Both iron-complex / bromine and cerium / vanadium systems are still at their early research stage. All authors suggested further studies on long term electrolyte stability and cell performance.

In particular, the low active species concentrations used in each of these systems would yield very low specific energy values that would make theses systems impractical. Even if the active ion concentration could be increased however, the issues of cross

contamination of the electrolytes by transfer of the different ions across the membrane would lead to gradual loss of capacity and would be difficult to recover.

2.3 Chemistry of vanadium in halide solution

2.3.1 Vanadium (II)

The outer electron configuration of Vanadium (II) is $3d^3$ in the ground state. Vanadium (II) is readily oxidised and is the least stable oxidation state of vanadium in aqueous solution [60]. V(II) compounds are strong reducing agents [61] , they oxidised rapidly in water, evolving hydrogen gas. In acidic solution, V(II) exists as $[V(H_2O)_6]^{2+}$ with an octahedral coordination. In acid solutions, $[V(H_2O)_6]^{2+}$ ion is more stable, and it would not be oxidised by water but by air instead. Although there is no sign of complex formation in solutions of HCl or H_2SO_4, V(II) ions do not reduce water in the presence of sulphuric acid.

V(II) hydrated crystals are formed by electrolytic reduction and evaporation of V(V) in halide solution. The electrolytic reduction of V_2O_5 in HF solution will form $[V(H_2O)_6]^{2+}$ ion. The evaporation of this solution yields a hydrated vanadium difluoride crystal $VF_2 \cdot nH_2O$, where the composition depends on the HF concentration [62].

In HCl solution, the electrolytic reduction of V(IV) followed by evaporation yields a blue complex ($VCl_2 \cdot 4H_2O$) that has a *trans*-octahedral structure [62, 63]. Whereas blue-violet needles of VBr_2 $6H_2O$ formed via the electrolytic reduction of V_2O_5 in HBr solution followed by evaporation [62, 63].

In strong perchloric acid, the reduction of dissolved V_2O_5 followed by evaporation yields red-violet needles of $V(H_2O)_6(ClO_4)_2$. This compound is not stable since perchlorates oxidise vanadium (II) to oxovanadium (IV) ions, VOV^{4+}[60].

The oxidation of V^{2+} to V^{3+} proceeds in several steps in acid solutions. First is the rapid oxidation of V^{2+} to VO^{2+} followed by the formation of intermediate ion VOV^{4+}. Finally the intermediate species reacts with V^{2+} and form V^{3+} [62].

Malin and Swinehart [64] agreed with the formation of an intermediate in V^{2+} oxidation. They determined the kinetics of the halogen and $V[(H_2O)_6]^{2+}$ reaction in perchloric acid. For bromine and tribromide with excess $V[(H_2O)_6]^{2+}$ both reaction (2.19 and 2.20) took place. The kinetics of this reaction was found to be in first-order where the rate constant, k = 3 x 10^4 $M^{-1}s^{-1}$. The kinetics were slower and deviated from first-order reaction when Br^- concentrations was greater than 10^{-2} M. From light absorbance measurements, the intermediate VOV^{4+} was found to be present in the solution.

$$2V^{2+} + Br_2 \Leftrightarrow 2V^{3+} + 2Br^- \qquad (2.19)$$

$$2V^{2+} + Br^-_3 \Leftrightarrow 2V^{3+} + 3Br^- \qquad (2.20)$$

2.3.2 Vanadium (III)

The outer electron configuration of V(III) is $3d^2$ in the ground state [63]. Compared to V(II), V(III) undergoes slow oxidation by air [60] and is stable in water [65]. By dissolving V_2O_3 in non-complexing acid, blue $[V(H_2O)_6]^{3+}$ ions with octahedral structure are obtained [63]. This agreed with $[V(H_2O)_6]^{3+}$ being the principle species in perchloric acid ($HClO_4$) [62]. When acid concentration decreases (ie pH increased), hydrolysis of $[V(H_2O)_6]^{3+}$ occurrs and green $V(OH)^{2+}$ ions are formed [60, 66]. Besides

the mononuclear hydroxo-species ($V(OH)^{2+}$), formation of binuclear ion $V_2(OH)_2^{4+}$ occurs via the Olation reaction described by Equation (2.21) [63].

$$2\left[V\left(H_2O\right)_6\right]^{3+} + 2H_2O \Leftrightarrow \left[\left(H_2O\right)_4V\begin{matrix}H\\O\\O\\H\end{matrix}V\left(H_2O\right)_4\right]^{4+} + 2H_3O^+ \qquad (2.21)$$

In complexing acids such as HCl and HBr, vanadium (III) forms complexes with halide ions [63]. Reaction in HCl solution can be described by reaction (2.22) [67], which yields $[VCl(H_2O)_5]^{2+}$ and $[VCl_2(H_2O)_4]^+$ ions [62]. By evaporation of dissolved V(III) in HCl and X-Ray examination of the solid powder, the existence of green *trans*-$[VCl_2(H_2O)_4]^+$ complex ion in HCl solution was confirmed [68].

$$\left[V\left(H_2O\right)_6\right]^{3+} + nCl^- \Leftrightarrow \left[V\left(H_2O\right)_{6-n}Cl_n\right]^{(3-n)+} + nH_2O \qquad (2.22)$$

In a more generic form, Niki and Mizota [69] described the complex ions in HX solution to be MX^{2+} and MX_2^+ at equilibrium (2.23, where M: metal; X: halide). This also suggested the formation of two complex ions in HBr (2.24 a) and HCl (2.24 b) solutions. However, equilibrium constant values were not available.

$$M^{3+} \Leftrightarrow MX^{2+} \Leftrightarrow MX_2^+ \qquad (2.23)$$

$$V^{3+} \Leftrightarrow VBr^{2+} \Leftrightarrow VBr_2^+ \qquad (2.24\ a)$$

$$V^{3+} \Leftrightarrow VCl^{2+} \Leftrightarrow VCl_2^+ \qquad (2.24\ b)$$

V(III) hydrated halide solid complex $VX_3 \cdot 6H_2O$ can be formed by evaporation of V(III) halide solution. The preparation of green solids $VCl_3 \cdot 6H_2O$ and $VBr_3 \cdot 6H_2O$ were described by Podomre and Smith [68]. They showed V(III) yield green complex ions in both HCl and HBr solutions, which are *trans*-$[V(H_2O)_4Cl_2]^+$ and *trans*-$[V(H_2O)_4Br_2]^+$ respectively.

2.3.3 Vanadium (IV)

V(IV) is the most stable oxidation state for vanadium, its outer electron configuration is $3d^1$ at the ground state [60]. In aqueous solution V(IV) is neither strongly oxidising nor reducing, over the years it has attracted a lot of attention [63, 70, 71]

When VO_2 is dissolved in non-complexing acid, the blue solution formed contains oxovanadium (IV) ($[VO(H_2O)_5]^{2+}$, VO^{2+}) as the principle species [60, 63]. In strong acid solution $[VO(H_2O)_5]^{2+}$ is stable to atmospheric oxidation for many months [62]. In concentrated sulphuric acids (>5 M) VO^{2+} ion is stable and does not form complex species with SO_4^{2-} and HSO_4^- ions [72]. This agreed with Kausar's [47] work, which is illustrated by a Raman spectrum of concentrated V(IV) solution, where the solution is a mixture of 3.5 M V(IV)/V(V) at 0% state of charge (SOC) of V(V). The solution gives a strong band at 900 cm^{-1} caused by the V=O stretch and indicates the dominance of VO^{2+} species.

Rossotti and Rossotti [73] studied the hydrolysis of VO^{2+} (0.005 – 0.5M) in perchloric acid (0.002 – 3 M), they explained the formation of two complexes $VO(OH)^+$ (or $[VO(OH)(H_2O)_4]^+$) and $(VO)_2(OH)_2^{2+}$ (or $[VO_2(OH)_2(H_2O)_4]^{2+}$). This can be described by reactions (2.25) and (2.26). The equilibrium constant for the former reaction is $10^{-6.0}$

whereas the later is $10^{-6.88}$ [71]. Israel [60] suggested there is no evidence of higher polymerised species formation in substantial amounts.

$$VO^{2+} + H_2O \Leftrightarrow VOOH^{+} + H^{+} \quad (2.25)$$

$$2VO^{2+} + 2H_2O \Leftrightarrow (VO)_2(OH)_2^{2+} + 2H^{+} \quad (2.26)$$

The majority of the oxovanadium (IV) complexes can be classified in terms of the generalised forms: $[VOL_5]^{n\pm}$, $[VOL_4]^{n\pm}$, $[VOL_xL_{5-x}]^{n\pm}$, $[VOL_xL_{4-x}]^{n\pm}$ [62]. For VO_2 dissolved in HCl or HBr solution, the formation of complex ion such as $[VOCl(H_2O)_4]^{+}$ or $[VOBr(H_2O)_4]^{+}$ is expected [70]. This is in agreement with the composition of hydrated compound ($VOCl_2 \cdot 4H_2O$) which is isolated from the solution of dissolved V_2O_5 in concentrated HCl [71]. A product with a similar composition ($VOSO_4.xH_2O$) is prepared by the reduction of V(V) in H_2SO_4 using SO_2 [71]. Most of the solid oxovanadium (IV) complex were identified by IR spectroscopy since it has a strong V=O stretching frequency [62].

The reduction of V(IV) to V(III) was described as the rate determining step for overall reduction of V(IV) to V(II). Since different intermediates would form in acid media, two possible routes for V(IV) reduction were found (cross ref reaction (2.27 to 2.29) and (2.30 to 2.32)). V(III) was not identified as an intermediate because the heterogeneous rate constant for V(III) reduction is larger than the rate of its formation. Therefore, V(III) concentration is not measurable on the electrode surface [60]. Concentrated HCl (12F) on the other hand was one of the very few media that allowed V(IV) to undergo stepwise reduction to V(III) without forming any intermediates [60].

$$VO^{2+} + H^{+} + 2e \Leftrightarrow VOH^{+} \qquad rds \qquad (2.27)$$

$$VOH^{+} + H^{+} \Leftrightarrow V^{2+} + H_2O \qquad fast \qquad (2.28)$$

$$V^{2+} \Leftrightarrow V^{3+} + e \qquad fast \quad at \quad E < -0.4V \qquad (2.29)$$

$$VO^{2+} + H^{+} + e \Leftrightarrow VOH^{2+} \qquad rds \qquad (2.30)$$

$$VOH^{2+} + H^{+} \Leftrightarrow V^{3+} + H_2O \qquad fast \qquad (2.31)$$

$$V^{3+} + e \Leftrightarrow V^{2+} \qquad fast \quad at \quad E < -0.6V \qquad (2.32)$$

2.3.4 Vanadium (V)

V(V) has an outer electron configuration of d^o and is the most strongly oxidising state. V_2O_5 is made from $VOSO_4 \cdot 5H_2O$ via thermal oxidation [62], or from NH_4VO_3 via heating [63]. There are various hydrolysis ions in aqueous solutions of V(V), which highly depend on solution acidity (Table 2.8). $[VO_2(H_2O)_4]^+$ ions (commonly refer as VO_2^+) only exists in concentrated acid (pH <1) [63].

Table 2.8 V(V) oxo-anion formation in different pH solution [63]

pH	V(V) oxo-anaions
<12	$[VO_4]^{3-}$
12	$[VO_3OH]^{2-}$
10	$[V_2O_6OH]^{3-}$
9	$[V_3O_9]^{3-}$
6.5	$V_2O_5(H_2O)_n$
2.2	$[V_{10}O_{28}]^{6-}$
<1	VO^{2+}

In concentrated hydrochloric acid (>8F [60] ; 37% HCl [74]), the addition of V_2O_5 leads to the reduction of V(V) to V(IV) and the evolution of Cl_2 gas [71, 75]. This blue

solution was found to be dominantly in $[VO(H_2O)_5]^{2+}$ ions [63]. Similarly in HBr, dissolved V_2O_5 forms $[VO(H_2O)_5]^{2+}$ ions and Br_2 gas is released [63, 76]. On the other hand Kurbatova et. al. [77] found that in a 0.1 M V(V) solution, $[VO_2Cl_4]^{3-}$ complex is formed at HCl concentrations less than 8.6 M, and becomes a tetrachloride complex $[VOCl_4]^-$ when the HCl concentration is greater than 8.6 M.

In sulphuric acid media, Kausar [47] and Kausar et al [78] showed the formation of different V(V) species depend upon the concentrations of V(V) and H_2SO_4. For a 4 M H_2SO_4 solution less than 1.5 M V(V), the dominant species were found to be VO_2^+, SO_4^{2-}, $VO_2SO_4^-$ and HSO_4^- ions. With increasing V(V) concentration up to 1.5 M at constant sulphuric acid concentration, there was a significant increase of $VO_2SO_4^-$ ions. A further increase in V(V) concentration (ie. > 1.5 M) at constant sulphuric acid concentration would cause the vanadium ions to form co-polymeric species with SO_4^{2-} / HSO_4^-. This led to the formation of $V_2O_3^{4+}$ and $V_2O_4^{2+}$ that caused the sudden increase in solution viscosity.

On the other hand the increase of H_2SO_4 concentration to 6 M for solutions with 1.5 M V(V), would decrease the amount of $VO_2SO_4^-$ ions. In such solution the presences of VO_3^- species is confirmed by the formation of a V_2O_5 precipitation at elevated temperatures. A further increase in total sulphate concentration (from 6 M to 8 M H_2SO_4) for solutions with 2 M V(V), favours the formation of the most stable species $VO_2(HSO_4)_2^-$ and $VO_2(SO_4)_2^{3-}$.

Kausar et al [78] also explained the sudden increase in positive electrolyte viscosity of all-vanadium redox flow cell (which the concentration of V(V) greater than 2 M in 5 M H_2SO_4), is caused by the formation of copolymer vanadium species. Therefore, to avoid

the precipitation at elevated temperature (> 30^{o}C), a higher H_2SO_4 concentration (> 5 M) is required for the all-vanadium redox flow cell.

2.3.5 Summery of vanadium complexes in different acids

Although vanadium ions form complex species in complexing acids (HCl, HBr), the dominate species is the same as in non-complexing media ($HClO_4$). Complex species that form in different vanadium states are summarised in (Table 2.9). In most cases the complex species exist in a small proportion.

Table 2.9 Vanadium complexes formed in different acid media and corresponding solid formation

Sate of V	Non-complexing acid	HCl	HBr	Solid Hydrated Complex	Ref.
V(II)	$[V(H_2O)_6]^{2+}$	No complex species	No complex species	$V(ClO_4)_2.6H_2O$ $VCl_2.4H_2O$, $VBr_2.6H_2O$	[60 –64]
V(III)	$[V(H_2O)_6]^{3+}$	$[VCl(H_2O)_5]^{2+}$ $[VCl_2(H_2O)_4]^{+}$	$[VBr(H_2O)_5]^{2+}$ $[VBr_2(H_2O)_4]^{+}$	$VCl_3.6H_2O$, $VBr_3.6H_2O$	[60, 63, 65 - 69]
V(IV)	$[VO(H_2O)_5]^{2+}$	$[VOCl(H_2O)_4]^{+}$	$[VOBr(H_2O)_4]^{+}$	$VOCl_2.4H_2O$	[60, 62–63, 70–73]
V(V)	$[VO_2(H_2O)_4]^{+}$	Reduced to V(IV) OR form anion complexes [HCl] < 8.6M forms: $[VO_2Cl_4]^{3-}$ [HCl] > 8.6M forms: $[VOCl_4]^{-}$	Reduced to V(IV)	NA	[47, 62–63, 71, 74– 78]

2.4 Electrochemical studies of V(III)/ V(II) in different acids

2.4.1 Cyclic voltammetry studies on V(II) / V(III) couple in H_2SO_4

Sum and co-workers studied the electrochemical behaviour of the V^{2+}/V^{3+} couple in H_2SO_4 using cyclic voltammetry [79]. Cyclic voltammogram experiments were conducted with a glassy carbon working electrode, graphite rod as the counter electrode and saturated caramel as the reference electrode (SCE) for solutions of 0.08M V^{3+} dissolved in 1.8 M H_2SO_4 (Figure 2.4). The V^{2+} / V^{3+} couple was found to be electrochemically irreversible, having a reduction peak at -0.7 V (vs SCE) and an oxidation peak around -0.35 V (vs SCE). Similar finding were obtained by Oriji and co-workers [80] for 1.61 g-atom (V) dm^{-3} of V(III) in H_2SO_4 solutions. Using a glassy carbon working electrode, platinum and Ag/AgCl as counter and reference electrodes, the reduction peak was found to occur at -0.7 V while the oxidation peak occurred at -0.2 V (vs Ag/AgCl).

2.4.2 Voltametric studies on V(II) / V(III) couple in HCl

The polarogram of V(II) in 12 F HCl solution showed a reversible anodic wave with a half-wave potential at -0.538 V (vs SCE), whereas a reversible cathodic wave with half-wave potential at -0.526 V (vs SCE) was produced by V(III). The half-wave potential obtained in 12 F HCl was slightly lower than that observed in diluted solution. In 1 F HCl the half-wave potential for V(III) reduction is -0.51 V (vs SCE) [60].

Meites and Moros [81] showed the presence of 1 F – 4.5 F HCl attributed to a Faraday current when V(IV) is reduced to V(II) at low concentrations (2.056 x 10^{-3} mol in 60

ml, ie. 3.43 x 10^{-4} M) Therefore, a background correction for the measured current was needed for controlled potential coulometric analysis.

With cyclic voltammetry, Sum et al [79] investigated the V(II)/V(III) electrochemical characteristics in HCl solution. Using lead as the working electrode, the voltammogram showed an anodic peak at -0.27 V (vs SCE) and a cathodic peak at -0.50 V (vs SCE). Further oxidation of the solution led to chorine gas formation that begins at 1.1 V (vs SCE).

2.4.3 Electrochemical parameters of V(III) / V(II) couple

Sum et. al. [79] studied the electrochemical parameters for the V(III)/V(II) couple in a 0.12 M VCl_3, 0.5 M H_2SO_4 solution using cyclic voltammetry. The formal potential of this redox couple was -0.6 V (vs SCE), with a cathodic peak and an anodic peak at -0.7 V and -0.35 V (vs SCE) respectively. Deduced from cyclic voltammograms, the diffusion coefficient and the heterogenous rate constant for V^{3+} reduction was found to be 1.41 x 10^{-6} cm^2s^{-1} and 1.7 x 10^{-5} cms^{-1} respectively.

In another study by Niki and Mizota [69] electrochemical parameters obtained were slightly different from a diluted V(III) solution (0.001 M V(III) in 0.5 M H_2SO_4). The formal potential, diffusion coefficient and heterogeneous rate constant were determined as -0.505 V (vs SCE), 6.33 x 10^{-6} cm^2s^{-1} and 1.1 x10^{-3} cms^{-1}respectively. The rate constant obtained in this study is similar to those shown in the review by Tanaka [82]

Niki and Mizota [69] also studied the electrochemical parameters of V(III)/V(II) in HCl and HBr solutions by d.c polarographic method using dropping mercury electrode (DME). The formal potential of V(III)/V(II) in HCl and HBr were slightly lower than

that obtained for non-complexing media ($HClO_4$). This indicated the formation of complex ions (see 2.4.7). Moreover, the rate constant for V(III) reduction in 1 M HBr is 100 times larger than that obtained in 1 M HCl solutions. On the other hand the diffusion coefficient was not highly affected by the use of HCl or HBr solutions. The kinetic parameters of V(III)/V(II) in different acid media, including the formal potential, diffusion coefficient and rate constant values reported by Niki and Mizota [69] are summarised in Table 2.10. The exchange current density of V(III)/V(II) in 1 M HBr was found to be 34 x 10^{-3} Acm^{-2}. This is consistent with the finding by Anson and Caja [83], who reported an exchange current density for the V(III) / V(II) couple in 1 M NaBr of 29 x 10^{-3} Acm^{-2}.

Table 2.10 Formal Potential of V(III)/V(II) and Diffusion Coefficient of V(III) in different acid medium [69]

Medium	[V(III)] (M)	$E^{o'}$ V(III)/ V(II) (V vs SCE)	Diffusion Coefficient (10^{-6} cm^2s^{-1})	α	k^o (cms^{-1})	Ref
$HClO_4$	0.001	-0.459	6.42	0.58	2.7 x10^{-3}	[69]
0.5 M H_2SO_4	0.001	- 0.505	6.33	0.51	1.1 x10^{-3}	[69]
1 M HCl	0.001	- 0.464	6.42	0.43	6.5 x10^{-5}	[69]
1 M HBr	0.001	- 0.460	6.77	0.4	0.33	[69]
0.5 M H_2SO_4 1.04 M $NaSO_4$	0.11	-0.6	1.41	0.67	1.7 x10^{-5}	[79]
4.2 M H_2SO_4	0.032	-0.5	0.57	0.5	2.0 x10^{-4}	[80]

2.4.4 The effect on CV by electrode treatment and prolonged immersion

Sum and co-workers [79] discovered that the treatment of the working electrode has a significant effect on the peaks obtained from the CV. A graphite electrode polished with 0.3 μm alumina tends to lose the characteristic peaks whereas with a P1200 sand paper treatment, the peaks corresponding to the V^{3+}/V^{2+} redox reaction could be observed (Figure 2.4). Prolonged immersion of the electrode in the solution was also found to produce a great shift of peak potential and peak currents.

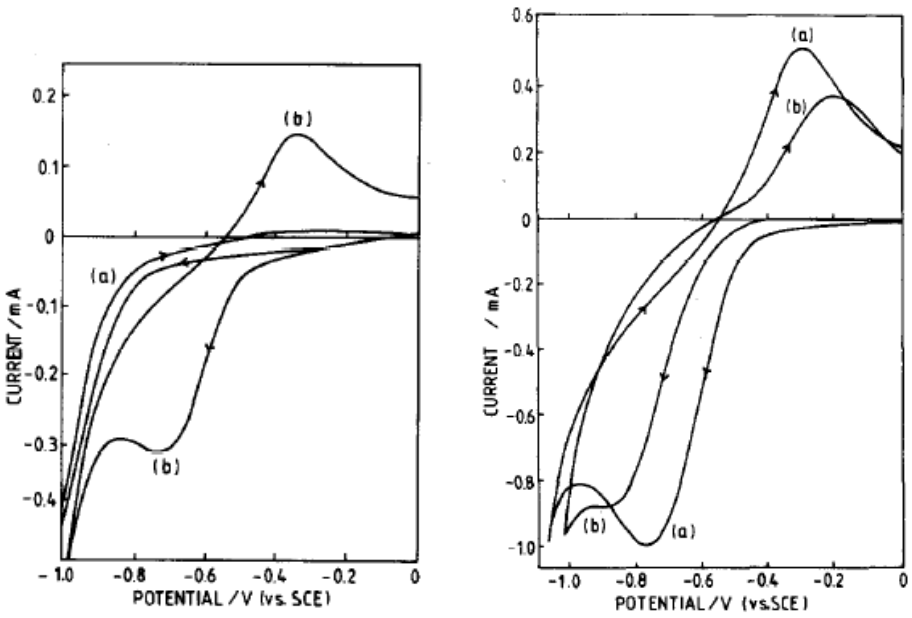

Figure 2.4 (Left) Cyclic Voltammetry of 0.08 M VCl_3 1.8 M H_2SO_4 with a scan rate of 5 $Vmin^{-1}$on 0.07cm^2 glassy carbon electrode with different electrode treatment (a) polish with P1200 sandpaper and 0.3 μm alumina then ultrasonic cleaning for 45min (b) polished with P1200 sandpaper only. [79] (Right) Cyclic voltammetry of 0.11 M VCl_3 1.6 M H_2SO_4 with a scan rate 8 $Vmin^{-1}$ showing prolonged immersion effect (a) First scan (b) Scan after 10 min of immersion in the solution. [79]

2.4.5 Cyclic voltammetry of vanadium electrode in hydrochloric acid

In the study of vanadium species in HCl, Barrado and co-workers [84] attempted to use a carbon paste electrode (CPE) with premixed V_2O_5 as working electrode while Pt wire and Ag/AgCl were used as counter and reference electrode. Figure 2.5 illustrates the electrochemical behaviour of the V_2O_5 / carbon paste electrode in a 1 M HCl solution from this study. Importantly, this cyclic voltammogram shows that once VO_2^+ has reduced to VO^{2+} the next reduction goes directly to V^{2+} instead of V^{3+}. Therefore, in order to study the electrochemical behaviour of the V^{3+}/V^{2+} couple a solution of V^{3+} ion needed to be prepared.

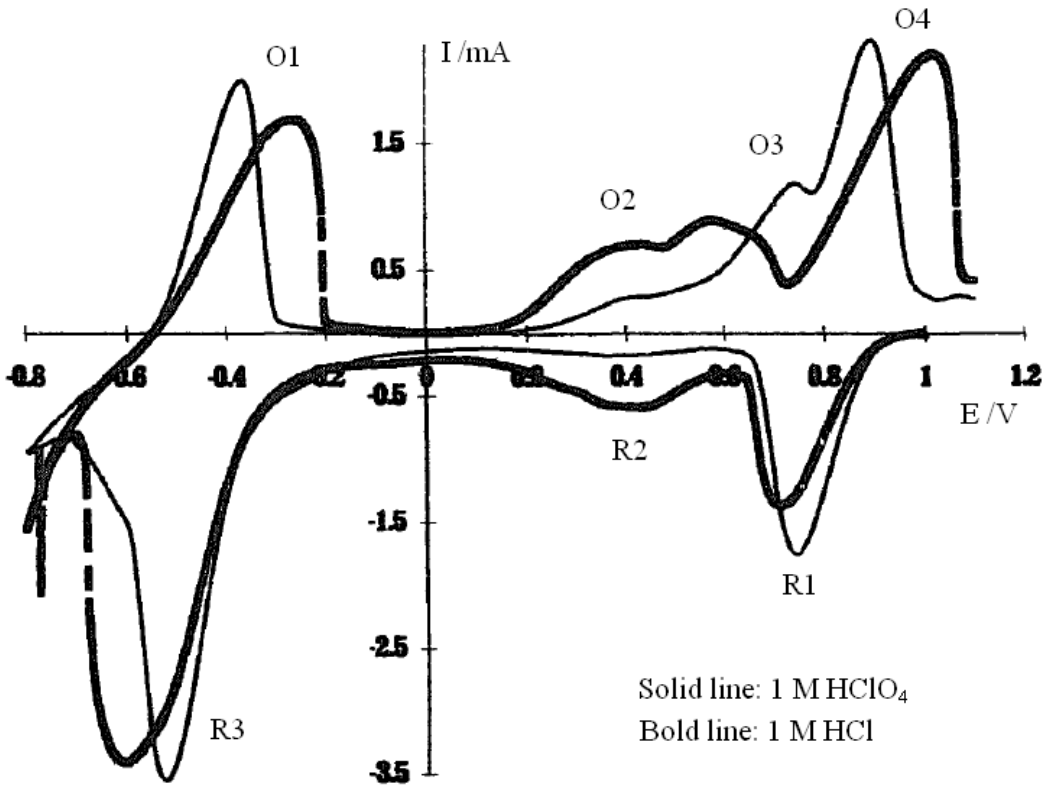

Figure 2.5 Cyclic voltammogram of V_2O_5 using a carbon paste electrode containing graphite and binder in supporting electrolytes (Solid line) 1 M $HClO_4$ and (Bold line) 1 M HCl [84] Where R1: V(V) → V(IV), R2: V(V) (s) → V(IV), R3: V(IV) → V(II), O1: V(II) → V(III),O2: V(III) → V(IV), O3: produced by dissolved species (not due to vanadium ions), O4:V(IV) → V(V)

2.4.6 Estimation of V(III) complex formation in HCl and HBr

It is known that V^{3+} does not form complexes with perchlorate ions [62]. Niki and Mizota [69] attempted to determine the complex ion distributions in different media using the formal potential. They followed the calculations by De Kreuk et al [85] repeated in Equation (2.33) and determined the complex ion percentage by the difference in the formal potentials between complexing (HCl, HBr) and non-complexing media ($HClO_4$) [69].

For this calculation Niki and Mizota [69] assumed higher complexes would form between chlorides and V(III), whilst complex between V(II) and chlorides were negligible, therefore the solution would only contain V^{3+} and VCl^{2+}.

$$E^{o'} = E^{o} - \frac{RT}{nF}\ln\left(\frac{r_o}{r_R}\right) \qquad (2.33)$$

Where,

Eo' = standard potential of the uncomplexed species
Eo = standard potential of the complexed species
ro = cO*/cOT*
rR = cR*/cRT* and
cO*, cR* are the bulk concentrations of uncomplexed species
cOT*, cRT* are the bulk concentrations of compelxed and uncomplexed species

From the formal potentials of V^{3+}/V^{2+} in different media are shown in Table 2.10, the difference between the potentials in HCl and $HClO_4$ was -0.005 V (vs SCE). By applying the potential difference to Equation 2.33, it was found that the solution contains 82.3% V^{3+} and 17.7% VCl^{2+}. Apply the same assumptions and calculation methods, the ion distribution in HBr solution for V^{3+} and VBr^{2+} was found to be 96% and 4% respectively. This also agreed with bromide ions being a milder complexing ion compared to chloride ions.

2.5 Bromide / bromine studies

2.5.1 Electrochemical process of bromide / bromine reaction

The Volmer-Heyrovsky (V-H) mechanism is commonly suggested to be the kinetic mechanism for bromide/ bromine reaction [86, 87]. Bromine oxidation occurs in several

steps. First, adsorbed Br species are formed on the electrode (2.34) which is considered to be the rate determining step (r.d.s) in many studies [86-88]. Then the adsorbed Br species are further oxidised to Br_2 (2.35), and followed by the tribromide complexation reaction in the solution (2.36) [86]. The kinetic mechanism for the bromide / bromine reaction is similar to the reaction of chlorine evolution in chloride solutions [89] .

$$Br^- \Leftrightarrow Br_{ads} + e \qquad (Volmer \quad step) \tag{2.34}$$

$$Br_{ads} + Br^- \Leftrightarrow Br_2 + e \qquad (Heyrovsky \quad step) \tag{2.35}$$

$$Br_2 + Br^- \underset{k_b}{\overset{k_f}{\rightleftharpoons}} Br_3^- \tag{2.36}$$

2.5.2 Kinetics of bromide/ bromine reaction

Mastragostiono and Gramellini [87] studied the electrochemical processes for the aqueous Br_2/Br^- reaction on a rotating disc electrode using two vitreous (glassy) carbon electrodes. On a reticulated vitreous carbon electrode (RVC) the equilibrium potential (OCP) for a 4.2×10^{-3} M bromide and 7.1×10^{-4} M bromine solution was 0.975 V (vs SCE), whereas the increase in bromide concentration reduced the OCP to about 0.76 V (vs SCE). The reduction in OCP is due to the formation of Br_3^- ions in solutions that have higher bromine and bromide concentrations.

In diluted bromine and bromide solutions, the transfer coefficient (α) for bromide oxidation on RVC was 0.23. The transfer coefficient of bromine reduction for solutions with and without Br_3^- formation varied between 0.22 and 0.26. The exchange current densities of bromide oxidation and bromine reduction on RVC for diluted solutions

were reported as 64 x 10^{-6} and 80 x 10^{-6} Acm^{-2} respectively. On the other hand the rate constant on RVC for bromide oxidation, bromine reduction and tribromide reduction were found to be 1.1 x 10^{-3}, 4.5 x 10^{-5} and 5.6 x 10^{-3} respectively.

Mastragostiono and Gramellini [87] also studied the bromine / bromide kinetics on a smooth vitreous carbon electrode (CVJ) and their results are summarised in Table 2.11.

Table 2.11 Kinetic parameters of Br_2/Br^- reaction on different electrodes at different concentrations [87]

	Br^- oxidation			**Br_2 reduction**		**Br_3^- reduction**	
Electrode	RVC	CVJ		RVC	CVJ	RVC	CVJ
$[Br_2]$ (M)	$7.1x10^{-4}$	$7.3x10^{-4}$	$7.1x10^{-5}$	$7.1x10^{-4}$	$7.1x10^{-4}$	$4.6x10^{-5}$	$5.0x10^{-5}$
$[Br^-]$ (M)	$4.2x10^{-3}$	$8.2x10^{-3}$	$8.2x10^{-3}$	$4.1x10^{-3}$	$8.9x10^{-3}$	1.0	1.0
$[Br_3^-]$ (M)	0	0	0	0	0	$1.0x10^{-3}$	$1.1x10^{-3}$
Eeq (mV, vs SCE)	975	915±5	880±5	965±5	925±5	760±5	730±5
α	0.23 ±0.02	0.32 ±0.02	0.3 ±0.01	0.22 ±0.02	0.45 ±0.01	0.26 ±0.1	0.42 ±0.4
i_o $10^{-6}Acm^{-2}$	64±4	219±4	124±2	80±1	137±1	143±3	111±2
RVC: Reticulated vitreous carbon electrode, CVJ: a smooth vitreous carbon electrode.							

Rubinstein [90] on the other hand study the mechanism for bromide / bromine reaction on Pt electrode. The exchange current density was found to be 0.083 Acm^{-2} on a reduced Pt electrode, and 0.02 Acm^{-2} on an oxidised Pt electrode. This study also agreed with the formation of adsorbed Br species on electrode surface being the r.d.s for bromide oxidation.

Ferro et al. [91] studied the bromide / bromine mechanism on a polycrystalline Pt electrode in a higher bromine concentration compared to the work of Mastragostiono and Gramellini [87]. In an equal molar solution of 0.375 M Br^- and Br_3^-, the exchange

current density and equilibrium potential were found to be 26.9 $mAcm^{-2}$ and 0.847 V (vs SCE) respectively. Their study also agreed that the bromide / bromine reaction undergoes a V-H mechanism. However, they indicated chemical desorption to be the r.d.s. for bromide oxidation, in agreement with the work by Conway et al [92].

2.5.3 Equilibrium of aqueous bromine contain chloride and bromide species

Bell and Pring [93] used the redox potential to determine the equilibrium constant of polybromide ion formation on addition of aqueous bromine to a solution containing bromide and chloride ions. They assumed there are Br_2Cl^- and $BrCl_2^-$ ions in the solution (2.37 to 2.40). They found that K = 16 M^{-1}, K_1 = 1.14 M^{-1} and K_2 = 7.2 x 10^{-3} M^{-1}

$$Br_2 + Br^- \underset{\longleftarrow}{\overset{K}{\longrightarrow}} Br_3^- \qquad (2.37)$$

$$Br_2 + Cl^- \underset{\longleftarrow}{\overset{K_1}{\longrightarrow}} Br_2Cl^- \qquad (2.38)$$

$$Br_2 + 2Cl^- \underset{\longleftarrow}{\overset{K_2}{\longrightarrow}} BrCl_2^- + Br^- \qquad (2.39)$$

$$Br_2 + Cl^- \underset{\longleftarrow}{\overset{K_3}{\longrightarrow}} BrCl + Br^- \quad neglected \quad when \quad \frac{[Br^-]}{[Cl^-]} > 0.03 \qquad (2.40)$$

As Bell and Pring [93] used the following Equations (2.41 to 2.43 where E^o = 1.065 V vs NHE) to obtained the equilibrium constants, the equilibrium potential can then be

estimated for solutions with known consternations in bromine, bromide and chloride at equilibrium.

$$E = E^o + \frac{RT}{nF} \ln \frac{[Br_2]}{[Br^-]^2} \tag{2.41}$$

$$E = E^o + \frac{RT}{nF} \ln \frac{[Br_2]}{(1 + K[Br^-])[Br^-]^2} \tag{2.41}$$

$$E = E^o + \frac{RT}{nF} \ln \frac{[Br_2]}{\left(1 + K[Br^-] + K_1[Cl^-] + \frac{K_2[Cl^-]^2}{[Br^-]}\right)[Br^-]^2} \tag{2.43}$$

Later study by Wang et al [94] showed the system for aqueous bromine, bromide and chloride would reach equilibrium in a slightly different route, which is described by the following reactions (2.44 to 2.47). The equilibrium constants were determined as K_1 = 6.0 M^{-1}, K_2 = 1.8 x 10^4 M^{-1}, K_3 = 1.3 $M^{-1}$and K_4 = 16.1 M^{-1}

$$Cl^- + BrCl_{(aq)} \underset{\longleftarrow}{\xrightarrow{K_1}} BrCl_2^- \tag{2.44}$$

$$Br^- + BrCl_{(aq)} \underset{\longleftarrow}{\xrightarrow{K_2}} Br_2Cl^- \tag{2.45}$$

$$Br_2 + Cl^- \underset{\longleftarrow}{\xrightarrow{K_2}} Br_2Cl^- \tag{2.46}$$

$$Br_2 + Br^- \underset{\longleftarrow}{\xrightarrow{K_4}} Br_3^- \tag{2.47}$$

2.5.4 Bromide oxidation in HCl solution from initial study of V/Br cell

From the initial study of the novel polyhailde redox cell, the formal potential of bromine / bromide was found to be 0.85 V for solutions containing 1 M HCl and 0.27 M NaBr (Figure 2.6) [5]. For solutions with increased bromide concentration the reduction peak potential is reduced while the oxidation peak potential increase.

As can be seen in the previous section (2.4.6) the oxidation potential of VO^{2+} to VO_2^+ is similar to that of bromide oxidation in HCl solutions. Bromide oxidation thus masks the V(IV) to V(V) oxidation reaction in an HBr supporting electrolyte, therefore no significant amount of VO_2^+ species are expected to form in the positive half-cell electrolyte of the V/Br cell during charging.

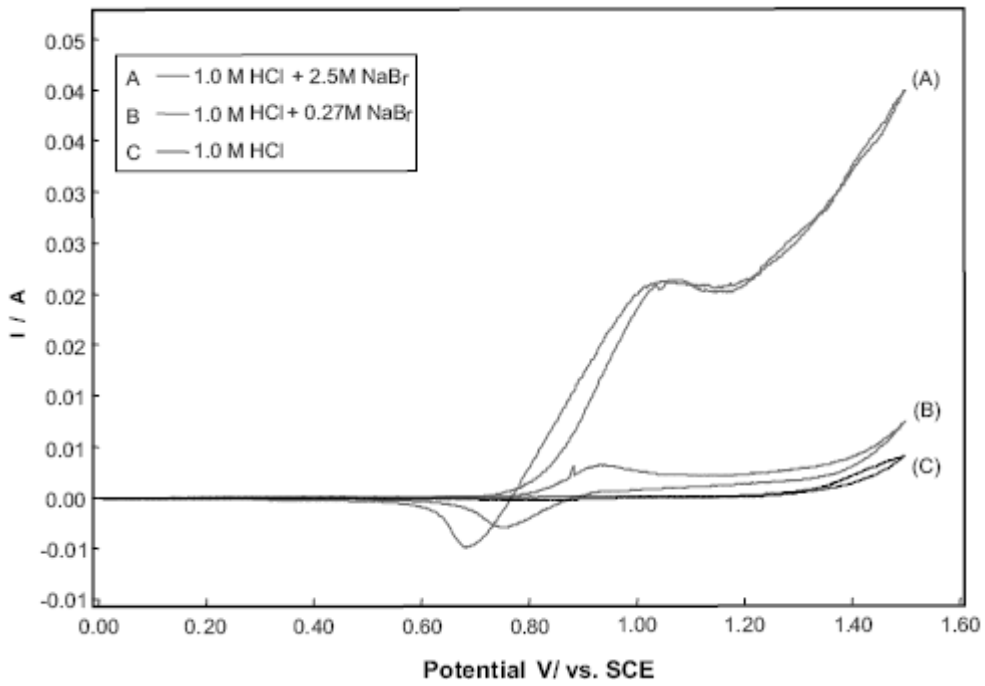

Figure 2.6 Cyclic Voltammogram of (A) 2.5 M (B) 0.27 M NaBr in 1 M HCl [5]

2.6 Bromine complexing agents in zinc bromine battery

A major problem that could occur with the V/Br cell is the possible emission of bromine gas during cell charging. This section aims to revise the available techniques that could be used to prevent bromine emission. Methods used in the zinc bromine flow battery including addition of propionitrile, gelling agent and quaternary ammonium bromine are described in the following sections.

2.6.1 Propionitrile

Singh et al. [40] proposed to use a dipolar aprotic solvent, propionitrile (PN) to obtain an aqueous phase with lower bromine concentration. An advantage of this method is the formation of charge-transfer complexes with bromine, which result in a highly conducting solution. In the study of Cathro [35] quaternary ammonium bromides (QBr) were added to the PN electrolyte in the positive side of the Zn/Br cell. This design is different from the conventional zinc bromine flow cell which has the same electrolyte composition in both tanks when discharged. It was shown that the aqueous bromine concentration reduced significantly when QBr is added to the PN electrolyte instead of using PN alone.

2.6.2 Gelling Agent

Three main types of silica can be used as gelling agents namely water-glass, fumed silica, and colloidal silica sols. Depending on the percentage of silica, the gel porosity and pore volume can be controlled [95]. The pore volume allows electrolytes to penetrate through and stay in the gel.

In advanced lead / acid batteries fumed silica and colloidal silica were mainly used as a mixture for electrolyte gelling [95]. By using of gelling agents, electrolyte strafication can be avoided and the capacity of the battery can be retained longer [96, 97].

Fumed silica was used as the gelling agent to capture bromine gas vapour in a preliminary study of vanadium bromide battery [98]. Vanadium bromide electrolyte was gelled by the addition of fumed silica that has two functional groups, silanol and siloxance (Aerosil 300). It was found that the vanadium bromide gel is able to capture bromine vapour during the charging of a lab scale static cell with electrode area of 25 cm^2 and it provided an energy efficiency of 60%. However, due to the high viscosity of the vanadium bromide gel it is not suitable for use in a flow cell.

2.6.3 Quaternary Ammonium Bromides

Since the early studies of a non-flowing zinc bromine battery patented by Bloch [22] the use of quaternary ammonium bromides as bromine complexing agents are disclosed. The addition of two types of solid aliphatic ammonium compounds to the graphite powder that surrounded the cathode was shown to prevent bromine attack during cell charging. Bloch discovered tetramethyl ammonium bromide is able to bind up to four molecules of bromine and form a conductive solid layer surrounding the cathode.

With this concept in mind De Rossi [99] attempted to use a quaternary ammonium bromide in a zinc bromine flow cell. It was shown that tetramethyl ammonium bromide (TMABr) combined with bromine to form two types of solids ($TMABr_3$ and $TMABr_9$) and a liquid eutectic mixture (2.48 and 2.49).

$$(TMA+Br^-)+Br_2 \rightarrow TMA^+ + Br_3^- + TMABr_3 \quad (2.48)$$

$$(TMA+Br^-)+3Br_2 \rightarrow TMA^+ + Br_9^- + TMABr_9 \quad (2.49)$$

However, in this particular design De Rossi aimed to eliminate the bromine rich liquid that flows around the cell, and the addition of TMABr addition would not be suitable. Therefore, De Rossi used tetramethly ammonium perchlorate ($TMAClO_4$) as the bromine complexing agent instead. Since $TMAClO_4$ has a low solubility in the zinc bromine electrolyte and forms a single solid ($TMABr_9$) when combined with bromine, it can be retained within the interior of the cathode [99].

In contrast to the above studies that suggested the formation of bromine rich solids to be critical, Eustace et. al. [34] reported the use of several asymmetrical cyclic quaternary ammonium bromides which allowed elemental bromine to be separated from the aqueous electrolyte in a form of liquid complex. The dense liquid complex is normally referred to as dense polybromide oil phase or fused salt. In Figure 2.7, the basic QBr reaction mechanism is shown alongside the charge and discharge reactions of a zinc bromine battery.

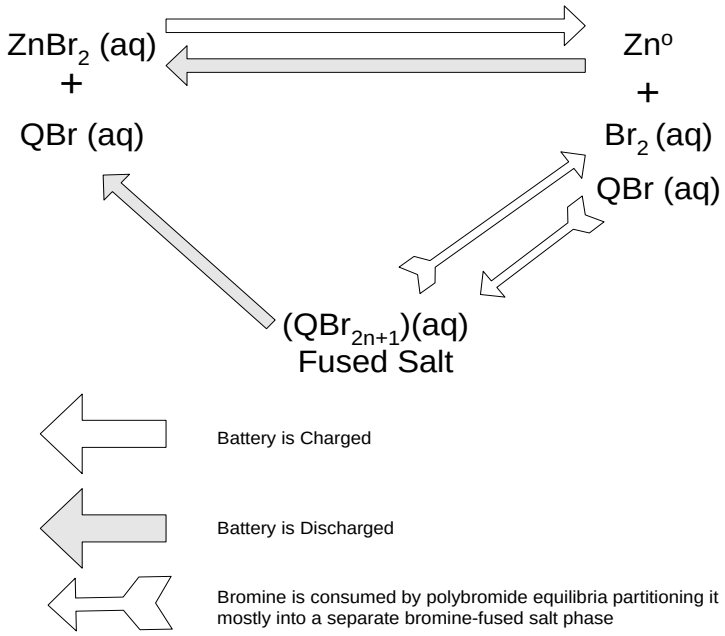

Figure 2.7 Chemical reactions of dense phase formation in a zinc bromine battery [55]

In a static cell containing small volumes of electrolytes (6 – 7 cm^3) Eustace et. al. [34, 100] showed that the addition of asymmetrical cyclic quaternary ammonium bromides can sufficiently improve the coulombic efficiency (Table 2.12). This study showed the static cell would have the highest coulombic efficiency (80 – 83%) for electrolytes containing 3 M $ZnBr_2$ and 1 M N-ethyl N-methyl-morpholinium bromide.

This explains the extensive use of N-ethyl N-methyl-morpholinium bromide in most later developed zinc bromine flow cells. Further, with the separation of a dense liquid polybromide phase now possible, all bromine rich material could be stored away from the cell electrode to prevent self discharge. This led to extensive studies in the search of suitable QBr compounds for the zinc bromine flow cell system that form a separable dense liquid polybromide phase when reacted with bromine.

Table 2.12 Coulombic efficiency of static cells with unsymmetrical cyclic QBr addition [34, 100]

Asymmetrical cyclic QBr	$ZnBr_2$ (M)	$ZnSO_4$ (M)	Coulombic Efficiency (%)
No complexing agent	3	0.2	30 – 41
0.94 M N-Carboxymethyl N-methyl piperidinium bromide	3	0.2	72 – 80
1 M N-ethyl N-methyl-morpholinium bromide	3	0.2	52 – 68
1 M N-ethyl N-methyl-morpholinium bromide (MEM)	3	0	80 – 83
0.85 M N-cholromethyl N-methyl morpholinium bromide	3	0	70 – 74
1 M N-cholromethyl N-methyl morpholinium bromide	3	0	73 – 77

2.6.4 Types of Quaternary Ammonium Bromides

Large numbers of quaternary ammonium bromide compounds have been tested for the zinc bromine flow cell and these can be grouped into three main types (Table 2.13). These are asymmetrical cyclic quaternary ammonium bromides [55, 101], asymmetrical aliphatic quaternary ammonium bromides [101] and symmetrical aliphatic quaternary ammonium bromides [36].

Eustace reported [34] that asymmetrical cyclic ammonium bromide forms a dense liquid polybromide phase and has a high bromine distribution coefficient when reacted with bromine. The bromine distribution coefficient (K_{Br2}) in the two liquid phases was determined according to Equation (2.50) K_{Br2} was found to be 8.1 for a 5 ml sample containing 2 M $ZnBr_2$ with 3.28 x 10^{-3} moles of dissolved N-Carboxymethyl N-methyl piperidinium bromide after 9.84 x 10^{-3} moles of liquid bromine was added. This is much higher than that of an asymmetrical aliphatic quaternary ammonium bromide ($C_5H_{12}O_2NBr$) that has a K_{Br2} of 1.6 determined by the same experimental method.

$$K_{Br2} = \frac{n_{Br2\_polybromie\_phase}}{9.84\times10^{-3} - n_{Br2\_polybromie\_phase}} \qquad (2.50)$$

Although the two asymmetrical cyclic ammonium bromides N-ethyl N-methyl-morpholinium bromide (MEM) and N-ethyl-N-methyl-pyrrolidinium bromide (MEP) were widely used in the zinc bromine flow cell, in later studies by Cathro et al [101] showed that MEP could form a white crystal with zinc while the addition of MEM could form a solid polybromide phase when reacted with bromine.

Table 2.13 Types of quaternary ammonium bromide (QBr) tested for zinc bromine flow cell

Types of QBr	Examples
Asymmetrical cyclic quaternary ammonium bromide [55, 101]	**N-ethyl N-methyl-morpholinium bromide (MEM)** **N-ethyl-N-methyl-pyrrolidinium bromide (MEP)** N-methoxymethyl N-methyl-piperidinium bromide N-chloromethyl N-methyl-pyrrolidinium bromide
Asymmetrical aliphatic quaternary ammonium bromide [101]	Tri-methyl-ethyl ammonium bromide **Di-methyl-diethyl ammonium bromides (2M2E)** **Methyl-tri-ethyl ammonium bromides** Tri-methyl-propyl ammonium bromides **Di-methyl-ethyl-propyl ammonium bromides (2MEP)** **Methyl-diethyl-propyl ammonium bromides (2EMP)** **Tri-ethyl-propyl ammonium bromides** Tri-methyl-chloro-methyl ammonium bromides Di-methyl-ethyl-chloro-methyl ammonium bromides Methyl-diethyl-chloro-methyl ammonium bromides Tri-ethyl-chloromethyl ammonium bromides
Symmetrical aliphatic quaternary ammonium bromide [36, 101]	Tetra methyl ammonium bromide Tetra ethyl ammonium bromide Tetra-butyl ammonium bromide (TBA)

As a result the use of asymmetrical aliphatic ammonium bromides for zinc bromine flow cell was further studied. Cathro [101] reported the observations of samples

containing $ZnBr_2$ and Br_2 and various unsymmetrical aliphatic ammonium bromides listed in Table 2.13.

The QBr in bold text shown in Talbe 2.13 denoted those would form a liquid bromine rich organic phase at 25^oC when bromine is added. Although an oil like phase is formed in all samples at 50^oC after bromine is added, most of them would form a solid or semi solid like material at 0^oC. Therefore, single asymmetrical aliphatic ammonium bromides would not be suitable for the zinc bromine flow cell between 0 – 50^oC.

The use of a single symmetrical quaternary ammonium bromide reported by Eustace [55], showed the formation of an insoluble solid polybromide phase in the $ZnBr_2$ electrolyte when reacted with bromine. This agreed with the work by Cartho and Cedzynska [101] showed that tetra-methyl ammonium bromide and tetra-ethyl ammonium bromide formed a solid polybromide phase when reacted with bromine. Therefore, symmetrical aliphatic quaternary ammonium bromides that have a high bromine reduction ability were selected as potential candidates to mix with asymmetrical cyclic ammonium bromide [36].

The above studies show that the use of single quaternary ammonium bromides will form a solid polybromide phase during the operation of a zinc bromine flow cell between 0 – 50^oC. If considering quaternary ammonium bromide as molten salts, it would be expected that a mixture of quaternary ammonium bromides would give a dense polybromide phase that has a lower freezing point than its individual compounds [101]. Similar findings reported by Walsh et al. [102] show that a mixture of salts would depress the freezing point. This means the dense polybromide phase formed when combined with bromine can remain as a liquid at lower temperatures and therefore can

be used in a wider temperature range. The freezing point depression phenomenon was quantified by the following Equation (2.51) [102]

$$\Delta T = \frac{R(T_x)^2 (mw_x)(m_y)}{1000\,\Delta H_{fux_x}} \qquad (2.51)$$

where ΔT represents the freezing point depression of specie x (^oK), R is gas constant, T_x is freezing point of specie x (^oK), mw_x is molecular weight of specie x, m_y is molality of specie y in the specie x and ΔH_{fusx} is heat of fusion of specie x. The freezing point of the two quaternary ammonium bromides would decrease when they are mixed together. Later research thus focused on mixtures of quaternary ammonium bromides for binding bromine in the Zn/Br battery.

2.6.5 Selection of QBr for zinc bromine flow cell

2.6.5.1 Electrolyte conductivity

Cathro et al. [103] measured the conductivity of $ZnBr_2$ electrolyte that contained a single compound of MEM or MEP. The electrolyte resistivity is shown (Table 2.14) to increase gradually with increasing state of charge. The addition of QBr has increased the electrolyte resistivity (Table 2.14) in 3 M $ZnBr_2$ electrolytes, while the addition of 1 M MEP causes the electrolyte to have a higher resistively than that for electrolyte with added 1 M MEM.

Table 2.14 Diffusion coefficient of bromine (0.01 M Br_2) and electrolyte resistivity in 3 M $ZnBr_2$ contained single QBr (MEM or MEP) at 25°C [36, 103]

SOC	Diffusion Coefficient of bromine (10^{-9} m^2s^{-1})				Electrolyte Resistivity (Ohm cm)			
	No QBr	MEM	MEP	MOD*	No QBr	MEM	MEP	MOD*
Fully charged	1.23	0.95	1.00	0.93	9.3	9.8	11.4	9.7
Half charged	1.06	0.59	0.61	0.5	8.7	11.2	12.1	12.0
Fully discharged	0.77	0.35	0.38	0.33	9.9	15.9	16.5	15.8
*MOD = modified electrolyte 0.5 M MEM + 0.25 M MEP + 0.15 M DEMP + 0.1 M TBA Where DEMP: Diethylmethylpropyl ammonium bromide TBA: Tetrabuthyl ammonium bromide								

2.6.5.2 Bromine diffusion coefficient

Cathro et al. [103] determined the diffusion coefficient of bromine with a rotating disc electrode in $ZnBr_2$ electrolytes containing a single QBr compound of MEM or MEP. As the electrolyte composition is dependent on the state of charge of the zinc bromine flow cell (Table 2.15), samples were prepared accordingly. From this study it was shown that the addition of QBr reduces the diffusion coefficient of bromine slightly (Table 2.14), where both MEM and MEP addition had similar effect.

Table 2.15 Electrolyte compositions in zinc bromine flow cell at different states of charge [103]

State of Charge (SOC)	$ZnBr_2$ (M)	QBr (M)
Fully charged	1	0.3
Half charged	2	0.65
Fully discharged	3	1

2.6.5.3 Stability tests

Cathro et al. [104] studied several single and binary mixtures of quaternary ammonium bromides for use in the $ZnBr_2$ flow cell. Observations of the polybromide and aqueous phase between 0 – 50 °C were reported. To simulate the electrolyte at three different

SOC, 25 ml samples contain 1 – 3 M $ZnBr_2$, 0.3 – 1 M QBr mixture were prepared then 0.5 – 2.5 ml of liquid bromine was added to each sample. The 1 M QBr solution was either a single compound or a binary mixture of asymmetrical cyclic ammonium bromide (MEM, MEP) and asymmetrical aliphatic ammonium bromide (2MEP, 2M2E). After the addition of liquid bromine, each sample was shaken and allowed to stand until the two phases are separated. Samples that formed a solid phase were eliminated from possible use in a zinc bromine flow cell. As mentioned in the previous section (section 2.6.4) both single QBr compounds (either MEM or MEP) would form a solid phase. This study showed the distinct effect of MEP addition to the $ZnBr_2$ electrolyte that formed white crystals in the aqueous phase and determined the compound has the formula $ZnBr_2$2QBr. The addition of 1 M MEM to $ZnBr_2$ mainly caused the formation of a solid polybromide phase with bromine concentrations less than 1 M at 0^oC. The solid polybromide phase depleted at higher bromine concentrations or at elevated temperature (50^oC). This study also stated that a QBr mixture (1:1 mole ratio) of MEP/2MEP has the lowest aqueous phase bromine concentration, whereas electrolytes containing a mixture of MEM/MEP had a higher aqueous bromine concentration. The performance of the two QBr mixtures was tested and these are further described later (section 2.6.5.4)

In a later study of Cathro [35], 1 M QBr was incorporated into a propionitrile (PN) /bromine mixture in the positive electrolyte. This is different from the study by Singh et al. [40] which only investigated bromine / PN mixtures. This study showed the addition of QBr in PN electrolytes will further reduce the bromine concentration in the aqueous phase (Table 2.16). In agreement with the previous study, 2MEP showed higher aqueous bromine reduction ability than MEM and MEP. Also the coulombic efficiency

has improved to 92.3% by the addition of 2MEP to PN in a cell using a Daramic® separator sandwiched between two layers of filter paper.

Table 2.16 Aqueous bromine concentration in $ZnBr_2$ with QBr and PN [35, 101]

	2 M $ZnBr_2$ 1.5 M Br_2 [101]		**1.5 M $ZnBr_2$ 1.25 M Br_2 with PN [35]**	
1 M QBr	25°C $[Br_2]aq$	50°C $[Br_2]aq$	25°C $[Br_2]aq$	50°C $[Br_2]aq$
2MEP	0.037	0.057	0.014	0.026
MEM	0.080	0.136	0.031	0.060
MEP	0.037	0.066	0.017	0.035
(1:1) MEM:MEP	0.07	0.109	--	--
MOD* [36]	0.078	0.137	--	--
* MOD – modified electrolyte with mixtures of four QBr 0.5 M MEM + 0.25 M MEP + 0.15 M 2EMP + 0.1 M TBA				

Cedzynska [104] reported the use of symmetrical quaternary ammonium bromides to reduce aqueous bromine concentration. By testing electrolytes with 2 M $ZnBr_2$ and 0.1 M Br_2, the addition of 0.1 M TBA showed the formation of an oily polybromide phase where the aqueous bromine concentration was measured to be 0.061 M. In comparison with MEM and MEP, TBA seemed to have a lower ability of reduce dissolved bromine in the aqueous phase (Table 2.16). The diffusion coefficient of bromine was found to be 0.95×10^{-9} m^2s^{-1} for a sample containing 2 M $ZnBr_2$, 0.01 M Br_2 and 0.1 M TBA. This is higher than the diffusion coefficient of bromine in MEM and MEP reported by Cartho et al. [103] mentioned earlier (Table 2.14). This study thus concluded that the use of TBA did not slow down bromine diffusion and indicated a low tendency to complex with bromine. According to the equation developed with which diffusion coefficient was assumed to be proportional to the rate of bromine transport, the self discharge rate could be determined for a known electrolyte composition, as follows (2.52) [104].

$$\frac{I}{C} = \frac{aFD}{d} \qquad (2.52)$$

Where

I = the determined bromine transport rate expressed as currents (Amp)

C = measured bromine concentration in the aqueous phase of the positive half cell

a = no. of electron involved (2 for Br_2)

F = Faraday constant

D = diffusion coefficient for Br_2 in electrolyte

d = equivalent thickness of the separator

(Where d is calculated from, d = (tortuosity factor)^2 (separator thickness)/ (porosity))

Table 2.17 Kinematic viscosity of $ZnBr_2$ with MEM, TBA [103, 104]

	Kinematic viscosity (10^{-6} m^2s^{-1})		
SOC (electrolyte concentrations)	No QBr	QBr = MEM	QBr = TBA
Fully charged (1 M $ZnBr_2$ 0.3 M QBr)	1.040	1.122	1.055
Half charged (2 M $ZnBr_2$ 0.65M QBr)	1.165	1.460	1.198

The use of TBA will thus result in a higher rate of bromine transport than the use of MEM or MEP, but due to the low kinematic viscosity of TBA in comparison with MEM (Table 2.17), it could be used in mixtures of QBr.

In another study by Cedzynska [36] a mixture of four different QBr was shown to allow the $ZnBr_2$ battery to operate in the temperature range from 5 – 50^{o}C. This study shows that the addition of aliphatic ammonium bromides (2MEP, 2EMP) will reduce aqueous bromine more than MEM, which agrees with Cathro [101]. Binary mixtures containing symmetrical ammonium bromides also proved to form solid polybromide phase within that temperature range. Although symmetrical QBr seemed not to be suitable, it improved electrolyte parameters such as low kinematic viscosity. These could therefore be used in a modified electrolyte at a low concentration (< 0.3 M) where no solid polybromide would form. The modified electrolyte (MOD) contained a mixture of 0.5

M MEM, 0.25 M MEP, 0.15 M 2EMP and 0.1 M TBA in the fully charged stage. Comparing electrolyte resistivity at 25^{o}C, MOD was found to be 15.8 ohm·cm, which is slightly higher than that for electrolytes containing MEM and MEP (Table 2.14). The diffusion coefficient of bromine in the MOD electrolyte was much lower than MEM or MEP alone. In terms of aqueous bromine reduction, bromine diffusion coefficient and electrolyte resistance, the MOD electrolyte was shown to be suitable for use in the $ZnBr_2$ flow cell between 5^{o}C and 50^{o}C. This is even better than the widely used 0.5 M MEM and 0.5 M MEP mixture.

2.6.5.4 Cycling Cell Performance with single and mixed QBr

Cathro and co-workers [101] studied the performance of the zinc bromine flow cell that utilised electrolytes with single or mixed quaternary ammonium bromides (Table 2.18) .

Table 2.18 $ZnBr_2$ single flow cell performance test with 2 M $ZnBr_2$ and Sandwich separator [101]

	2 M $ZnBr_2$			**2 M $ZnBr_2$ 3 M KCl**		
1 M QBr	Coulombic Eff (%)	Voltaic Eff (%)	Energy Eff (%)	Coulombic Eff (%)	Voltaic Eff (%)	Energy Eff (%)
MEM	93.6	81.1	75.9	93.9	88.1	82.7
MEP	94.6	81.0	76.6	95.5	88.4	84.4
(1: 1) MEM:MEP	93.4	80.2	74.9	94.7	87.9	83.3
(1:1) MEP:2MEP	95.3	78.1	74.4	96.2	87.4	84.1

Experiments were undergone in a single cell setup using an electrode with working area of 16 cm^2 and a microporous polyethylene separator. Platinum on a titanium substrate was used as the negative electrode, a titanium sheet being the positive electrode. For electrolyte contained MEP, the cell provide an energy efficiency of 76.6% where the

aqueous bromine concentration were 0.041 M, while an addition of 3 M KCl has reduced the electrolyte resistance and improved the energy efficiency to 84.4%.

2.6.5.5 Summary of QBr selection in zinc bromine flow cell

With the gathered information, it can be seen that the use of a single QBr compound will either form a solid polybromide phase with bromine or white crystals with $ZnBr_2$ electrolytes. Later research thus focused on mixtures of QBr. Among the three major types of QBr, asymmetrical quaternary ammonium bromide was the most effective in terms of aqueous bromine reduction, followed by MEP and MEM. From the study of the diffusion coefficients of bromine in electrolytes containing cyclic QBr, bromine was found to be more diffusive in electrolytes containing MEP than those containing MEM. Electrolyte resistively was increased by the addition of MEP whereas MEM addition had a minor effect. Electrolytes of propionitrile in the positive half-cell that incorporated 2MEP further reduced aqueous bromine concentration. Later studies focused on QBr mixtures containing up to four different QBr. The use of MOD electrolyte produced showed further reduction in bromine transport without solid formation between 0^oC and 50^oC, however cell efficiency data was not available. Therefore, in terms of cell efficiency, a bindery mixture containing MEP and 2MEP proved to have the best performance for the $ZnBr_2$ flow cell

In this thesis three QBr were selected for study, two from asymmetrical cyclic quaternary ammonium bromide group and one from the aliphatic ammonium bromide. These were N-ethyl-N-methyl morpholinium bromide, N-ethyl-N- methyl pyrrolidinium bromide and Tetra-butyl ammonium bromide, their structures being presented in Figure 2.8.

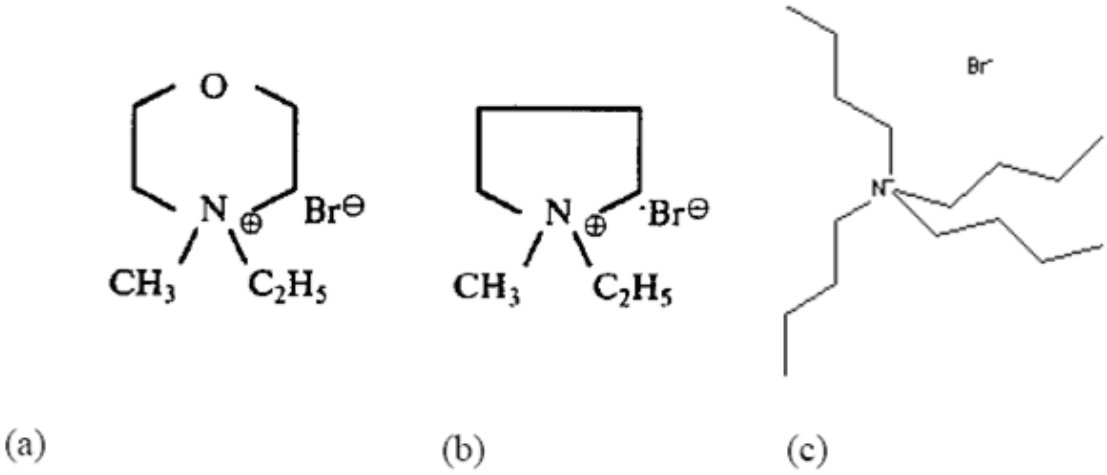

Figure 2.8 (a) N-ethyl-N-methyl-morpholinium bromide (MEM) $C_7H_{16}BrNO$ [105] (b) N-ethyl-N-methyl-pyrrolidinium bromide (MEP) $C_7H_{16}NBr$ [106] (c) Tetra-butyl ammonium bromide (TBA) $C_{16}H_{36}BrN$ [107]

2.7 Studies in Quaternary Ammonium bromides

2.7.1 Chemistry of bromine complexation

In early studies on the subject, focus was made on the chemistry and physical properties of quaternary ammonium bromide (QBr) solutions after bromine addition [55, 101]. Eustace [55] suggested that when aqueous bromine is dissolved in bromide ion rich solution, they are in equilibrium with polybromide complexes Br_n^- where n = 3, 5, 7 etc, which is by reactions (2.53) and (2.54). For these reactions the equilibrium constants obtained by Scaife and Tyrrel [108] were $K_1 = 16\ M^{-1}$ and $K_2 = 25.3\ M^{-2}$. Eustace [55] was the only group that suggested the formation of more complex polybromide ions represented by (2.55), however the equilibrium constant was not determined.

$$Br_2 + Br^- \underset{\longleftarrow}{\xrightarrow{K_1}} Br_3^- \qquad (2.53)$$

$$Br_3^- + Br_2 \underset{\longleftarrow}{\xrightarrow{K_2}} Br_5^- \qquad (2.54)$$

$$Br_5^- + Br_2 \rightleftharpoons Br_7^- \qquad (2.55)$$

Eustace [55] also suggested there is anion radical exchange between dissolved QBr and polybromide ions in the aqueous phase, which can be described by reaction (2.56). On the other hand the oily second phase that formed was described by reactions (2.57) and (2.58). In later works as described by Bolstad et al [25] the reaction between bromine and QBr was generalised in the form as described by reaction (2.59). Both groups state that each QBr typically complexes up to 3 molecules of bromine. The addition of quaternary ammonium bromides to bromine solution would reduce the aqueous bromine concentration by binding free bromine to form a separate dense bromine rich organic phase. As a result the evolution of bromine vapour is reduced. Bauer et al [109, 110] later found that MEP^+ in the aqueous phase incorporated into the bromine rich organic phase more rapidly than MEM^+. In another study Bauer et al [109] also found that MEP^+ and Br_5^- were the main species in the organic phase of a typical zinc bromine electrolyte during cell charging.

$$Q^+Br^- + Br_7^- \rightleftharpoons Q^+Br_7^- + Br^- \qquad (2.56)$$

$$Q^+Br_3^- + Br_2 \rightleftharpoons Q^+Br_5^- \qquad (2.57)$$

$$Q^+Br_5^- + Br_2 \rightleftharpoons Q^+Br_7^- \qquad (2.58)$$

$$Q^+Br^- + nBr_2 \rightleftharpoons Q^+(Br_2)_nBr^- \qquad (2.59)$$

Suggested by Eustace [55], bromine is partitioned between the aqueous and the bromine rich organic phase, which can be expressed by the distribution coefficient Equation (2.60). The bromine distribution coefficient is highly affected by the bromide concentration as it has a major influence on the aqueous phase equilibrium.

$$Distribution \quad coefficient = \frac{[Br_2]_{Br_2-rich}}{[Br_2]_{aqueous}} \tag{2.60}$$

Walsh et al. [102] studied several symmetrical aliphatic QBr, they discovered that the QBr halogen complex would either be amorphous or form solids when the aliphatic QBr has a symmetry number lower than 3. They also observed that the decrease in QBr symmetry number lowered the freezing point of the QBr halogen complex solutions.

In all ceases, the addition of the quaternary ammonium bromide would bind with a large amount of dissolved bromine, the resultant electrolyte will contain a low equilibrium aqueous bromine concentration [111]. Bajpal et al. [112] reported that the addition of quaternary ammonium bromides can reduce bromine vapour by almost 100 fold. The measured bromine vapour pressure for aqueous bromine and after the addition of quaternary ammonium salts decrease in the following order: bromine > Tetramethylammonium bromide > triocylmethylammonium chloride > N-ethyl N-methyl-morpholinium bromide. It can be deduced that, the reduction of bromine vapour pressure by the addition of an aliphatic ammonium halide would be less effective than the addition of a cyclic quaternary ammonium halide.

The use of bromine complexing agents to reduce bromine vapour emissions has been extensively studied in relation to the zinc-bromine battery. Early studies in this area are detailed in the previous section (2.6)

2.7.2 Electrode mechanism of bromide, bromine and QBr

Kautek et. al [113, 114] studied the mechanism of the reaction between bromine and QBr in a solution containing 3 M $ZnBr_2$, 0.5 M MEM and 0.5 M MEP solution with gold and glassy carbon electrodes using *In Situ* FTIR and cyclic voltammetry. Adsorption of MEM-Br was found to be much stronger than for MEM-Br_n on both gold and glassy carbon electrodes [113, 114]. Bauer et al. [109] reported a Raman spectroscopic study of bromine complex. They showed that the reaction mechanism of bromine, bromide and MEP^+ proceeds as a heterogeneous electron transfer from Br^-, followed by a rapid homogenous reaction of dissolved MEP^+ that leads to the formation MEP-Br_n. This can be described by reaction (2.61) and (2.62). On the other hand the heterogenous reaction of adsorbed MEM-Br_{ad} ion pair only plays a minor role (2.63).

$$3Br^- \longrightarrow Br_3^- + e^- \tag{2.61}$$

$$MEP_{aq}^{\ +} + Br_2 + Br^- \longrightarrow MEP\cdots Br_{3naq} \tag{2.62}$$

$$MEM\cdots Br_{ad} + 2Br^- \longrightarrow MEM\cdots Br_{3naq} + 2e^- \tag{2.63}$$

Chapter 3 Theoretical Background

3.1 Redox Flow Cell

3.1.1 Specific Energy

The theoretical specific energy (W_e^{th}, Wh kg^{-1}) of a cell is commonly used as the parameter to compare the theoretical maximum energy a cell can deliver with different redox systems. This can be found by dividing Gibbs energy with the mass of the reactants [6]. In general, the practical specific energy is less than 35% of the theoretical value since the solvent, pumps, electrodes and cell component all add weight without contributing to the delivered energy of the system. Despite the fact that weight is not the major concern of a flow cell system, theoretical specific energy is often used to compare between different flow cell systems. Some researchers may choose to report the theoretical energy density ($W_{denisty}^{th}$, Wh L^{-1}) [24, 53].

3.1.2 Open circuit potential (OCP)

The theoretical open circuit potential OCP is also referred to as the reversible cell potential ΔE (V) [115]. This can be estimated from the standard reduction potential of each half cell reaction.

3.1.3 Flow Cell Charge / Discharge cycle

In order to test the performance of a flow cell the most common technique is to monitor the cell voltage with time when the cell is charged and discharged at a constant current. A typical charge / discharge response (Figure 3.1) would have an increasing cell voltage during the charging stage and a gradual decrease when the cell discharges.

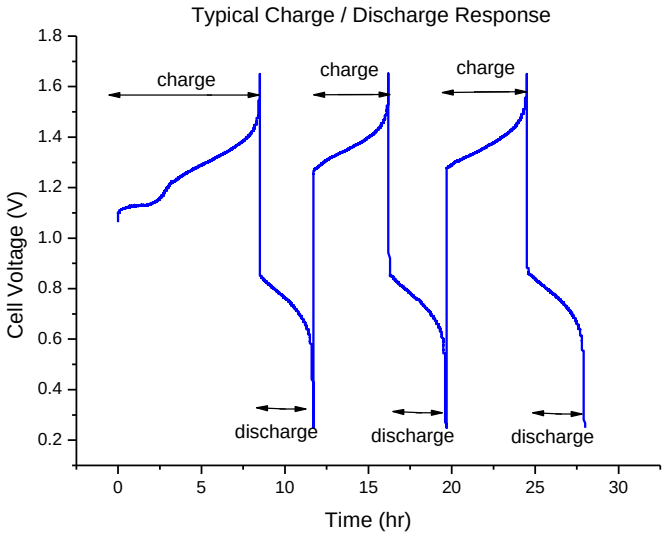

Figure 3.1 Typical charge/discharge responses of 2 M V/Br flow cell

3.1.4 Flow Cell Performance

The three commonly used performance measures of a flow cell that are obtained from the resultant charge-discharge response are coulombic, voltaic and energy efficiency. Coulombic efficiency also known as the Amp-hour efficiency is a ratio of the discharge to charge capacity of the cell. Theoretical capacity or electrical charge (Q_T) can be calculated from Faraday's Law, therefore in theory Q_T is the product of the cell charging current (I, Amps) and the theoretical discharging time ($t_{T,}$ seconds).

Experimentally, the capacity of a cell would be lower than theoretical value which is calculated as an integral of charge or discharge current (I, Amps or Cs^{-1}) with time. After the charge and discharge capacity (Ahr) are calculated separately, the coulombic efficiency (%) can be found.

The theoretical available energy ($Energy_T$, J) is calculated by multiplying the electrical charge (Q_T, C) and cell potential (E_{cell}, V or JC^{-1}). Energy is normally recorded in a more common unit, Watt-hours (Wh) which can be converted from Joules (J) with the knowledge of 1Wh = 3600J, while the practical available energy found experimentally, is an integration of the product of cell potential (V, JC^{-1}) and the current (I, Cs^{-1}) with time. After the calculation of charge and discharge practical available energy, the energy efficiency (sometimes known as total efficiency) of the cell can be found.

For an experimental setup with constant charge and discharge current, energy efficiency calculation would be slightly different from the above description.

Since the energy efficiency is also a product of coulombic and voltaic efficiency, where the voltaic efficiency (η_V) can then be found.

Alternately, voltaic efficiency can be estimated as the ratio between discharge and charge voltage at 50% state of charge (50% SOC) from the voltage response curve obtained experimentally.

3.2 Electrochemical Studies of redox species

When studying electrode kinetics, electroanalytical techniques such as cyclic voltammetry and linear voltammetry are commonly used. These techniques are relative

easy and fast they often used for the selection of suitable redox couples and electrode materials.

3.2.1 Cyclic Voltammetry

Cyclic voltammetry has become the most frequently used technique in preliminary electrochemical studies of new redox system, as it can obtain information from complex electrode reactions [116, 117]. The basic concept is to measure the faradic current that passes through the electrochemical cell as a function of the applied potential [118]. The applied potential at the working electrode changes linearly with time (Figure 3.2) in the forward direction and sweeps backward when it reaches the switching potential (point C and E) [119] . From the literature [46, 79, 80] , properties such as diffusion coefficient and kinetic rate constant can be derived from the cyclic voltammograms at various scan rates.

Cyclic voltammetry experiments normally start at the open circuit voltage (A), where no potential is applied and hence no reaction is taking place. In the forward scan the potential is moved toward the negative direction (B) which causes the reduction to occur. When it reaches the switching potential (C) the scan direction is reversed (as to point E). The resulting voltammogram is a measure of current as a function of potential (Figure 3.3). The time span of the reaction is controlled by the scan rate (ν) because it is the rate of change in potential with time $E(t) = Ei - \nu t$

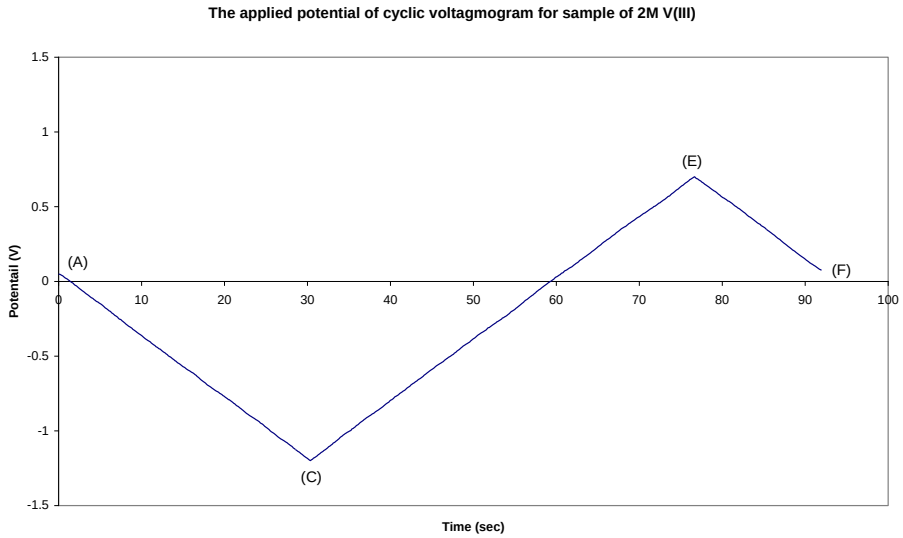

Figure 3.2 Variation of applied potential to the working electrode with time

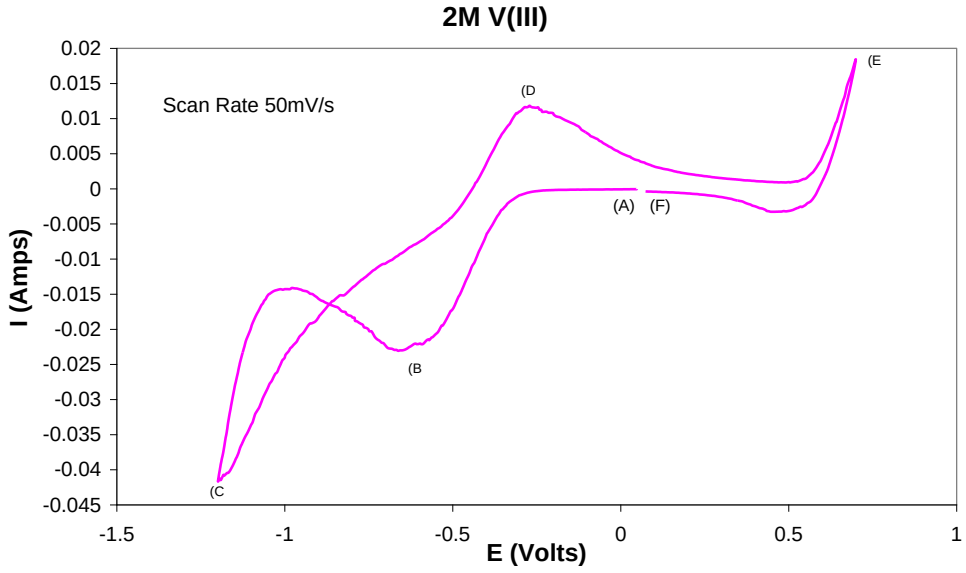

Figure 3.3 Corresponding cyclic voltammogram

3.2.2 Stirred solution with linear sweep voltammetry

Linear sweep voltammetry is similar to the cyclic voltammetry, with potential changed linearly with time but only in one direction and at a very low scan rate. In a stirred solution the effect of mass transfer would be eliminated or reduced to a minimal.

Kinetic properties of the electrochemical cell can be found from a Tafel plot (See section 3.2.3) in the activation controlled region.

3.2.3 Electrochemical Properties determined from cyclic voltammetry

3.2.3.1 Reversible Reactions

For reversible reactions in the form O + ne ⇔ R it is possible to use peak current data from cyclic voltammetry to calculate diffusion coefficient. As peak current is dependent on testing solution temperature, the equation can be reformulated accordingly.

3.2.3.2 Irreversible reactions

Irreversible reactions can be identified by a peak potential separation (ΔE_p) in the cyclic voltammogram, which would be greater than the calculated value for a reversible system (ie $\Delta Ep > 0.056/n$ at 25^oC). For irreversible reactions, the following Equation (3.1) is used to determine the diffusion coefficient [116].

$$i_p = 0.4958nFAD^{1/2}C^o\upsilon^{1/2}\left(\frac{\alpha n_a F}{RT}\right)^{1/2} \qquad (3.1)$$

By plotting peak current against square root of scan rate, a straight line would result that has a slope proportional to the diffusion coefficient. The rate constant is related to the peak current and the peak potentials. A plot of $\ln(i_p)$ against $(E_p - E^{o'})$ at different scan rates, should have an intercept proportional k^o with a slope of $-\alpha f$.

Although the peak current calculation depends on temperature, the intercept of the $\ln(i_p)$ vs $(E_p - E^{o'})$ is independent of temperature. Therefore, this equation can be used to calculate the reaction rate constant (k^o) at any particular temperature.

3.3 Electrochemical properties obtained from linear sweep voltammetry

According to the Butler-Volmer Equation, the net current density consists of an anodic and cathodic component [116]. A linear relationship between current density and overpotential would hold in regions of low over potential ($\eta < 100$ mV), while at high overpotentials ($\eta > 100$ mV), there is an exponential relationship between current density and overpotential. With cathodic polarisation, at large overpotential the Butler-Volmer Equation would become the Tafel Equation.

A Tafel plot is a graph of ln(i) against overpotential (η), with linearity at large overpotentials. From the linear region of this graph (Figure 3.4), the equilibrium exchange current density (i_o) can be obtained from the intercept, while the symmetry factor (β) can be found from the slope.

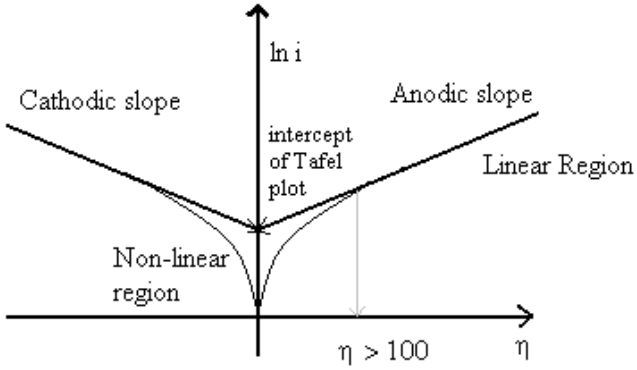

Figure 3.4 A typical Tafel Plot

3.4 EIS Theory

Electrochemical impedance is determined from the respond current through the electrochemical cell when an AC potential is applied to a 3-electrodes cell. When a sinusoidal potential excitation (3.2) is applied to the electrochemical cell, the respond is an AC current signal containing an excitation frequency and its harmonics illustrated by Equation 3.3. The impendence of the system is calculated according to Ohm's Law (3.4). The impendence is more commonly expressed as a complex function as illustrated in Equation (3.5).

$$E(t) = E_o \cos(\omega t) \tag{3.2}$$

$$I(t) = I_o \cos(\omega t - \phi) \tag{3.3}$$

$$Z = \frac{E(t)}{I(t)} = \frac{E_o \cos(\omega t)}{I_o \cos(\omega t - \phi)} = Z_o \frac{\cos(\omega t)}{\cos(\omega t - \phi)} \tag{3.4}$$

$$Z = \frac{E}{I} = Z_o \exp(j\phi) = Z_o(\cos\phi + j\sin\phi) \tag{3.5}$$

As seen above, the expression of impendence (Z) consists of a real and an imaginary part. By plotting the imaginary part against the real part on an XY graph would result the commonly known Nyquist plot (Figure 3.5). The semicircle in Figure 3.5 (a) is the characteristic of a Randles equivalent circuit represented by Figure 3.5 (c) which indicates the system to be kinetic controlled. Another common presentation is the Bode plot, which both the impedance (log|Z|) and the phase shift (Φ) is plotted against the log of frequency (log(ω)) in two separate graphs shown in Figure 3.5(b). For mixed kinetic and charge transfer controlled systems, the equivalent circuit, Nyquist plot and the Bode

plot are slightly different with an additional Warburg element representing the diffusion controlled (Figure 3.6). However in both cases the Ohmic solution resistance (R_e) is found where the Nyquist curve intersects with the real axes.

In practice the current respond of a potentiostated electrochemical cell is non-linear. Therefore, in order to ensure the cell response to be in pseudo-linearity, AC excitation signal is usually small (1 to 10 mV). Also the electrochemical system has to be in steady state throughout the measuring process of the EIS spectrum.

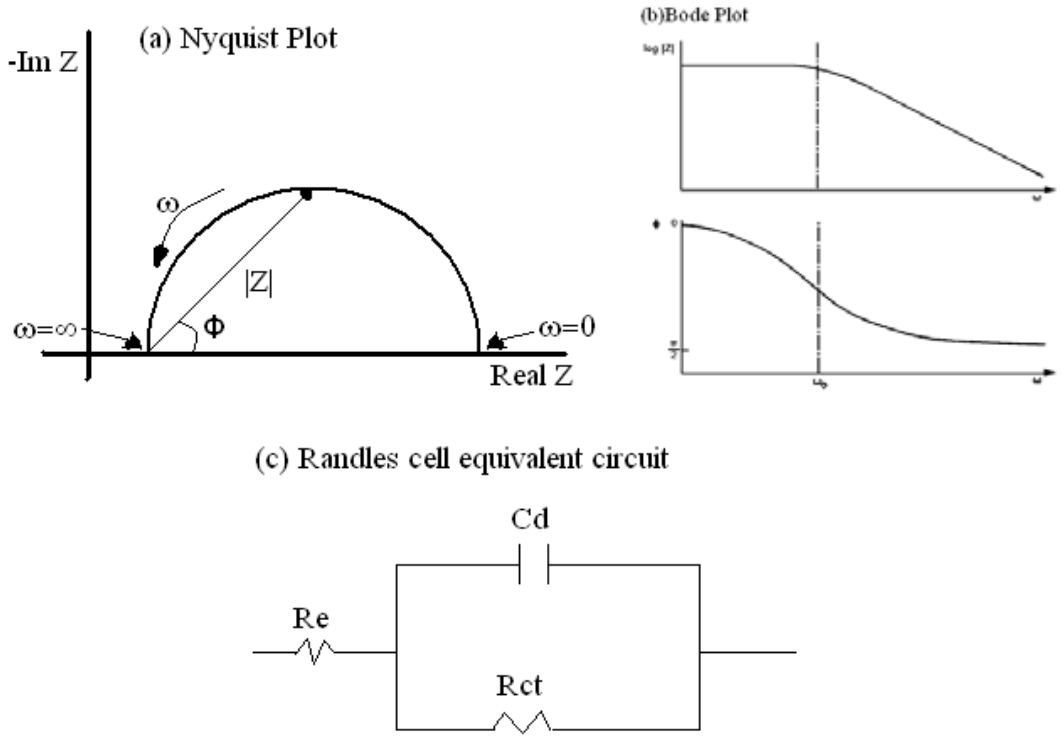

Figure 3.5 Impedance spectrums for kinetic controlled system (a) Nyquist Plot (b) Bode Plot (c) Equivalent circuit

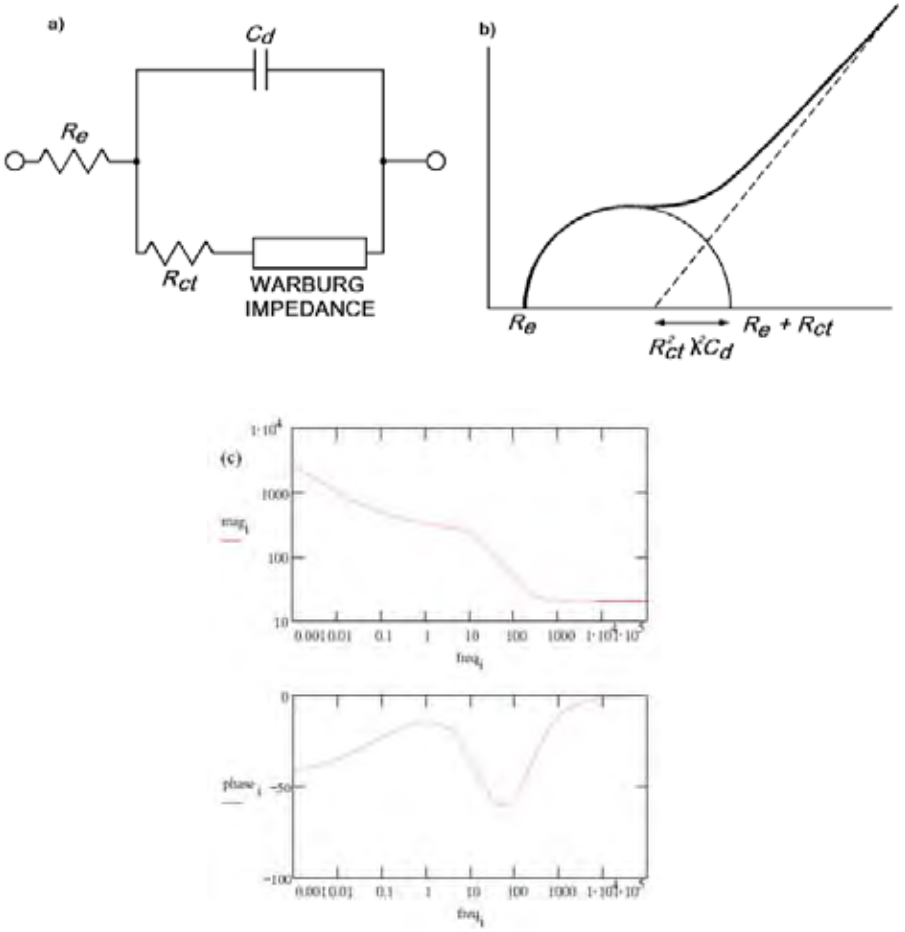

Figure 3.6 (a) an equivalent circuit with mixed kinetic and charge transfer control R_e = Ohmic solution resistance, R_{ct} = charge transfer resistance, Warburg impedance = Warburg resistance or mass transfer resistance, C_d = Double layer capacitance (b) Nyquist diagram for mixed control circuit (c) Bode Plot for system with mixed kinetic and charge transfer control [120, 121]

3.4.1 Impedance measurements for membrane resistance

Although the membrane resistance was also determined by EIS, the experimental setup would be slightly different from the 3-electrodes cell. Membrane would be clamped between two plates connected to an electrode at each side where the electrolytes of interest would be filled between the gap. Membrane resistance is equal to the difference in cell resistance with and without a membrane in place [122].

Chapter 4 Experimental Method

4.0 Overview

This chapter summarises the experimental procedures for stability tests, cyclic voltammetry and the lab scale vanadium bromide testing cell used to evaluate the charge-discharge behaviour of the complexed electrolytes and membranes.

4.1 Chemicals and Equipments

4.1.1 Chemicals

Vanadium Trioxides V_2O_3 (s) (Mitsubishi Chemical Corporation, Japan)

Vanadium Trioxides V_2O_3 (s) (Stratcor, Pittsburgh, Pennsylvania)

Vanadium Pentaoxides V_2O_5 (s) (Mitsubishi Chemical Corporation, Japan)

48% Hydrobromic Acid HBr, 8.84 M (Univar, USA)

32% Hydrocholric Acid HCl, 10.44 M (Ajax –APS, Australia)

40-70% N-ethyl-N-methylmorpholiniumbromide (MEM) $C_7H_{16}BrNO$ (aq), (Dead Sea Bromine Group (DSBG) Beer-Sheva, Israel)

40 – 70% N-ethyl-N-methylpyrrolidiniumbromide (MEP) $C_7H_{16}NBr$ (aq), (Dead Sea Bromine Group (DSBG) Beer-Sheva, Israel)

Tetra-butyl ammonium bromide (TBA) $C_{16}H_{36}BrN$ (s) (Sigma-Aldrich, Australia)

Liquid Bromine Br_2 (Ajax –APS, Australia)

All Clear® Co-polymer sealer, (Selley, Australia)

4.1.2 Materials for working electrode preparations

Silver loaded epoxy adhesive (RS components, Australia)

Silver loaded epoxy hardener (RS components, Australia)

Araldite® F Resin, Thixotropic paste (Huntsman, Queensland, Australia)

Araldite® HY 905 Hardener, Thixotropic paste (Huntsman, Queensland, Australia)

Graphite rod, Graphite disc

4.1.3 Equipments

1287A Potentiostat, (Solartron Analytical, England)

1255B Frequency Response Analyzer (Solartron Analytical, England)

Corrware® and CView® 2.8 (softwares for CV) (Solartron Analytical, England)

Zplots and ZView (softwares for EIS) (Solartron Analytical, England)

Saturated calomel electrode (SCE)

Magnetic stirrer and magnet bar

Battery testing unit (RePower, China)

Cell Test V2.5 (software) (RePower, China)

Connection cables with four alligator clips (RePower, China)

MD-10 Magnetic drive pumps (Tokyo Iwaki Co. Ltd., Japan)

3057 Yokogawa Portable Recorder (Yokogawa Electric Co., Japan)

KB53Temperature Incubator (Binder, Germany)

4.2 Electrolytes preparation for stability test observations

During normal operations of a vanadium bromide flow cell, bromine vapour is detected. In order to reduce the amount of bromine emission, this project proposes to use a mixture of quaternary ammonium bromides as bromine complexing agents as previously studied in the zinc bromine flow cell [29, 36, 55]. Three types of quaternary

ammonium bromide (QBr) namely, MEM, MEP and TBA were evaluated over a wide range of concentration ratios.

4.2.1 Batch vanadium solutions

Pure V_2O_3 (Stratcor) normally stored in a glove box to ensure minimal air oxidation was used for stability and voltametric studies of V(III) samples. 2.5 M V(III) solutions were prepared by dissolving 187.3g of V_2O_3 in 1 L of 7.6 M HBr and 1.46 M HCl solutions. While V(IV) was prepared by dissolving equal molar of V_2O_3 (Mitsubishi Chemicals) and V_2O_5 (Mitsubishi Chemicals) in 1 L of 7.6 M HBr and 1.46 M HCl solutions. For 2.76 M V(IV) solutions, 103.4g of V_2O_3 and 125.5g of V_2O_5 was used.

For flow cell and static cell cycling experiments, electrolytes contained 50: 50 molar ratios of V(III) : V(IV) ions referred to $V^{3.5+}$ here after. This was prepared by dissolving V_2O_3 (Mitsubishi Chemicals) and V_2O_5 (Mitsubishi Chemicals) in 3:1 mole ratio. For 2.5 M $V^{3.5+}$ solution 140.5 g V_2O_3 and 56.8 g V_2O_5 are dissolved in 1 L of 7.6 M HBr and 1.46 M HCl solutions. However, it was later found that 26% of the V_2O_3 (Mitsubishi) had been oxidised to V(IV) (ie V_2O_3 powder contained 26% V(IV)) . This was determined by dissolving 0.1 M V_2O_3 in 5 M H_2SO_4 and titrating against 0.02 M potassium permanganate. The electrolyte used for all flow cell and static cell testing in this study thus contained 30 : 70 ratio of V(III) and V(IV) and is later referred as $V^{3.7+}$.

4.2.2 Simulated positive electrolyte

V(IV) solutions containing single, binary or ternary QBr were prepared by adding different amounts of QBr to the measured volumes of 2.5 M or 2.76 M V(IV) solutions. This was followed by adding a measured volume of HBr and HCl mixture and finally

liquid Br_2 was added. Solutions were measured with pipettes and placed in 25 ml glass tubes that are later sealed with electric tapes to prevent bromine evaporation. After each glass tubes were sealed, each sample was shaken for 15 seconds. Two different total QBr concentrations 0.75 M and 1 M were of interest and samples were prepared by varying the molar ratio of MEM, MEP and TBA.

Table 4.1 Some examples of samples prepared for simulated positive electrolytes

Sample Content	Volume (ml) / Mass (gram)						
	2.5 M V(IV)	**2.76 M V(IV)**	**Br_2**	**MEM**	**MEP**	**TBA (gm)**	**7.6 M HBr + 1.46 M HCl**
2 M V(IV) + 1 M MEM + 1 M Br_2	0.0	5.0	0.4	1.6	0.0	0.0	0.0
1.96 M V(IV) + 0.54 M MEM + 0.44 M MEP + 1.11 M Br_2	0.0	5.0	0.4	0.9	0.8	0.0	0.0
1.94 M V(IV) + 0.38 M MEM 0.17 M MEP + 0.18 M TBA + 1.05M Br_2	7.2	0.0	0.5	0.8	0.4	0.6	0.4
2.03 M V(IV) + 1.16 M MEM	0	10.0	0.0	3.6	0.0	0.0	0.0
1.95 M V(IV) + 0.54 M MEM + 0.45 M MEP	0.0	10.0	0.0	1.8	1.6	0.0	0.7

It is important to note that MEM and MEP are in aqueous form, for each gram of aqueous MEP or MEM only contained 0.643 g of MEP and 0.738 g of MEM, where the balancing is comprised of water (see Appendix B for full calculations). Samples of V(IV) containing single and binary QBr in the absence of bromine were also prepared. Table 4.1 lists some examples of the V(IV) solutions prepared. A detailed summary of all V(IV) samples prepared are given in Table B.1,Table B.2 and Table B.3 in the appendix.

4.2.3 Simulated negative electrolyte

For V(III) solutions, only binary QBr mixtures were of interest. Samples were prepared in the same way as the V(IV) solutions. Table 4.2 shows some examples of V(III) solutions prepared, while a detailed summary of all V(III) solutions prepared is given in Table B.5 in Appendix B.

Table 4.2 Examples of simulated negative electrolytes

Sample content	Volume (ml)					
	2.5 M V(III)	**Br_2**	**MEM**	**MEP**	**7.6 M HBr + 1.46 M HCl**	**H_2O**
2 M V(III) + 0.19 M Br_2	16	0.2	0.0	0.0	0.0	3.8
2 M V(III) + 0.37 M MEM + 0.38 M MEP	16	0.0	1.7	1.9	0.4	0.0
2 M V(III) + 0.19 M Br_2 + 0.37 M MEM + 0.38 M MEP	16	0.2	1.7	1.9	0.2	0.0

4.2.4 Bromine with ternary QBr solutions

Besides the simulated positive and negative V/Br electrolytes, several samples were prepared without vanadium. Ternary QBr mixture was first dissolved in HBr and HCl solution, followed by bromine addition. Ternary QBr mixture with final concentration of 1 M and 0.75 M were prepared (Table 4.3). Detailed summary of samples contained bromine and ternary QBr is given in the Appendix (Table B.4)

Table 4.3 Examples for bromine and ternary QBr solutions

Sample Content	**Br_2 (ml)**	**MEM (ml)**	**MEP (ml)**	**TBA (g)**	**7.6 M HBr + 1.46 M HCl (ml)**
6.2 M HBr + 1.2 M HCl + 0.36 M MEM + 0.17 M MEP + 0.18 M TBA + 1.04 M Br_2	0.50	0.80	0.40	0.55	7.60
5.6 M HBr + 1.1 M HCl + 0.43 M MEM + 0.41 M MEP + 0.2 M TBA + 1.02 M Br_2	0.50	1.00	1.00	0.60	7.00

4.2.5 Observation of physical stability by changing environment temperature

The physical appearance of each sample was observed daily for a period of 10 days between 11 – 40^{o}C. Sample solutions were first observed at 25^{o} C, then observations were made at 40^{o}C and finally at 11^{o}C for solutions containing 2 M V(III) or 2 M V(IV) with various MEM and MEP concentrations.

4.3 Cyclic Voltammetry Measurement

4.3.1 Preparation of working electrodes

The working electrode was made from a 6 mm graphite rod set in epoxy resin with an exposed surface area of 0.28 cm^{2}. In order to reduce resistance, the 20 mm length of graphite rod was attached to a stainless steel rod with silver epoxy (Figure 4.1). Silver adhesive and silver hardener paste mixed in one to one ratio was used to join the two rods. The silver paste was thoroughly mixed in a small watch glass prior applying to the silver rod. When the two rods were well attached, the assembly was oven dried at 100^{o}C for 15 min. The rod was allowed to cool down and then inserted in a PVC mould (D = 15 mm. Subsequently, a paste like mixture of epoxy resin and epoxy hardener (3:1 ratio) was poured into the PVC mould to cover the sides of graphite rod. Once the epoxy resin had dried, the PVC mould was removed. The surface was polished with 240 grit sand paper to remove the excess epoxy and expose the graphite surface. Finally, the electrode surface was polished with 1200 grit sand paper and washed with distilled water. For better results and reproducibility the final step was repeated each time a fresh solution was tested.

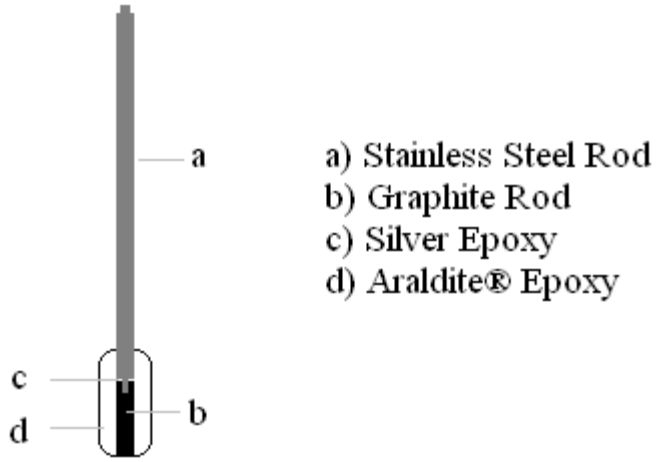

Figure 4.1 Cross-section of Working Electrode

4.3.2 Experimental Setup

A three electrode cell (Figure 4.2) was set up for both cyclic voltammetry and linear sweep voltammetry experiments. Firstly, 20 ml of test electrolyte was poured in the glass cell. The working electrode was positioned into one of the three holes in a PVC lid that tightly covered the glass cell. A 6 mm diameter 10 cm long carbon rod was used as the counter electrode, while the saturated calomel electrode (SCE) acted as a reference electrode for all voltammetry experiments in this thesis. A magnetic stirrer was used in linear sweep voltammetry experiment for measurement of Br^-/Br^{3-} kinetics in simulated positive half-cell samples.

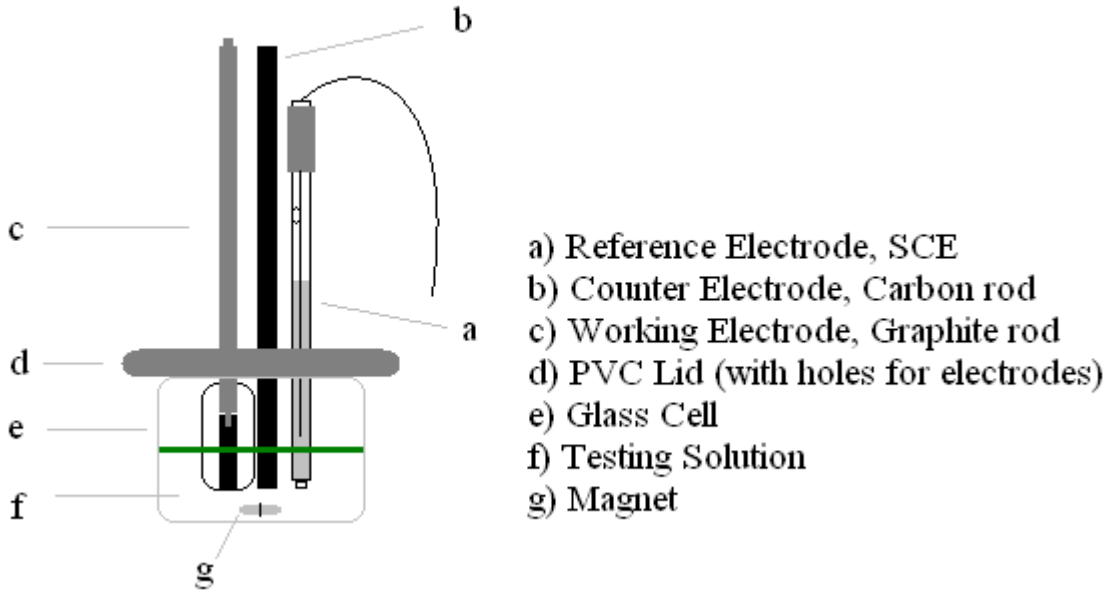

Figure 4.2 Three electrode cell for cyclic voltammetry and linear voltammetry

4.3.3 V(III) solution for cyclic voltammetry

Two series of samples were prepared for cyclic voltammetric measurements to monitor the effect of QBr addition in simulated negative half cell solutions. The first series had a fixed QBr concentration that only varied the ratio between MEM and MEP, while the second series had a fixed amount of one type of QBr whilst the other type was being varied. Samples of both series were made from 2.5 M V(III) batch solutions by dissolving pure V_2O_3 (Stratcor) as described in section 4.2.2.

Six samples of 2 M V(III) with a fixed concentration of 0.75 M QBr were prepare each with a different ratio of MEM to MEP. Supporting electrolyte was added to maintain the final concentration. As MEM and MEP is an aqueous solution with densities varying between 1.10 – 1.25 gcm^{-3}, MEM and MEP densities were measured in order to calculate the volume needed for each sample. The weight percent of MEM and MEP were found to be 73.8% and 64.3% respectively, a detailed calculation is presented in Appendix B. The volume needed to prepared the 2 M V(III) with 0.75 M QBr is

tabulated below (Table 4.4). A detailed lists of solutions prepared is provided in Appendix B.

Table 4.4 2 M V(III) 0.75 M QBr sample preparation for cyclic voltammetry

Sample Content	2.5 M V(III) (ml)	MEM (ml)	MEP (ml)	7.6 M HBr + 1.46 M HCl (ml)	H_2O (ml)
2 M V(III)	16.0	0.0	0.0	0.0	4
2 M V(III) + 1 M MEM	14	4.5	0.0	0.0	0
2 M V(III) + 1 M MEP	14	0	4.9	0.0	0
2 M V(III) + 0.20 M MEM + 0.56 M MEP	16.0	0.9	2.8	0.3	0
2 M V(III) + 0.57 M MEM + 0.18 M MEP	16.0	2.6	0.9	0.5	0

For samples in the second series MEM concentration was fixed while the MEP concentration was gradually increased and vice versa. In each case the vanadium concentration was maintained at 1.76 M V(III) (Table 4.5).

Table 4.5 1.76 M V(III) solutions with one fixed QBr concentration for cyclic voltammetry

Sample Content	2.2 M V(III) (ml)	MEM (ml)	MEP (ml)	7.6 M HBr + 1.46 M HCl (ml)
1.67 M V(III) + 0.15 M MEM + 0.47 M MEP	13.6	0.6	2.1	1.6
1.67 M V(III) + 0.15 M MEM + 0.65 M MEP	13.6	0.6	2.9	0.9
1.67 M V(III) + 0.15 M MEM + 0.83 M MEP	13.6	0.6	3.7	0
1.67 M V(III) + 0.49 M MEM + 0.16 M MEP	13.6	2.0	0.7	1.6
1.67 M V(III) + 0.66 M MEM + 0.16 M MEP	13.6	2.7	0.7	0.9
1.67 M V(III) + 0.86 M MEM + 0.16 M MEP	13.6	3.5	0.7	0.1

4.3.4 V(IV) and bromine / bromide solutions for linear sweep voltammetry

A series of samples was prepared for linear sweep voltammograms to observe the effect of complexing agent addition on the positive half cell reaction. From the linear voltamograms the kinetics of the bromine / bromide couple was studied both with and without the addition of the bromine complexing agents. Table 4.6 and Table 4.7 lists the solutions compositions used for these studies.

Table 4.6 Solutions containing 2 M V(IV) 6.1 M HBr 1.2 M HCl 0.2 M Br_2 with 0.75 M QBr for linear sweep voltammetry

Content	2.5 M V(IV) (ml)	Br_2 (ml)	MEM (ml)	MEP (ml)	7.6 M HBr + 1.46 M HCl (ml)	H_2O (ml)
2 M V(IV) + 0.2 M Br_2	14.4	0.2	0.0	0.0	0	3.4
2 M V(IV) + 0.2 M Br_2 + 0.36 M MEM + 0.38 M MEP	14.4	0.2	1.5	1.7	0.2	0
2 M V(IV) + 0.2 M Br_2 + 0.24 M MEM + 0.51 M MEP	14.4	0.2	1.0	2.3	0.1	0
2 M V(IV) + 0.2 M Br_2 + 0.19 M MEM + 0.56 M MEP	14.4	0.2	0.8	2.5	0.1	0
2 M V(IV) + 0.2 M Br_2 + 0.51 M MEM + 0.24 M MEP	14.4	0.2	2.1	1.1	0.2	0
2 M V(IV) + 0.2 M Br_2 + 0.56 M MEM + 0.18 M MEP	14.4	0.2	2.3	0.8	0.3	0

Table 4.7 Solutions containing 0.2 M and 1 M Br_2 with and without QBr for linear sweep voltammetry

Content	8.84 M HBr (ml)	Br_2 (ml)	MEM (ml)	MEP (ml)	7.6 M HBr + 1.46 M HCl (ml)	H_2O (ml)
6.2 M HBr + 0.2 M Br_2	14	0.2	0	0	0	4.8
6.2 M HBr + 1 M Br_2	14	1	0	0	0	4
6.2 M HBr + 1.2 M HCl + 0.2 M Br_2	0	0.2	0	0	16.3	3.5
6.2 M HBr + 1.2 M HCl + 1 M Br_2	0	1	0	0	16.3	2.7
6.2 M HBr + 1.2 M HCl + 0.2 M Br_2 + 0.19 M MEM + 0.56 M MEP	0	0.2	0.9	2.9	16.1	0

4.3.5 Cyclic Voltammetry

The three electrode cell setup is connected to the potentiosat for voltammetry measurements. Voltage is swept from the open circuit potential to a switching potential at -0.7 V, then scanned in the other direction to the positive switching potential at 1.2 V and finally stopped at the open circuit potential. Measurements were carried out at different scan rates to calculate the diffusion coefficient. Stirring of the solution is needed after each scan to ensure a homogeneous electrolyte for all measurements. All measurements were conducted at room temperature (25 – 28^{o}C). The working electrode

was polished with P1200 sand paper and rinsed with distilled water each time the solution was changed.

4.3.6 Linear sweep voltammetry

The same three electrode setup was used for linear sweep voltammetry of simulated positive half cell electrolyte samples. Voltage was swept from the open circuit to 1.1 V and solutions were stirred with a magnetic stirrer to maintain homogeneity after each scan. Scan rates between 1 – 10 mVs^{-1} were used, they are much slower than those for CV experiments.

4.3.7 EIS measurements for solution resistance estimation

EIS measurements were conducted to estimate solution and cell resistance to allow iR correction of the linear sweep voltammograms. EIS measurements were conducted using the same three electrode cell as for linear sweep voltammetry. A frequency response analyser (1255B, Solatron) was employed with the use of Zplot program. The frequency sweep occurred between the working and the reference electrode while the potential was held constant at 10 mV. This is similar to the procedures mentioned by Mathur and co-workers [123] for the solution resistance in a study of the Fe^{2+}/Fe^{3+} redox system. EIS measurements for each sample were carried out prior to the linear sweep measurement. By assuming the test system to be a reversible electrons transfer system, it can be represented by an equivalent circuit of mixed kinetic and diffusion controlled system (Figure 4.3). Solution resistance (Ohms) was estimated from the Nyquist Plot where the curve intersected with the real axis (Figure 4.4).

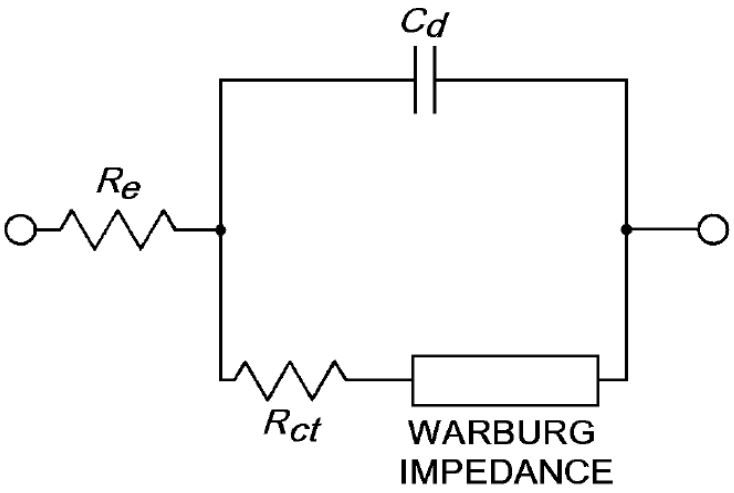

Figure 4.3 Equivalent circuit with mixed kinetic and charge transfer control R_e = Ohmic solution resistance, R_{ct} = charge transfer resistance, Warburg impedance = Warburg resistance or mass transfer resistance, C_d = Double layer capacitance

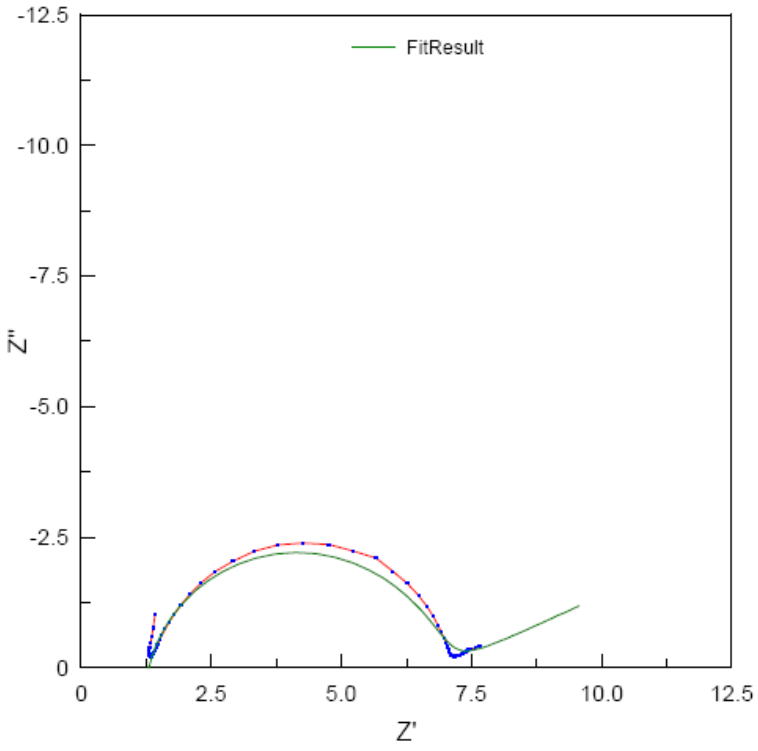

Figure 4.4 A typical Nyquist Plot for solution resistance estimation

4.4 Vanadium bromide flow cell testing

4.4.1 Battery analyser

The charge and discharge response of each cell was measured by a RePower Battery Testing unit (5 A, 10 V) controlled by a desktop computer. The battery testing unit was connected to the copper terminals of the test cell by a cable at one of the channel outlets. The cable had two sets of two alligator clips; each set was connected to one terminal of the cell with one clip for current and the other for voltage measurements. Constant current was applied and the potential measurement was obtained as a function of time by the software provided (Cell Test V2.5). As corrosion of the alligator clips was mild to rapid, each was cleaned with sandpaper before each test.

4.4.2 Static cell setup

A static cell is normally used for initial testing and voltage cut off limit detection. Static cells were built from two halves, each with an end plate, a copper plate, a glassy carbon, a rubber gasket and a PVC frame stacked on top of one another (Figure 4.6). Four 3 mm (1.5 mm when squeezed) thick carbon felts were soaked in 50 ml of testing electrolyte then kept under vacuum for one hour to ensure maximum solution absorption. After removing the carbon felts from the electrolytes the remaining solution volume was measured to estimate the amount of electrolyte retained in the felts. Two carbon felts were then inserted in the 3 mm cavity of each frame and the pre-treated ion exchange membrane was placed on top of the PVC plastic before sealing the two halves together. Synthetic polymer sealer (All Clear®, Selley) was used to stick and seal each layer, and then eight bolts were used to tighten the two outmost PVC end plates and to keep all the layers tight. The static cell was then allowed to stand for 30 minutes. The idle time

allowed the membrane to be fully soaked in the testing electrolyte, and to confirm that the cell was properly sealed. All cell leakages have to be repaired and finally the copper plate terminals were cleaned with sandpaper before connecting to the battery analyser for cell charging and discharging measurements.

4.4.3 Lab scale flow cell setup

The major components of a flow cell are similar to those of a static cell with the only difference being in the PVC frames that hold the carbon felts. As electrolytes should flow though the carbon felts, an inlet and outlet tube is incorporated in each frame. In this study, 3 mm and 4.5 mm thick flow frames are used, in each case four 3 mm thick carbon felts are inserted between the frames. Electrolytes were circulated from the external reservoirs by magnetic drive pumps (Iwaki), and connected to the cell by plastic tubing. Electric fans were used to prevent the pumps being overheated.

For the electrolytes containing complexing agents (MEM / MEP) the construction of the lab scale vanadium bromide flow cell was slightly altered from the setup of previous studies within the department [124]. The major modification was the addition of a magnetic stirrer below the reservoir for positive half-cell electrolytes (Figure 4.5), to ensure a good mixing between the aqueous phase and the dense bromine rich organic phase. The original flow cell setup was only used when testing electrolytes had no complexing agents.

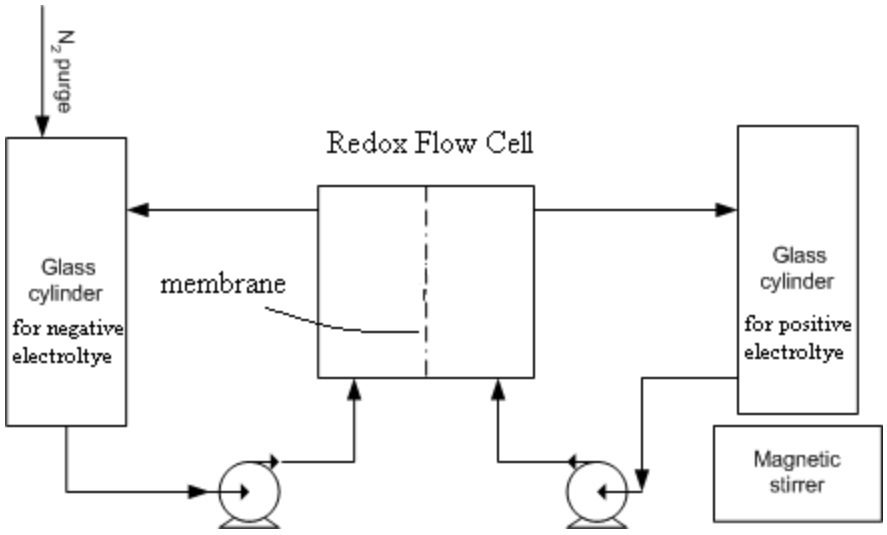

Figure 4.5 Schematic Diagram of the flow cell

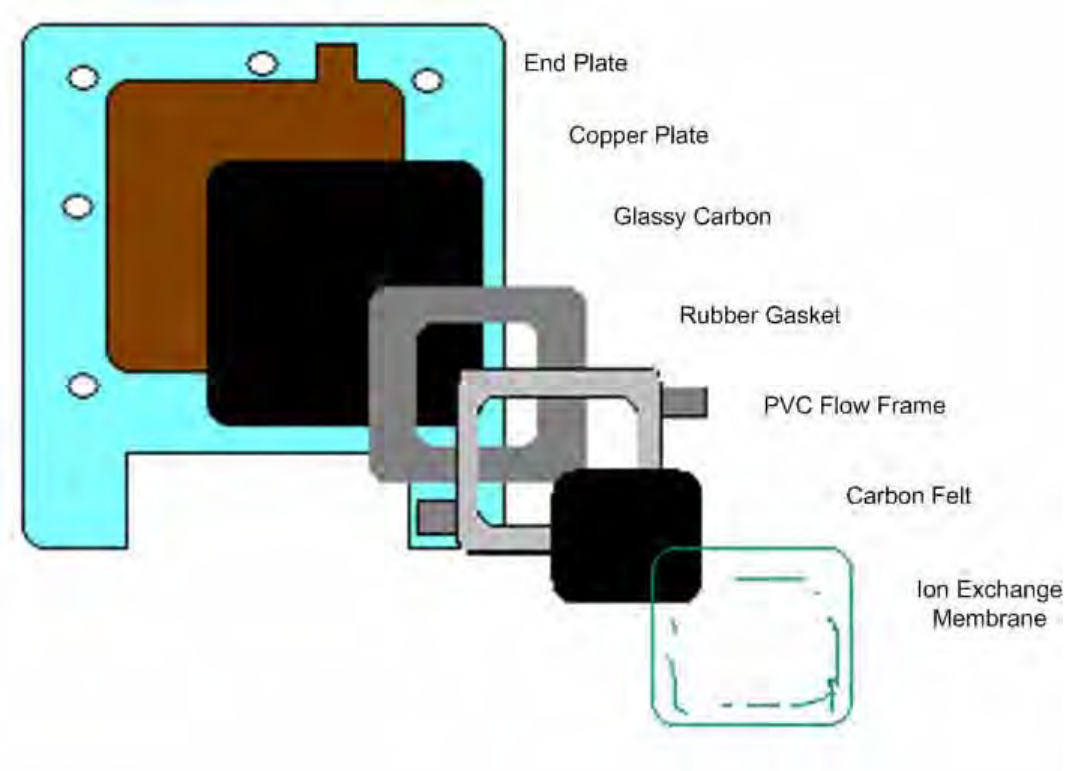

Figure 4.6 Components of one half of the redox cell

4.4.4 Charge and discharge procedures

Using the battery analyser from RePower and software Celltest V2.5, a constant charge/discharge current was applied to the test cell while monitoring the voltage response. As described previously, the battery analyser is connected to the copper plates

of the test cell with a connection cable before starting the Celltest V2.5 program. The Celltest V2.5 program allowed user to control the voltage limit and applied current for each charge and discharge cycle, also user can specify the umber of cycles to be repeated. For safety reasons, measuring voltage range and current limit has to be set to prevent the occurrence of extreme voltages or currents. For a continued charge / discharge process, the applied constant current can be changed after a fixed number of cycles with a limit of 20 programmed steps. With this feature, the cell efficiency versus current plot can be obtained without manually restarting the charging process, eliminating the idle time.

4.4.5 Half-cell potential measurement

The experimental setup for the measurement of half-cell potential was similar to that mentioned previously. The major difference was the addition of a chart recorder (Yokogawa) and an SCE in one reservoir as the reference electrode to monitor the two half cell potentials separately (Figure 4.7). The open circuit cell potential was measured every 60 minutes during a charge / discharge cycle for a one minute zero current interruption. The potential obtained during current interruption is the open circuit potential of the cell at each state-of-charge.

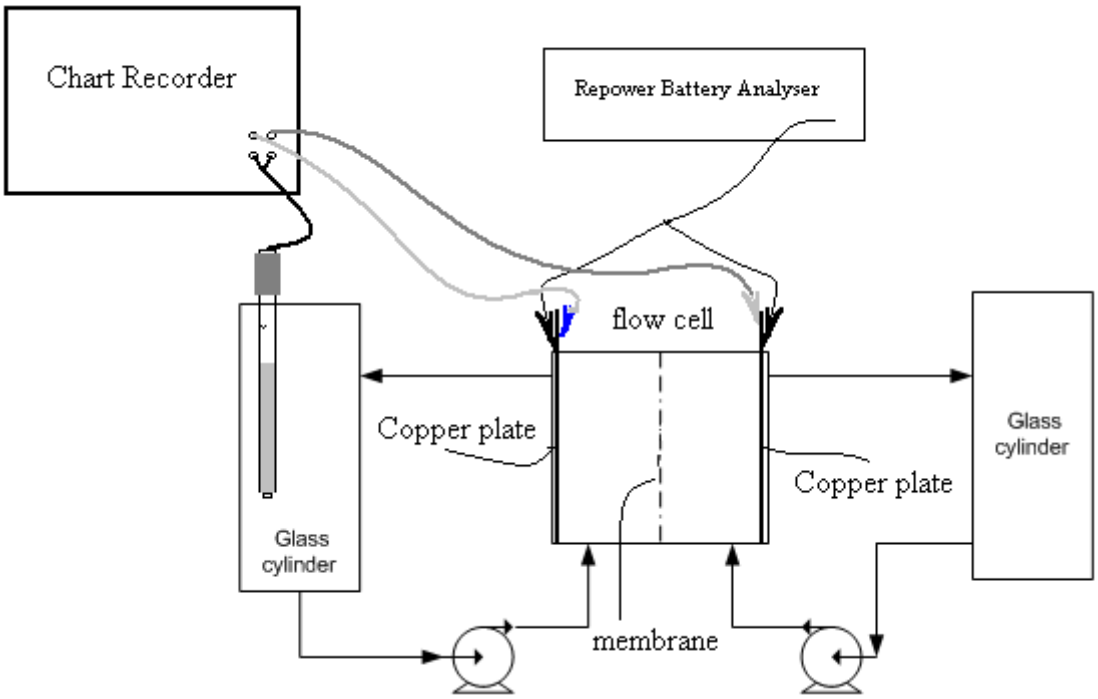

Figure 4.7 Flow cell setup for open circuit potential measurements

4.4.6 Cell performance at constant temperature

To obtain the cell performance at different operating temperatures, the test cell was placed in a temperature incubator (Binder). The static cells used contained 2 M $V^{3.7+}$ with complexing agents and these were tested at 10, 15, 25 and 35^{o}C. Most of the flow cell studies were carried out at room temperature (25^{o}C); some tests were also conducted at 10^{o}C.

4.5 Membrane Conductivity

4.5.1 Membrane conductivity with EIS measurements

The conductivity of two membranes (ChiNaf and VF11) soaked in vanadium solutions with and without complexing agent (MEM, MEP) was tested with impendence measurements using two constant surface area electrodes.

The conductivity cell setup consisted of two PVC holders, two rubber gaskets, a fixed distance constant area electrode and the test membrane. The rubber gasket containing a circular hole with a known area (0.64 cm^2) at the centre (Figure 4.8) was attached on the side of each PVC holder (Figure 4.8) with co-polymer sealant. Each test membrane was positioned between the holes before the two PVC holders were glued together. Blank measurements were made for each vanadium solution (ie. with no membrane) prior to testing resistance of the cell with the membranes. All measurements were recorded with 50 ml of vanadium solutions in each PVC holder.

The fixed distance electrode assembly was made of two identical electrodes. Each electrode was made from a 6 mm carbon disc attached to a stainless steel rod by silver epoxy (Figure 4.9). Each electrode was oven dried at 100^oC for 15 minutes, before covering the side with epoxy resin.

For constant surface area, the back of the carbon disc and part of the stainless steel rod were covered with epoxy. After air drying overnight and sanding to a constant surface area, both electrodes were inserted though a PVC plate at a constant distance of 3 cm apart. The schematic diagram in Figure 4.8 shows a cross section of the setup.

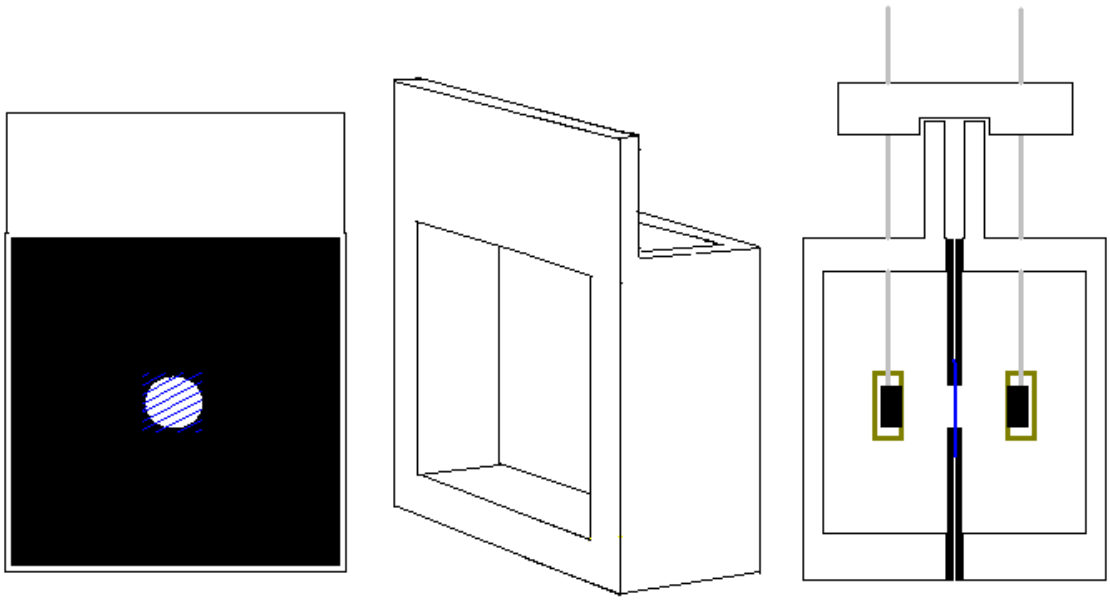

Figure 4.8 (Left) Rubber gasket contained circular hole with known area glued on PVC holder. (Middle) Side view of a PVC holder. (Right) Cross-section of the whole conductivity testing cell setup

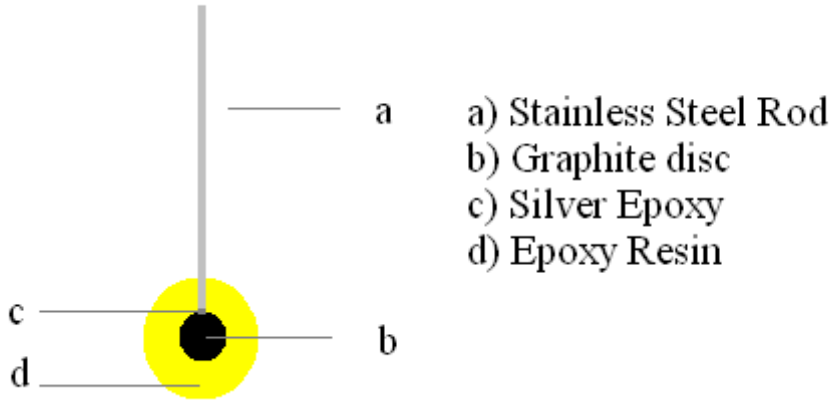

Figure 4.9 Cross-section of one of the fixed distance electrodes

Chapter 5 Physical and electrochemical studies of quaternary ammonium bromide in V/Br electrolytes

5.1 Screening test/ Stability test

5.1.1 Aim of screening test

For zinc bromine electrolytes the addition of quaternary ammonium bromide had caused solid formation in either the bromine rich organic phase or the aqueous phase under certain conditions. This section reports the qualitative study of three quaternary ammonium bromides at different combinations in the vanadium bromide (V/Br) electrolytes. Mixtures that formed solid when added to simulated charged or discharged vanadium electrolyte would be eliminated. Samples preparations are described in the section 4.2.

5.1.2 QBr addition to simulated charged positive electrolyte

Physical observation of simulated charged positive electrolyte containing V(IV) ions, Br_2 and three types of QBr at various concentrations, were made at 11, 25 and 40^{o}C.

5.1.2.1 Single QBr compounds

Observation of 2 M V(IV) solutions with single QBr compound is summarised in Table 5.1. Different from zinc bromine electrolyte, MEP did not form any solid particles with

V(IV) ions in the aqueous phase. However, MEP formed solid particles at low bromine concentration (0.2 M) in the bromine rich phase. When the bromine concentration is increased (1 M) this bromine rich phase became an orange layer. After bromine was added to MEP solutions no bromine vapour was observed at 25^{o}C. Since solid formed at room temperature, samples with MEP would not be tested at 11 and 40^{o}C.

Similar to MEP, the addition of MEM did not precipitate with V(IV) and remained as a green liquid 10 days after the addition. However, orange solid appeared in the bromine rich phase after 0.2 M Br_2 was added to 1.2 M MEM at 25^{o}C. At the same concentration of MEM, the addition of 1 M Br_2 formed some orange needle like solid instead of an oily layer (Figure 5.1), while in samples with lower MEM concentrations (0.6 and 0.8 M), addition of Br_2 (0.2 and 1 M) would form orange oily droplets or layers. For samples containing 0.6 – 1.2 M MEM, no bromine vapour was observed 10 days after the addition of 1 M Br_2 at 25^{o}C. However when the temperature was raised to 40^{o}C, bromine vapour could be seen in sample with lower MEM concentration (0.6 M).

TBA powder was found to be soluble in 7.6 M HBr + 1.46 M HCl acid. After TBA was dissolved in 2 M V(IV) solution, there was no apparent precipitation. However when 1 M Br_2 was added to the solution, it became very viscous and yellowish solid appeared in the bromine rich phase. (Table 5.1) There was no bromine vapour in the sample containing 0.75 M TBA, 10 days after the addition of 1 M Br_2 at 25^{o}C.

All the three tested QBr compounds would not precipitated with V(IV) when used as a single compound, however, it formed solid particles or some needle like crystals with aqueous bromine at 25^{o}C. Therefore, the use of single QBr compound is not suitable as bromine complexing agents for the positive electrolyte for V/Br flow cell.

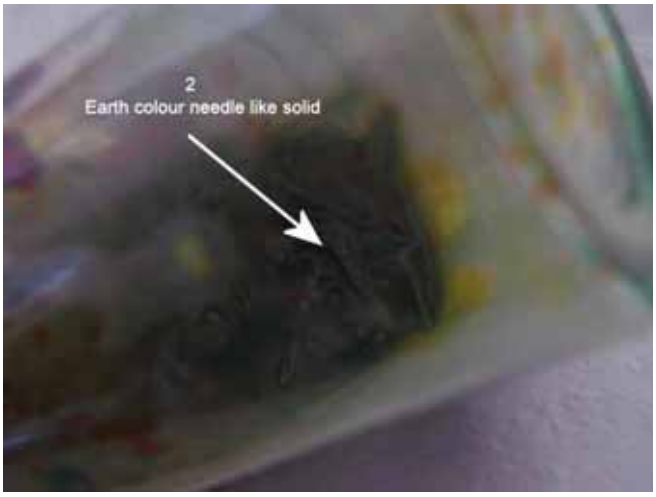

Figure 5.1 Orange needle like crystal formed at 25°C in 2 M V(IV) 1 M Br_2 and 1 M MEM containing total concentrations of 5.5 M HBr and 1.1 M HCl

5.1.2.2 Binary and ternary mixture of QBr compound

From the study of single QBr compounds it was known that the formation of an orange solid is likely to proceed when bromine concentration is less than or equal to 1 M. Therefore, binary and ternary QBr mixtures were first tested in 1 M Br_2 solutions at 25°C. This could eliminate QBr mixtures that formed solid particles in a simulated fully charged positive electrolyte. Observation records are summarised in Table 5.2.

When bromine was added to binary QBr mixtures that contained TBA, it either formed a viscous orange layer or some yellowish particles. When TBA concentrations are higher than 0.25 M the aqueous phase became very viscous. Therefore, binary mixtures with TBA should not be used for V/Br electrolytes.

In the study of single QBr compounds, bromine vapour can be retained in the solution between 11 – 40°C for samples that contained greater than 0.6 M QBr. Therefore, mixtures of MEM and MEP with a total concentration of 0.75 M and 1 M were compared at 25°C. (Table 5.2)

Simulated positive V/Br electrolytes containing binary mixtures of MEM and MEP are likely to form a dense orange layer after 1 M Br_2 is added at 25^{o}C. The sample 2 M V(IV) + 0.84 M MEM + 0.23 M MEP + 1 M Br_2 is the only exception that formed an orange solid at 25^{o}C.

On the other hand, the addition of 1 M Br_2 to mixtures of MEM and MEP with a lower QBr concentration (0.75 M QBr) neither formed solid particles nor bromine vapours at 25^{o}C. Therefore, these samples were further tested at 11°C and 40^{o}C with 0.2 M and 1 M Br_2 addition. Observations are summarised in Table 5.3. This is in agreement to the work by Cathro et al. [101] as the authors mentioned mixtures of QBr compounds would give a liquid polybromide phase even though each individual compound may result in a highly viscous or solid polybromide phase. Therefore, MEM and MEP mixtures are considered to be a reasonable choice for bromine vapour reduction in vanadium bromide electrolytes between 11 – 40^{o}C.

Samples of simulated positive V/Br electrolytes containing ternary mixture of MEM, MEP and TBA at 25^{o}C showed a repetitive pattern that the bromine rich phase became viscous with increasing TBA concentration. Meanwhile the aqueous phase turned viscous when the TBA concentration was higher than 0.25 M. Therefore, the choice of using a ternary mixture for the vanadium bromide flow cell was eliminated. Therefore, the use of a binary mixture containing MEM and MEP as the bromine complexing agent seemed to be a better option for the V/Br flow cell.

5.1.3 Observation of V(IV) after QBr addition

It is known that the use of single QBr compound (MEM, TBA) would cause the simulated charge positive V/Br electrolyte samples to form solids in the bromine rich

organic phase. In order to verify solid formation occurring between bromine and QBr rather than a product formed between V(IV) and QBr, V(IV) samples containing QBr in the absence of bromine were prepared. It was found that all the samples remained as a single phase dark green liquid at 11 – 40^{o}C. Therefore, this showed that there are no major interference between V(IV) and QBr (Table 5.1 – Table 5.3).

5.1.4 Stability of TBA with bromine addition

5.1.4.1 TBA with bromine addition

As discussed in section 5.1.2.1, samples containing TBA in simulated positive V/Br electrolytes either formed solids in the bromine rich organic phase or that phase would become very viscous. A series of TBA control samples were prepared to confirm the yellowish solid formation caused by a reaction between bromine and TBA. Weighed TBA powder was dissolved in 7.5 M HBr + 1.5 M HCl to prepare samples of 0.05 M, 0.1 M, 0.15 M, 0.25 M 0.5 M and 1 M TBA, then 1 M Br_2 was added to each sample (Figure 5.2). Yellowish solids were found in 0.5 M and 1 M TBA (Figure 5.3 left), while the sample of 0.25 M TBA formed a highly viscous organic phase (Figure 5.3 right). Therefore, TBA concentrations had to be lower than 0.25 M to allow the bromine rich organic phase to remain as an orange liquid layer.

5.1.4.2 TBA mixtures with added bromine

Although samples containing TBA as a single QBr would form solid particles in the bromine rich organic phase, the use of TBA in a ternary QBr mixture allowed the phase to remain as an orange oily layer. It was also found that a 1 M ternary QBr mixture is

better in bromine gas reduction than for samples containing 0.75 M ternary QBr after the addition of 1 M Br_2 and sorted at 40^{o}C (Figure 5.4)

Figure 5.2 Samples of TBA in various concentrations after the addition of 1 M Br_2 at 25^{o}C

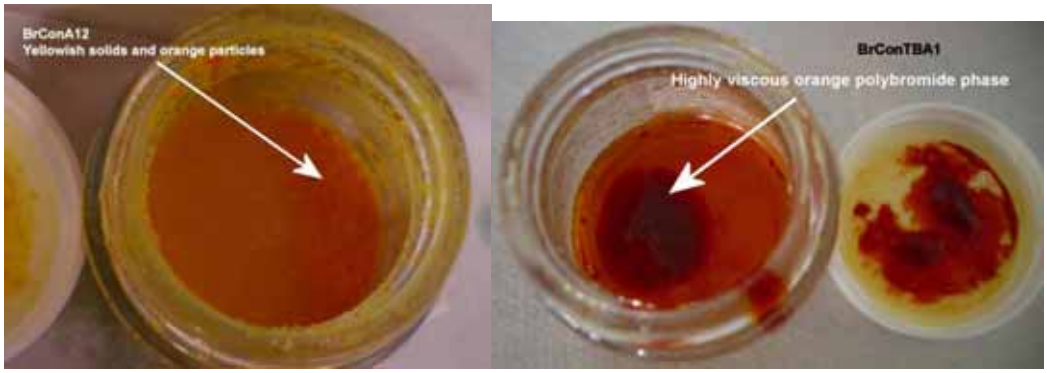

Figure 5.3 1 M Br_2 in 7.5 M HBr + 1.5 M HCl with added (left) 1 M TBA (right) 0.25 M TBA

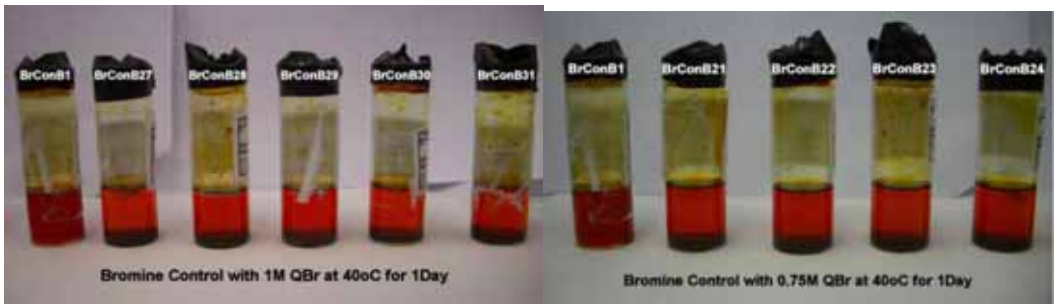

Figure 5.4 Samples of (left) 1 M QBr (right) 0.75 M QBr in 7.5 M HBr + 1.5 M HCl with added 1 M Br_2

Table 5.1 Observation of simulated positive electrolyte (supporting electrolyte 7.6 M HBr 1.4 M HCl) containing single QBr compound, total acid concentrations: 6.1 ± 0.6 M HBr and 1.1 ± 0.1 M HCl

QBr	Temp (°C)	V(IV) (M)	MEM (M)	MEP (M)	TBA (M)	Bromine Concentration (M)				
						0 M	0.2 M		1 M	
						(aq) phase	Bromine rich phase	(aq) phase	Bromine rich phase	(aq) phase
No QBr	25	2	0	0	0	Green liquid	**Brown Gas**	Green liquid	**Brown Gas**	Green liquid
Single QBr Compounds	25	2	1.2	0	0	Green liquid	**Orange solid**	Green liquid	**Needle like crystal**	Green liquid
		2	0.8	0	0	Green liquid	Orange droplets	Green liquid	Orange Oil layer	Green liquid
		2	0.6	0	0	Green liquid	Orange droplets	Green liquid	Orange Oil layer	Green liquid
		2	0	0.9	0	Green liquid	**Orange solid**	Green liquid	Orange Oil layer	Green liquid
		2	0	0.7	0	Green liquid	Orange solid	Green liquid	Orange Oil layer	Green liquid
		2	0	0	0.75	Green liquid	Yellow solid	Green liquid	Yellow / Orange solid	Viscous Green slurry
	11	2	0.7	0	0	Green liquid	Orange droplets	Green liquid	Orange Oil layer	Green liquid
		2	0.6	0	0	Green liquid	Orange droplets	Green liquid	Orange Oil layer	Green liquid
	40	2	0.7	0	0	Green liquid	Orange droplets	Green liquid	Orange Oil layer	Green liquid
		2	0.6	0	0	Green liquid	Orange droplets	Green liquid	Orange Oil layer with brown gas	Green liquid

Table 5.2 Observation of simulated positive electrolyte (2 M V(IV), 7.6 M HBr and 1.4 M HCl) with binary and ternary QBr mixture at 25°C, total acid concentrations: 5.8 ± 0.5 M HBr and 1.2 ± 0.1 M HCl

QBr mixture	Temp (°C)	V(IV) (M)	MEM (M)	MEP (M)	TBA (M)	Addition of 0 M Br_2	Addition of 1 M Br_2	
						Aqueous phase	Bromine rich phase	Aqueous phase
Binary QBr mixture	25	2	0.54	0.45	0	Green liquid	Orange Oil layer	Green liquid
	25	2	0.73	0.30	0	Green liquid	Orange Oil layer	Green liquid
	25	2	0.84	0.23	0	Green liquid	**Orange solid**	Green liquid
	25	2	0.37	0.62	0	Green liquid	Orange Oil layer	Green liquid
	25	2	0.28	0.71	0	Green liquid	Orange Oil layer	Green liquid
	25	2	0.39	0.35	0	Green liquid	Orange oil layer	Green liquid
	25	2	0.24	0.49	0	Green liquid	Orange oil layer	Green liquid
	25	2	0.15	0.58	0	Green liquid	Orange oil layer	Green liquid
	25	2	0.49	0.22	0	Green liquid	Orange oil layer	Green liquid
	25	2	0.58	0.18	0	Green liquid	Orange oil layer	Green liquid
	25	2	0.38	0	0.36	Green liquid	**Viscous orange layer**	Viscous Green liquid
	25	2	0.24	0	0.5	Green liquid	**Viscous orange layer**	Viscous Green liquid
	25	2	0.14	0	0.59	Green liquid	**Viscous orange layer**	Viscous Green liquid
	25	2	0.47	0	0.26	Green liquid	Orange oil layer with brown gas	Green liquid
	25	2	0.56	0	0.17	Green liquid	Orange oil layer with brown gas	Green liquid
	25	2	0	0.34	0.39	Green liquid	**Viscous orange layer**	Viscous Green liquid
	25	2	0	0.21	0.52	Green liquid	**Viscous orange layer**	Viscous Green liquid
	25	2	0	0.17	0.57	Green liquid	**Orange Solid**	Viscous Green liquid
	25	2	0	0.47	0.26	Green liquid	**Viscous orange layer**	Green liquid
	25	2	0	0.56	0.18	Green liquid	**Viscous orange layer**	Green liquid
Ternary QBr Mixture	25	2	0.23	0.26	0.25	Green liquid	**Viscous orange layer**	Viscous Green liquid
	25	2	0.38	0.17	0.18	Green liquid	Slightly viscous orange oil layer	Green liquid
	25	2	0.47	0.13	0.13	Green liquid	Slightly viscous orange oil layer	Green liquid
	25	2	0.19	0.39	0.16	Green liquid	Slightly viscous orange oil layer	Green liquid
	25	2	0.14	0.43	0.17	Green liquid	Slightly viscous orange oil layer	Green liquid
	25	2	0.19	0.17	0.37	Green liquid	**Orange Solid**	Viscous Green liquid
	25	2	0.14	0.13	0.47	Green liquid	**Orange Solid**	Viscous Green liquid

Table 5.3 Observation of simulated positive electrolyte (7.6 M HBr + 1.4 M HCl) with MEM and MEP at different ratio, total acid concentration : 6.1 ± 0.2 M HBr and 1.1 ± 0.1 M HCl

Temp (^oC)	V(IV) (M)	MEM (M)	MEP (M)	0 M Br_2	0.2 M Br_2		1 M Br_2	
				(aq) phase	Bromine rich	(aq) phase	Bromine rich	(aq) phase
11	2	0.39	0.35	Green liquid	Orange oil droplets	Green liquid	Orange Oil layer	Green liquid
	2	0.24	0.49	Green liquid	Orange oil droplets	Green liquid	Orange Oil layer	Green liquid
	2	0.15	0.58	Green liquid	Orange oil droplets	Green liquid	Orange Oil layer	Green liquid
	2	0.49	0.22	Green liquid	Orange oil droplets	Green liquid	Orange Oil layer	Green liquid
	2	0.58	0.18	Green liquid	Orange oil droplets	Green liquid	Orange Oil layer	Green liquid
25	2	0.39	0.35	Green liquid	Orange oil droplets	Green liquid	Orange Oil layer	Green liquid
	2	0.24	0.49	Green liquid	Orange oil droplets	Green liquid	Orange Oil layer	Green liquid
	2	0.15	0.58	Green liquid	Orange oil droplets	Green liquid	Orange Oil layer	Green liquid
	2	0.49	0.22	Green liquid	Orange oil droplets	Green liquid	Orange Oil layer	Green liquid
	2	0.58	0.18	Green liquid	Orange oil droplets	Green liquid	Orange Oil layer	Green liquid
40	2	0.39	0.35	Green liquid	Orange oil droplets	Green liquid	Orange Oil layer	Green liquid
	2	0.24	0.49	Green liquid	Orange oil droplets	Green liquid	Orange Oil layer	Green liquid
	2	0.15	0.58	Green liquid	Orange oil droplets	Green liquid	Orange Oil layer	Green liquid
	2	0.49	0.22	Green liquid	Orange oil droplets	Green liquid	Orange Oil layer	Green liquid
	2	0.58	0.18	Green liquid	Orange oil droplets	Green liquid	Orange Oil layer	Green liquid

Table 5.4 Observation of bromine samples at various QBr concentrations, total acid concentrations 5.9 ± 0.3 M HBr and 1.1 ± 0.1 M HCl * Brown gas started to evolved for all samples with 0.75 M QBr at 40°C after 24hr

Total QBr (M)	Temp (°C)	HBr (M)	HCl (M)	MEM (M)	MEP (M)	TBA (M)	Bromine added, ml (concentration, M)		
							0 ml (0 M)	0.5 ml (1 M)	
							(aq) phase	Bromine rich phase	(aq) phase
0	11,25,40	6.0	1.1	0	0	0	Yellow liquid	Brown Gas	Yellow liquid
0.7	11,25,40*	6.2	1.2	0.36	0.17	0.18	Yellow liquid	Orange oil layer	Yellow liquid
		6.1	1.2	0.44	0.13	0.13	Yellow liquid	Orange oil layer	Yellow liquid
		6.1	1.2	0.18	0.38	0.16	Yellow liquid	Orange oil layer	Yellow liquid
		6.1	1.2	0.13	0.42	0.17	Yellow liquid	Orange oil layer	Yellow liquid
1	11,25,40	5.6	1.1	0.43	0.41	0.2	Yellow liquid	Orange oil layer	Yellow liquid
		5.6	1.1	0.52	0.33	0.2	Yellow liquid	Viscous orange layer	Yellow liquid
		5.6	1.1	0.61	0.25	0.2	Yellow liquid	Viscous orange layer	Yellow liquid
		5.6	1.1	0.35	0.49	0.2	Yellow liquid	Orange oil layer	Yellow liquid
		5.6	1.1	0.26	0.57	0.2	Yellow liquid	Viscous orange layer	Yellow liquid

Table 5.5 Observations of simulated negative electrolyte with binary QBr mixture at 0 M and 0.2 M bromine addition, total acid concentrations: 6.2 ± 0.1 M HBr and 1.2 ± 0.1 M HCl

QBr Compound	Temp (°C)	V(III) (M)	MEM (M)	MEP (M)	TBA (M)	Bromine Concentration (M)		
						0 M	0.2 M	
						(aq) phase	Bromine rich phase	(aq) phase
Binary QBr Mixture	11,25,40	2	0	0	0	Green liquid	Brown Gas	Green liquid
		2	0.37	0.38	0	Green liquid	Orange oil droplet	Green liquid
		2	0.24	0.5	0	Green liquid	Orange oil droplet	Green liquid
		2	0.20	0.56	0	Green liquid	Orange oil droplet	Green liquid
		2	0.50	0.26	0	Green liquid	Orange oil droplet	Green liquid
		2	0.57	0.18	0	Green liquid	Orange oil droplet	Green liquid

5.1.5 Simulated negative electrolytes

5.1.5.1 Stability of 2 M V(III) solutions containing binary QBr mixtures

Samples simulating the discharged negative half cell of V/Br electrolyte were prepared (Ch4). Observations of any interference between V(III), MEM and MEP in the mixtures were recorded (Table 5.5). All solutions remained as a single green liquid phase at 11 and 40 ^{o}C, and proved that the addition of MEM and MEP to V(III) is stable.

5.1.5.2 Stability of simulated negative electrolyte with low level of Br_2 addition

To simulate the situation when low levels of bromine passed through the membrane from the positive half-cell, samples of simulated negative V/Br electrolyte containing 0.2 M Br_2 were prepared and observations were made (Table 5.5). Similar to V(IV) solutions, the addition of Br_2 to MEM and MEP mixtures in 2 M V(III) formed an orange oily layer. On the other hand, the aqueous phase of each sample has remained as a green liquid. No solid formation has been observed when 0.2 M Br_2 is added to 2 M V(III) samples containing MEM and MEP at 11 and 40^{o}C.

5.1.6 Summary of QBr stability for 2 M Vanadium electrolyte

V(IV) samples with binary mixtures of QBr containing TBA had formed a highly viscous solution in the bromine rich organic phase after bromine addition. Therefore, the use of TBA is not suitable for the V/Br flow cell. Secondly, V(IV) containing ternary QBr mixtures only proved to retain bromine vapour when the total QBr concentration is greater than 1 M. As this would lead to an increase in QBr consumption

and higher cost, V/Br electrolytes that utilised ternary QBr mixture would not be the ideal choice. Thirdly, both V(III) and V(IV) solutions contained binary QBr mixtures of MEM and MEP formed an orange oil layer when liquid bromine is added. Finally, both V(III) and V(IV) solution remained as a homogenous liquid phase after the addition of MEM and MEP in the absence of Br_2 and proved to be stable between 11 – 40 ^{o}C.

It is important to note that both MEM and MEP used in this study are in an aqueous form. Increasing the QBr concentration will therefore reduce the concentration of both HBr and HCl acid. This could lead to a reduction of the total bromide concentration in the electrolyte even though each QBr is attached to a bromide ion.

From the above results therefore, in terms of physical stability, the use of MEM and MEP as a binary mixture with a total concentration of 0.75 M would be suitable for use in the V/Br electrolyte as bromine complexing agents.

5.2 Electrochemical study by cyclic voltammetry

The electrochemical interference caused by the addition of quaternary ammonium bromide was studied by cyclic voltammetry. This included the effect of QBr addition on the diffusion coefficient of V^{3+} and the bromide / bromine reaction kinetics. A graphite electrode with a constant surface area (A = 0.28 cm^2) was used as the working electrode for all electrochemical studies reported in this thesis.

5.2.1 Reproducibility of working electrode

Several graphite working electrodes were fabricated for the use in the voltammetry experiments. Each was checked individually for its reproducibility before data

collection (Figure 5.5). Although each electrode was made by the same method as described earlier (Chapter 4.3), voltammograms varied for different electrodes measuring the same solution. This might be caused by different internal resistances and polishing levels for each electrodes. Therefore, comparisons were only made amongst results measured with the same electrode.

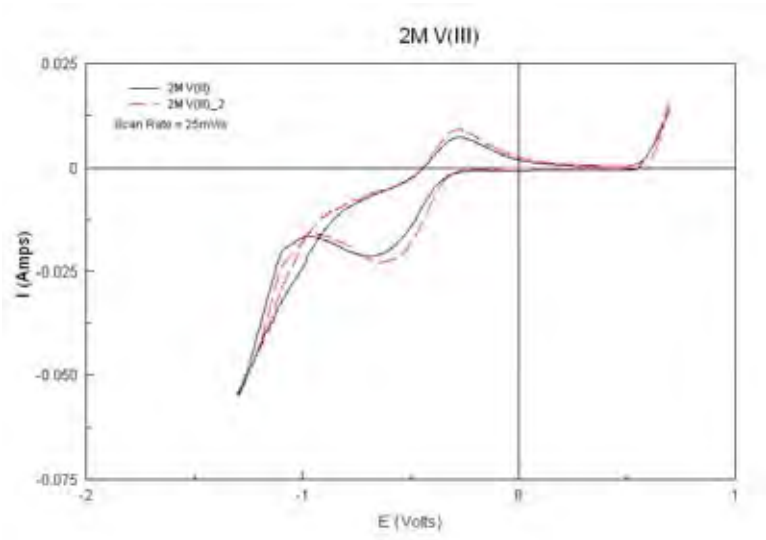

Figure 5.5 Reproducibility check for graphite working electrode in 2 M V(III) in 6.1 M HBr + 1.2 M HCl E_{OCP} = 0. 24 V (vs SCE), scan rate 25 mVs^{-1}, scan directions: from OCP to -1.3 V then backward scan to 0.8 V and finally stop at OCP

5.3 Electrochemical Studies of V^{3+} / V^{2+} Couple

5.3.1 Diffusion Coefficient of V^{3+} in simulated negative half-cell electrolyte of V/Br flow cell

The preparation of 2 M V(III) in 7.6 M HBr + 1.46 M HCl is described in section 4.2.2. Cyclic voltammetry was carried out at 28^{o}C and at four different scan rates. In each case the initial potential was 0.25 V and the initial scan was in the negative direction.

The cyclic voltammogram of 2 M V(III) (Figure 5.6) at a scan rate of 50 mVs^{-1} shows a cathodic peak at -0.72 V corresponding to the reduction of V^{3+} to V^{2+} . An anodic peak at -0.26 V is corresponding to the re-oxidation of V^{2+} to V^{3+}. The beginning of

hydrogen evolution is observed at about -1.0 V where the cathodic current started to increase sharply. Experimental data of cathodic peak current and potential at each scan rate are summarised in Table 5.6.

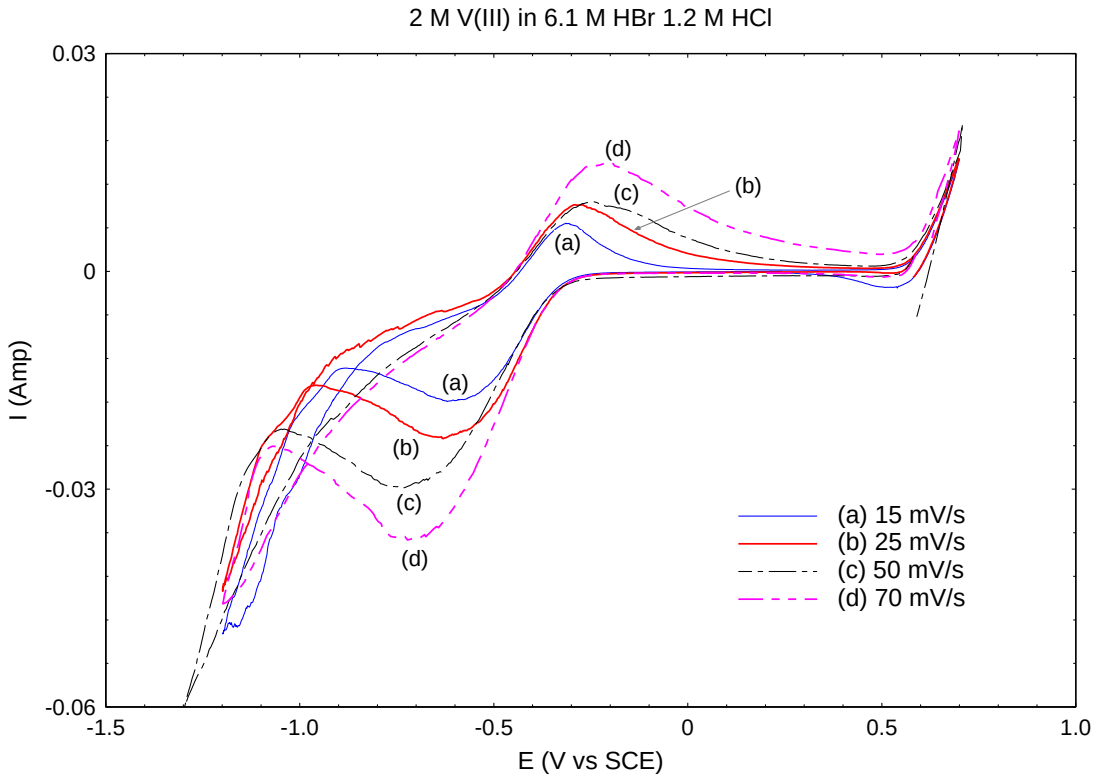

Figure 5.6 Cyclic Voltammogram of 2 M V(III) + 6.1 M HBr + 1.2 M HCl at scan rate of 15, 25, 50 and 70 mVs^{-1}

Table 5.6 Data of cathodic peak potential (E_p), peak current (i_p) and calculated formal potential ($E^{o'}$), peak potential difference (ΔE_p) for CV of 2 M V(III) + 6.1 M HBr + 1.2 M HCl

Scan rate (mV/s)	E_p (V)	I_p (Amps)	ΔE_p (V)	$(E_{pa}+E_{pc})/2$	$E^{o'}$ (V vs SCE)
15	-0.62	0.02	0.31	-0.47	-0.47
25	-0.64	0.02	0.35	-0.47	
50	-0.72	0.03	0.46	-0.49	
70	-0.72	0.04	0.51	-0.47	

From the same cyclic voltammogram (Figure 5.6), the peak potential separation (ΔEp) was found to be greater than 0.056 mV at each scan rate. Therefore, the reaction V^{3+} + e ⇔ V^{2+} is considered to be electrochemically irreversible.

The diffusion coefficient of V^{3+} was calculated from the peak current equation for an irreversible reaction, which is presented in Equation 5.1. The formal potential of the V^{3+} / V^{2+} couple was determined as the average value of the mid points between the anodic and cathodic peaks at different scan rates, illustrated by Equation (5.2) [79].

At 28°C, $$i_p = 2.97 \times 10^5 n(\alpha n)^{1/2} A D^{1/2} C^o \upsilon^{1/2} \quad (5.1)$$

$$E^{o'} = \frac{\sum (E_{pa} + E_{pc})/2}{no.\ of\ \ scans} \quad (5.2)$$

The plot i_p versus $\nu^{1/2}$ (Figure 5.7) showed a straight line with a slope of 0.13 that is equal to 2.97 x $10^5 n(\alpha n)^{1/2} A D^{1/2} C^o$. With a known electron transfer for V^{3+} / V^{2+} couple (n = 1), a constant working electrode surface area (A = 0.28 cm^2) and V(III) concentration (C^o = 2 M or 0.002 mol cm^{-3}), when αn is assumed to be 0.5, the diffusion coefficient of V^{3+} in 2 M V(III) was found to be 1.2 x 10^{-6} $cm^2 s^{-1}$. This is about 5 times lower than the values obtained by Niki and Mizota for a 10 mM V(III) dissolved in 1 M HBr solution which was 6.77 x 10^{-6} $cm^2 s^{-1}$. This deviation is probably due to variations in surface roughness of the electrodes used, leading to difference in effective surface areas. The formal potential of the V^{3+}/V^{2+} couple calculated at four scan rates was –0.47 V. This agreed with the values determined by Niki and Mizota [69] for 10 mM V(III) in 1 M HCl or 1 M HBr which were -0.464 and -0.460 V (vs SCE) respectively.

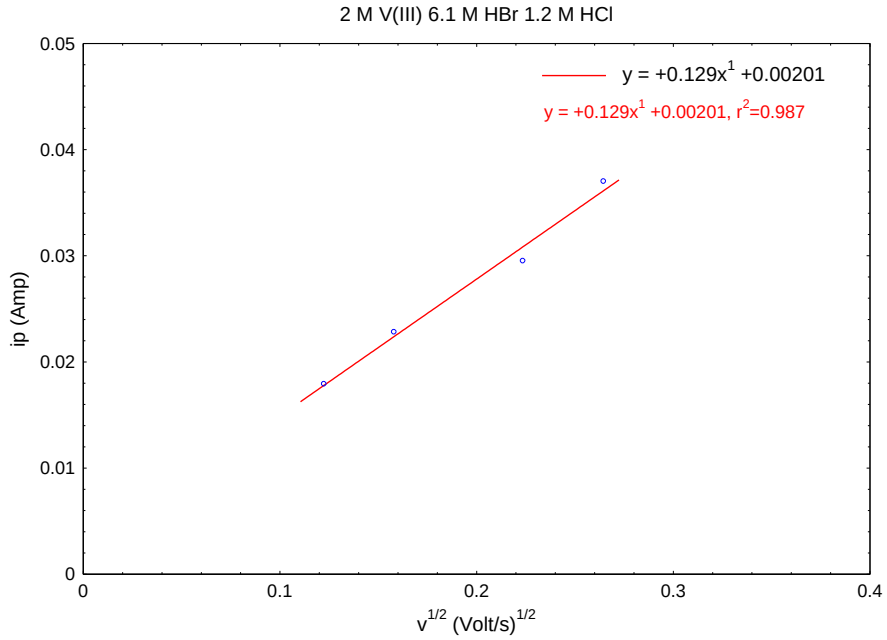

Figure 5.7 Peak current (i_p) against square root of scan rate ($v^{1/2}$) for 2 M V(III) + 6.1 M HBr and 1.2 M HCl

5.3.2 Effect of QBr addition on V^{3+} diffusion coefficient

Cyclic voltammograms of V^{3+} solutions containing MEM and MEP for scan rates 10 – 100 mVs^{-1} are presented at in Appendix C Figure C.1 and C.2. Peak potentials, peak currents and peak separation values are tabulated in Table 5.7. The diffusion coefficient of V^{3+} in each solution was determined from plots of i_p versus $v^{1/2}$ shown in Appendix C Figure C.6 and C.7. The calculated formal potential and V^{3+} diffusion coefficient values for each solution are tabulated in Table 5.8.

As shown in the cyclic voltammogram of Figure 5.8, the addition of MEM and MEP had caused a reduction in the cathodic peak current and had shifted the peak potential slightly. Cyclic voltammograms (Figure 5.8) for solution containing 1 M MEM and 1 M MEP showed with increasing QBr concentration the cathodic currents were slightly decreased. This effect is further discussed in section 5.3.4. From the stability studies it is known that the use of MEM and MEP as a single QBr compound in V/Br electrolytes

could lead to the possibility of solid formation when combined with bromine. Hence, CV for V(III) solutions with MEM or MEP added as single compound presented here only aimed to show their effect on the electrochemical parameters of V(III).

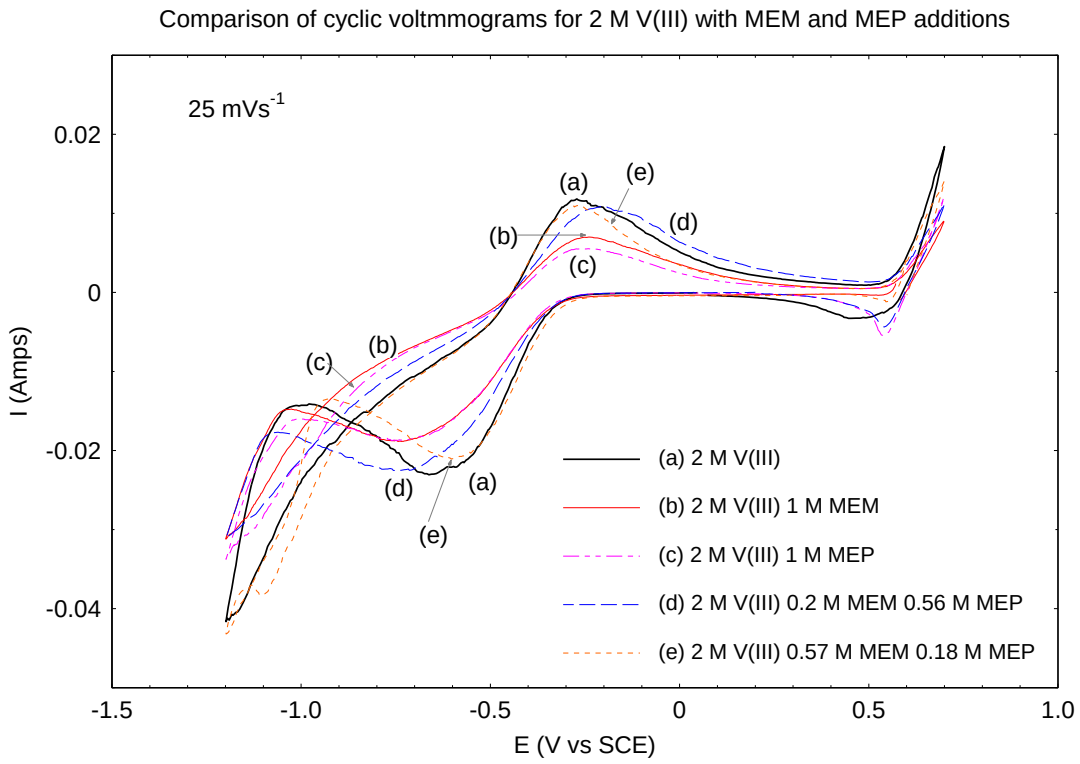

Figure 5.8 Cyclic voltammograms in 2 M V(III), 6.0 ± 0.2 M HBr and 1.1 ± 0.1 M HCl with various concentrations of MEM and MEP at a scan rate of 25 mVs^{-1}

From the results shown in Table 5.7 and Table 5.8 there are no major changes in peak potential separation and formal potential after the addition of MEM and MEP. However the addition of MEM and MEP had decreased the diffusion coefficient of V^{3+}. Compare to a V(III) solution the diffusion coefficient of V^{3+} for solution containing 0.75 M QBr has decreased by nearly one half, whereas a further reduction was observed for solution containing 1 M QBr. Despite such deviation, the diffusion coefficients obtained were of the same order of magnitude, therefore the effect of QBr addition is considered to be minimal. The addition of MEM and MEP had no major effect on the formal potential and peak potential separation, showing that its interference on the kinetics of the V^{3+}/

V^{2+} redox couple is minimal. Since the kinetics of V^{3+}/ V^{2+} couple is critical for the effective separation of the V/Br redox cell, it is quantitatively analysed in the following section.

Table 5.7 Data of cathodic E_p, i_p and calculated $E^{o'}$ and ΔE_p from CV Appendix C Figure C.1 and C.2 in comparison with 2 M V(III), 6.0 ± 0.2 M HBr and 1.1 ± 0.1 M HCl

Sample Content	scan rate mV	E_{pc} (V)	I_{pc} (Amp)	ΔE_p	$(E_{pa}+E_{pc})/2$
2 M V(III)	15	-0.62	0.02	0.31	-0.47
	25	-0.64	0.02	0.35	-0.47
	50	-0.72	0.03	0.46	-0.49
	70	-0.72	0.04	0.51	-0.47
2 M V(III) + 1 M MEM	15	-0.67	0.01	0.39	-0.48
	25	-0.75	0.02	0.50	-0.50
	50	-0.82	0.02	0.61	-0.51
	70	-0.93	0.03	0.79	-0.53
2 M V(III) + 1 M MEP	15	-0.69	0.02	0.40	-0.49
	25	-0.71	0.02	0.45	-0.48
	50	-0.79	0.02	0.65	-0.46
	70	-0.83	0.03	0.72	-0.47
2 M V(III) + 0.20 M MEM + 0.56 M MEP	15	-0.65	0.02	0.36	-0.48
	25	-0.67	0.02	0.40	-0.47
	50	-0.74	0.02	0.53	-0.47
	70	-0.78	0.03	0.60	-0.48
2 M V(III) + 0.57 M MEM + 0.18 M MEP	10	-0.57	0.01	0.24	-0.45
	25	-0.60	0.02	0.33	-0.44
	50	-0.68	0.03	0.49	-0.44
	70	-0.77	0.03	0.53	-0.51

Table 5.8 Diffusion coefficient and formal potential for 2 M V(III) 6.0 ± 0.2 M HBr and 1.1 ± 0.1 M HCl 0.75M QBr

Sample Content	**slope**	**Intercept**	**$E^{o'}$(V)**	**$D^o x10^{-7}$ (cm^2/s)**
2 M V(III)	0.13	0.002	-0.47	12.0
2 M V(III) + 1 M MEM	0.09	0.004	-0.50	5.4
2 M V(III) + 1 M MEP	0.08	0.006	-0.48	4.4
2 M V(III) + 0.20 M MEM + 0.56 M MEP	0.10	0.005	-0.48	6.1
2 M V(III) 0.57M MEM 0.18M MEP	0.11	0.002	-0.46	8.6

5.3.3 Kinetics of V^{3+} in 2 M V(III) and QBr addition

The effect of QBr addition on V^{3+} kinetic parameter was further studied. According to Equation (5.3) the heterogeneous rate constant (k^o) and transfer coefficient (α) can be found from the slope and intercept of a ln (i_p) vs ($E_p - E^{o'}$) plot respectively [116].

$$i_p = 0.227nFAC^o k^o e^{\left[-\alpha f\left(E_p - E^o\right)\right]} \qquad (5.3)$$

The kinetic parameters for the V^{3+}/V^{2+} couple in 2 M V(III), 6.2 M HBr and 1.2 M HCl were determined from Figure 5.9 where values of i_p, E_p, and $E^{o'}$ were obtained from Table 5.6. From this plot the transfer coefficient and heterogenous rate constant at 28°C were found to be 0.14 and 1.39 x 10^{-4} cms^{-1} respectively.

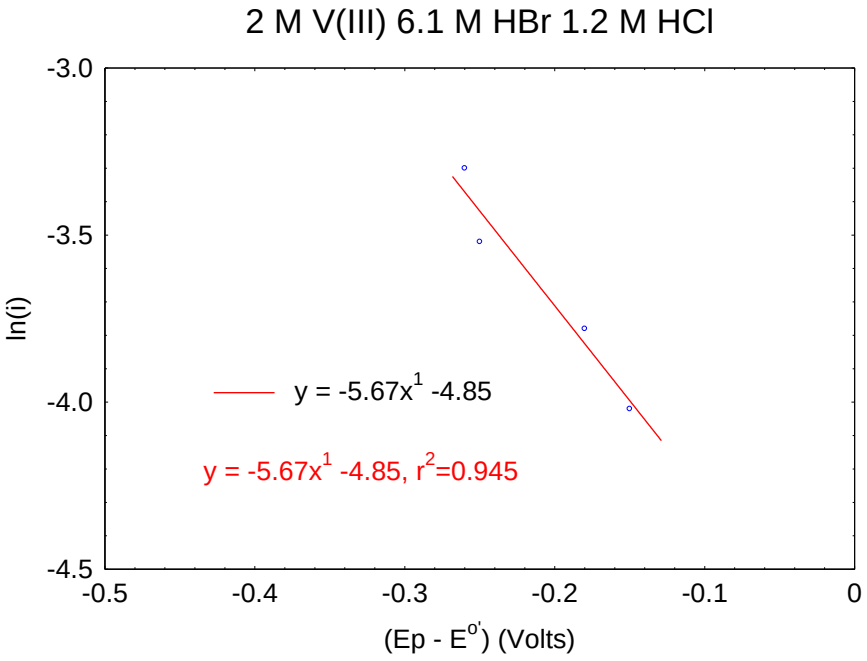

Figure 5.9 A plot of ln(i_p) against vs ($E_p - E^{o'}$) for cyclic voltammogram of 2 M V(III) in 6.2 M HBr and 1.2 M HCl

Similar plots (Appendix C Figure C.9 and C.10) and calculations were made for V(III) solutions after the addition of MEM and MEP to illustrate its effect on kinetic parameters. By assuming V^{3+} ions to be the only electroactive species in this potential

region and the results of α and k^o for samples containing MEM and MEP are summarised in Table 5.9. This showed the addition of MEM and MEP had no major effect on α, since α values for all samples tested are similar (Table 5.9). The heterogenous rate constants were only slightly affected by the addition of MEM or MEP but with no particular trend had been observed.

Table 5.9 Kinetics properties of 2 M V(III) 0.75 M QBr containing 6.0 ± 0.2 M HBr 1.1 ± 0.1 M HCl at 28°C

Sample Content	slope	Intercept	α	k^o (10^{-4}) cms^{-1}
2 M V(III)	-5.7	-4.9	0.14	1.5
2 M V(III) + 1 M MEM	-2.7	-4.7	0.07	1.7
2 M V(III) + 1 M MEP	-3.4	-4.8	0.09	1.5
2 M V(III) + 0.20 M MEM + 0.56 M MEP	-4.5	-4.9	0.12	1.4
2 M V(III) + 0.57 M MEM + 0.18 M MEP	-4.0	-4.6	0.10	1.9

In Table 5.9, the α values do not lie in the usual range of $0.3 < \alpha < 0.7$. This inconsistency in α values is probably caused by the discrepancies between the values of effective and geometric electrode surface area.

Diffusion coefficient of V^{3+} recalculated using experimental α values are presented in Table 5.10. Compared to those calculated by assuming $\alpha = 0.5$, it was found that the diffusion coefficient of V^{3+} in a 2 M solution determined by the experimental calculated α is much closer to the literature value (6.77×10^{-6} cm^2s^{-1}) [69].

From Table 5.10 it is also shown that the addition of MEM has less effect on the diffusion coefficient of V^{3+} compared to those with MEP addition. Moreover, the increase of total QBr concentration had slightly reduced the diffusion coefficient.

Table 5.10 Comparison of diffusion coefficient of V^{3+} calculated by experimental transfer coefficient (α) and by assuming $\alpha = 0.5$

Sample Content	D^o ($\alpha = 0.5$) (10^{-7} cm^2/s)	α	D^o (10^{-6} cm^2/s)
2 M V(III)	12.0	0.14	4.2
2 M V(III) + 1 M MEM	5.4	0.07	3.8
2 M V(III) + 1 M MEP	4.4	0.09	2.4
2 M V(III) + 0.20 M MEM + 0.56 M MEP	6.1	0.12	2.6
2 M V(III) + 0.57 M MEM + 0.18 M MEP	8.6	0.10	4.1

5.3.4 The effect of increasing QBr concentration

As presented earlier the increasing in QBr concentrations would lead to a reduction in cathodic current and V^{3+} diffusion coefficient. In order to examine the individual effects of MEM and MEP when added to V(III) electrolytes, several samples were prepared with increasing concentration of one complexing agent while the other was fixed. The resultant cyclic voltammograms (Appendix Figure C.3, C.4 and C.5) at scan rates 25 – 100 mVs^{-1}, showed similar features either with increasing MEM or MEP concentration. In comparison with 2 M V(III) samples, the addition of MEM and MEP had caused a larger reduction in cathodic current for solutions with 1.67 M V(III). From the cyclic voltammogram measured at 50 mVs^{-1} (Figure 5.10), i_p had nearly reduced by 0.01 Amps after the addition of MEM or MEP. Calculated formal potentials were found to be similar among tested samples (Table 5.11). They are also in agreement with previous results for 2 M V(III). Diffusion coefficient values of V^{3+} in each solution obtained from the plots of i_p against $v^{1/2}$ (Appendix C Figure C.8) are tabulated in Table 5.11. Kinetic parameters α, k^o were also determined (Table 5.12). Finally, comparisons were made between the diffusion coefficients found using experimental α and $\alpha = 0.5$ (Table 5.13).

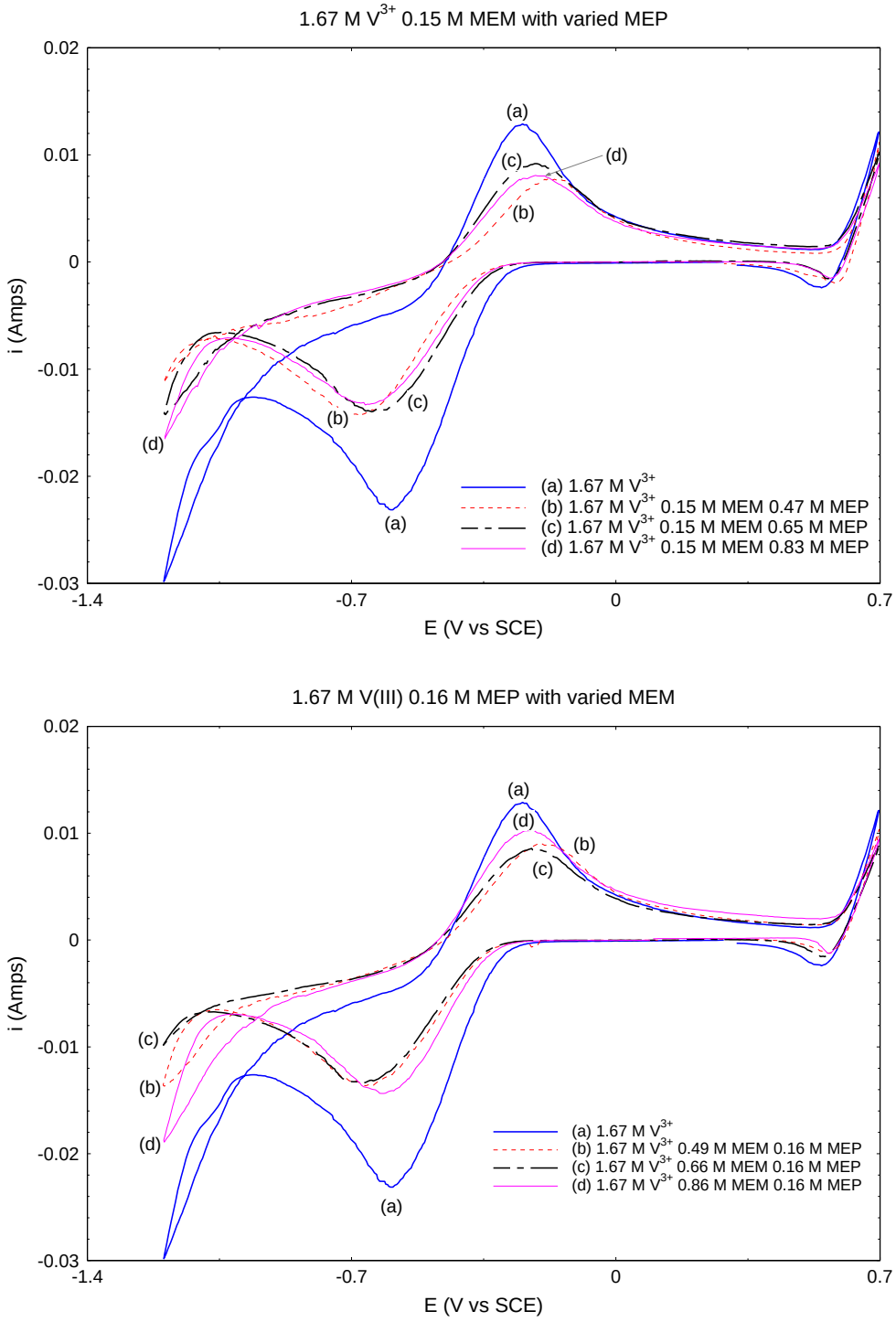

Figure 5.10 CV at 50 mVs^{-1} of (top) 1.67 M V(III), 6.2 ± 0.4 M HBr, 1.1 ± 0.1 M HCl, 0.15 M MEM and with varied MEP (bottom) 1.67 M V(III), 6.2 ± 0.4 M HBr, 1.1 ± 0.1 M HCl, 0.16 M MEP and with varied MEM

Table 5.11 Formal potential, slope and intercept of i_p vs $v^{1/2}$ plot (Appendix C Figure C.8) and the calculated diffusion coefficient (solution containing 6.2 ± 0.4 M HBr, 1.1 ± 0.1 M HCl)

Content	$E^{o'}$ (V)	slope	intercept	V^{3+} Diffusion Coefficient D^o at 28°C (10^{-7} cm^2/s)
1.67 M V(III)	-0.43	0.08	0.003	6.3
1.67 M V(III) + 0.15 M MEM + 0.47 M MEP	-0.43	0.07	0.0006	4.4
1.67 M V(III) + 0.15 M MEM + 0.65 M MEP	-0.44	0.05	0.002	2.6
1.67 M V(III) + 0.15 M MEM + 0.83 M MEP	-0.44	0.05	9×10^{-4}	2.6
1.67 M V(III) + 0.49 M MEM + 0.16 M MEP	-0.43	0.08	-0.004	6.3
1.67 M V(III) + 0.66 M MEM + 0.16 M MEP	-0.43	0.05	0.001	2.3
1.67 M V(III) + 0.86 M MEM + 0.16 M MEP	-0.46	0.05	0.003	2.3

Table 5.12 Slope and intercept of $\ln(i_p)$ vs $(E_p - E^{o'})$ plot (Appendix C Figure C.11) and the calculated transfer coefficient and heterogenous rate constant (solution containing 6.2 ± 0.4 M HBr, 1.1 ± 0.1 M HCl)

Content	slope	Intercept	α	k^o (10^{-4}) cms^{-1}
1.67 M V(III)	-6.94	-5.01	0.18	1.23
1.67 M V(III) + 0.15 M MEM + 0.47 M MEP	-7.15	-6.09	0.18	0.42
1.67 M V(III) + 0.15 M MEM + 0.65 M MEP	-3.73	-5.07	0.10	1.16
1.67 M V(III) + 0.15 M MEM + 0.83 M MEP	-4.64	-5.47	0.12	0.78
1.67 M V(III) + 0.49 M MEM + 0.16 M MEP	-6.43	-5.78	0.17	0.57
1.67 M V(III) + 0.66 M MEM + 0.16 M MEP	-4.82	-5.48	0.12	0.77
1.67 M V(III) + 0.86 M MEM + 0.16 M MEP	-4.60	-5.18	0.12	1.04

Table 5.13 Comparison of diffusion coefficient of V(III) calculated by experimental transfer coefficient with assumption of $\alpha = 0.5$ (solution containing 6.2 ± 0.4 M HBr, 1.1 ± 0.1 M HCl)

Content	QBr (M)	D^o ($\alpha = 0.5$) (10^{-7} cm^2/s)	α	D^o (10^{-6} cm^2/s)
1.67 M V(III)	0	6.3	0.18	1.76
1.67 M V(III) + 0.15 M MEM + 0.47 M MEP	0.62	4.4	0.18	1.21
1.67 M V(III) + 0.15 M MEM + 0.65 M MEP	0.79	2.6	0.10	1.29
1.67 M V(III) + 0.15 M MEM + 0.83 M MEP	0.97	2.6	0.12	1.07
1.67 M V(III) + 0.49 M MEM + 0.16 M MEP	0.65	6.3	0.17	1.72
1.67 M V(III) + 0.66 M MEM + 0.16 M MEP	0.82	2.3	0.12	0.97
1.67 M V(III) + 0.86 M MEM + 0.16 M MEP	1.01	2.3	0.12	0.95

In Table 5.11 it is shown that there is a reduction in V^{3+} diffusion coefficient with increasing QBr concentrations. At low total QBr concentrations (0.6 M), the decrease in D^o caused by MEM is less than that caused by MEP addition. At higher QBr

concentration (0.8 M and 1.0 M), the increase in MEM concentrations has caused D^o to reduce more rapidly than the increase in MEP concentrations.

5.3.5 Summary of the use of QBr on V^{3+}/V^{2+} couple

The formal potential of V^{3+}/V^{2+} was found to be between -0.43 to -0.47 V (vs SCE), and the addition of MEM or MEP had caused minimal changes. The rate constants and formal potential remained constant after addition of QBr.

The diffusion coefficient and transfer coefficient were less affected by the addition of MEM in comparison with MEP at lower QBr concentration and showed a similar effect when the total QBr concentration was increased.

This confirms that the addition of MEM and MEP does not affect the electrochemical properties of the V^{3+}/V^{2+} couples and therefore these compounds can be used as bromine complexing agents in the V/Br redox flow cell electrolytes.

5.4 Electrochemical Studies on simulated positive electrolyte

From a previous study [54] the Br^-/Br_3^- couple is known to be the dominant redox reaction in the positive half cell of V/Br redox flow cell rather than the VO^{2+}/VO_2^+ couple occurs in a H_2SO_4 system. Linear voltammetry was performed in the positive potential range in the V/Br electrolyte to study the kinetics of the Br^-/Br_3^- couple. Solutions were found to have a highly resistive behaviour, as preliminary linear sweep voltammograms were found to be linear instead of the expected exponential current versus voltage feature. An iR correction was therefore needed for each voltammogram before any Tafel calculation could be performed. Cell resistances were estimated by

electrochemical impedance spectroscopy (EIS) and an equivalent circuit fit simulation. For each solution, EIS measurements were made prior to linear sweep voltammetry.

5.4.1 Impendence measurement of solution resistance

With a three electrode cell setup illustrated in Figure 4.2, EIS measurements were performed by sweeping frequency between 10 – 1 x 10^6 Hz at constant potential of 10 mV (vs SCE). The results are presented as Nyquist and Bode plots in Figure 5.11. By impedance software (ZView2, Solartron), each cell resistance was found as R_{cell} where the curve in Nyquist plot intersects with the real axis at high frequency (see section 3.4). Results of five samples containing various amounts of MEM and MEP are tabulated below (Table 5.14). The cell resistance showed a minor increase by the addition of MEM and MEP. Although the total concentrations of QBr has been maintained constant (0.75 M), by changing the ratio between MEM and MEP the cell resistance had fluctuated slightly, however, no major trend has been observed.

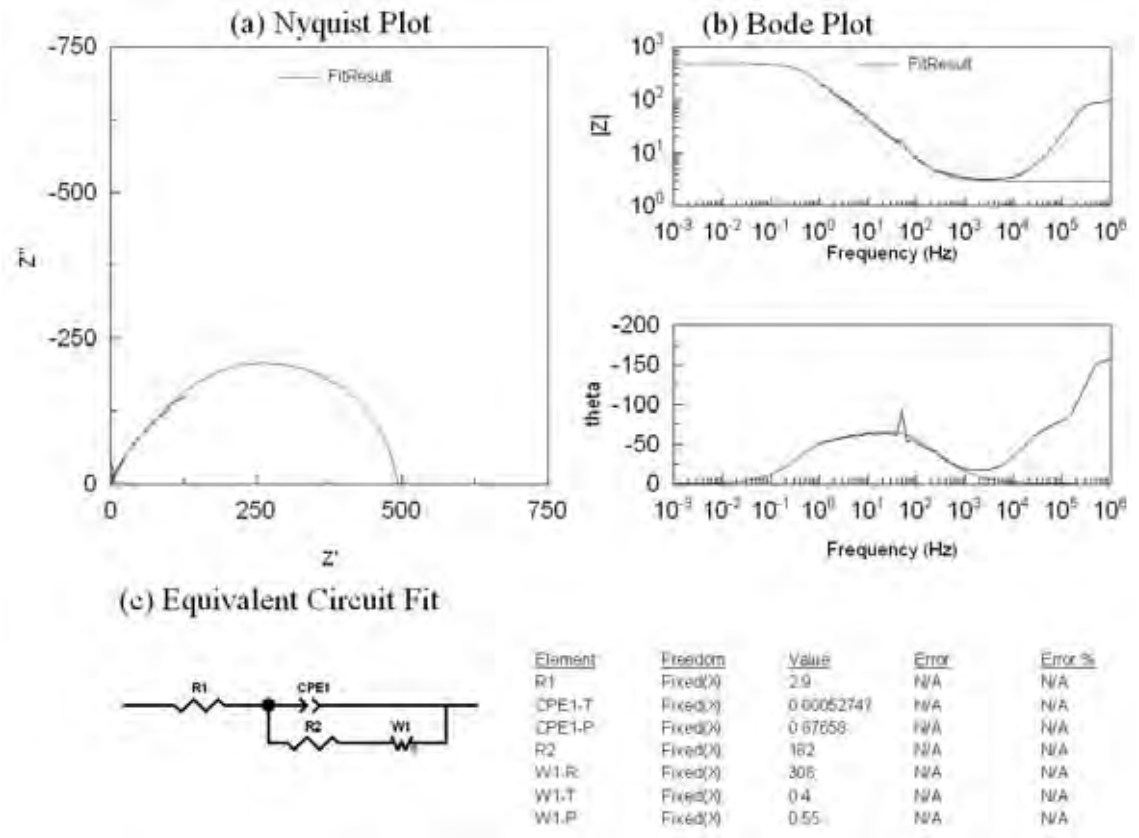

Figure 5.11 Typical results from circuit fit simulation (a) Nyquist Plot (b) Bode Plot (c) Equivalent Circuit Fit Model and results where R_{cell} is the cell resistance, in this case for 2 M V(IV) 6.1 M HBr 1.2 M HCl 0.2 M Br_2 0.19 M MEM 0.56 M MEP R_{cell} = 2.9 Ohms Electrode area = 0.28 cm^2

Table 5.14 Cell Resistance for samples of simulated positive half cell from EIS

V(IV) (M)	Br_2 (M)	MEM (M)	MEP (M)	HBr (M)	HCl (M)	Cell resistance (Ohms)	Cell resistance area (Ohms cm^2)
2	0.2	0.00	0.00	6.1	1.2	2.3	0.64
2	0.2	0.36	0.38	6.2	1.2	2.9	0.81
2	0.2	0.24	0.51	6.1	1.2	3.2	0.90
2	0.2	0.19	0.56	6.1	1.2	2.9	0.81
2	0.2	0.51	0.24	6.2	1.2	2.9	0.81
2	0.2	0.56	0.18	6.2	1.2	3.5	0.98

5.4.2 Linear sweep voltammograms of simulated positive solutions with iR correction

The cell resistance value was entered to the data modification function of CView program that automatically computes the iR correction for a selected curve. After the iR correction was applied, an exponential relationship between current density and

potential was found for a 2 M V(IV) 6.1 M HBr 1.2 M HCl 0.2 M Br_2 solution as seen in Figure 5.12. Then by the same method, i-E plot of solutions containing QBr are presented in Figure 5.13. By comparing the linear sweep voltammograms before and after the addition of QBr, Figure 5.13 showed that MEM and MEP had caused the slope to change and suggested the kinetics of the Br^-/Br^{3-} couple were significantly affected. This could have also resulted from the presence of vanadium ions however, linear sweep voltametric measurement of samples in the absence of vanadium species, were also conducted and are discussed later in this chapter (Chapter 5.5)

Linear sweep voltammograms at different scan rates showed similar features and are reported in Appendix D.

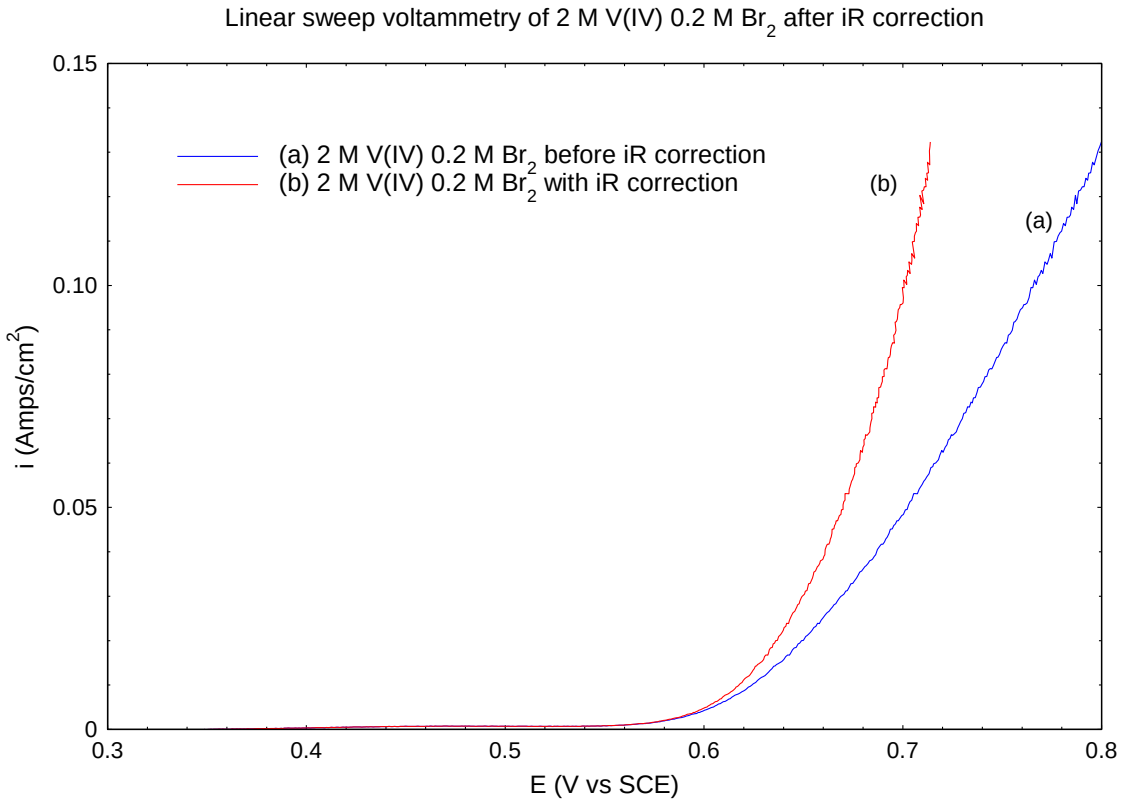

Figure 5.12 2 M V(IV) + 6.1 M HBr + 1.2 M HCl + 0.2 M Br_2 comparison with iR correction (a) original linear voltammogram (b) linear voltammogram with iR correction

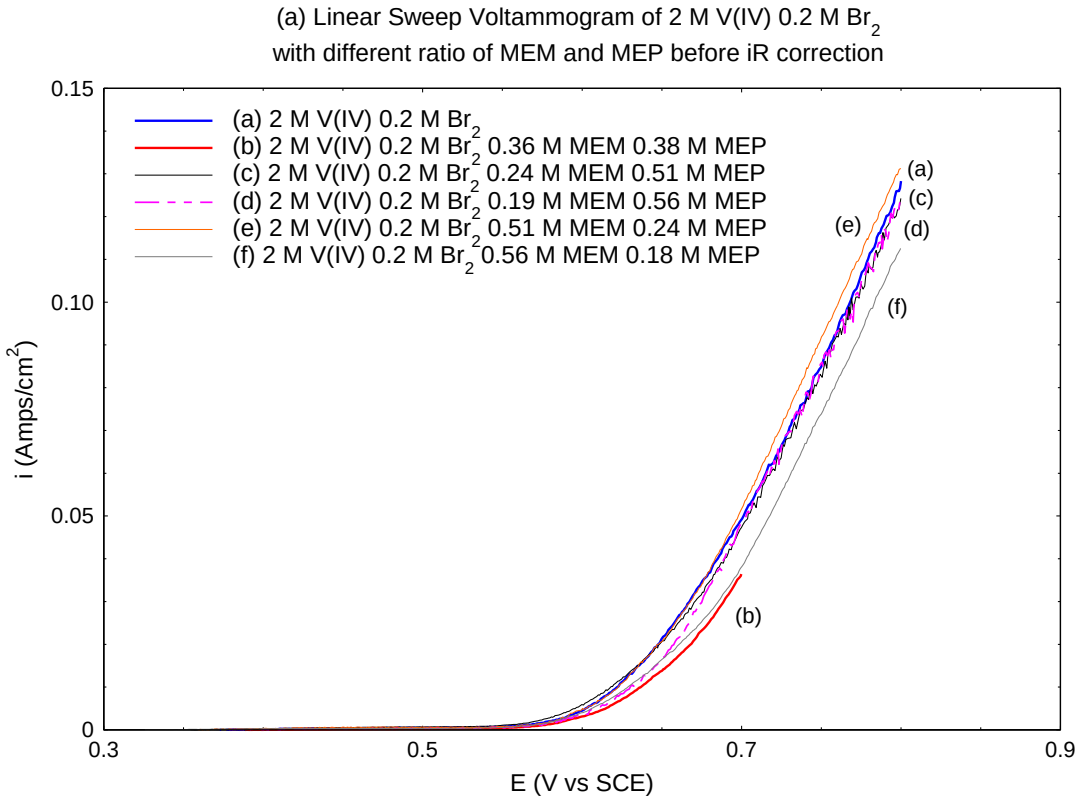

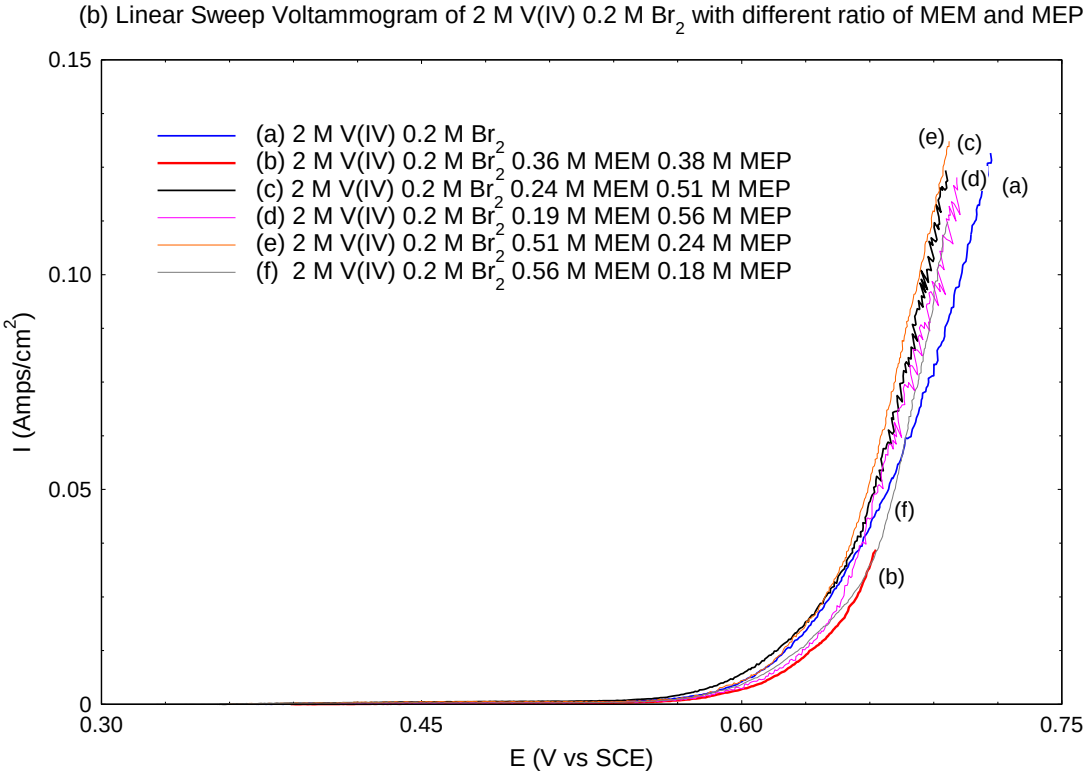

Figure 5.13 Linear sweep voltammograms of Br^-/Br_3^- reaction in 2 M V(IV), 6.1 ± 0.1 M HBr, 1.2 M HCl containing 0.75 M QBr (a) before and (b) after iR correction at 5 mVs^{-1}

5.5 Kinetic parameters of bromine/bromide in HBr, HCl on graphite electrode

Due to the complexity of Br^-/Br_3^- reaction in simulated positive electrolyte caused by possible interference from any V(IV) to V(V) reactions in the Br^- linear sweep voltammograms. Linear sweep voltammetry was also performed for samples containing similar bromine and bromide concentrations in the absence of vanadium species.

5.5.1 Bromine / bromide solution resistance

Cell resistance was obtained from impedance measurements using the same steps described above (5.4.1). Measurements were made with a graphite working electrode of 0.28 cm^2, and cell resistance values for each solution are presented in Table 5.15. Results showed that cell resistances in different supporting electrolytes were similar. However, the addition of MEM and MEP had increased the resistance slightly.

Table 5.15 Bromine / bromine solution resistance obtained by EIS measurements with 3 electrode cell (graphite working electrode A = 0.28cm^2, graphite counter electrode, SCE reference electrode)

Samples concentrations					Cell Resistances	
HBr (M)	HCl (M)	Br_2 (M)	MEM (M)	MEP (M)	R (Ohm)	R (Ohm cm^2)
6.2	0	0.2	0	0	1.3	0.36
6.2	0	1	0	0	1.35	0.38
6.2	1.2	0.2	0	0	1.36	0.38
6.2	1.2	1	0	0	1.35	0.38
6.2	1.2	0.2	0.19	0.56	1.5	0.42

5.5.2 Linear sweep voltammogram of bromine / bromide solutions

Linear sweep voltammograms were recorded at scan rates of 2, 3 and 5 mVs^{-1} for five bromine / bromide solutions with an upper potential limit of 1.1 V. iR correction was

applied to each linear sweep voltammogram using the corresponding solution resistance. Each voltammograms has an exponential feature, which is not affected by the charge of scan rates. Therefore, voltammogram with scan rate of 2 mVs^{-1} has been used for comparison and discussions while voltammograms with other scan rates is reported later in Appendix D.

5.5.2.1 Results of linear sweep voltammogram

Linear sweep voltammograms of five bromine / bromide solutions with scan rates of 2 mVs^{-1} has been superimposed in Figure 5.14. The graph showed the increase of bromine concentration and the addition of HCl has no major effect on the exponential curve feature. However, the addition of complexing agent had highly altered the curve at potentials above 0.8 V (vs SCE). In that region, the current density had nearly reduced by one third compared with the other solutions.

The potential range studied in Figure 5.14 is much larger than the previous voltammograms for V(IV) solutions (Figure 5.13), and this explains the significant increase in the measured current densities. Furthermore, the current density range studied here would be higher than that encountered during normal operation of the V/Br cell.

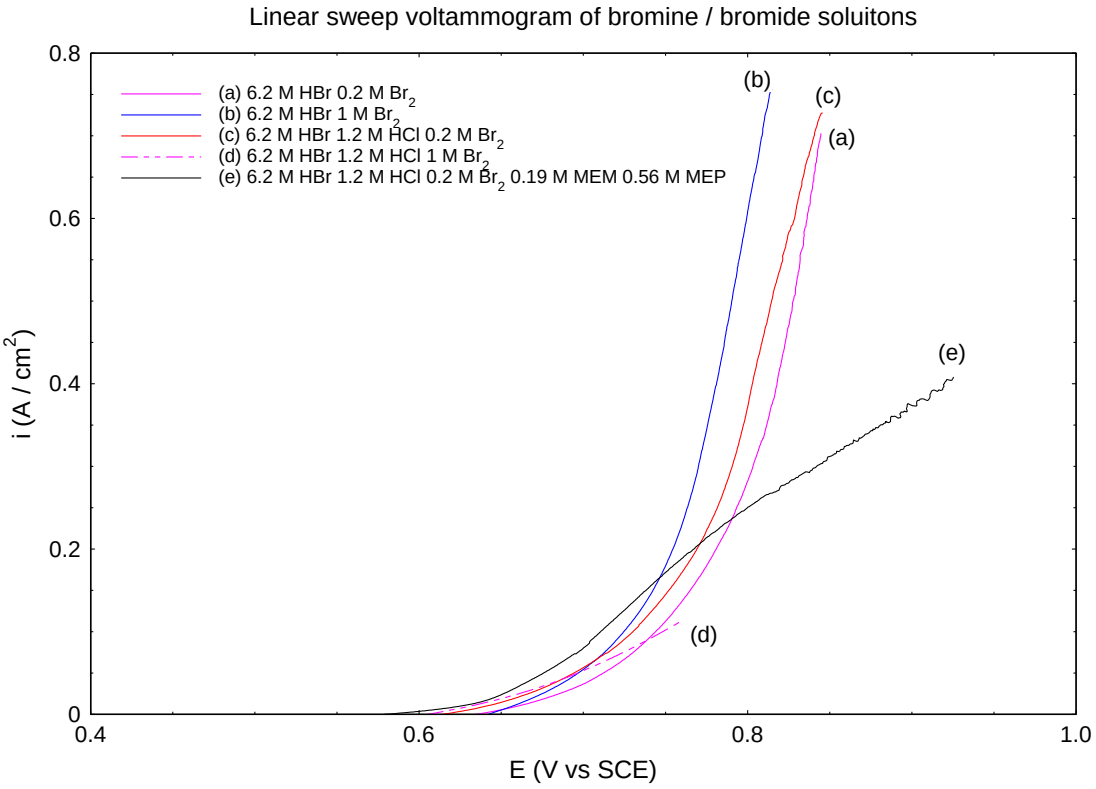

Figure 5.14 Linear sweep voltammogram at 2 $mVs^{-1}$for bromine / bromide solutions with iR correction

5.5.2.2 Effect of QBr addition

Besides the reduction of current density at high positive voltages, physical changes in the operation were observed during and after each oxidation sweep. Unlike samples that had no complexing agent, a layer of orange oil was formed on the surface of the working electrode after each oxidation sweep. Although the formation of orange oil was expected, the oil layer stayed on the working electrode instead of diffusing and mixing with the bulk solution. This oil adsorption might lead to two theories that caused the mass transport controlled region to appear in the linear voltammogram for samples with MEM and MEP.

The first hypothesis assumes that bromine reacts with complexing agent and formed small oil droplets dispersed on the surface of working electrode and lead to a reduction

in the effective surface area. When the effective surface area had been reduced this would logically reduce the current through the electrode. This matches with the observation in the linear voltammogram beyond 0.8 V (Figure 5.16).

In the second hypothesis it is assumed that the working electrode is entirely covered by the oily layer and this reduced the rate of bromide ion diffusion to the working electrode surface. The diffusion of bromide ions thus becomes the rate determining step in the bromide oxidation reaction giving rise to a limiting current as observed at high overvoltage.

In the literature there are a few electrochemical studies [111, 113, 114] on solutions containing bromine, bromide, and QBr. Two studies by Kautek et al [113, 114] reported the adsorption of MEM-Br_{ad} and MEP-Br_{ad} on glassy carbon and gold electrode. They reported an increase in MEM-Br_{ad} adsorption on glassy carbon from -1.6 V (vs saturated mercury sulphate electrode (MSE), +0.658 V vs SHE) until the oxidation of adsorbed bromide ions at 0.4 V (vs MSE). The adsorption of MEM-Br_{ad} is much stronger than that of the MEP-Br_{ad} ion pair due to the ether oxygen in the morpholinium molecule (Figure 2.8). Therefore, the major mechanism for the reaction between bromine, bromide and MEP^+ proceeds as a heterogeneous electron transfer from bromide ion followed by a homogenous reaction between bromine and dissolved MEP^+. The heterogeneous reaction of adsorbed MEM-Br_{ad} is a minor reaction (Ch3.5.2).

When the theory by Kautek et al [113, 114] is applied to our system, the MEM-Br_{ad} ion pair is adsorbed on the graphite working electrode until the oxidation of bromide ions at 0.7 V (vs SCE) in Figure 5.14. The electrochemically oxidised Br^- forms Br_2 that reacts with the dissolved MEP_{aq}^+ to form a non-aqueous organic bromine phase (MEP-Br_{3naq})

in the solution. Although the heterogenous reaction of adsorbed MEM-Br_{ad} is comparatively minor, it is the major route for the organic bromine formed on the electrode surface. Therefore, the organic bromine phase formed on the electrode surface will contain MEM-Br_{3naq} as the dominant species. However, the reason for the current plateau above 0.8 V is still unclear and could be caused by either of both of the hypotheses mentioned or in a stepwise process.

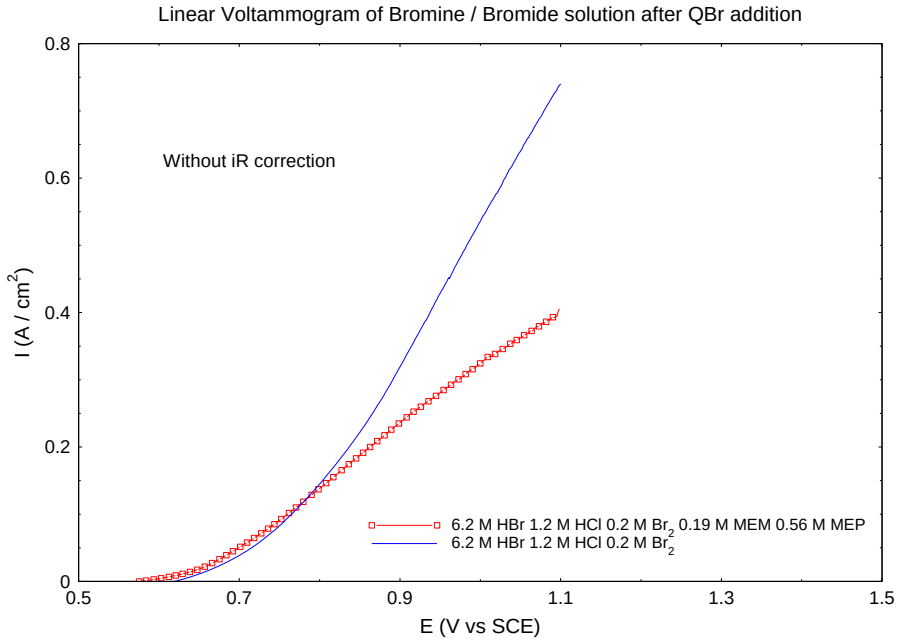

Figure 5.15 Comparison of linear sweep voltammogram of 6.2 M HBr + 1.2 M HCl + 0.2 M Br_2 after MEM and MEP addition (with out iR correction) at 2 mVs^{-1}

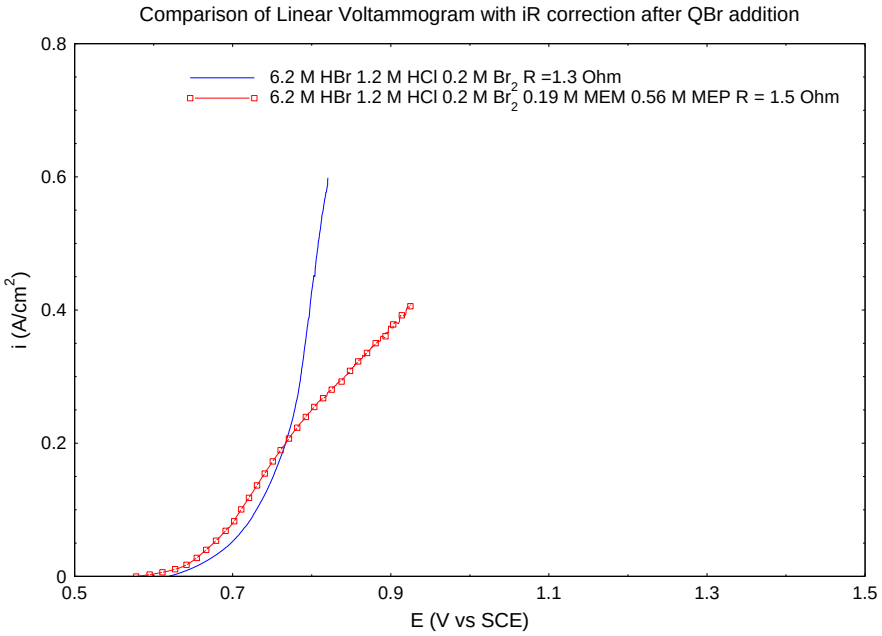

Figure 5.16 Effect of QBr addition on linear sweep voltammogram at 2 mVs^{-1} (after iR correction)

5.5.3 Open circuit potential

The measured open circuit potential (OCP) values of the bromine / bromide solutions (Table 5.16) were close to the theoretical values calculated with the equations suggested by Bell and Pring [93] (see Chapter 2 and Appendix E). In comparison, the OCP values reported in section 5.4.2 for 2 M V(IV) 0.2 M Br_2 solutions were much lower. The decrease in OCP is due to the contribution of the V(IV) ion to the solution potential.

Theoretically the reversible potential or OCP of a bromine / bromide solution will increase with increasing bromine concentration. However, measured OCP showed otherwise. First there is only a minimal change in the OCP with increasing bromine concentration in the same supporting electrolyte. Secondly, the OCP is reduced by HCl addition. The theoretical OCP of the solution in the presence of QBr is similar to the experimental value if 30% of bromine is assumed to be remained in the aqueous phase.

Table 5.16 Open circuit potential of various bromine bromide solutions

Sample	$E^o_{theoretical}$ * (V vs SCE)	E^o_{OCP} (V vs SCE)
6.2 M HBr 0.2 M Br_2	0.6392	0.6489
6.2 M HBr 1 M Br_2	0.6622	0.6497
6.2 M HBr 1.2 M HCl 0.2 M Br_2	0.6390	0.6370
6.2 M HBr 1.2 M HCl 1 M Br_2	0.6620	0.6209
6.2 M HBr 1.2 M HCl 0.2 M Br_2 0.19 M MEM 0.56 M MEP	0.6197^	0.6091
^ Assumed bromide in the QBr also contributed to $[Br^-]$ for calculation $[Br^-]_{total}$ = 6.868M . Assumed 30% of bromine remained in aqueous phase after equilibrium		

5.5.4 Kinetic parameters

Kinetic parameters of the bromine / bromide couple were determined from a Tafel plot for each linear sweep voltammogram at different scan rate. For solution containing 6.2 M HBr and 0.2 M Br_2, the linear voltammograms at 2, 3 and 5 mVs^{-1} are shown in Figure 5.17. Overpotential can then be calculated by subtracting OCP from measured potential, together with the measured current densities Tafel plots are constructed (Figure 5.18). From the slope and intercept of the linear region in the Tafel plot, the transfer coefficient (β) and equilibrium exchange current density (i_o) were found to be 0.49 and 0.013 Acm^{-2} respectively for a scan rate of 2 mVs^{-1}. In a similar manner, i_o and β of four other solutions were determined at various scan rates (Appendix D). Results at sweep rate of 2 mVs^{-1} are presented in Table 5.17.

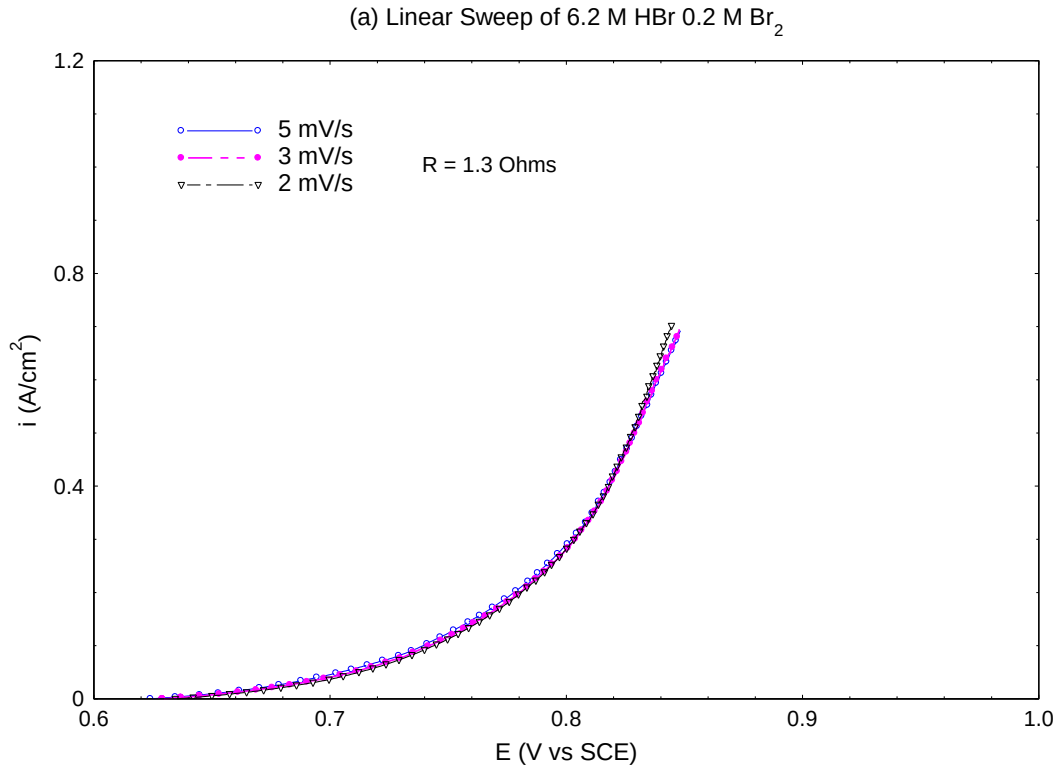

Figure 5.17 iR corrected linear sweep voltammogram of 6.2 M HBr 0.2 M Br_2 at scan rate of 2, 3 and 5 mVs^{-1}

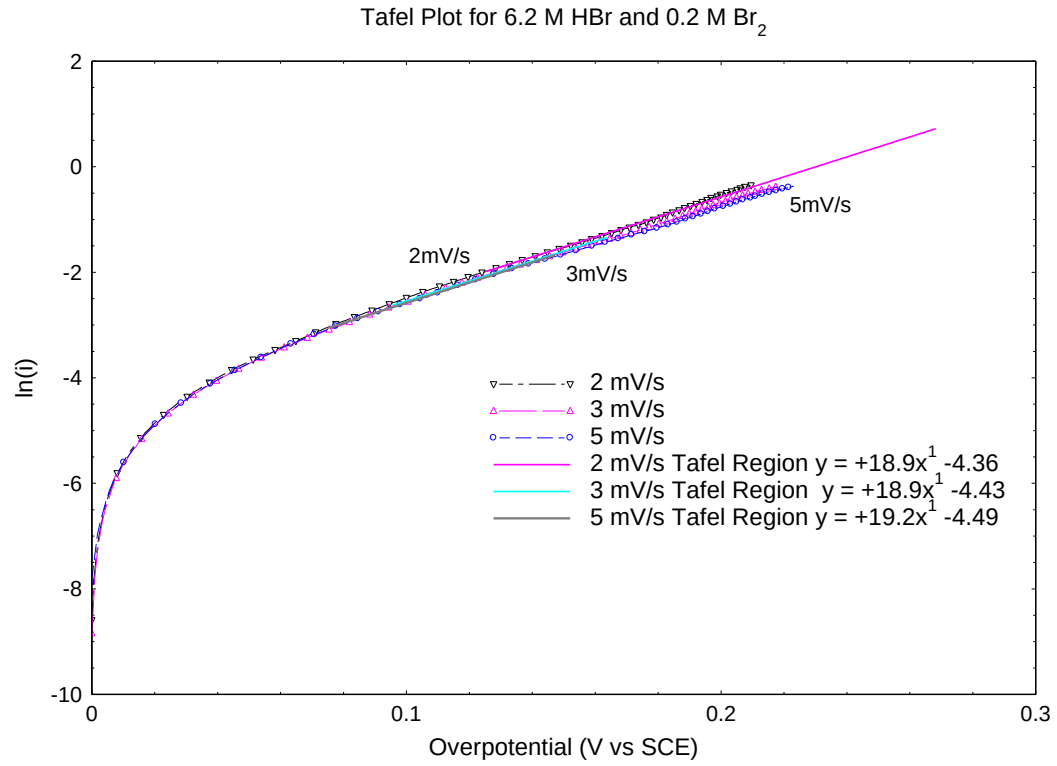

Figure 5.18 Tafel Plot for 6.2 M HBr and 0.2 M Br_2 at scan rate of 2, 3 and 5 mVs^{-1}

Table 5.17 Kinetic parameters of bromine / bromide couple from Tafel plots at linear sweep rate of 2 mVs^{-1}

Solution Concentrations					Electrochemical Parameters				
HBr (M)	HCl (M)	Br_2 (M)	MEM (M)	MEP (M)	E_{OCP} (V vs SCE)	Slope	Intercept	i_o (Acm^{-2})	α
6.2	0	0.2	0	0	0.64	18.9	-4.36	0.013	0.49
6.2	0	1	0	0	0.65	22.0	-4.00	0.018	0.56
6.2	1.2	0.2	0	0	0.61	19.6	-4.48	0.012	0.50
6.2	1.2	1	0	0	0.61	17.4	-4.60	0.010	0.45
6.2	1.2	0.2	0.19	056	0.58	17.1	-4.69	0.010	0.44

5.5.4.1 Comparison with theoretical i_o obtained by impedance measurement

In the literature, kinetic studies of Br_2/ Br^- solutions were made from equal molar of Br_2 / Br_3^- ions at low concentrations, where most studies used dropping mercury electrode as the working electrode. In order to observe the kinetics of simulated positive V/Br electrolyte, 6.2 M HBr has been used in the present study. In this study, the equilibrium exchange current densities obtained with the graphite electrode were lower than those obtained by impedance measurement reported in the literature. The transfer coefficients obtained are between 0.45 – 0.56 which are slightly higher than the literature values. These discrepancies could be due to different electrode surface roughness causing differences in effective surface area.

Table 5.18 Kinetic parameters of Br_2/Br^- from the literatures

Br^- (M)	Br_2 (M)	Br_3^- (M)	α	i_o (A cm^{-2})	Ref
0.1	0.275	0.275	0.25 – 0.5	0.033	[89]
0.1	0.01	0.01	0.25 -0.5	0.017	[89]
0.005 -1	0.5	0.001	0.24	0.024	[86]
0.5	0.27	Did not considered	0.3 -0.45	0.005	[125]

5.5.4.2 Effect of different supporting electrolyte

Tafel plots for supporting electrolytes with and without HCl showed a similar linear region at overpotential between 0.1 – 0.2 V (Figure 5.19). Both Tafel curves deviate sharply from linearity at low overpotential $\eta < 0.1V$ as expected and reached a deviation caused by mass transfer at large overpotentials $\eta > 0.2$ V. There is no major difference in the Tafel plot for samples containing 0.2 M Br_2 added to both supporting electrolytes (Figure 5.19). A deviation becomes apparent when the bromine concentration was increased to 1 M, in the presences of HCl (Figure 5.19). However, the deviation in Tafel plot has minimal impact on the calculated i_o and β, which is close to 0.01 Acm^{-2} and 0.5 Acm^{-2} respectively (Table 5.17).

5.5.4.3 Effect of QBr addition

For samples with the same supporting electrolyte and bromine concentration, the addition of MEM and MEP had reduced ln(i) in a Tafel plot and caused an extra hump to appear near $\eta = 0.08$ V (Figure 5.20). Tafel plots of the samples containing MEM and MEP deviated from linearity at overpotential $\eta > 0.16$ V as a result of mass transfer effects. The range of the Tafel region is much smaller in comparison with that obtained in the sample with no complexing agent. The addition of QBr only caused a marginal change on calculated i_o and β. Also, the plateau region that appeared at large overpotential is likely to be caused by mass transfer effects. Again this suggested the formation of bromine had reacted with MEM and MEP on the surface of the working electrode, and this organic layer causes the Tafel plot to show a mass transfer limited region at large overpotential.

5.5.4.4 Resistance Correction effect

Tafel plots of 6.2 M HBr and 0.2 M Br_2 with different iR correction factor showed that the kinetic parameter is highly affected by the cell resistance value used (Figure 5.21). From observation, the degree of coverage of the working electrode surface by organic bromine layer increases with increasing current. This could lead to an increase in cell resistance by increasing current. However, iR correction conducted in this study has assumed the measured cell resistance to be constant. Therefore, this could lead to discrepancies in the results reported.

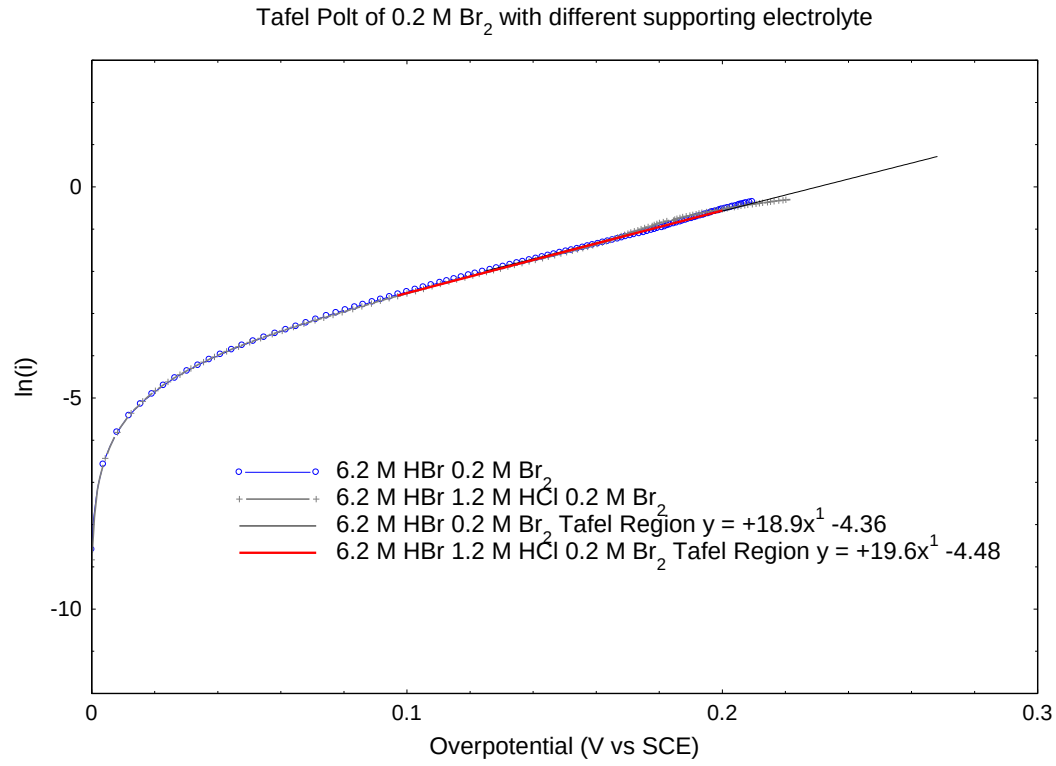

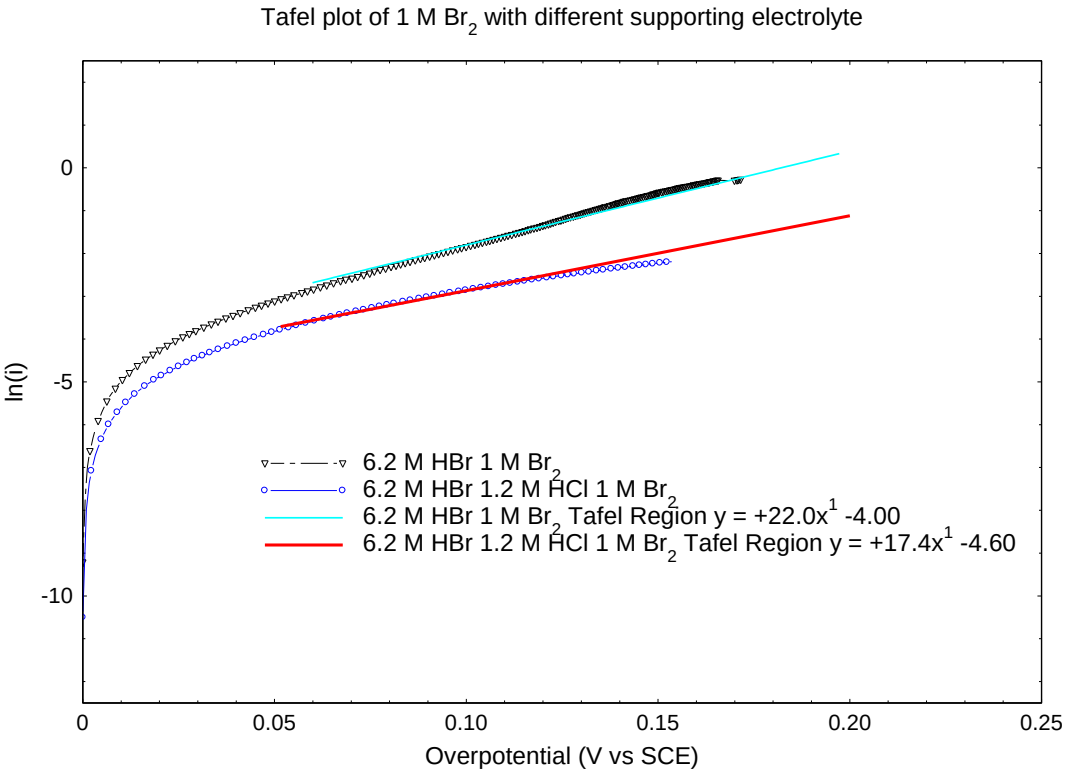

Figure 5.19 Tafel plots from iR-corrected Linear sweep voltammograms (top) 0.2 M Br_2 with 6.2 M HBr as supporting electrolyte at linear scan rate of 2 mVs^{-1} (bottom) 1 M Br_2 with 6.2 M HBr and 1.2 M HCl as supporting electrolyte at linear scan rate of 2 mVs^{-1}

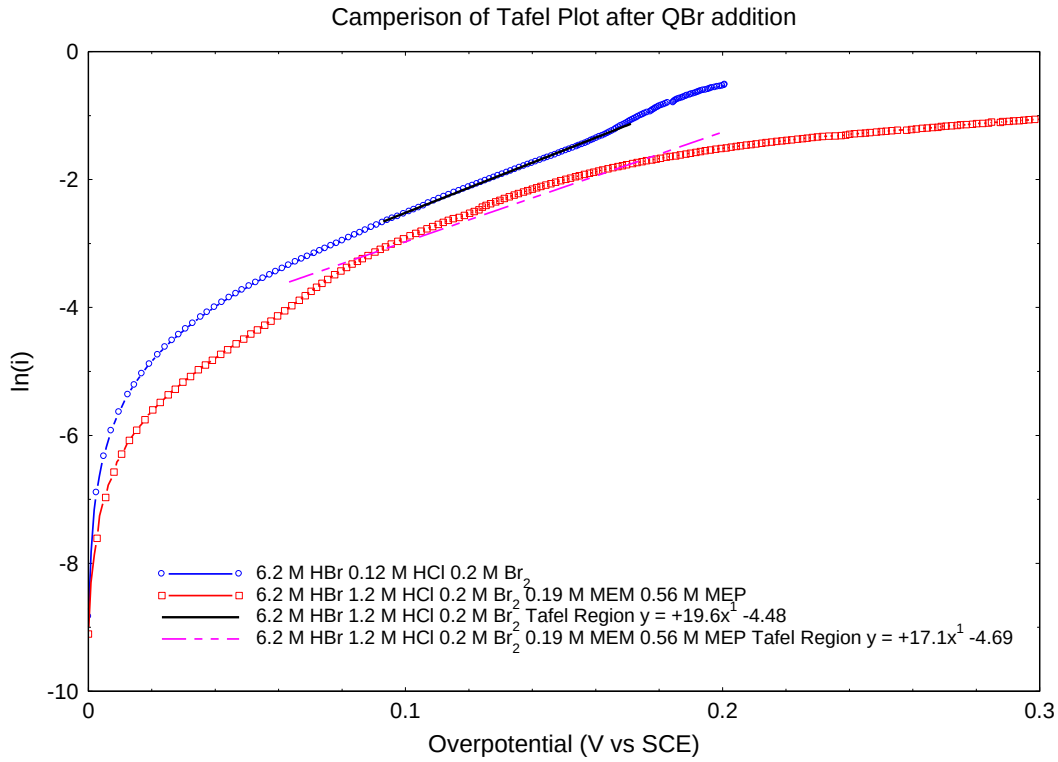

Figure 5.20 Tafel plot of 6.2 M HBr + 1.2 M HCl + 0.2 M Br after QBr addition obtained from iR-corrected Linear sweep voltammograms at scan rate of 2 mVs^{-1}

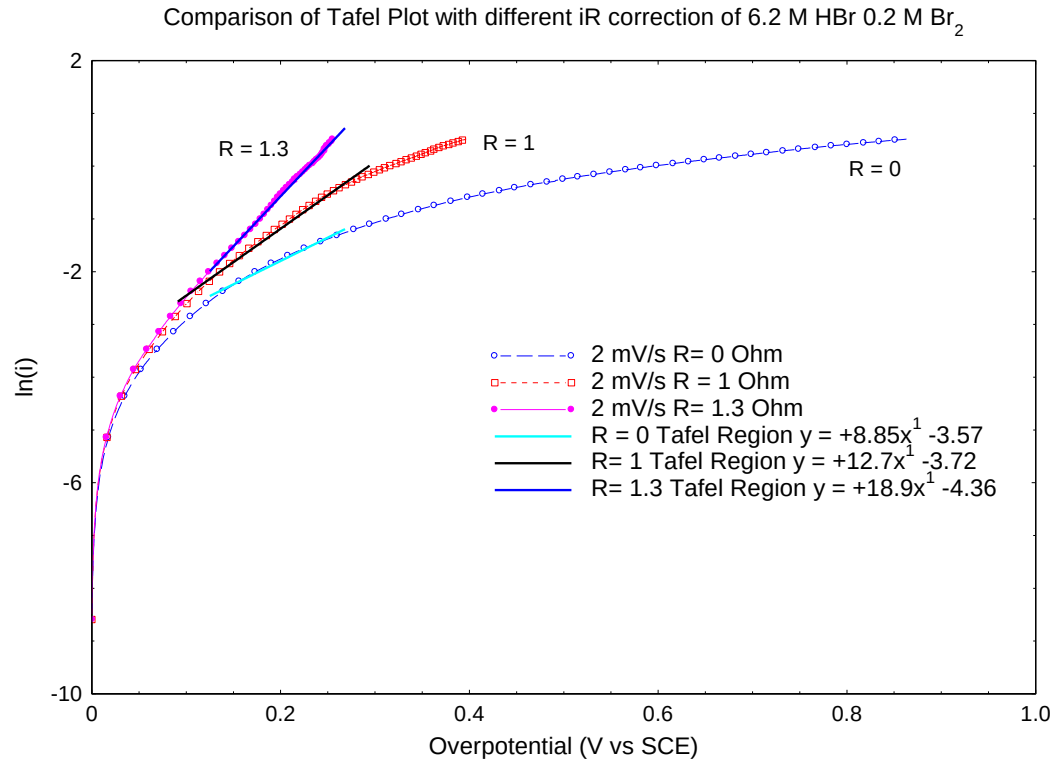

Figure 5.21 Comparison of Tafel plots of 6.2 M HBr + 0.2 M Br_2 at linear scan rate of 2 mVs^{-1} with different iR correction

Chapter 6 Performance of modified electrolytes in V/Br redox cell

6.0 Overview

The performance of the Vanadium bromide Redox Cell (V/Br) is reported in this chapter. The effect of complexing agent addition and temperature effect for static cell will be discussed. Current density and cell efficiency relationship is presented. Open circuit potential and Cell polarisation resistance of a lab scale flow cell is also reported.

6.1 Preliminary studies on membrane characteristics

Before the performance of a modified V/Br electrolyte could be evaluated in a redox flow cell, preliminary membrane studies were needed to identify a suitable membrane for use in the cell. These results are presented below.

6.1.1 Membrane treatment and wetability

Observations were made for the wetability of ChiNaf and VF11 membrane before and after their corresponding pre-treatment. For membranes without treatment, they were wet with distilled water prior to each test. The treatment for ChiNaf was heating in 5 M H_2SO_4 at 70^oC for 30 minutes and VF11 was soaked in 5 M H_2SO_4 at room temperature for 24 hours. Droplets of three solutions 2M $V^{3.7+}$, 2M $V^{3.7+}$ + 0.19M MEM + 0.56 M MEP and 2M $V^{3.7+}$ + 0.56 M MEM + 0.19M MEP were placed on the membranes. It was found that all solutions stayed as droplets on the surface of membranes for those

without treatment. After membrane treatments, both ChiNaf and VF11 allowed all three solutions to spread on the surface in a uniform manner. This showed the pre-treatment has converted the hydrophobic membranes to hydrophilic materials that could be used in the redox cell test.

6.1.2 Membrane Conductivity

The membrane conductivity of ChiNaf and VF11 was determined in V/Br electrolytes with and without complexing agent (MEM, MEP). Tests were carried out with the impendence techniques and utilised two constant surface area electrodes. The membrane area was set at 0.64 cm^2 and the membrane resistance for each membrane is determined from the difference in cell resistance with and without a membrane in place (section 4.5). Table 6.1 showed that the cell resistance increased after complexing agents were added, and ChiNaf had an area resistance nearly twice of that of the VF11 membrane in 2 M $V^{3.7+}$. After the addition of complexing agents membrane area resistance of VF11 and ChiNaf were 2.0 and 2.7 ohms cm^2 respectively, showing that the presence of MEM and MEP is somehow reducing the conductivity of each of the membranes.

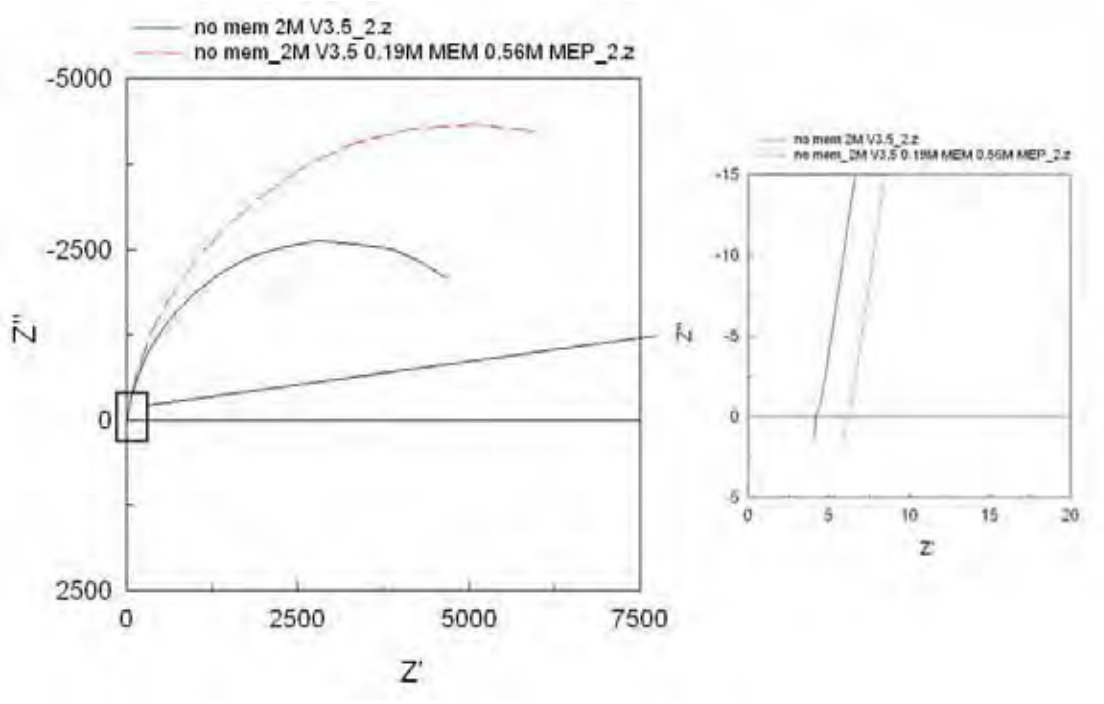

Figure 6.1 Nyquist Plot of Solution conductivity with EIS method

Table 6.1 Results of solution and membrane resistance summary

Electrolyte	Cell Resistance without membrane (Ohms)	Membrane	Cell resistance with membrane (Ohms)	Membrane resistance (Ohms)	Membrane area resistance (Ohms cm^2)
2 M $V^{3.7+}$	4.2	ChiNaf	5.5	1.3	1.3
		VF11	4.9	0.7	0.7
2 M $V^{3.7+}$ 0.19M MEM 0.56M MEP	6.1	ChiNaf	8.9	2.8	2.7
		VF11	8.1	2.0	2.0

6.2 Cell performance Calculations

6.2.1 Cell efficiency

Numerical integration by the trapezoidal method was used to calculate the coulombic (η_C), voltaic (η_V) and energy (η_E) efficiencies throughout this thesis. Based on the trapezoidal method, the integration equations can be written into Equation (6.1) to (6.3) as described by Vafiadis [124]. Measured data can be directly imported to the Excel file with embedded macro written by M. Lindsay, from which cell efficiencies for

consecutive charge and discharge cycles were determined. A step by step instruction is included in Appendix G

$$\eta_C = \frac{\sum_0^{m-1} \frac{1}{2}\left(I_j + I_{j+1}\right)\left(t_{j+1} - t_j\right)}{\sum_0^{n-1} \frac{1}{2}\left(I_k + I_{k+1}\right)\left(t_{k+1} - t_k\right)} \tag{6.1}$$

$$\eta_E = \frac{\sum_0^{m-1} \frac{1}{2}\left(V_j + V_{j+1}\right)\left(t_{j+1} - t_j\right)}{\sum_0^{n-1} \frac{1}{2}\left(V_k + V_{k+1}\right)\left(t_{k+1} - t_k\right)} \tag{6.2}$$

$$\eta_E = \eta_C \eta_V \tag{6.3}$$

6.3 V/Br cells without complexing agents

6.3.1 V/Br static cell without complexing agents

As discussed in the previous section, VF11 membrane has a lower membrane area resistance in $V^{3.7+}$ than ChiNaf. However, the cell efficiencies of each membrane had yet been considered. This section thus aims to determine the cell efficiencies of each cation exchange membrane in the vanadium bromide static cells without complexing agents. Comparisons were made for static cell efficiencies determined at room temperature (25^{o}C).

6.3.1.1 Static cell of 2 M $V^{3.7+}$ using VF11 membrane

Static cells were made with PVC frame of 3 mm thickness for experiments conducted both in the constant temperature chamber and at room temperature. Two 3 mm thick carbon felts (1.5 mm when compressed) with a surface area of 25 cm^2 containing

different amount of electrolytes were placed in each half-cell cavity. The membrane held between the two half-cells had a contact surface area of 25 cm^2. The experimental procedure for static cell assembly was described earlier (Chapter 4.4.2).

6.3.1.1.1 Cell efficiencies at room temperature (25^oC)

At room temperature (25^oC), a static cell was built with the VF11 membrane and two carbon felts soaked with 11 ml of 2 M $V^{3.7+}$ in each half-cell. The theoretical charging times for the first and consecutive cycles are 120.3 min and 70.8 min respectively. The charge / discharge diagram in Figure 6.2 showed the first cycle was not properly charged to 1.65 V due to equipment malfunction however, as the cell charging times of consecutive cycles were close to theoretical values, results from cycle 2 to 10 were considered to be valid for comparison. Average coulombic, voltaic and energy efficiencies from cycles 2 to 10 were 75.4 %, 79.6% and 60.0% respectively. They are also tabulated in Table 6.3. Detailed results of each cycle are reported in Appendix H.

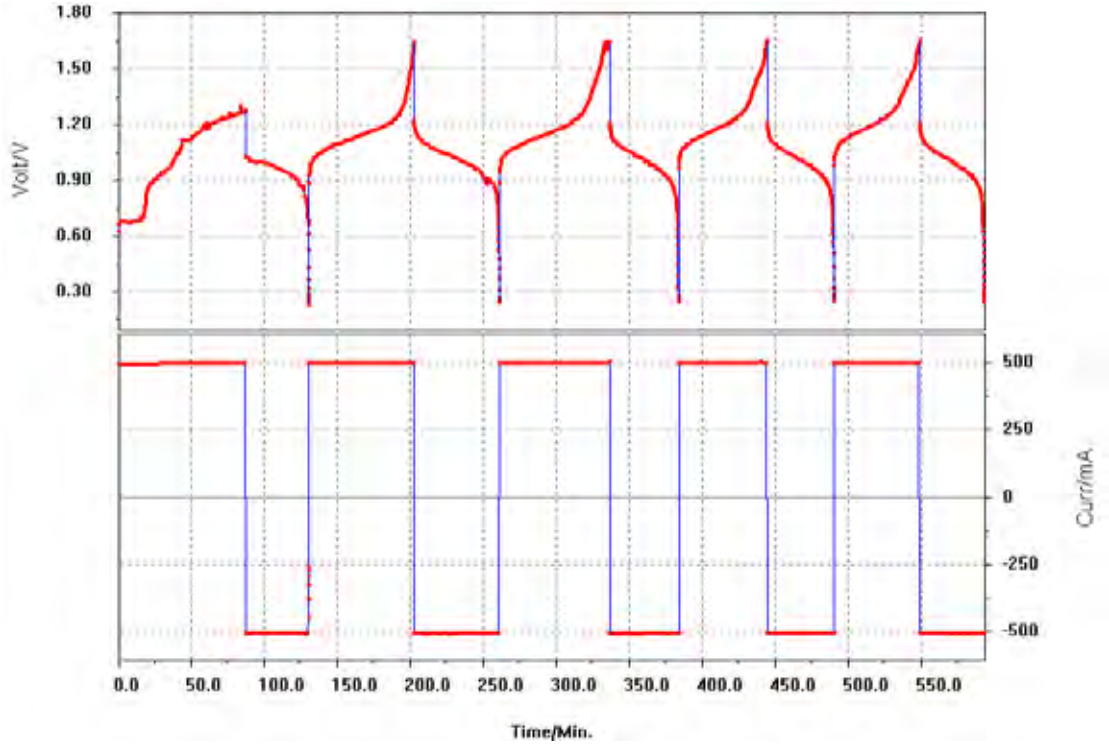

Figure 6.2 The first five charge / discharge cycles of static cell using VF11 membrane containing 11 ml of 2 M $V^{3.7+}$ 6.1 M HBr 1.2 M HCl in each half-cells at room temperature (25°C) (File: 11apr.cel)

6.3.1.1.2 Effect of various current densities and temperatures on cell efficiency

Another static cell using VF11 membrane was built from PVC frame with thickness of 3 mm and containing two carbon felts filled with 7 ml of 2 M $V^{3.7+}$ in each half-cell. The experiments were conducted in the constant temperature chamber. From this experiment, the effects of current density and temperature on cell efficiency were determined. The static cell was charged and discharged at constant current densities of 10, 20 and 40 $mAcm^{-2}$ consecutively. Charge-discharge tests were carried out at 10, 15, 25 and 35°C. A typical cell potential curve and the corresponding applied current are shown in Figure 6.3 for measurements at 25°C.

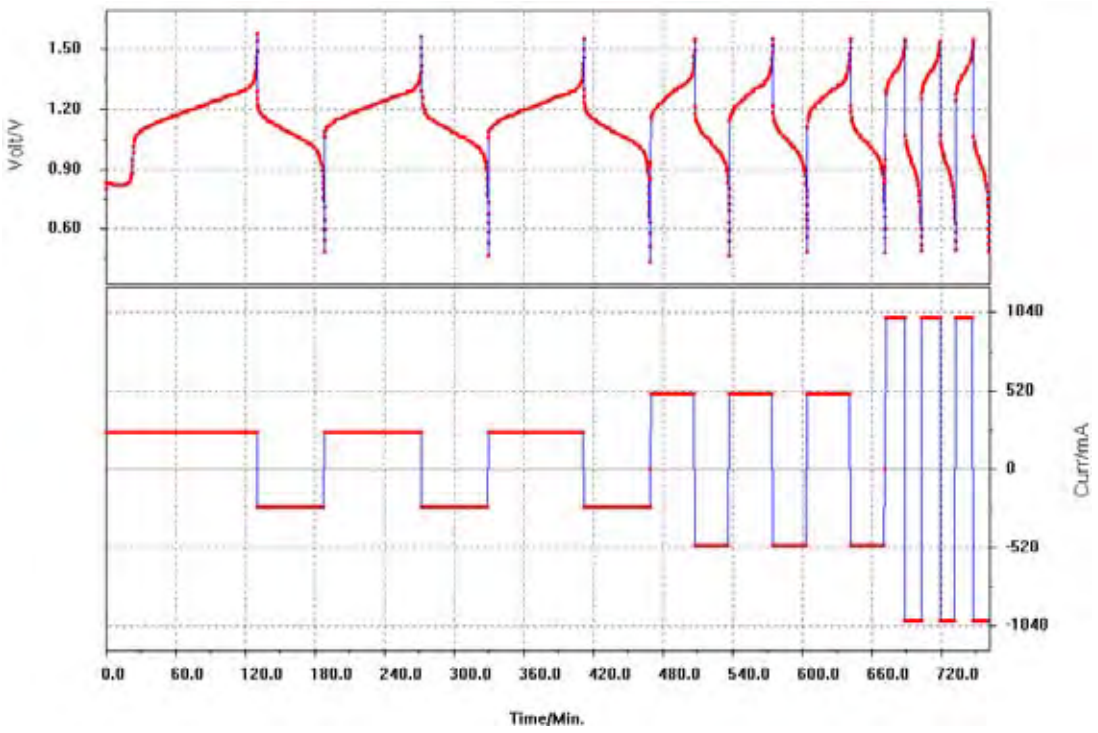

Figure 6.3 Cell potential of 2 M $V^{3.7+}$ + 7.6 M HBr + 1.46 M HCl (7 ml in each half-cell) static cell at 25°C with current densities of 10, 20 and 40 $mAcm^{-2}$ (File: T25_0329)

With the same method mentioned in 6.2.1, the average coulombic, voltaic and energy efficiencies were determined and summarised in Table 6.2. A combined graph (Figure 6.4) of coulombic, voltaic and energy efficiency for 2 M $V^{3.7+}$ at 25°C showed that the cell reached a highest energy efficiency of 63% at 20 $mAcm^{-2}$.

Cell efficiencies were plotted against current density for each temperature tested and these are presented in Figure 6.5 (a – c). Coulombic efficiency increased linearly with increasing current density, while voltaic efficiency followed an opposite trend. Because of the increase in iR drop, voltaic efficiency decreases linearly with current density. Energy efficiency is the product of coulombic and voltaic efficiency which can be seen as a parabolic curve in Figure 6.5(c).

The plots (Figure 6.5 (a – c)) also show the rise in temperature caused a decrease in coulombic efficiencies, while an opposite effect is observed in voltaic efficiencies. This

observation is similar to the all-vanadium flow cell. Therefore, the decrease in coulombic efficiency could be explained by the preferential vanadium ion transport through the cation membrane at higher temperatures [45], while the increase in voltaic efficiency is caused by the reduction in solution resistance and activation overvoltage for both half cells at higher temperatures [45].

Determined from the cell energy efficiency, the optimal operating temperature of 2 M $V^{3.7+}$ static cell would be at 25^{o}C. Also the energy efficiency curves of Figure 6.5 (c) show that the cell reached a maximum efficiency value at 20 mAcm^{-2}.

Table 6.2 Average Coulombic, Voltaic and Energy Efficiencies of static cell using VF11 membrane and containing 2 M $V^{3.7+}$ + 7.6 M HBr + 1.46 M HCl

Temp (^{o}C)	Current (mAcm^{-2})	Avg. C. Eff (%)	Avg. V. Eff (%)	Avg. E. Eff (%)
10	10	70.6	84.7	59.8
	20	80.0	73.2	58.6
	40	87.8	54.5	47.9
15	10	66.2	85.3	56.5
	20	77.2	74.3	57.3
	40	85.0	57.9	49.2
25	10	68.8	87.9	60.5
	20	79.8	79.1	63.1
	40	85.0	63.9	54.3
35	10	61.3	88.7	54.4
	20	75.8	79.9	60.6
	40	82.6	65.0	53.7

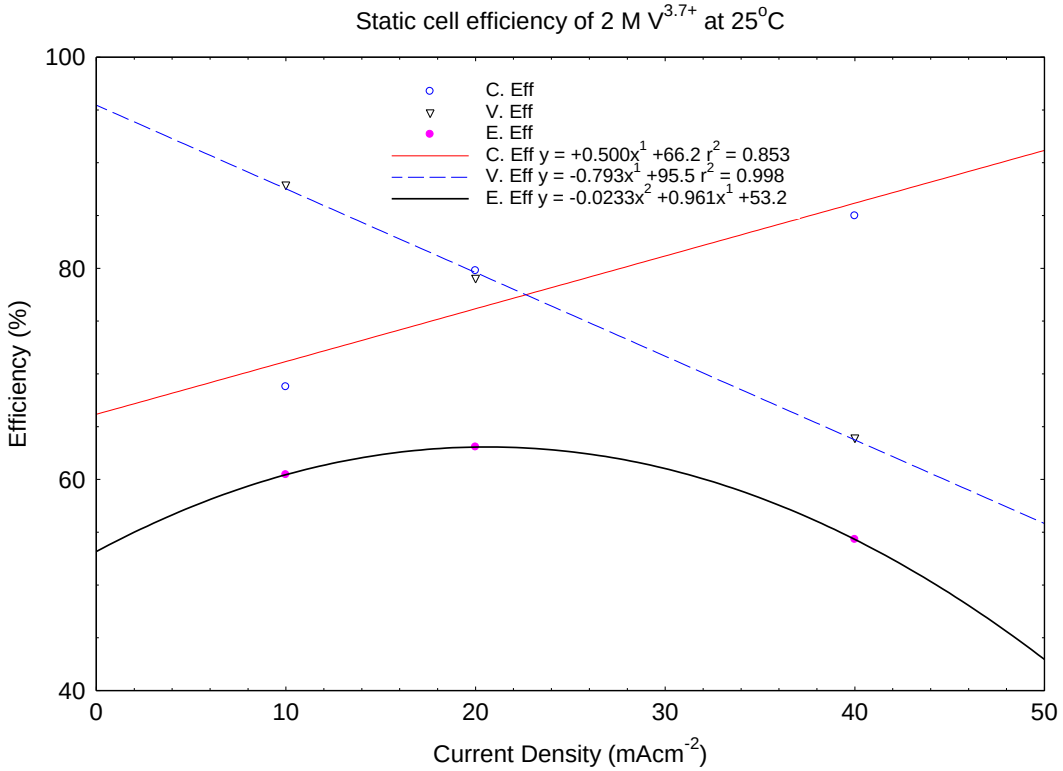

Figure 6.4 Coulombic, Voltaic and energy efficiency of 2 M $V^{3.7+}$ + 7.6 M HBr + 1.46 M HCl using VF11 membrane at 25°C

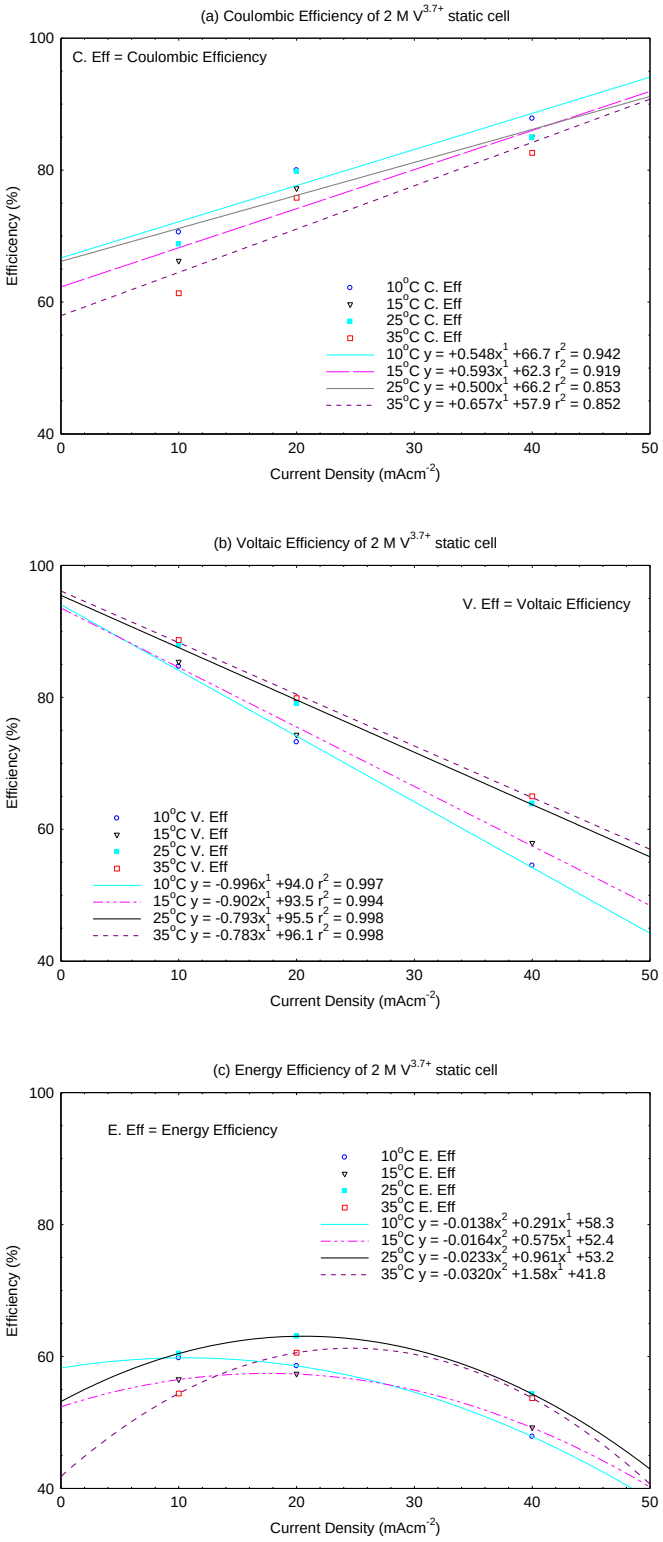

Figure 6.5 (a) Coulombic, (b) Voltaic and (c) Energy efficiency of 2 M $V^{3.7+}$ + 7.6 M HBr + 1.46 M HCl static cell using VF11 membrane at various temperature

6.3.1.2 Static cell of 2 M $V^{3.7+}$ using ChiNaf membrane

Experiments were also carried out at room temperature (25^{o}C) for 2 M $V^{3.7+}$ static cell using ChiNaf membrane. The static cell used a frame of 3 mm thickness and was filled with two 3 mm carbon felts (1.5 mm when compressed) that contained 8 ml 2 M $V^{3.7+}$ in each half-cell. The ChiNaf membrane held between the carbon felts has a contact area of 25 cm^2. This cell was charged and discharged at a constant current density of 20 $mAcm^{-2}$

The first and consecutive theoretical charging cycles (Figure 6.6) are 87.5 min and 51.5 min respectively. The theoretical reduction time of $V^{3.7+}$ to V^{3+} in the negative half cell is much longer than its oxidation to VO^{2+} in the positive half cell. This will lead to at least two apparent potential steps in the first charging cycle.

For clear comparison, the charge – discharge curves of the first two cycles are superimposed on the same time axis in Figure 6.7. The potential change that corresponds to each redox reaction was assigned according to the calculated theoretical time. In the first charging cycle (Figure 6.7), a clear potential step occurred at 13.9 min which is close to the theoretical time of VO^{2+} oxidation in the positive half cell. Then a minor step occurred at 25.3 min and can be assigned to the reduction of VO^{2+} to V^{3+} in the negative half cell. Finally a second sharp potential step before the cut-off potential resulted from the reduction of V^{3+} to V^{2+} in the negative half cell. During cell discharge, the oxidation of V^{2+} to V^{3+} would be the limiting reaction and hence a single potential step is observed. From the second cycle onwards, V^{3+} and Br^{-} would be the reactive redox species. Therefore, only one potential step occurs in subsequent charge and

discharge cycles. Theoretical and experimental times of each step for the first and second cycles are marked in Figure 6.7.

Since the cell potential versus time graph (Figure 6.6) showed a slight overcharge in the first two cycles, the voltage cut-off limit of the charging step was reduced to 1.55 V from the 3rd cycle onwards, while the discharge limit remained at 0.25 V. The average values of coulombic, voltaic, and energy efficiencies obtained from cycle 3 to 10 were calculated to be 85%, 79.2% and 68.5% respectively. All cell performance results and efficiencies of each cycle are reported in Appendix H.

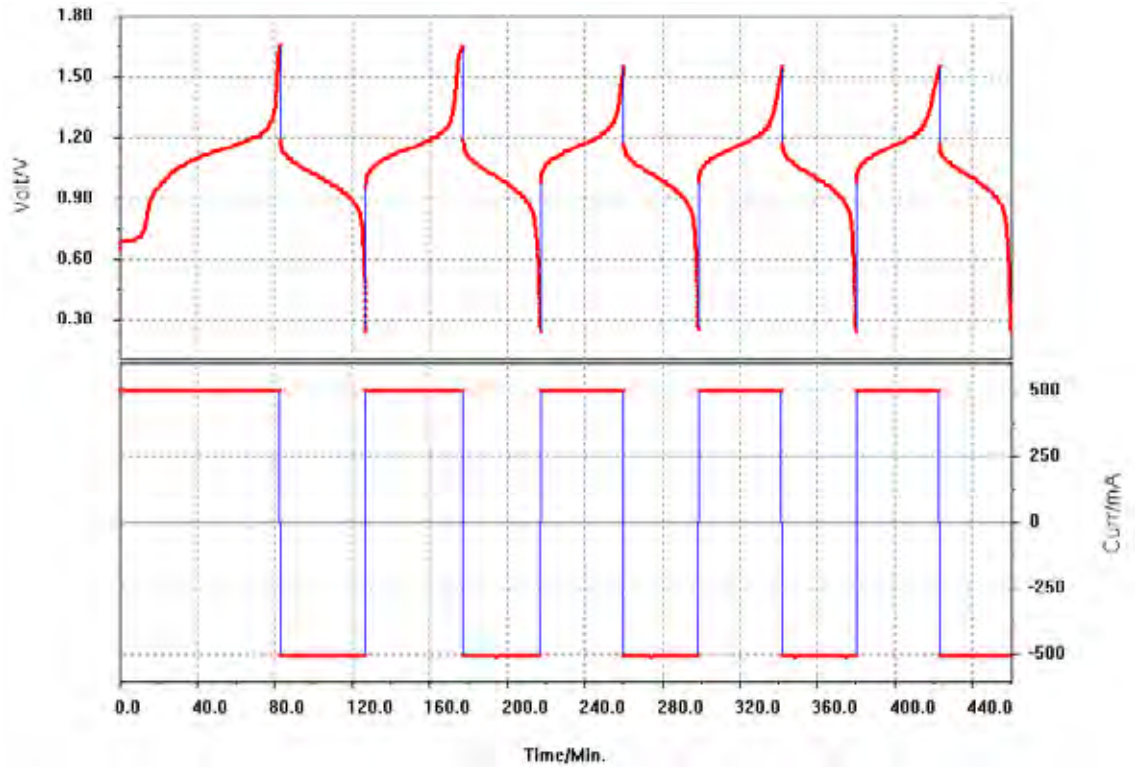

Figure 6.6 First five charge / discharge cycles of 2 M $V^{3.7+}$ (8 ml in each half-cells) using ChiNaf membrane at room temperature (25^{o}C) with charge-discharge current density of 20 mAcm^{-2} (File: 6aprsa.cel)

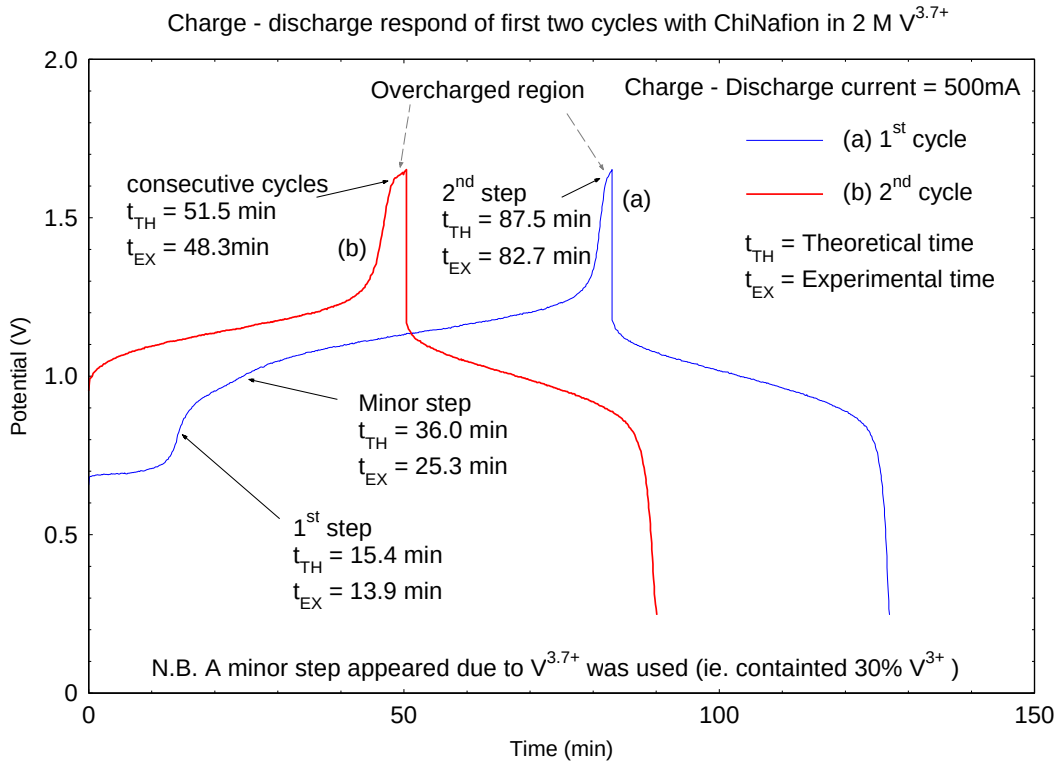

Figure 6.7 Charge – Discharge potential respond of first two cycles with ChiNaf in 2 M $V^{3.7+}$ + 7.6 M HBr + 1.46 M HCl when 20 $mAcm^{-2}$ constant charge – discharge current is applied

6.3.1.3 Comparison of 2 M $V^{3.7+}$ static cell using ChiNaf and VF11 membranes at room temperature

Static cell efficiencies obtained at room temperature (25^{o}C) from ChiNaf and VF11 membranes were compared for cycles with the same cut-off voltage limit. The charge and discharge response for cycle 2 of ChiNaf is superimposed on to the same graphs as the 2nd and 4th cycle of VF11 (Figure 6.8). Cell efficiencies for the corresponding cycles are labelled on the graph. It is observed that the voltaic efficiency obtained from VF11 membrane is higher than ChiNaf in cycle 2. Also, the voltaic efficiency only drops gradually with increasing number of cycles.

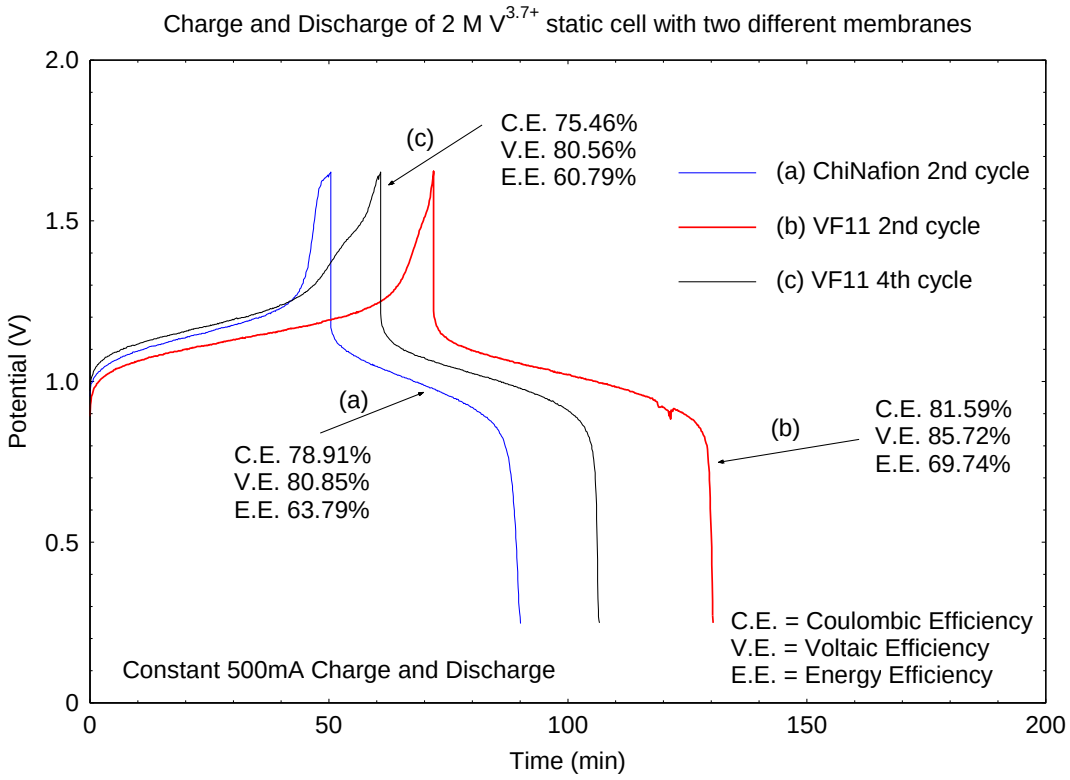

Figure 6.8 Charge and discharge respond of 2 M $V^{3.7+}$ static cell built with ChiNaf and VF11 at room temperature (25°C) and 20 $mAcm^{-2}$

Table 6.3 Efficiency of 2 M $V^{3.7+}$ static cell built with different membranes at 25°C

Membrane	Current Density ($mAcm^{-2}$)	Charge voltage limit (V)	No. of cycles for average calculations	Avg. C.E. (%)	Avg. V.E. (%)	Avg. E.E (%)
ChiNaf	20	1.55	8	86.5	79.2	68.5
VF11	20	1.65	9	75.4	79.6	60.0

The summarised data in Table 6.3 showed the average voltaic efficiencies are similar for both membranes but ChiNaf provided a higher average coulombic efficiency. This is because ChiNaf has a thickness of 50 microns while VF11 has a thickness of 25 microns. The thicker ChiNaf is better in separating the migration of electroactive species and therefore exhibits a higher coulombic efficiency. Therefore, ChiNaf appears to be a better option for use in the V/Br redox cell. Preliminary flow cell studies with this membrane are reported in Section 6.3.2.2.

6.3.2 V/Br flow cell without complexing agent

6.3.2.1 Flow cell with 2 M $V^{3.7+}$ using VF11 membrane

A flow cell (T10_1206) containing 2 M $V^{3.7+}$ + 7.6 M HBr + 1.46 M HCl without complexing agent was charged and discharged at constant current densities of 20 and 40 $mAcm^{-2}$ consecutively. The cell potential versus time curve is shown in Figure 6.9. The average coulombic, voltaic and energy efficiencies at 20 $mAcm^{-2}$ are 77.2%, 77.4% and 59.7% respectively. At 40 $mAcm^{-2}$, only two cycles was successful due to the low voltage cut-off limit. The coulombic, voltaic and energy efficiencies at 40 $mAcm^{-2}$ determined from the second cycle were 84.4%, 60.4% and 51.0% respectively.

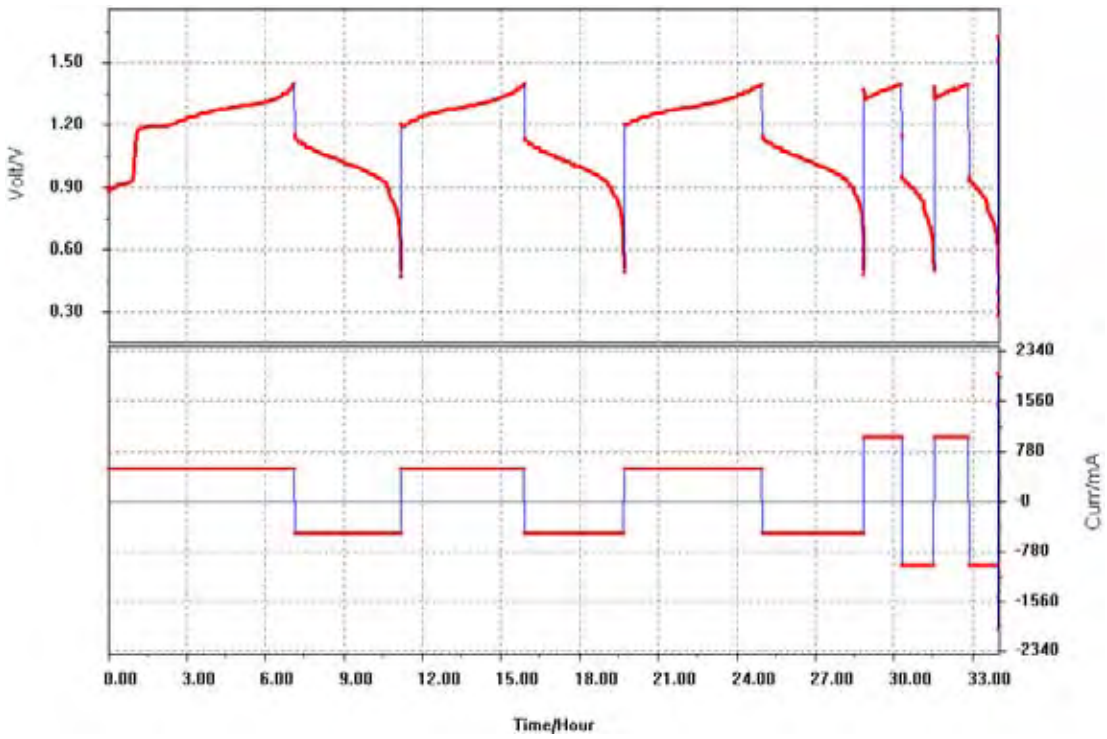

Figure 6.9 Cell potential of 2 M $V^{3.7+}$ + 7.6 M HBr + 1.46 M HCl (50 ml each half cell) using VF11 membrane at 10°C with charge-discharge current densities at 20 and 40 $mAcm^{-2}$(T10_1206.cel)

6.3.2.2 Flow cell with 2 M $V^{3.7+}$ using ChiNaf membrane

Several flow cells using ChiNaf membrane are built and tested to determine the effect of flow frame thickness, current densities and temperature on cell performance. The open circuit profile in a charge-discharge cycle of the flow cell with 2 M $V^{3.7+}$ + 7.6 M HBr + 1.46 M HCl using ChiNaf membrane is also observed.

6.3.2.2.1 The effect of flow frame thickness at room temperature (25^{o}C)

The flow-frame thickness was found to affect the coulombic and voltaic efficiencies of a flow cell using 2 M $V^{3.7+}$ + 7.6 M HBr + 1.46 M HCl electrolyte and ChiNaf membrane at 25^{o}C. For the flow cell with a 4.5 mm thick flow-frame, a large iR drop occurred throughout the charge-discharge cycles at 40 mAcm^{-2} (Figure 6.10). By comparison, the cell potential measured during charge-discharge cycling showed a lower iR drop when the flow-frame thickness is reduced to 3 mm (Figure 6.11). The average coulombic, voltaic and energy efficiencies of both flow cells are presented in Table 6.4. As expected the voltaic efficiency has increased with the reduction in flow-frame thickness. This flow-frame thickness was therefore used in all later flow cell studies.

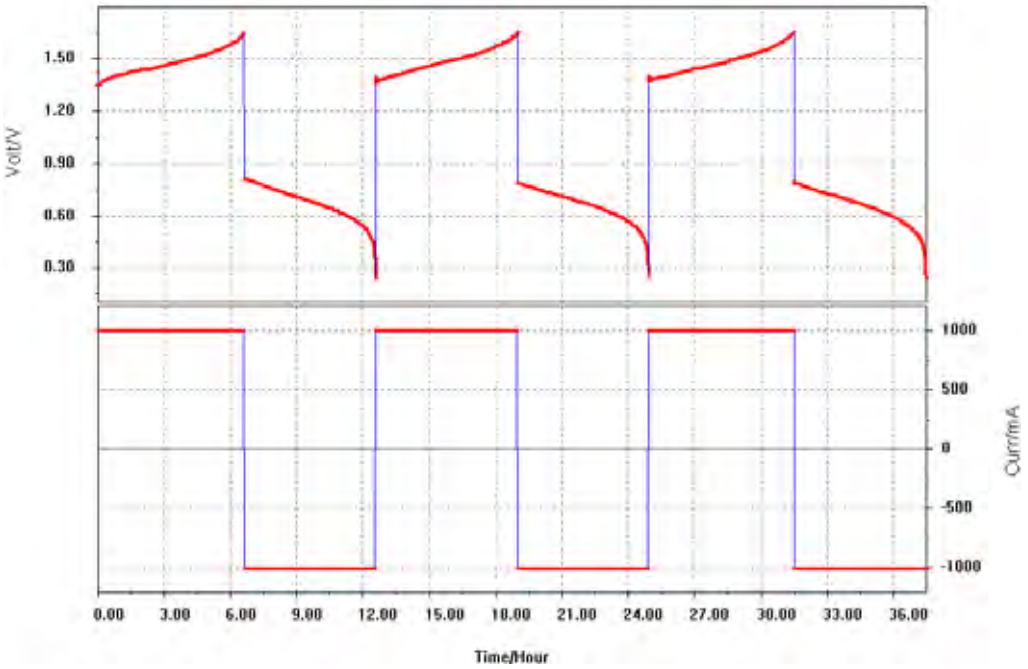

Figure 6.10 Charge / discharge cycles of 2 M $V^{3.7+}$ + 7.6 M HBr + 1.46 M HCl (100 ml each half cell) using ChiNaf membrane and 4.5 mm flow frame with charge-discharge current density of 40 $mAcm^{-2}$ at 25°C (30maycyc.cel)

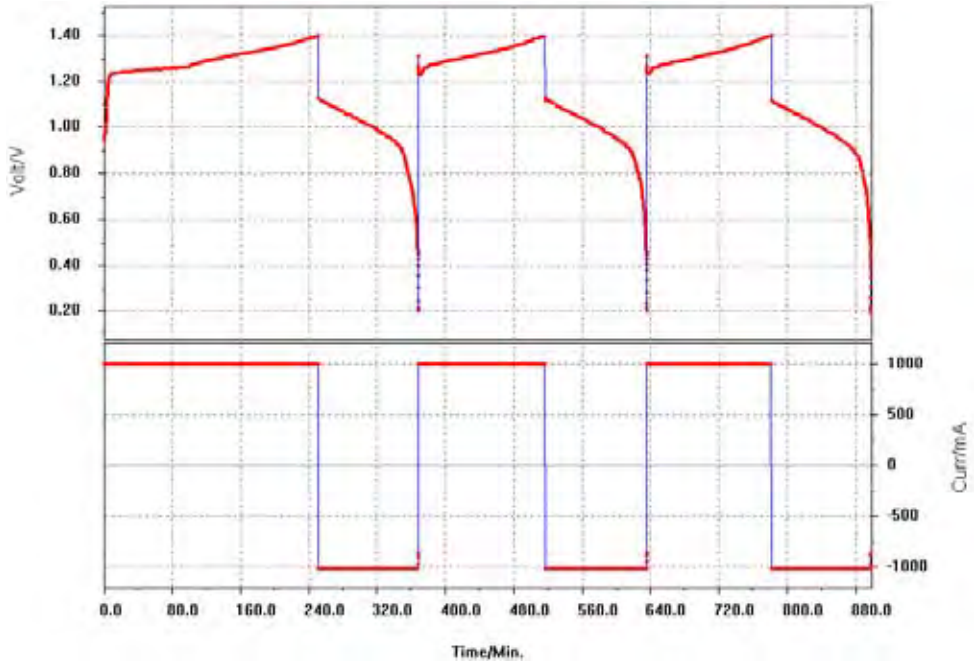

Figure 6.11 Charge / discharge cycles of 2 M $V^{3.7+}$ + 7.6 M HBr + 1.46 M HCl (50ml each half cell) using ChiNaf membrane and 3 mm flow-frame with charge-discharge current density of 40 $mAcm^{-2}$ at 25°C (CY061204.cel)

Table 6.4 Cell efficiencies of 2 M $V^{3.7+}$ + 7.6 M HBr + 1.46 M HCl flow cell using ChiNaf membrane with different flow-frame thickness at 25°C

Flow-frame thickness (mm)	Current Density ($mAcm^{-2}$)	Avg. C.E. (%)	Avg. V.E. (%)	Avg. E.E (%)
4.5	40	91.3	43.4	39.6
3	40	79.9	73.6	58.8

6.3.2.2.2 The effect of varying current densities and temperatures on cell performance

In this section the effect of changing current densities and temperatures on the cell performance of the 2 M $V^{3.7+}$ + 7.6 M HBr + 1.46 M HCl flow cell using ChiNaf membrane is studied. The performance of this flow cell was measured in the constant temperature chamber at 10 and 15°C. The flow cell was charged and discharged at constant current density of 20, 40, 60 and 80 $mAcm^{-2}$ at both temperatures.

Cell potential measurements at 10°C (Figure 6.12), showed significant fluctuations in coulombic efficiency at 80 $mAcm^{-2}$ (Appendix H.6) Therefore, the cell efficiency at 20, 40 and 60 $mAcm^{-2}$ were compared between 10 and 15°C (Figure 6.13). The plot of efficiencies versus current density again agrees with the trend of increase in coulombic efficiency and decrease in voltaic efficiency with increasing current density. At 10°C, the cell potential profile with charge-discharge current density of 40 $mAcm^{-2}$ (Figure 6.14) is similar to that obtained at 25°C (Figure 6.11), whereas the energy efficiency has been slightly reduced (Table 6.5). The polarisation curves of a vanadium bromide flow cell at 10°C were found to be linear (Figure 6.15). From the slopes, polarisation resistance for the charge and discharge of V/Br flow cell at 10°C were found to be 3.9 and 3.6 Ωcm^2 respectively. This is different from the all vanadium flow cells, which has a polarisation resistance that is lower during charge cycle than that of the discharge cycle at 23°C, being 4.5 Ωcm^2 and 5.4 Ωcm^2 respectively [45].

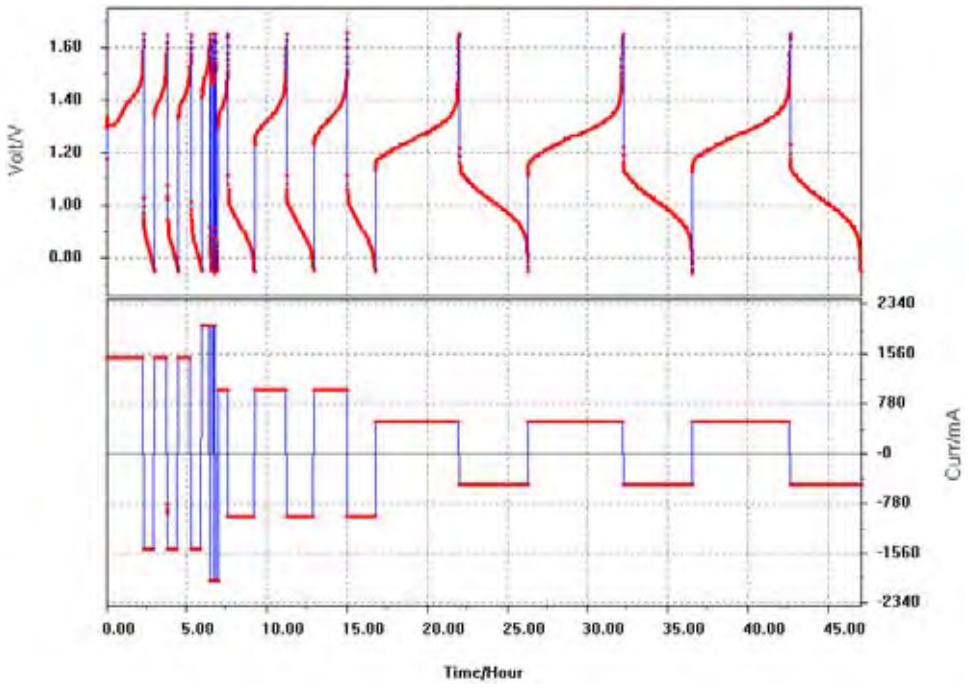

Figure 6.12 Charge / discharge cycles of 2 M $V^{3.7+}$ + 7.6 M HBr + 1.46 M HCl (50 ml each half cell) using ChiNaf membrane with charge-discharge current densities of at 20, 40 and 60 $mAcm^{-2}$ at 10°C (T10_0221.cel)

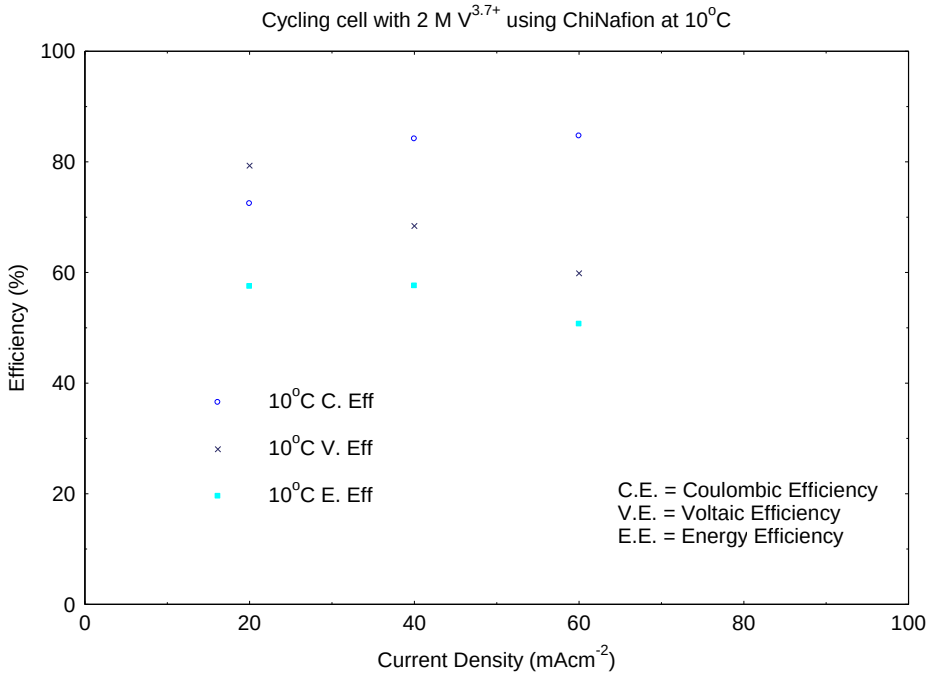

Figure 6.13 Coulombic, Voltaic and energy efficiency of 2 M $V^{3.7+}$ + 7.6 M HBr + 1.46 M HCl flow cell at 10°C using ChiNaf membrane with charge-discharge current densities of at 20, 40 and 60 $mAcm^{-2}$

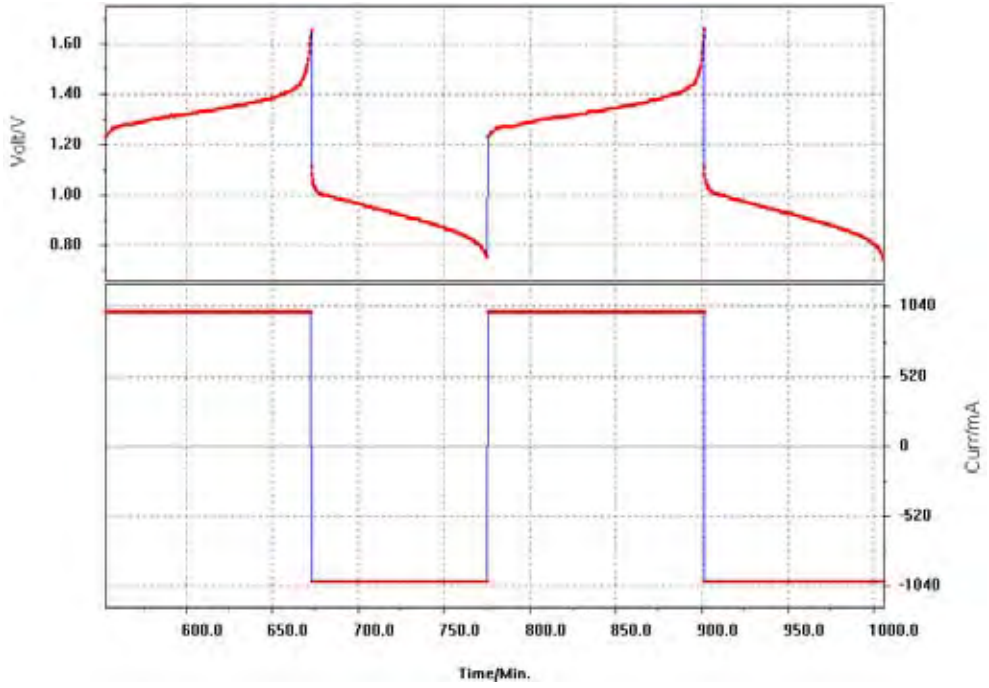

Figure 6.14 Charge / discharge cycles of 2 M $V^{3.7+}$ + 7.6 M HBr + 1.46 M HCl (50ml each half cell) using ChiNaf membrane with charge-discharge current density of 40 $mAcm^{-2}$ at 10°C (cycle 8 and 9 of T10_0221.cel)

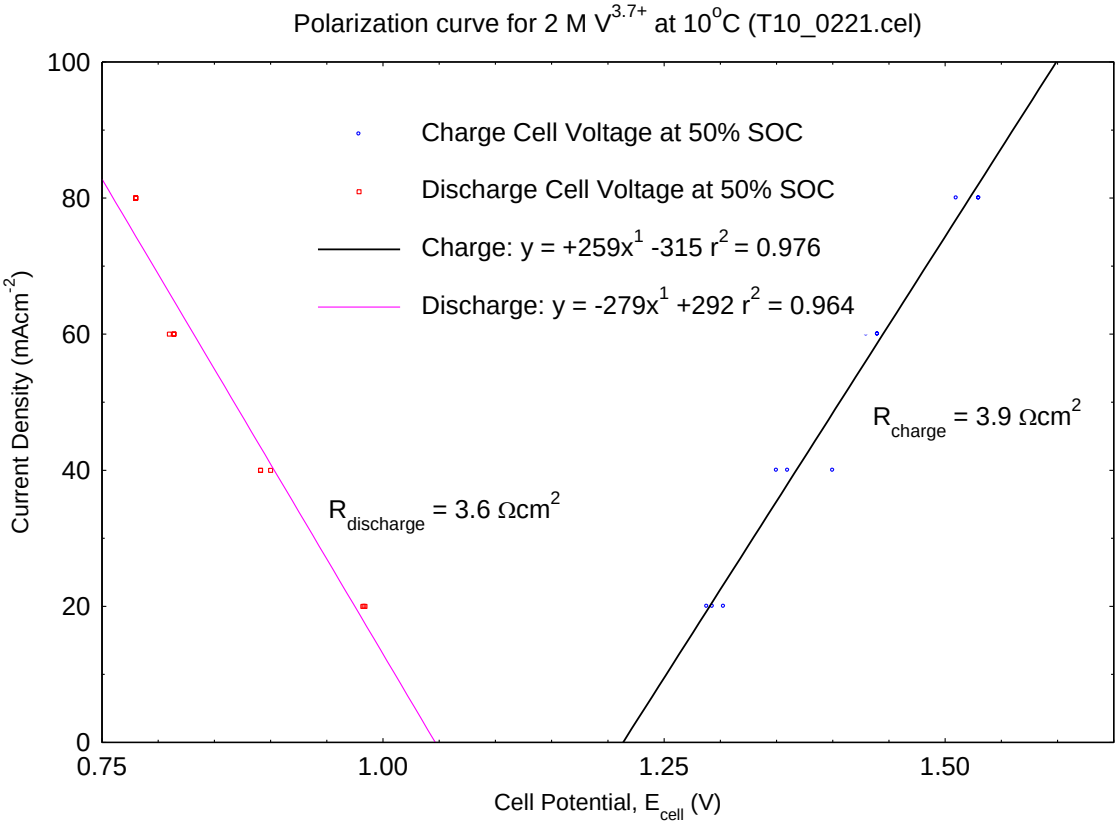

Figure 6.15 Polarization curve for 2 M $V^{3.7+}$ + 7.6 M HBr + 1.46 M HCl flow cell at 10°C using ChiNaf membrane (T10_0221.cel)

Figure 6.16 showed that the cell potential versus time profile of the same flow cell operated at 15^{o}C in the constant temperature chamber, and was charge-discharge at constant current densities of 20, 40, 60 and 80 mAcm^{-2}. Since an abnormal discharge potential occurred in the 2nd cycle at 80 mAcm^{-2} and a shortened discharge time in the 3rd cycle, the cell efficiencies obtained after that cycle were not considered for comparisons. As shown in Table 6.5, results obtained at 60 mAcm^{-2} showed a decrease in coulombic efficiency whereas voltaic efficiency increased when temperature increased from 10 to 15^{o}C, as expected.

Table 6.5 Cell efficiencies of 2 M $V^{3.7+}$ + 7.6 HBr + 1.46 M HCl flow cell at different temperatures and charge-discharge current density

Temperature (^{o}C)	Current Density (mAcm^{-2})	Avg. C.E. (%)	Avg. V.E. (%)	Avg. E.E (%)
10	20	72.5	79.3	57.5
10	40	84.2	68.4	57.6
10	60	84.7	59.9	50.7
15	60	84.5	60.6	51.2
25 (Room Temperature)	40	79.9	73.6	58.8

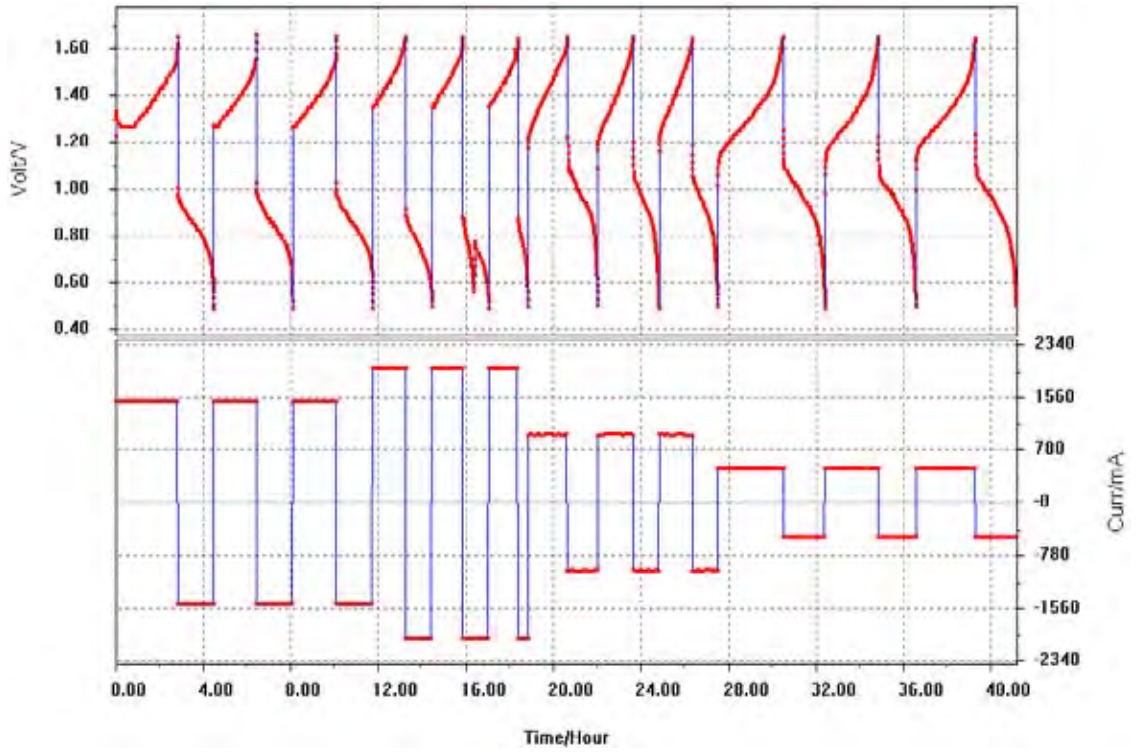

Figure 6.16 Charge / discharge cycles of 2 M $V^{3.7+}$ + 7.6 M HBr + 1.46 M HCl (50ml each half cell) using ChiNaf membrane at 15°C (T15_0301.cel)

6.3.2.2.3 Open circuit potential profile of 2 M $V^{3.7+}$ flow cell using ChiNaf membrane

With a slightly different setup as described in section 4.4.5, the open circuit potential (OCP) in each half cell was measured for a flow cell containing 2 M $V^{3.7+}$ + 7.6 M HBr + 1.46 M HCl electrolyte. Measurements were made at several current interruption steps throughout one charge and discharge cycle. A detailed description of the experimental setup is reported in section 4.4.5. The measured cell potential and applied current are shown in Figure 6.17. The sudden drop of cell potential every sixty minutes denotes the open circuit potential measurement at each current interruption step. Half cell potential (vs SCE) was recorded by a chart recorder continuously during the charge and discharge cycle. OCP obtained during charge and discharge of each half cell is plotted in Figure 6.18.

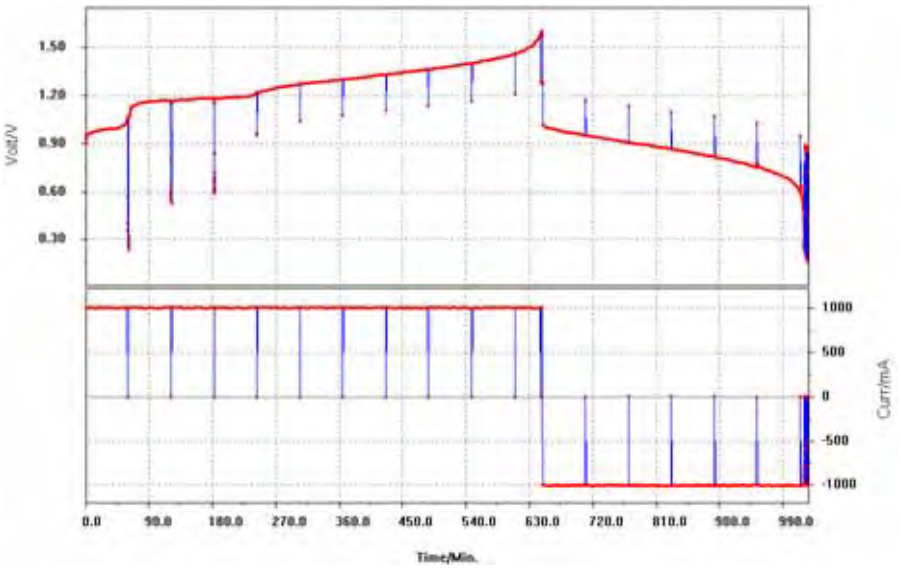

Figure 6.17 First charge / discharge cycle of 2 M $V^{3.7+}$ + 7.6 M HBr + 1.46 M HCl (100ml in each half-cell) using ChiNaf membrane at 25°C for OCP measurements (18maycyc.cel)

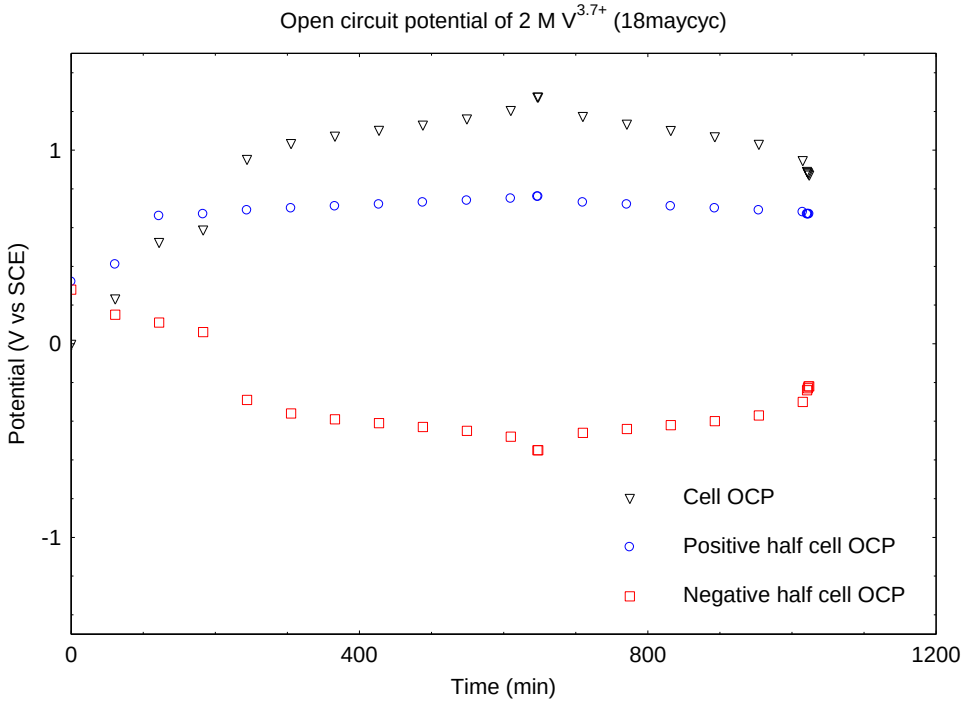

Figure 6.18 Measurements of positive, negative and overall open circuit potential (OCP) of 2 M $V^{3.7+}$ + 7.6 M HBr + 1.46 M HCl corresponding cycling cell 18maycyc.cel

In the positive half cell (Figure 6.18), the OCP increased significantly from 0.32 V to 0.67 V (vs SCE) in two hours which indicates that the V^{3+} ion is oxidised to VO^{2+} during this time. This was followed by the oxidation of Br^- ions, as shown by the

gradual increase in OCP until 0.76 V when the cell is fully charged. The fully charged sate of a V/Br flow cell is governed by the complete conversion of V^{3+} to V^{2+} ions in the negative half-cell electrolyte. During cell discharge, the OCP in the positive half cell declined gradually from 0.76 V to 0.67 V (vs SCE), this pointed out a single reduction step of Br_3^-, where the vanadium ion remained as VO^{2+}.

In the negative half cell, the OCP decreased gradually from 0.28 V to 0.06 V (vs SCE) in three hours, followed by the sudden decrease to -0.29 V (vs SCE) in one hour, which indicated the complete reduction of VO^{2+} to V^{3+}. Potential was then constantly decreased until the electrolyte was fully reduced to V^{2+} with OCP equal -0.55 V (vs SCE). When the cell was discharged, OCP of the negative half cell increased to -0.22 V. This indicated V^{2+} was oxidised to V^{3+} in the negative half cell after discharge.

From the potential change description, V^{3+} had been oxidised to VO^{2+} in the positive half cell much earlier than the reduction of VO^{2+} to V^{3+} in the negative half cell. This agrees with the theoretical calculation, for the electrolyte contained 30% V^{3+} and 70% VO^{2+}. Also this explains the occurrence of the extra step in the cell potential at 96 min (Figure 6.17).

It is important to note that the ideal initial solution of the V/Br cell should contain a 50:50 mixture of V(III) and V(IV) ions. However due to the problem of V_2O_3 powder oxidation in the batch $V^{3.5+}$ solution prepared for this study, a higher than expected V(IV) : V(III) ion ratio was obtained in the stock solution used for cell cycling. This imbalance in the vanadium oxidation state will have a negative impact on cell capacity and cell performance. However, the effect should be the same throughout so the results obtained are still useful for comparison of membrane performance.

6.3.2.3 Comparisons of 2 M $V^{3.7+}$ flow cells using VF11 and ChiNaf membrane at 10^oC

Cell efficiencies for flow cells at 10^oC that used VF11 and ChiNaf membrane at various charge-discharge current densities are repeated below (Table 6.6) for comparison. In contrast to the discussion on static cell experiments, which ChiNaf had a higher coulombic efficiency at 25^oC. The coulombic efficiencies of the ChiNaf flow cell at 10^oC is lower than that of VF11 membrane at the same current density. The only advantage of using ChiNaf in the flow cell system is the higher voltaic efficiency compared to a VF11 flow cell, but these results may require further verification.

Table 6.6 Cell efficiencies of 2 M $V^{3.7+}$ + 7.6 M HBr + 1.46 M HCl flow cell using different membranes at 10^oC

Membrane	Current Density ($mAcm^{-2}$)	Avg. C.E. (%)	Avg. V.E. (%)	Avg. E.E (%)
VF11	20	77.2	77.4	59.7
VF11	40	84.4	60.4	51.0
ChiNaf	20	72.5	79.3	57.5
ChiNaf	40	84.2	68.4	57.6

6.4 Cells with complexing agents

6.4.1 Static cells with complexing agents

6.4.1.1 Static cells with complexing agents using ChiNaf membrane

In Chapter 5 it was found that the diffusion coefficient of V^{3+} in a 2 M V(III) + 0.57 M MEM + 0.18 M MEP was higher than that in 2 M V(III) + 0.2 M MEM + 0.56 M MEP. On the other hand 2 M V(IV) + 0.2 M Br_2 + 0.56 M MEM + 0.18 M MEP solution was found to be more resistive than that containing 2 M V(IV) + 0.2 M Br_2 + 0.19 M MEM + 0.56 M MEP. In order to select the appropriate MEM to MEP ratio for the vanadium

bromide flow cell, the performance of two static cells containing different MEM and MEP concentrations was monitored. Both static cells used carbon felts electrode and ChiNaf membrane with contact area of 25 cm^2, while the frame thickness is 3 mm. Both static cell experiments were undergone at room temperatures (25^oC).

6.4.1.1.1 Static cell with 2 M $V^{3.7+}$ 0.56M MEM 0.19M MEP using ChiNaf membrane

In this static cell, two 3 mm carbon felts containing approximately 5 ml of 2 M $V^{3.7+}$ + 0.56 M MEM + 0.19 M MEP + 6.2 M HBr + 1.2 M HCl are filled in each half-cell. The cell was charged and discharged at 4 $mAcm^{-2}$. The cell potential versus time curve (Figure 6.19) showed the second cycle experiences an overcharged at 1.9 V, so the cut-off limit was reduced to 1.8 V in subsequent cycles. The major concern of this electrolyte was the uncertainty of the fully discharged state, as the normal sharp potential drop is not apparent (Figure 6.19). Average coulombic, voltaic and energy efficiencies are summarised in Table 6.7

6.4.1.1.2 Static cell with 2 M $V^{3.7+}$ 0.19 M MEM 0.56 M MEP using ChiNaf membrane

Another static cell containing 7 ml of 2 M $V^{3.7+}$+ 0.19 M MEM + 0.56 M MEP + 6.2 M HBr + 1.2 M HCl in each half-cells was charged and discharged under the same conditions. The cell potential versus time curve showed that overcharge occurred only in the first cycle, and disappeared in the subsequent cycles (Figure 6.20). During cell discharge an expected sharp drop in potential is seen at 0.25 V. Coulombic, voltaic and energy efficiencies are summarised in Table 6.7.

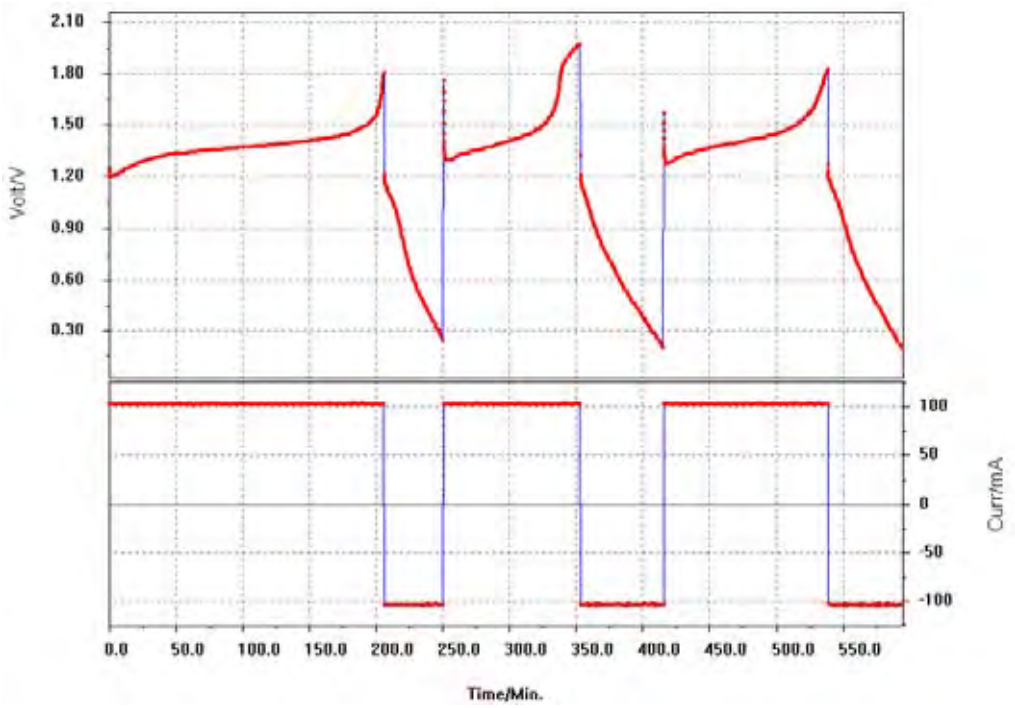

Figure 6.19 First 3 charge / discharge cycles of 2 M $V^{3.7+}$ + 0.56 M MEM + 0.19 M MEP + 6.1 M HBr + 1.2 M HCl (5 ml in each half-cells) with ChiNaf membrane (21JULSA2.cel)

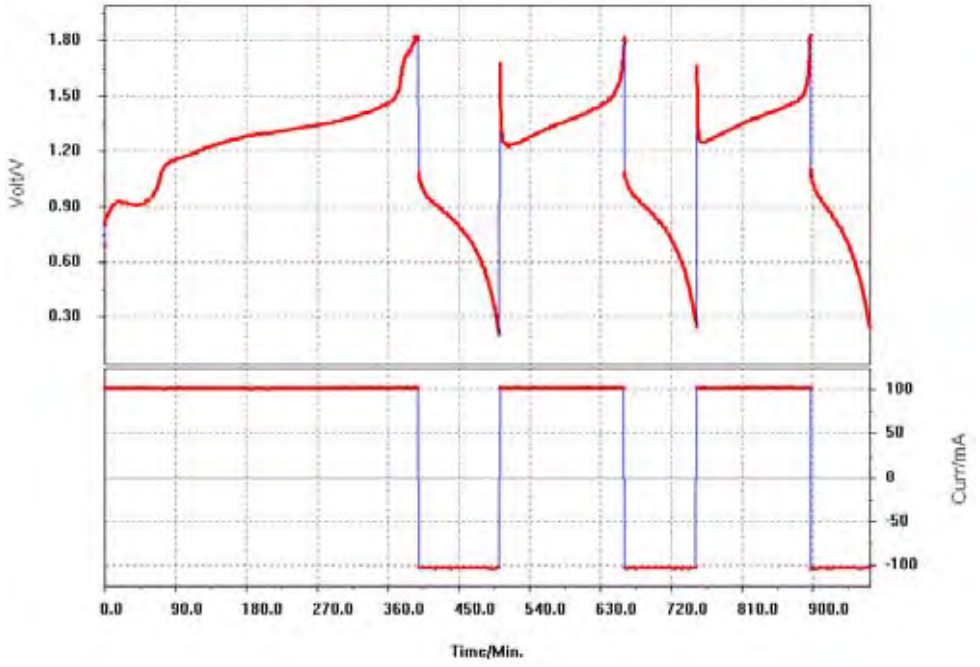

Figure 6.20 First 3 charge / discharge cycles of 2 M $V^{3.7+}$ + 0.19 M MEM + 0.56 M MEP + 6.1 M HBr + 1.2 M HCl (7 ml in each half-cells) with ChiNaf membrane (20JULSA1.cel)

6.4.1.1.3 Comparison of static cells using ChiNaf membrane with different MEM and MEP concentrations in the electrolytes

The major similarities between the two static cells were the sudden jump of cell potential instantaneously after current is applied. As this only occurred from the 2nd cycle onwards, this sudden increase in cell resistance is likely caused by the formation of the oily layer after bromine reacted with MEM and MEP. In order to compare the two sets of data numerically, overcharge needs to be avoided. Therefore, results obtained from both static cells were corrected to the same voltage limit of 1.65 and 0.36 V. It was found that for both static cells, the coulombic efficiency has been reduced whereas the voltaic efficiency was improved after voltage limit correction.

The cell potentials in the 2nd and 4th cycle for the two static cells were superimposed on the same graph (Figure 6.21). Cell efficiencies calculated from the corrected voltage limit showed that the cell with 2 M $V^{3.7+}$ + 0.19 M MEM + 0.56 M MEP + 6.1 M HBr + 1.2 M HCl electrolyte has a higher coulombic and voltaic efficiency than a static cell containing 2 M $V^{3.7+}$ + 0.56 M MEM + 0.19 M MEP + 6.1 M HBr + 1.2 M HCl. This agrees with the results from solution resistance as this electrolyte has a lower resistance, which possibly leads to better voltaic efficiency.

In conclusion, 2 M $V^{3.7+}$ + 0.19 M MEM + 0.56 M MEP + 6.1 M HBr + 1.2 M HCl was thus selected as the preferred composition for further studies. However results presented in Table 6.7 showed the overall energy efficiencies to be relatively low for these static cells employing the ChiNaf membrane. Therefore, further cell testing was performed with the VF11 membrane and the results are presented in the following sections for comparisons (6.4.1.2). Moreover, temperature effect on the performance of a V/Br cell containing this electrolyte is also reported.

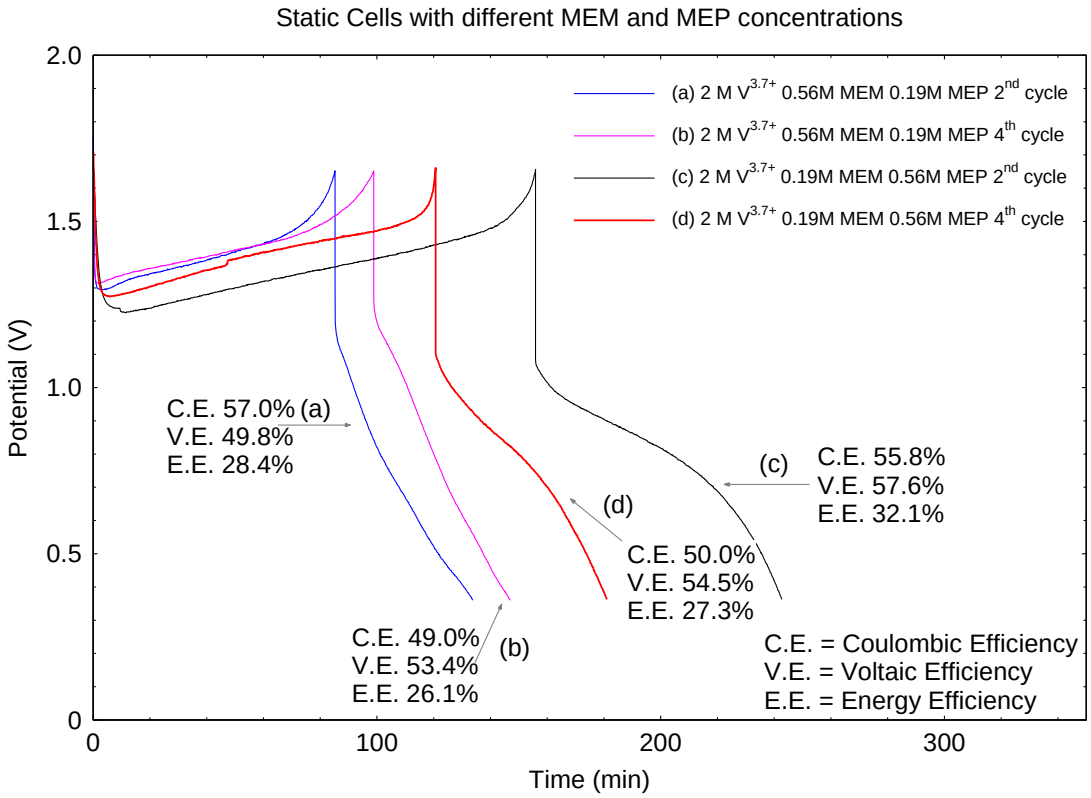

Figure 6.21 4 mAcm^{-2} charge and discharge respond of 2 M $V^{3.7+}$ + 0.56 M MEM + 0.19 M MEP + 6.1 M HBr + 1.2 M HCl and 2 M $V^{3.7+}$ + 0.56 M MEM + 0.19 M MEP + 6.1 M HBr + 1.2 M HCl static cell using ChiNaf membrane and voltage corrected to 1.65 and 0.36 V cut-off limit

Table 6.7 Average cell efficiencies of static cell with different MEM and MEP concentrations (5 cycles) at room temperature (25°C) and at 4 mAcm^{-2}

	$V^{3.7+}$ (M)	MEM (M)	MEP (M)	Voltage limit (V)	Avg. Coulombic Efficiency (%)	Avg. Voltaic Efficiency (%)	Avg. Energy Efficiency (%)
Original data	2	0.56	0.19	1.8, 0.2	59.6	42.9	25.4
	2	0.19	0.56	1.8, 0.2	54.2	51.3	27.9
Voltage limit correction	2	0.56	0.19	1.65, 0.36	48.1	52.8	25.4
	2	0.19	0.56	1.65, 0.36	50.4	54.1	27.3

6.4.1.2 V/Br static cell using VF11 membrane with added MEM and MEP

A static cell using VF11 membrane and a frame of 3 mm thickness was built. It was filled with two 3 mm carbon felts containing 7 ml of 2 M $V^{3.7+}$ 0.19 M MEM 0.56 M

MEP electrolytes in each half-cells and was separated by the VF11 membrane with a contact area of 25 cm^2. The performance of the V/Br static cell after the addition of MEM and MEP complexing agents was determined from the charge-discharge curves at temperatures of 10, 15, 25 (Figure 6.22) and 35^oC. For each temperature current densities of 10, 20 and 40 $mAcm^{-2}$ were applied.

Figure 6.22 showed the cell potential versus time for a static cell containing 2 M $V^{3.7+}$ + 0.19 M MEM + 0.56 M MEP with various applied current densities at 25^oC. There is a distinct cell potential step in both the charge and discharge stages. Similar features were also observed at other temperatures (10, 15, and 35^oC). Furthermore the experimental charging time was significantly lower than the theoretical value. This could have been caused by the formation and separation of complexed bromine oil in the positive half cell that limited the bromine / bromide transport in the absence of electrolyte flow.

The relationship between coulombic, voltaic and energy efficiencies with current density is shown in Figure 6.23. In Figure 6.23, the optimum operating condition was found to be 30 $mAcm^{-2}$ and 15^oC, at which the energy efficiency was 60%. The cell efficiencies obtained at 15^oC are shown in Figure 6.24, whereas the results obtained at each temperature are summarised in Table 6.8.

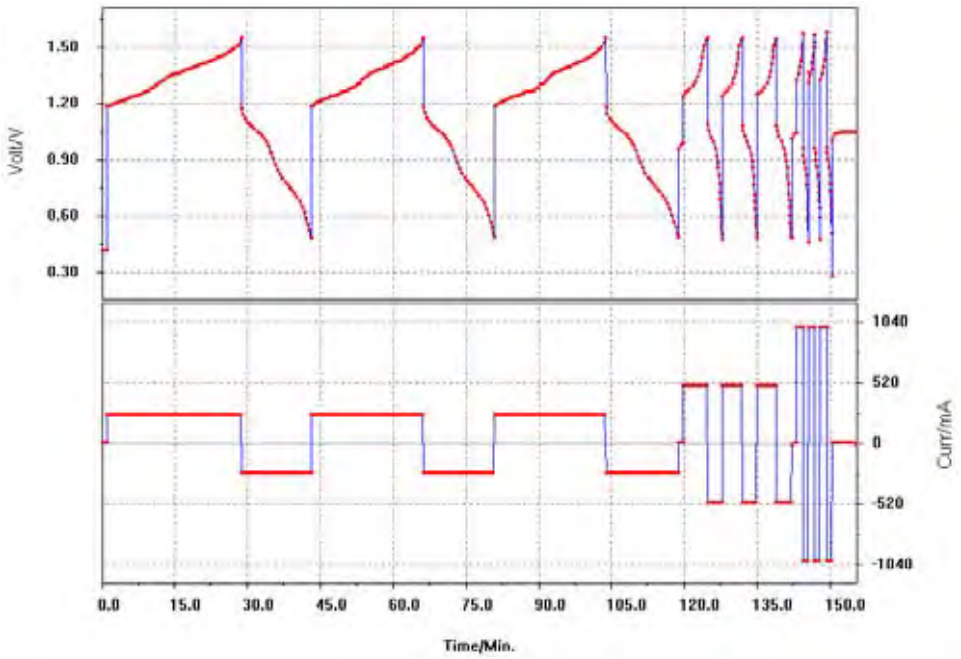

Figure 6.22 Charge-discharge curves for 2 M $V^{3.7+}$ + 0.19 M MEM + 0.56 M MEP + 6.1 M HBr + 1.2 M HCl (7 ml in each half-cells) static cell using VF11 membrane at 25^{o}C (T25_0322.cel)

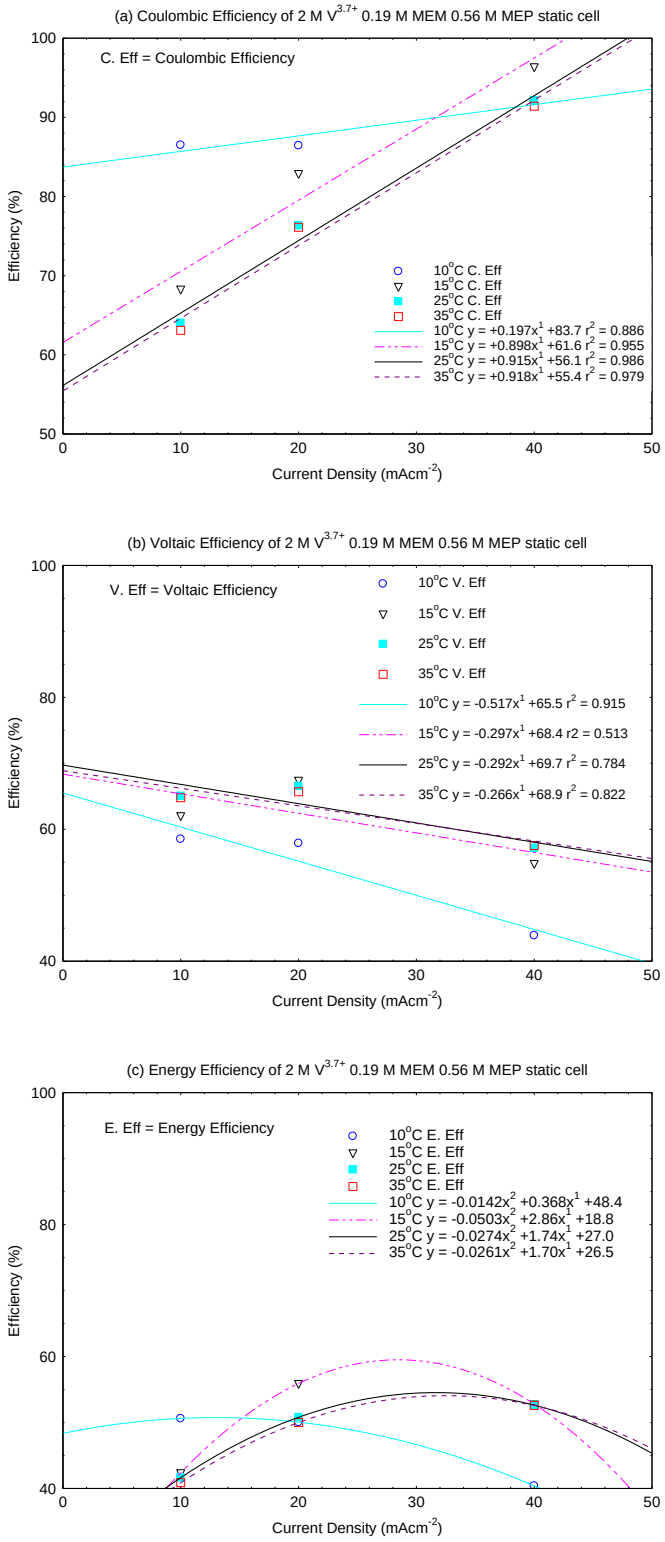

Figure 6.23 (a) Coulombic, (b) Voltaic and (c) Energy efficiency at various temperature for static cell using VF11 membrane and containing 2 M $V^{3.7+}$ + 0.19 M MEM + 0.56 M MEP + 6.1 M HBr + 1.2 M HCl

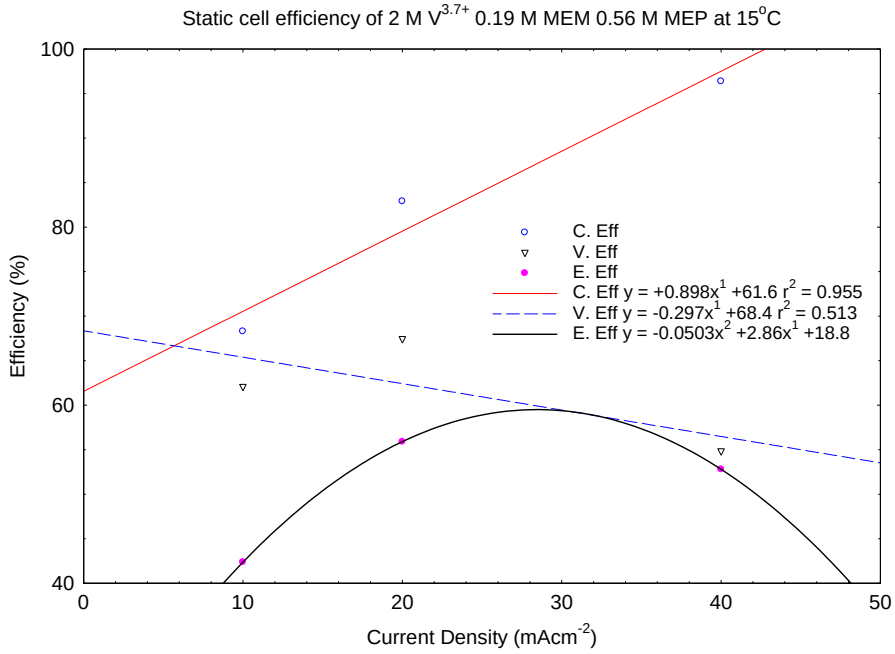

Figure 6.24 Coulombic, Voltaic and energy efficiency of the static cell containing 2 M $V^{3.7+}$ + 0.19 M MEM + 0.56 M MEP + 6.1 M HBr + 1.2 M HCl electrolyte and using VF11 membrane at 15°C

Table 6.8 Average Coulombic, Voltaic and Energy Efficiency of static cell containing 2 M $V^{3.7+}$ + 0.19 M MEM + 0.56 M MEP + 6.1 M HBr + 1.2 M HCl using VF11 membrane

Temp (°C)	Current ($mAcm^{-2}$)	Avg. C. Eff (%)	Avg. V. Eff (%)	Avg. E. Eff (%)
10	10	86.5	58.5	50.6
	20	86.4	57.9	50.1
	40	92.0	43.9	40.4
15	10	68.3	62.1	42.4
	20	82.9	67.4	55.9
	40	96.4	54.8	52.8
25	10	64.0	65.0	41.6
	20	76.3	66.5	50.8
	40	92.1	57.2	52.6
35	10	63.1	64.8	40.9
	20	76.1	65.7	50.0
	40	91.4	57.5	52.6

6.4.1.3 Comparison of static cells using ChiNaf and VF11 membrane with electrolytes containing 2 M $V^{3.7+}$ 0.19 M MEM and 0.56 M MEP

The static cell using ChiNaf membrane provided a low overall energy efficiency as mentioned in section 6.4.1.1.2. This static cell was filled with electrolytes containing 2 M $V^{3.7+}$ + 0.19 M MEM + 0.56 M MEP with a charge-discharge current of 4 $mAcm^{-2}$. The coulombic, voltaic and energy efficiency measured at room temperature was found to be 50.4, 54.1 and 27.3 % respectively.

Direct comparison between ChiNaf and VF11 cannot be made due to the difference in charge-discharge current densities and temperatures. Therefore, cell efficiencies for the static cell using VF11 membrane were estimated from Figure 6.23 to the nearest charge-discharge current density and operation temperature. Coulombic, voltaic and energy efficiency estimated at 4 $mAcm^{-2}$ and 25^{o}C is 60%, 69% and 41% respectively.

Therefore, the energy efficiency of a static cell using VF11 membrane was found to be higher than that obtained from a static cell using ChiNaf membrane for electrolytes containing MEM and MEP complexing agents. As a result, static cell using VF11 membrane would be more suitable for electrolytes containing MEM and MEP complexing agents than ChiNaf membrane. The reason for this difference in performance is unclear and further studies are needed to clarify the membrane / electrolyte interactions in the presence of the bromine complexing agents and organic complex phase in the V/Br cell. However, the major issue of oily layer formed in the positive half-cell that caused the two potential steps in the potential verse time curve has yet to be considered for membrane selection.

6.4.2 Flow cell with complexing agents

6.4.2.1 Flow cell using VF11 membrane with electrolytes containing 2 M $V^{3.7+}$ 0.19 M MEM and 0.56 M MEP

A flow cell (T10_0314) using VF11 membrane and containing 2 M $V^{3.7+}$ + 0.19 M MEM + 0.56 M MEP + 6.1 M HBr + 1.2 M HCl electrolytes was charged and discharged with constant current density of 10 and 20 $mAcm^{-2}$ at $10^{o}C$. The cell was assembled with electrolyte flowing in from the bottom and out for the top as illustrated in (Figure 4.5). From the graph of cell potential versus time in Figure 6.25, the third cycle at 10 $mAcm^{-2}$ showed a significant reduction in discharge time that could not be explained. The coulombic, voltaic and energy efficiency determined at 10 and 20 $mAcm^{-2}$ are tabulated in Table 6.9. Furthermore, the two steps in cell potential previously observed for static cells described in section 6.4.1.2 disappeared in the flow cell experiments. As discussed in section 6.4.1.2, the mass transfer limitation in the positive half cells may have caused the two steps in the cell potential in static cells. In flow cell, the movement of electrolyte allowed the organic phase to move to and from the electrode during cycling, providing a more uniform emulsion for reaction, this explained the disappearance of the two potential steps.

The charge-discharge time at 20 $mAcm^{-2}$ was one-third lower than the theoretical value for flow cell containing 60 ml of 2 M $V^{3.7+}$ + 0.19 M MEM + 0.56 M MEP electrolytes. This could have been caused by the poor mixing of aqueous and polybromide oil phase, but is more likely to be a result of the $V^{3.7+}$ oxidation state in the electrolyte that does not provide an equal molar of V(III) : V(IV) content which is needed to provide the stoichiometric amounts of V^{2+} and Br_3^- species during charging.

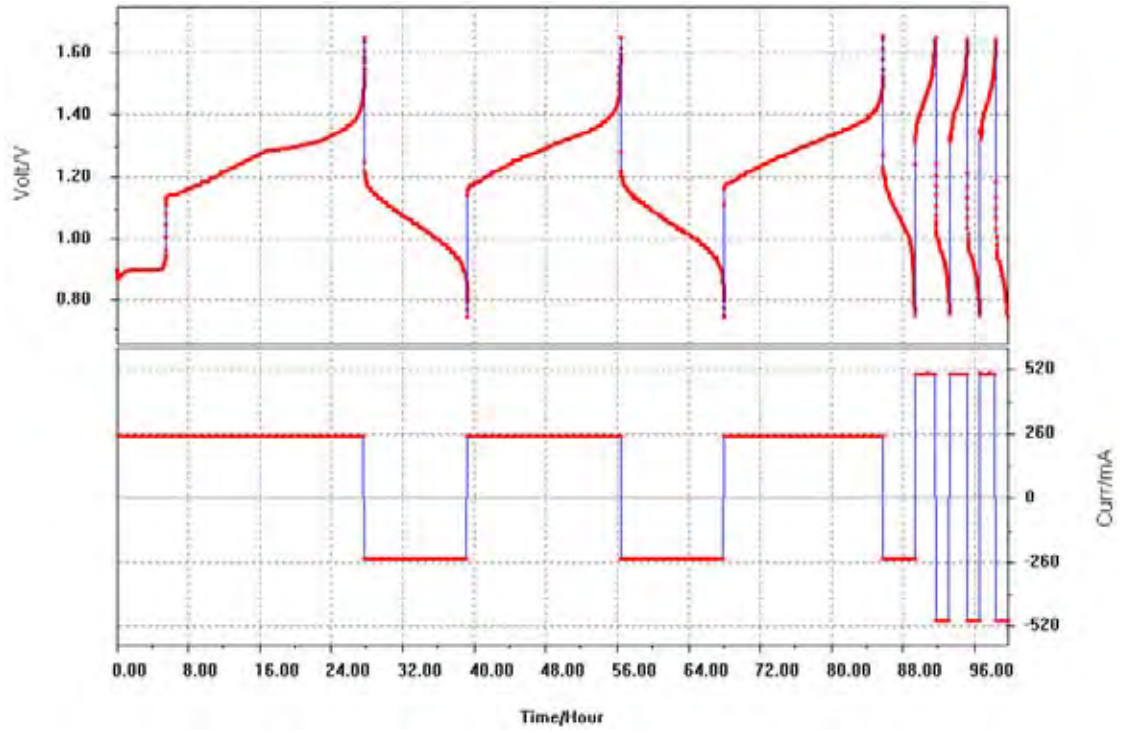

Figure 6.25 Charge / discharge cycles of 2 M $V^{3.7+}$ 0.19 M MEM 0.56 M MEP 6.1 M HBr 1.2 M HCl (60 ml each half cell) using VF11 membrane at 10°C (T10_0314.cel)

Table 6.9 Cell efficiencies of flow cells using VF 11 membrane with electrolyte containing 2 M $V^{3.7+}$ 0.19 M MEM 0.56 M MEP 6.1 M HBr 1.2 M HCl at 10°C

Current Density ($mAcm^{-2}$)	Cycle	Coulombic Efficiency (%)	Voltaic Efficiency (%)	Energy Efficiency (%)
10	2^{nd}	67.5	81.0	54.7
20	5^{th} and 6^{th}	70.8	61.3	43.4

6.4.2.2 Flow cell using ChiNaf membrane with electrolytes containing 2 M $V^{3.7+}$ + 0.19 M MEM + 0.56 M MEP

Figure 6.26 showed the cell potential versus time of a flow cell using ChiNaf membrane containing 50 ml of 2 M $V^{3.7+}$ + 0.19 M MEM + 0.56 M MEP + 6.1 M HBr + 1.2 M HCl electrolytes in each half-cell. The cell was charged and discharge at constant current density of 10 $mAcm^{-2}$ at room temperature (25°C). Average coulombic, voltaic and energy efficiency of the cell are tabulated in Table 6.10. With increasing number of cycles there is a drop both in coulombic and voltaic efficiency. Also cell potential fluctuated vigorously towards the end of the fifteen cycles (Figure 6.27). The major

explanation is the formation of complex polybromide phase in the positive half cell which did not fully mixed with the aqueous phase and caused the potential fluctuation.

Table 6.10 Cell efficiencies of 2 M $V^{3.7+}$ + 0.19 M MEM + 0.56 M MEP + 6.1 M HBr + 1.2 M HCl flow cell at room temperature (25^{o}C)

No of Cycles	Temperature (^{o}C)	Current Density (mAcm^{-2})	Avg. C.E. (%)	Avg. V.E. (%)	Avg. E.E (%)
5	25	10	86	69	59
Next 10	25	10	80	54	43

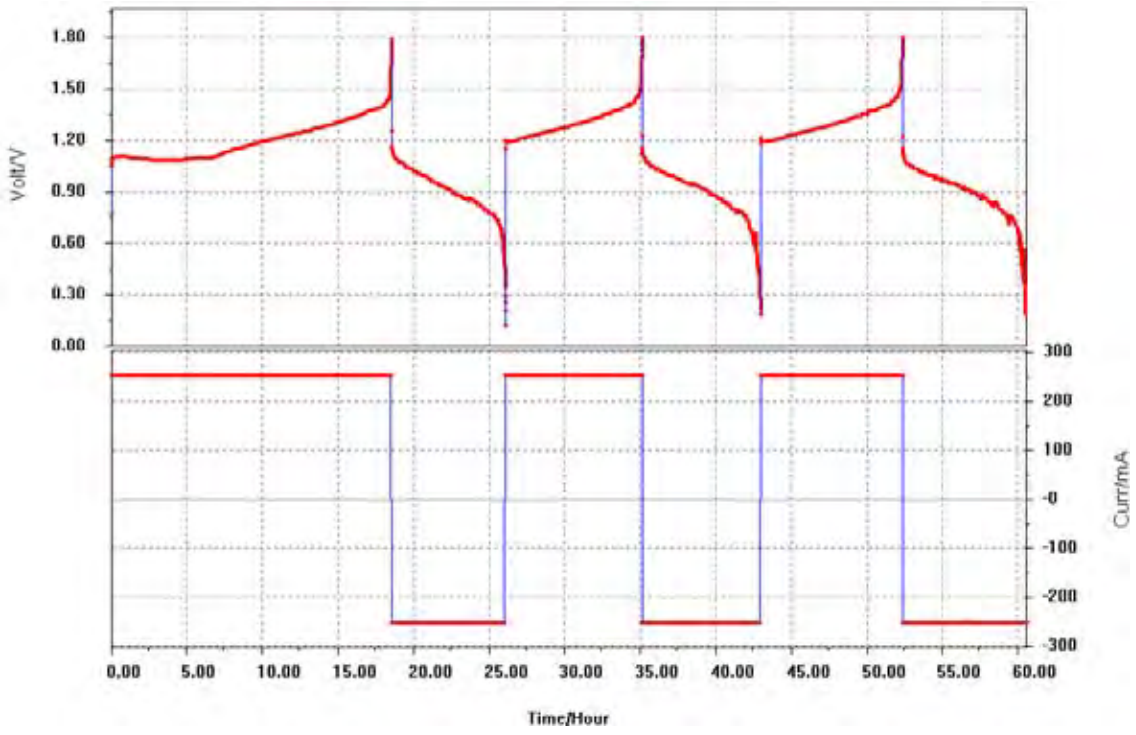

Figure 6.26 Charge / discharge cycles of 2 M $V^{3.7+}$ + 0.19 M MEM + 0.56 M MEP + 6.1 M HBr + 1.2 M HCl (50 ml each half-cells) using ChiNaf membrane at room temperature (25^{o}C), (cycle 1 to 3 of CY060929.cel)

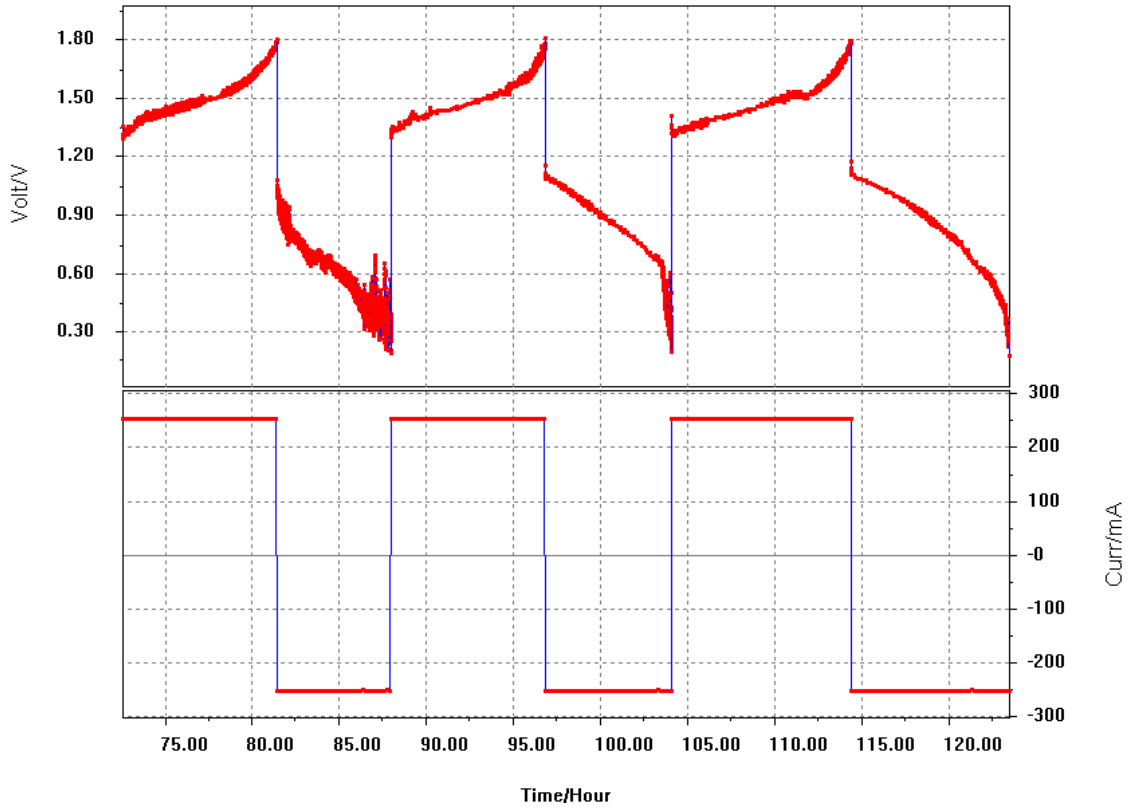

Figure 6.27 Charge / discharge cycles of 2 M $V^{3.7+}$ 0.19 M MEM 0.56 M MEP (50 ml each half cell) using ChiNaf membrane at room temperature (25°C), (cycle 7 to 10 of CY060930.cel)

6.5 Summary

Cell efficiencies for static cells using VF11 membrane before and after the addition of MEM and MEP complexing agents are presented in Table 6.2 and Table 6.8. For the same current density and temperatures, the addition of MEM and MEP increased the coulombic efficiency, while the voltaic efficiency was reduced by such addition.

After the addition of MEM and MEP complexing agents to a static cell using VF11 membrane, the trends in cell efficiencies with increasing current densities were similar to that of a static cell without complexing agents. However the oily layer formed in the positive half-cell lead to the poor mixing between the aqueous and the organic phase which caused the abnormal two steps in the potential versus time curve.

Due to a possibility in a bromide limited transport in the static cell after complexing agent addition, a flow cell containing electrolytes with the same compositions was also studied. Flow cells were built and test at 10^{o}C, as described in section 4.4.3.

The coulombic efficiency obtained by a flow cell was lower than the static cell, whereas the voltaic efficiency was higher than that of the static cell. This is expected, since solution flow will reduce concentration overvoltage losses, giving rise to increased voltage efficiency, while a higher rate of transfer of electrolyte across the membrane will reduce the coulombic efficiency compared with the static cell.

In flow cells before and after MEM and MEP addition a similar effect on cell efficiencies with increasing current density was observed. With increasing current density there was an increase in coulombic efficiency, and a decrease in voltaic efficiency. This agrees with the trend observed in static cells using VF11 membrane before and after MEM and MEP addition (compare Tables 6.2 6.5 and 6.8). At the same current density and temperature, the coulombic efficiency increased and the voltaic efficiency decreased after MEM and MEP addition.

The energy efficiency of a 2 M $V^{3.7+}$ electrolyte in a ChiNaf flow cell was found to be 59 % at a current density of 40 mAcm^{-2}, whereas the energy efficiency of 2 M $V^{3.7+}$+ 0.19 M MEM + 0.56 M MEP + 6.1 M HBr + 1.2 M HCl was found to be 59 % at 10 mAcm^{-2} and reduced to 43 % after 15 cycles. The addition of MEM and MEP had similar effect on flow cell at 10^{o}C utilising VF11 membrane for which the energy efficiency reduced by 10 % (compare section 6.3.2.1 with Table 6.9), after MEM and MEP addition.

As the positive half cell reaction is mass transport limited in the presence of the bromine complexing agents, the uniform mixing of the organic and aqueous phase was found to be the major problem affecting the performance of cells employing MEM and MEP complexing agents to bind the Br_2 produced during the charge cycle.

In the flow configuration used in this study the electrolyte is fed into each half-cell from the bottom, flowing out at the top of the cell. The higher density of the organic bromine phase could lead to a settling of the complexed bromine layer at the bottom of the cell cavity preventing its uniform distribution with the porous carbon felt electrode. A possible solution to this problem maybe to reverse the electrolyte flow so that it enters the cell at the top and exits from the bottom, thereby flushing out any oily bromine complex that might settle and build up in the lower part of the cell cavity.

Further work is thus required to improve the cell design and flow configuration to ensure uniform mixing of the organic and aqueous solution phases within the cell cavity, so that higher energy efficiency can be achieved with the complexed vanadium bromide electrolyte for the V/Br redox cell.

Chapter 7 Conclusions and Recommendation

In this thesis, three quaternary ammonium bromides N-ethyl-N-methyl-morpholinium bromide (MEM) N-ethyl-N-methyl-pyrrolidinium bromide (MEP) Tetra-butyl ammonium bromide (TBA), were tested for their suitability as bromine complexing agents in vanadium bromide (V/Br) flow cell to improve the stability of the electrolyte.

From electrolyte stability studies, MEM, MEP and TBA were found to be stable in V/Br electrolytes in the absence of bromine and did not form any solid particles. However in the presence of bromine, electrolytes with binary QBr mixtures containing TBA resulted in viscous solutions. When bromine is added to V/Br electrolytes containing a ternary QBr mixture, it was found that this mixture is less effective in bromine capturing if the total QBr concentration was less than 1 M at 40^{o}C, where bromine gas evolution was observed. In this study it was found that V/Br electrolytes containing a binary QBr mixture (0.75M) of MEM and MEP to be the best combination that formed an orange oily layer in the presence of bromine without solidification between 11 – 40^{o}C.

The electrochemical studies of V^{3+}/V^{2+} were carried out in HBr / HCl supporting electrolyte similar to that of the V/Br flow cell. The formal potential was found to be between -0.43 and -0.47 V (vs SCE), and only a slight fluctuation occurred after the

addition of MEM or MEP. Similarly the addition of MEM and MEP had a minimal effect on the $V^{2+} \Leftrightarrow V^{3+}$ transfer coefficient and the diffusion coefficient of V^{3+}. Since the electrochemical parameters of V^{3+}/V^{2+} couple was not affected by the addition of MEM and MEP, it can be added to the negative half-cell of a V/Br flow cell without major interference.

Both in the presence and absences of vanadium ions, the kinetics of Br^-/Br_3^- redox couple were found to be mass transfer controlled. In the absence of vanadium ions, the kinetic parameters of the Br^-/Br_3^- couple including the exchange current density and the transfer coefficient were determined. The exchange current density was found to decrease from 0.013 Acm^{-2} to 0.01 Acm^{-2} after the addition of MEM and MEP mixture. On the other hand the transfer coefficient before and after MEM and MEP addition was found to be 0.5 and 0.44 respectively. Since the kinetic parameters were not significantly affected by the addition of MEM and MEP mixture, they can be added to the positive half-cell of the V/Br flow cell as bromine complexing agents.

The cell performance of 2 M $V^{3.7+}$ vanadium bromide electrolyte was studied both in static and flow cell setup using two different membrane (ChiNaf and VF11). From preliminary membrane studies it was found that ChiNaf showed a higher membrane resistance than VF11, but the coulombic efficiency of a 2 M $V^{3.7+}$ static cell utilising ChiNaf was over 85%. The polarization resistance of a lab scale V/Br flow cell utilising ChiNaf membrane and 2 M $V^{3.7+}$ electrolytes was found to be slightly higher during cell charging (3.9 $\Omega\ cm^2$) than during the discharge process (3.6 $\Omega\ cm^2$). This is opposite to what was observed in the all-vanadium redox cell.

The effect of MEM and MEP addition on cell performance was also investigated. Flow cell performance for 2 M $V^{3.7+}$ + 0.19 M MEM + 0.56 M MEP electrolytes utilising ChiNaf membrane at 10 $mAcm^{-2}$ gave an energy efficiency of 59%, decreasing to 43% after 15 cycles. For the static cell utilising VF11 membrane, the addition of MEM and MEP reduced the energy efficiency from 59.7% to 43.4%. It is believed that this is caused by the mass transfer controlled Br^-/Br_3^- couple in the complexed positive half-cell solution. Therefore, uniformity between the organic and aqueous phase is important for flow cells utilising electrolytes with MEM and MEP.

For future studies, it is recommended to investigate the organic phase of the vanadium bromide electrolytes either with FTIR or Raman spectroscopy. This will allow a comparison to be made with the organic phase formed in zinc bromine electrolytes. The kinetics of Br^-/Br_3^- system could be further investigative by rotating disc voltammetry, to determine the redox mechanism in the V/Br electrolytes.

Although a reasonable degree of bromine capture was achieved with the use of a 1:0.75 molar ratio of Br_2 to QBr in the 2 M vanadium bromide solutions investigated in this study. A small amount of bromine vapour was still generated in the cell above room temperature. Further studies should therefore be considered with 1:1 molar ratio of Br_2 to QBr in both 2 M and in 3 M vanadium electrolytes for higher energy density applications. When preparing 3 M vanadium solution with 1.5 M QBr addition, stepwise procedures will need to be developed to reduce dilution effect.

Reference

[1] M. Skyllas-Kazacos and F. Grossmith, J. Electrochem. Soc. 134 (1987) 2950.

[2] M. Skyllas-Kazacos, D. Kasherman, R. Hong and M. Kazacos, J. Power Sources 35 (1991) 399.

[3] R. Largent, M. Skyllas-Kazacos and J. Chieng, Proceedings IEEE 23rd Photovoltaic Specialists Conference, Louisville, Kentucky, (May 1993).

[4] M. Skyllas-Kazacos, R. G. Robins and M. Rychick, U.S. Patent No. 4,786,567 22 November, (1988).

[5] M. Skyllas-Kazacos, J. Power Sources 124 (2003) 299.

[6] O. Haas and E. J. Cairns, Annual Reports on the Progress of Chemistry, Section C 95 (1999) 163.

[7] M. Bartolozzi, J. Power Sources 27 (1989) 219.

[8] C. Ponce de Leon, A. Frias-Ferrer, J. Gonzalez-Garcia, D. A. Szanto and F. C. Walsh, J. Power Sources 160 (2006) 716.

[9] N. H. Hagedorn. NASA Redox Storage System Development Project: Lewis Research Center; 1984. Report No NASA-TM-83677.

[10] L. H. Thaller. Redox Flow Cell Energy Storage System: Lewis Research Center; 1979. Report No NASA-TM-79143.

[11] M. Lopez-Atalaya, G. Codina, J. R. Perez, J. L.Vazquez and A. Aldaz, J. Power Sources 39 (1992) 147

[12] L. Swette and V. Jalan. Development of Electrodes for the NASA Iron/Chromium Redox System and Factors Affecting Their Performance: GINER INC; 1984. Report No NASA-CR-174724.

[13] A. Price, S. Bartley, S. Male and G. Cooley, Power Engineering Journal 13 (1999) 122.

[14] N. Wilks in *Whatever the weather: Advances in battery technology could hold the key to the successful development of alternative sources of energy*, *Vol. 17* 2004, 33.

[15] VRB Corporate Brochure: VRB Power System Incorporated.

[16] R. Zito, U.S. Patent No. 5612148, (1997).

[17] P. J. Morrissey, P. J. Mitchell and S. E. Male, US Patent No. US 6841294 B1, (2005).

[18] P. J. Morrissey, World Intellectual Property Organization No. WO/2001/073882, (2001).

[19] H. Zhou, H. Zhang, P. Zhao and B. Yi, Electrochimica Acta 51 (2006) 6304.

[20] P. Zhao, H. Zhang, H. Zhou and B. Yi, Electrochimica Acta 51 (2005) 1091.

[21] C. S. Bradley, United Stated Patent No. 312802, (1885).

[22] R. Bloch, U.S. Patent No. 2566114, (1951).

[23] P. C. Butler, P. A. Eidler, P. G. Grimes, S. E. Klassen and R. C. Miles, Ch 39 Zinc/Bromine Batteries, (2002).

[24] P. C. Symons and P. C. Butler. Introduction to advanced batteries for emerging applications. Albuquerque, NM: Sandia National Laboratories; 2001. Report No SAND2001-2022P.

[25] J. J. Bolstad and R. C. Miles, Energy Conversion Engineering Conference 1989 IECEC-89. Proceedings of the 24th Intersociety Washington, DC 6 - 11 August, (1989), 1311.

[26] P. Singh and B. Jonshagen, J. Power Sources 35 (1991) 405.

[27] W. L. Towle and R. A. Rizzo, Zinc/Bromine Batteries, (1984).

[28] L. Warren and R. A. Rizzo, CH29 Zinc/Bromine Batteries, in: D. Linden (Ed.) Handbook of Batteries and Fuel Cell, McGraw-Hill, New York (1984).

[29] R. J. Bellows, D. J. Eustace, P. Grimes, J. A. Shrophsire, H. C. Tsien and A. F. Venero, Proceedings of the 11th International Symposium, Brightion, (1978), 301.

[30] Y. Ando and T. Ochiai, U.S. Patent No. 4510218, April 9, (1985).

[31] E. Kantner, U.S. Patent No. 4491625, 1 January, (1985).

[32] P. A. Eidler and P. J. Lex, U.S. Patent No. January 7, (1997).

[33] P. Eidler. Development of zinc/bromine batteries for load-leveling applications: Phase1 final report: Sandia National Laboatories; 1999 July. Report No SAND99-1853.

[34] D. J. Eustace, U.S. Patent No. 4,064,324 December 20, (1977).

[35] K. J. Cathro, J. Power Sources 23 (1988) 365.

[36] K. Cedzynska, Electrochimica Acta 40 (1995) 971.

[37] R. J. Bellows and E. Kantner, U.S. Patent No. 4818642, 4 April, (1989).

[38] F. G. Will, Interface Phenomena in Advanced Batteries, in: Material for Advanced Batteries, Plenum Press, (1980), 190.

[39] P. Lex and B. Jonshagen, Power Engineering Journal June (1999) 142.

[40] P. Singh, K. White and A. J. Parker, Journal Power Sources 10 (1983) 309

[41] P. G. Grimes, Proceeding of the 2nd Annual Battery Conference on Applications and Advances, California State University, Long Beach, 14-16 Jan, (1986), 131.

[42] T. Fujii, M. Igarashi, K. Fushimi, T. Hashimoto, A. Hirota, H. Itoh, K. Jin-Nai, Y. Tagami, I. Kouzuma, Y. Sera and T. Nakayama, Energy Conversion

Engineering Conference, 1989. IECEC-89. Proceedings of the 24th Intersociety, Washington, DC, 6-11 Aug, (1989), 1319

[43] T. Fujii and A. Kokado, U.S. Patent No. 4550065, 29 October, (1985).

[44] M. Skyllas-Kazacos, US Patent No. 4786567, 22 Nov, (1988).

[45] M. Kazacos and M. Skyllas-Kazacos, Journal of The Electrochemical Society 136 (1989) 2759

[46] E. Sum, M. Rychcik and M. Skyllas-kazacos, J. Power Sources 16 (1985) 85.

[47] N. Kausar in *Studies of V(IV) and V(V) species in vanadium cell electrolyte*, *Ph.D* The University of New South Wales, Sydney, 2002.

[48] T. Mohammadi and M. S. Kazacos, J. Power Sources 63 (1996) 179.

[49] S. Miyake and N. Tokuda, Power Engineering Society Summer Meeting, 2001. IEEE, 15-19 July (2001), 450

[50] M. Gattrell, J. Park, B. MacDougall, J. Apte, S. McCarthy and C. W. Wu, 54th Annual Meeting of International Society of Electrochemistry, Symposium 5: Electrochemical Energy Conversion and Storage: Fundamental and Technological Advances., Sao Pedro, Brazil, (2003).

[51] M. Skyllas-Kazacos in *Recent Progress with the UNSW Vanadium Battery*, *Vol.* 2002.

[52] VRB. An Electrochemical Energy Storage Company - Executive Summary: VRB Power System Incorporated; 2004.

[53] F. Beck and P. Ruetschi, Electrochimica Acta 45 (2000) 2467.

[54] M. Skyllas-Kazacos, Power and Energy Systems EuroPES 2004, Rhodes, Greece, 28 - 30 June, (2004), 226.

[55] D. J. Eustace, J. Electrochem. Soc. 127 (1980) 528.

[56] Y. H. Wen, H. M. Zhang, P. Qian, H. T. Zhou, B. L. Yi and Y. S. Yang, Electrochimica Acta 51 (2006) 3769.

[57] Y. H. Wen, H. M. Zhang, P. Qian, H. T. Zhou, P. Zhao, B. L. Yi and Y. S. Yang, Journal of the Electrochemical Society 153 (2006) A929

[58] X. Xia, H.-T. Liu and Y. Liu, Journal of the Electrochemical Society 149 (2002) A426.

[59] B. Fang, S. Iwasa, Y. Wei, T. Arai and M. Kumagai, Electrochimica Acta 47 (2002) 3971.

[60] Y. Israel and L. Meites, Vanadium, in: A. J. Bard (Ed.) Encyclopedia of Electrochemistry of the Elements Marcel Dekker Inc. Pub, New York, (1976).

[61] O. G. Holmes and D. S. McClure, Journal of the Chemical Physics 26 (1957) 1686

[62] R. J. H. Clark, The Chemistry of Titanium And Vanadium, Elsevier Publishing Company, (1968).

[63] D. Nicholls, Complexes and First-Row Transition Elements, The Macmillan Press Ltd, (1974).

[64] J. Malin and J. H. Swinehart, Inorganic Chemistry 8 (1969) 1407

[65] A. S. Tracey, G. R. Willsky and E. S. Takeuchi, Vanadium: chemistry, biochemistry, pharmacology, and practical applications, CRC Press, Boca Raton, (2007).

[66] S. C. Furman and C. S. Garner, Journal of American Chemical Society 72 (1950) 1785

[67] C. J. Jones, d- and f-Block Chemistry, The Royal Society of Chemistry, Thomas Graham House, Cambridge, (2001).

[68] L. P. Podmore and P. W. Smith, Australian Journal of Chemistry 25 (1972) 2521.

[69] K. Niki and H. Mizota, Journal of Electroanalytical Chemistry 72 (1976) 307.

[70] J. Selbin, Coordination Chemistry Reviews 1 (1966) 293

[71] J. Selbin, Chemical Reviews 65 (1965) 153

[72] G. Oriji, Y. Katayama and T. Miura, Electrochimica Acta 49 (2004) 3091.

[73] F. J. C. Rossotti and H. S. Rossotti, Acta Chem Scand. 9 (1955) 1177.

[74] M. M. Brezinski and O. Duncan, European Patent No. EP1 318 271 A1, (2003).

[75] E. H. Swift and R. W. Hoeppel, Journal of the American Chemical Society Vol. 51, (1929) 1366

[76] M. Skyllas-Kazacos and Y. Limantari, Journal of Applied Electrochemistry 34 (2004) 681–685.

[77] L. D. Kurbatova, T. I. Polupanova and D. I. Kurbatov, Russian Journal of Applied Chemistry 75 (2002) 1216

[78] N. Kausar, R. Howe and M. Skyllas-kazacos, Journal of Applied Electrochemistry 31 (2001) 1327.

[79] E. Sum and M. Skyllas-Kazacos, J. Power Sources 15 (1985) 179.

[80] G. Oriji, Y. Katayama and T. Miura, J. Power Sources 139 (2005) 321.

[81] L. Meites and S. Moros, Journal of Analytical Chemistry 31 (1959) 23.

[82] N. Tanaka and R. Tamamushi, Electrochimica Acta 9 (1964) 963

[83] F. C. Anson and J. Caja, Journal of Electrochemical Society : Electrochemical Science and Technolygy 117 (1970) 306

[84] E. Barrado, R. Pardo, Y. Castrillejo and M. Vega, Journal of Electroanalytical Chemistry 427 (1997) 35.

[85] C. W. D. Kreuk, M. Sluyters-Rehrach and J. H. Sluyters, Journal of Electroanalytical Chemistry 33 (1971) 267

[86] P. K. Adanuvor, R. E. White and S. E. Lorimer, Journal of The Electrochemical Society 134, (1987) 1450.

[87] M. Mastragostino and C. Gramellini, Electrochimica Acta 30 (1985) 373.

[88] W. D. Cooper and R. Parsons, Journal of the Chemical Society. Faraday Transactions 66 (1970) 1698.

[89] J. Llopis and M. Vazquez, Electrochimica Acta 6 (1962) 177.

[90] I. Rubinstein, J. Phys. Chem. 85 (1981) 1899.

[91] S. Ferro, C. Orsan and A. D. Battisti, Journal of Applied Electrochemistry 35 (2005) 273.

[92] B. E. Conway, Y. Phillips and S. Y. Qian, Journal of the Chemical Society, Faraday Transactions 91 (1995) 283

[93] R. P. Bell and M. Pring, Journal of the Chemical Society A: Inorganic, Physical, Theoretical (1966) 1607

[94] T. X. Wang, M. D. Kelley, J. N. Cooper, R. C. Beckwith and D. W. Margerum, Inorganic Chemistry 33 (1994) 5872.

[95] D. W. H. Lambert, P. H. J. Greenwood and M. C. Reed, J. Power Sources 107 (2002) 173.

[96] R. Newnham and W. Baldsing, Journal Power Sources 59 (1996) 137.

[97] J. Strebe, B. Reichman, B. Mahato and K. Bullock, Journal Power Sources 31 (1990) 43.

[98] S. McKinlay in *Investigation into the Prevention of the Loss of Bromine in the Vanadium Bromide Flow Cell*, *Honours Thesis* UNSW, Sydney, 2003.

[99] M. DeRossi, U.S. Patent No. 3811945, May 21, (1974).

[100] D. J. Eustace and P. AMalachesky, No. 4,068,046, January 10, (1978).

[101] K. J. Cathro, K. Cedzynska, D. C. Constable and P. M. Hoobin, J. Power Sources 18 (1986) 349.

[102] F. M. Walsh, D. N. Crouse and A. M. Ajami, U.S. Patent No. 4104447, 1 Aug, (1978).

[103] K. J. Cathro, K. Cedzynska and D. C. Constable, J. Power Sources 16 (1985) 53.

[104] K. Cedzynska, Electrochimica Acta 34 (1989) 1439.

[105] ICL-IP in *N-ethyl-N-methylmorpholiniumbromide, Vol. 2005* 2005.

[106] ICL-IP in *N-ethyl-N-methylpyrrolidiniumbromide, Vol. 2005* 2005.

[107] MP-Biomedicals in *Tetra-butyl ammonium bromide Catalogue number: 152101*, *Vol. 2005* 2005.

[108] D. B. Scaife and H. J. V. Tyrrell, Journal of the Chemical Society (1958) 386

[109] G. Bauer, J. Drobits, C. Fabjan, H. Mikosch and P. Schuster, Journal of Electroanalytical Chemistry 427 (1997) 123.

[110] G. Bauer, J. Drobits, C. Fabjan, H. Mikosch and P. Schuster, Chemie Ingenieur Technik - CIT 68 (1996) 100

[111] K. Kinoshita, S. C. Leach and C. M. Ablow, Journal of The Electrochemical Society 129 (1982).

[112] S. N. Bajpal, Journal of Chemical Engineering Data 26 (1981) 2.

[113] W. Kautek, A. Conradi, M. Sahre, C. Fabjan, J. Drobits, G. Bauer and P. Schuster, Journal of The Electrochemical Society Volume 146 (1999) 3211.

[114] W. Kautek, A. Conradi, C. Fabjan and G. Bauer, Electrochimica Acta 47 (2001) 815.

[115] J. Larminie and A. Dicks, Fuel cell systems explained, John Wiley & Sons Ltd, England, (2003).

[116] A. J. Bard and L. R. Faulkner, Electrochemical methods : fundamentals and applications, Wiley, New York, (2001).

[117] S. P. Kounaves, Voltammetric Techniques, in: F. A. Settle (Ed.) Handbook of Instrumental Techniques for Analytical Chemistry, Prentice Hall, (1997), 709

[118] D. A. Skoog, D. M. West and F. J. Holler, Fundamentals of Analytical Chemistry, Saunders College Publishing, USA, (1996).

[119] D. H. Evans, K. M. O'Connell, R. A. Petersen and M. J. Kelly, Journal of Chemical Education 60 (1983) 290.

[120] C. Gabrielli. Identification of electrochemical electrochemical processes by frequency response analysis: Solartron analytical; 1998. Report No 004/83.

[121] Electrochemical Impedance Spectroscopy Primer: Gamry Instruments; 2005.

[122] R. A. Assink, Journal of Membrane Science 17 (1984) 205.

[123] P. B. Mathur, C. S. Rajagopalan and D. P. Bhatt, J. Power Sources 19 (1987) 269.

[124] H. Vafiadis and M. Skyllas-Kazacos, Journal of Membrane Science 279 (2006) 394.

[125] I. Vogel and A. Möbius, Electrochimica Acta 36 (1991) 1403.

Appendixes

Appendix A Determining the oxidation states of vanadium solutions

Solution preparation

Dissolve an adequate amount of vanadium oxide (V_2O_3) powder in a 5 M H_2SO_4 25 ml solutions to make a 2 M V(III) solution. Then make a dilute solution as 0.1 M V(III). Pipette 10ml of the 0.1 M V(III) to a 40 ml glass cell for $KMnO_4$ titration. Cover glass cell with the PCV lid with 3 holes that allowed electrodes and pipette outlet to get though. Make sure the magnet does not hit the electrodes and the pipette outlet is directly on top of the stirring bar. Addition of zinc pallets to 2 M $VOSO_4$ before dilute to 0.1 M analyte. If zinc is added to dilute solutions it would react with water.

Oxidizing agent

0.02 M $KMnO_4$ used as oxidizing agent

Electrodes

$Hg/HgSO_4$ is used as reference electrode

Pt wire or Pt rod as counter electrode

Equipment

Autoburette ABU11, Copen-Hagen NV, Denmark

3057 Yokogawa Portable Recorder (Yokogawa Electric Co., Japan)

Chart recorder settings

Channel H: Pt wire or Pt rod

Channel L: $Hg/HgSO_4$ reference electrode

Voltage range: 2V full range, Chart speed: 60cm/ hr

Auto pipette settings

Speed of $KMnO_4$ delivery: 1ml/min

Titration and analysis

After electrodes are connected and the auto burette is properly filled, start the $KMnO_4$ delivery and the chart recorder measurement at the same time. Look for colour change in the analyte and observe the potential change. Stop the $KMnO_4$ flow when the analyte reaches the VO^{2+} state (yellow).

$$MnO_4^- + 8H^+ + 5e \rightarrow Mn^{2+} + 4H_2O$$

$$MnO_4^- + 8H^+ + 5V^{2+} \rightarrow 5V^{3+} + Mn^{2+} + 4H_2O$$

Resulting chart analysis

$V^{3+} + e \rightarrow V^{2+}$	E^o = -0.255 V
$VO^{2+} + 2H^+ + e \rightarrow V^{3+} + H_2O$	E^o = 0.337 V
$VO_2^+ + 2H^+ + e \rightarrow VO^{2+} + H_2O$	E^o = 1.00 V
$Hg/HgSO_4$	E^o = 0.6154 V

An ideal potential curve for a pure V(III) solution is illustrated in Figure A.1, which the potential is plotted as a function of $KMnO_4$ addition to the solution. The potential of green V (III) solution is about -0.28V (vs $Hg/HgSO_4$). The solution colour turns to blue when it reaches V(IV) state where the potential is about 0.3 V (vs $Hg/HgSO_4$). Finally turns to pale yellow when solution reaches V(V) state where the potential goes to 0.8 V. Since the oxidation of vanadium involves a one electron process for each stage, the length of each step should be the same.

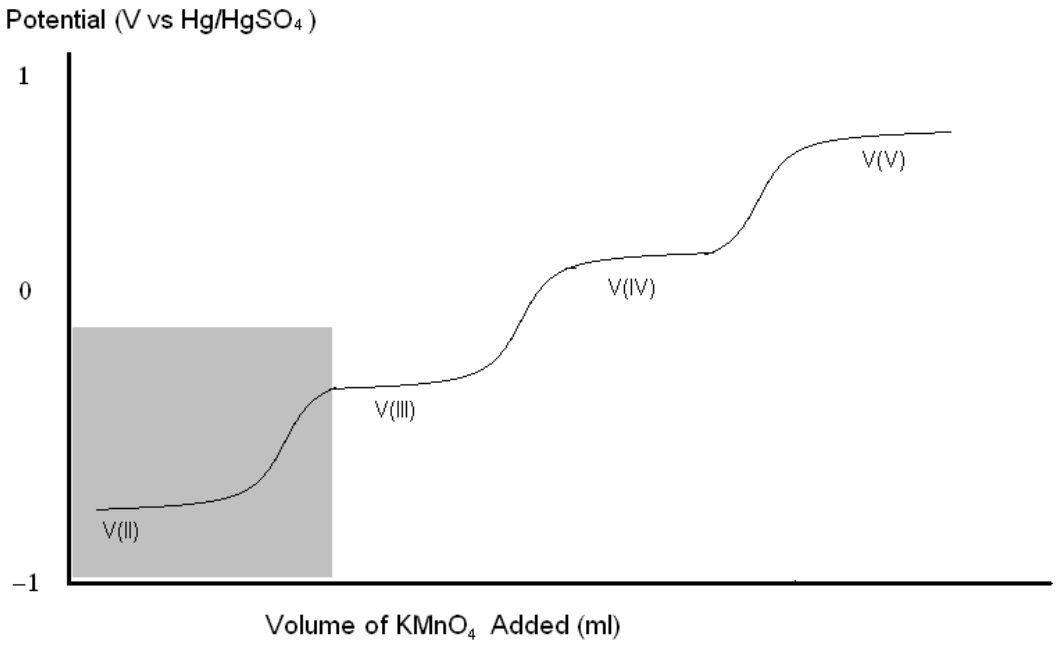

Figure A.1 Ideal potential curve for 100% V(III) excepted greyed area which only happens to a solution which is fully reduced to V(II) by zinc pallets

To determine what the percent of V_2O_3 had been air oxidized to VO^{2+} by measuring the length of the V(III) step on the chart was compare with the V(IV) step as in Figure A.1. For a pure V(III) solution the length of the V(III) step should equal the length of the V(IV) step. Any excess in the length of V(IV) step would indicate the existence of

VO^{2+} in the V_2O_3 powder. Therefore this factor had to be taken into account when vanadium batch solutions are prepared.

For solutions with V(V) in H_2SO_4 system, zinc pallets are used to reduce electrolyte to V^{2+} sate before the total concentration of the vanadium solution is found from the length of the V(IV) step. By converting the length of step V(IV) to the volume of $KMnO_4$ added, then calculated the moles of $KMnO_4$ was used. From equilibrium equations we know each mole of $KMnO_4$ convert 5 moles of vanadium ions, and then the number of moles of vanadium can be determined. Finally, as the volume of analyte is known its concentration can be found.

Appendix B V(III) Solution preparation calculations

Samples of 2 M V(III) with 0.75 M QBr were prepared by adding measured volumes of QBr to a fixed amount of 2.5 M V(III) and topping up with HBr and HCl to keep the supporting electrolyte concentration constant.

As vanadium concentration was fixed at 2 M and with a known amount of sample volume, the number moles of vanadium are calculated. The number of moles of QBr needed to maintain the total at 0.75 M concentration. To vary the ratio between MEM and MEP for different samples, the number of moles for each is calculated separately.

Equation B.1 $$\frac{n_{V3.5}}{c_{V3.5}} = \frac{n_{QBr}}{c_{QBr}} = V_{sample}$$

Equation B.2 $$n_{QBr} = \frac{n_{V3.5}}{c_{V3.5}} c_{QBr}$$

Equation B.3 $$n_{MEM} = n_{QBr}\left(\frac{ratio_{MEM}}{ratio_{MEM} + ratio_{MEP}}\right)$$

Equation B.4 $$n_{MEM} = \frac{n_{V3.5}}{c_{V3.5}} c_{QBr}\left(\frac{ratio_{MEM}}{ratio_{MEM} + ratio_{MEP}}\right)$$

Equation B.5 $$n_{MEP} = \frac{n_{V3.5}}{c_{V3.5}} c_{QBr}\left(\frac{ratio_{MEP}}{ratio_{MEM} + ratio_{MEP}}\right)$$

As MEM and MEP are in dissolved aqueous form a number of assumptions were needed to determine how much of each should be added to the different samples. The weight percentage and densities may vary from batch to batch and the manufacture only

provided the weight percentage as a range (40 – 75%) with the corresponding specific gravities between 1.10 and 1.25.

Therefore the mass of MEM and MEP samples were measured with a 25.376 cm^3 glass cell and the densities of each were determined to be 1.245 and 1.205 gcm^{-3} respectively. Both MEM and MEP were assumed to have a linear relationship between the weight percentage and its density, therefore the weight percentage was determined from a simple plot (Figure B.1). It was found that for each gram of added aqueous MEP or MEM, corresponded to 0.643 g of MEP and 0.738 g of MEM.

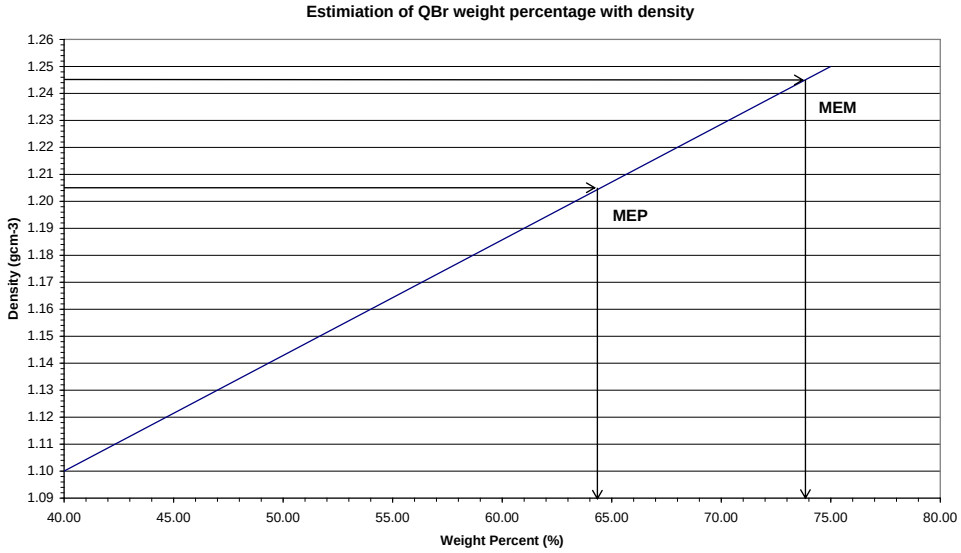

Figure B.1 Weight percent estimation of MEM and MEP with measured densities

Once the densities and weight percent were found, the volume of MEM and MEP for each sample was calculated and added to the measured 2.5 M V(III) solution. Finally, supporting electrolyte was added to the sample to maintain the final concentration of HBr and HCl

Table B.1 Sample Preparations for simulated positive electrolytes with single QBr (Stability tests observations summarised in Table 5.1)

	Concentrations (M)							Volume (ml)							
Sample	V(IV)	MEM	MEP	TBA	Br_2	HBr	HCl	2.5 M V(IV)	2.76 M V(IV)	Br_2	MEM	MEP	TBA	7.6 M HBr + 1.46 M HCl	H_2O
ConA1	2.03	0.00	0.00	0.00	0.00	6.1	1.2	0	10.0	0.0	0.0	0.0	0.0	1.0	2.6
ConA2	2.03	1.16	0.00	0.00	0.00	5.6	1.1	0	10.0	0.0	3.6	0.0	0.0	0.0	0
V4ConB2	2.00	0.75	0.00	0.00	0.00	6.3	1.2	7.2	0	0.0	1.5	0.0	0.0	0.3	0
ConB2	2.00	0.59	0.00	0.00	0.00	6.6	1.3	0	5.0	0.0	0.9	0.0	0.0	1.0	0
ConA6	2.08	0.00	0.99	0.00	0.00	5.7	1.1	0	10.0	0.0	0.0	3.3	0.0	0.0	0
ConB6	2.00	0.00	0.79	0.00	0.00	6.1	1.2	0	5.0	0.0	0.0	1.4	0.0	0.5	0
ConB12	2.00	0.00	0.00	0.75	0.00	6.1	1.2	0	5.0	0.0	0.0	0.0	1.7	0.5	1.4
02A	2	0	0	0	0.2	6.1	1.2	7.2	0.0	0.1	0.0	0.0	0.0	0.0	1.7
02V4A2	2	1.17	0	0	0.2	5.5	1.1	0	10.0	0.1	3.7	0.0	0.0	0.0	0
02II	2.02	0.79	0	0	0.2	6.2	1.2	7.2	0.0	0.1	1.6	0.0	0.0	0.0	0
02V4B2	2.02	0.59	0	0	0.2	6.5	1.2	7.2	0.0	0.1	1.2	0.0	0.0	0.4	0
02V4A6	2.04	0	1	0	0.2	5.6	1.1	0.0	10	0.1	0.0	3.4	0.0	0.0	0
02V4B6	2.04	0	0.68	0	0.2	6.2	1.2	0.0	10	0.1	0.0	2.3	0.0	1.1	0
02V4B12	2	0	0	0.75	0.2	6.0	1.2	0.0	10.0	0.1	0.0	0.0	3.3	1.0	2.7
I	2	0	0	0	1	6.1	1.2	0.0	5	0.4	0.0	0.0	0.0	0.5	1
2	2	1	0	0	1	5.5	1.1	0.0	5.0	0.4	1.6	0.0	0.0	0.0	0
II, B	2	0.79	0	0	1	5.8	1.1	0.0	5.0	0.4	1.2	0.0	0.0	0.3	0
B2	2	0.59	0	0	1	6.2	1.2	0.0	5.0	0.4	0.9	0.0	0.0	0.6	0
6	1.99	0	0.91	0	1	5.5	1.1	0.0	5.0	0.4	0.0	1.6	0.0	0.0	0
VI	2	0	0.68	0	1	5.9	1.1	0.0	5.0	0.4	0.0	1.2	0.0	0.4	0
V4B12	1.95	0	0	0.75	1	6.0	1.1	7.2	0	0.5	0.0	0.0	2.2	0.0	1.5
V4B2	1.95	0.73	0	0	1	5.9	1.1	7.2	0.0	0.5	1.5	0.0	0.0	0.0	0

Table B.2 Sample Preparations for simulated positive electrolyte with binary and ternary QBr mixture at 25oC (Stability Observation summarised in Table 5.2)

	Concentrations (M)							Volumes (ml)							
Sample	V(IV)	MEM	MEP	TBA	Br2	HBr	HCl	2.5 M V(IV)	2.76 M V(IV)	Br_2	MEM	MEP	TBA	7.6 M HBr + 1.46 M HCl	H_2O
ConA3	1.95	0.54	0.45	0	0	5.8	1.1	0.0	10.0	0.0	1.8	1.6	0.0	0.7	0
ConA4	1.95	0.74	0.30	0	0	5.7	1.1	0.0	10.0	0.0	2.4	1.1	0.0	0.6	0
ConA5	1.95	0.84	0.23	0	0	5.7	1.1	0.0	10.0	0.0	2.7	0.8	0.0	0.6	0
ConA7	1.95	0.37	0.62	0	0	5.8	1.1	0.0	10.0	0.0	1.2	2.2	0.0	0.7	0
ConA8	1.95	0.28	0.71	0	0	5.8	1.1	0.0	10.0	0.0	0.9	2.5	0.0	0.7	0
V4ConB3	2.00	0.39	0.35	0.00	0.00	6.2	1.2	7.2	0.0	0.0	0.8	0.8	0.0	0.2	0
V4ConB4	2.00	0.24	0.49	0.00	0.00	6.2	1.2	7.2	0.0	0.0	0.5	1.1	0.0	0.2	0
V4ConB5	2.00	0.15	0.58	0.00	0.00	6.2	1.2	7.2	0.0	0.0	0.3	1.3	0.0	0.2	0
V4ConB7	2.00	0.49	0.22	0.00	0.00	6.3	1.2	7.2	0.0	0.0	1.0	0.5	0.0	0.3	0
V4ConB8	2.00	0.58	0.18	0.00	0.00	6.2	1.2	7.2	0.0	0.0	1.2	0.4	0.0	0.2	0
3	1.96	0.54	0.44	0	1.11	5.4	1.0	0.0	5.0	0.4	0.9	0.8	0.0	0.0	0
4	1.92	0.73	0.33	0	1.08	5.3	1.0	0.0	5.0	0.4	1.2	0.6	0.0	0.0	0
5	1.92	0.85	0.22	0	1.08	5.3	1.0	0.0	5.0	0.4	1.4	0.4	0.0	0.0	0
7	1.94	0.37	0.62	0	1.11	5.3	1.0	0.0	5.0	0.4	0.6	1.1	0.0	0.0	0
8	1.94	0.25	0.73	0	1.11	5.3	1.0	0.0	5.0	0.4	0.4	1.3	0.0	0.0	0
V4B3	1.94	0.38	0.34	0.00	1.04	5.9	1.1	7.2	0.0	0.5	0.8	0.8	0.0	0.0	0
V4B4	1.94	0.24	0.47	0.00	1.04	5.9	1.1	7.2	0.0	0.5	0.5	1.1	0.0	0.0	0
V4B5	1.94	0.14	0.56	0.00	1.04	5.9	1.1	7.2	0.0	0.5	0.3	1.3	0.0	0.0	0
V4B7	1.95	0.48	0.22	0.00	1.04	5.9	1.1	7.2	0.0	0.5	1.0	0.5	0.0	0.0	0
V4B8	1.94	0.56	0.17	0.00	1.04	5.9	1.1	7.2	0.0	0.5	1.2	0.4	0.0	0.0	0
V4B9	1.94	0.38	0.00	0.36	1.05	6.2	1.2	7.2	0.0	0.5	0.8	0.0	1.1	0.4	0.4

	Concentrations (M)							Volumes (ml)							
Sample	V(IV)	MEM	MEP	TBA	Br2	HBr	HCl	2.5 M V(IV)	2.76 M V(IV)	Br_2	MEM	MEP	TBA	7.6 M HBr + 1.46 M HCl	H_2O
V4B10	1.94	0.24	0.00	0.50	1.05	6.0	1.1	7.2	0.0	0.5	0.5	0.0	1.5	0.1	1
V4B11	1.94	0.14	0.00	0.59	1.05	6.1	1.2	7.2	0.0	0.5	0.3	0.0	1.8	0.3	1
V4B13	1.93	0.47	0.00	0.26	1.04	5.9	1.1	7.2	0.0	0.5	1.0	0.0	0.8	0.0	0.6
V4B14	1.94	0.56	0.00	0.17	1.05	6.2	1.2	7.2	0.0	0.5	1.2	0.0	0.5	0.4	0
V4B15	1.94	0.00	0.34	0.39	1.05	5.9	1.1	7.2	0.0	0.5	0.0	0.8	1.2	0.0	0.8
V4B16	1.94	0.00	0.21	0.52	1.05	6.0	1.1	7.2	0.0	0.5	0.0	0.5	1.6	0.1	1
V4B17	1.94	0.00	0.17	0.57	1.05	6.0	1.2	7.2	0.0	0.5	0.0	0.4	1.7	0.2	1
V4B18	1.94	0.00	0.47	0.26	1.05	6.3	1.2	7.2	0.0	0.5	0.0	1.1	0.8	0.5	0
V4B19	1.94	0.00	0.56	0.18	1.05	6.1	1.2	7.2	0.0	0.5	0.0	1.3	0.5	0.3	0
V4B20	1.94	0.23	0.26	0.25	1.05	6.3	1.2	7.2	0.0	0.5	0.5	0.6	0.7	0.5	0
V4B21	1.94	0.38	0.17	0.18	1.05	6.2	1.2	7.2	0.0	0.5	0.8	0.4	0.6	0.4	0
V4B22	1.94	0.47	0.13	0.13	1.05	6.1	1.2	7.2	0.0	0.5	1.0	0.3	0.4	0.3	0
V4B23	1.94	0.19	0.39	0.16	1.05	6.1	1.2	7.2	0.0	0.5	0.4	0.9	0.5	0.3	0
V4B24	1.94	0.14	0.43	0.17	1.05	6.1	1.2	7.2	0.0	0.5	0.3	1.0	0.5	0.3	0
V4B25	1.94	0.19	0.17	0.37	1.05	5.9	1.1	7.2	0.0	0.5	0.4	0.4	1.1	0.0	0.8
V4B26	1.94	0.14	0.13	0.47	1.05	5.9	1.1	7.2	0.0	0.5	0.3	0.3	1.4	0.0	1

Table B.3 Sample preparations for simulated positive electrolyte with MEM and MEP at different ratio (Stability Observation summarised in Table 5.3)

	Concentrations (M)							Volumes (ml)						
Sample	V(IV)	MEM	MEP	TBA	Br_2	HBr	HCl	2.5 M V(IV)	2.76 M V(IV)	Br2	MEM	MEP	TBA	7.6M HBr + 1.46M HCl
V4ConB3	2.00	0.39	0.35	0.00	0.00	6.2	1.2	7.2	0.0	0.00	0.80	0.80	0.0	0.2
V4ConB4	2.00	0.24	0.49	0.00	0.00	6.2	1.2	7.2	0.0	0.00	0.50	1.10	0.00	0.20
V4ConB5	2.00	0.15	0.58	0.00	0.00	6.2	1.2	7.2	0.0	0.00	0.30	1.30	0.00	0.20
V4ConB7	2.00	0.49	0.22	0.00	0.00	6.3	1.2	7.2	0.0	0.00	1.00	0.50	0.00	0.30
V4ConB8	2.00	0.58	0.18	0.00	0.00	6.2	1.2	7.2	0.0	0.00	1.20	0.40	0.00	0.20
V4B3	1.94	0.38	0.34	0.00	1.04	5.9	1.1	7.2	0.0	0.5	0.80	0.80	0.0	0.0
V4B4	1.94	0.24	0.47	0.00	1.04	5.9	1.1	7.2	0	0.5	0.50	1.10	0.0	0.0
V4B5	1.94	0.14	0.56	0.00	1.04	5.9	1.1	7.2	0	0.5	0.30	1.30	0.0	0.0
V4B7	1.95	0.48	0.22	0.00	1.04	5.9	1.1	7.2	0	0.5	1.00	0.50	0.00	0.0
V4B8	1.94	0.56	0.17	0.00	1.04	5.9	1.1	7.2	0	0.5	1.20	0.40	0.00	0.0
B3	2.00	0.39	0.35	0.00	0.22	6.2	1.2	14.4	0.0	0.2	1.60	1.60	0.0	0.2
B4	2.00	0.24	0.49	0.00	0.22	6.2	1.2	14.4	0.0	0.2	1.00	2.20	0.00	0.20
B5	2.00	0.15	0.58	0.00	0.22	6.2	1.2	14.4	0.0	0.2	0.60	2.60	0.00	0.20
B6	2.00	0.49	0.22	0.00	0.22	6.2	1.2	14.4	0.0	0.2	2.00	1.00	0.00	0.40
B7	2.00	0.58	0.18	0.00	0.22	6.2	1.2	14.4	0.0	0.2	2.40	0.80	0.00	0.20

Table B.4 Sample preparations for bromine solutions with various QBr concentrations (Stability Observation summarised in Table 5.4)

	Concentrations (M)						Volumes (ml)					
Sample	MEM	MEP	TBA	Br_2	HBr	HCl	Br_2	MEM	MEP	TBA	7.6 M HBr + 1.46 M HCl	H_2O
BrConB1	0.00	0.00	0.00	1.00	6.0	1.1	0.50	0.00	0.00	0.00	7.6	1.6
BrConB21	0.36	0.17	0.18	1.04	6.2	1.2	0.50	0.80	0.40	0.55	7.60	0
BrConB22	0.44	0.13	0.13	1.04	6.1	1.2	0.50	1.00	0.30	0.40	7.50	0
BrConB23	0.18	0.38	0.16	1.04	6.1	1.2	0.50	0.40	0.90	0.48	7.50	0
BrConB24	0.13	0.42	0.17	1.04	6.1	1.2	0.50	0.30	1.00	0.50	7.50	0
BrConA27	0.43	0.41	0.20	1.02	5.6	1.1	0.50	1.00	1.00	0.60	7.00	0
BrConA28	0.52	0.33	0.20	1.02	5.6	1.1	0.50	1.20	0.80	0.60	7.00	0
BrConA29	0.61	0.25	0.20	1.02	5.6	1.1	0.50	1.40	0.60	0.60	7.00	0
BrConA30	0.35	0.49	0.20	1.02	5.6	1.1	0.50	0.80	1.20	0.60	7.00	0
BrConA31	0.26	0.57	0.20	1.02	5.6	1.1	0.50	0.60	1.40	0.60	7.00	0

Table B.5 Samples preparations for simulated negative electrolyte with binary QBr mixture at 0M and 0.2M bromine (Observation summarised in Table 5.5)

	Concentrations (M)						Volumes (ml)						
Sample	V(III)	MEM	MEP	Br_2	HBr	HCl	2.2 M V(III)	2.5 M V(III)	Br_2	MEM	MEP	7.6 M HBr + 1.46 M HCl	H_2O
V3ConB1	2.00	0.00	0.00	0.00	6.1	1.2	0	16.00	0.00	0.00	0.00	4.00	4
V3ConB3	2.00	0.37	0.38	0.00	6.2	1.2	0	16.00	0.00	1.70	1.90	0.40	0
V3ConB4	2.00	0.24	0.50	0.00	6.2	1.2	0	16.00	0.00	1.10	2.50	0.40	0
V3ConB5	2.00	0.20	0.56	0.00	6.2	1.2	0	16.00	0.00	0.90	2.80	0.30	0
V3ConB7	2.00	0.50	0.26	0.00	6.2	1.2	0	16.00	0.00	2.30	1.30	0.40	0
V3ConB8	2.00	0.57	0.18	0.00	6.3	1.2	0	16.00	0.00	2.60	0.90	0.50	0
V3B1	2.00	0.00	0.00	0.19	6.1	1.2	0	16.00	0.20	0.00	0.00	3.80	3.8
V3B3	2.00	0.37	0.38	0.19	6.2	1.2	0	16.00	0.20	1.70	1.90	0.20	0
V3B4	2.00	0.24	0.50	0.19	6.2	1.2	0	16.00	0.20	1.10	2.50	0.20	0
V3B5	2.00	0.20	0.56	0.19	6.1	1.2	0	16.00	0.20	0.90	2.80	0.10	0
V3B7	2.00	0.50	0.26	0.19	6.2	1.2	0	16.00	0.20	2.30	1.30	0.20	0
V3B8	2.00	0.57	0.18	0.19	6.2	1.2	0	16.00	0.20	2.60	0.90	0.30	0

Table B.6 Simulated positive and negative half-cell electrolytes for Linear Voltammetry and Cyclic Voltammetry

	Concentrations (M)						Volumes (ml)						
Solutions for Linear Voltammetry	**V(IV)**	**MEM**	**MEP**	**Br_2**	**HBr**	**HCl**	**2.5M V(IV)**	**2.76M V(IV)**	**Br_2**	**MEM**	**MEP**	**7.6M HBr + 1.46M HCl**	**H_2O**
02V4B1	2.00	0.00	0.00	0.22	6.1	1.2	14.4	0.0	0.2	0.0	0.0	0.0	3.4
02V4B3	2.00	0.36	0.38	0.22	6.2	1.2	14.4	0.0	0.2	1.5	1.7	0.2	0.0
02V4B4	2.00	0.24	0.51	0.22	6.1	1.2	14.4	0.0	0.2	1.0	2.3	0.1	0.0
02V4B5	2.00	0.19	0.56	0.22	6.1	1.2	14.4	0.0	0.2	0.8	2.5	0.1	0.0
02V4B7	2.00	0.51	0.24	0.22	6.2	1.2	14.4	0.0	0.2	2.1	1.1	0.2	0.0
02V4B8	2.00	0.56	0.18	0.22	6.2	1.2	14.4	0.0	0.2	2.3	0.8	0.3	0.0
Solutions for Cyclic Voltammetry	**V(III)**	**MEM**	**MEP**	**Br_2**	**HBr**	**HCl**	**2.2M V(III)**	**2.5M V(III)**	**Br_2**	**MEM**	**MEP**	**7.6M HBr + 1.46M HCl**	**H_2O**
1.67M V(III)	1.67	0.00	0.00	0	5.8	1.1	13.60	0	0.00	0.0	0.0	0.0	4.3
1.67M V(III) 0.15M MEM 0.47M MEP	1.67	0.15	0.47	0	6.5	1.2	13.60	0	0	0.6	2.1	1.6	0
1.67M V(III) 0.15M MEM 0.65M MEP	1.67	0.15	0.65	0	6.1	1.2	13.60	0	0	0.6	2.9	0.9	0
1.67M V(III) 0.15M MEM 0.83M MEP	1.67	0.15	0.83	0	5.8	1.1	13.60	0	0	0.6	3.7	0.0	0
1.67M V(III) 0.49M MEM 0.16M MEP	1.67	0.49	0.16	0	6.5	1.2	13.6	0	0	2.0	0.7	1.6	0
1.67M V(III) 0.66M MEM 0.16M MEP	1.67	0.66	0.16	0	6.2	1.2	13.60	0	0	2.7	0.7	0.9	0
1.67M V(III) 0.86M MEM 0.16M MEP	1.67	0.86	0.16	0	5.8	1.1	13.60	0	0	3.5	0.7	0.1	0
2M V(III)	2.00	0.00	0.00	0.00	6.1	1.2	0	16.0	0.0	0.0	0.0	0.0	4
2M V(III) 1M MEM	2.00	1.04	0.00	0	5.8	1.1	0	14	0.0	4.5	0.0	0.4	0
2M V(III) 1M MEP	2.00	0.00	1.04	0	5.6	1.1	0	14	0	0.0	4.9	0.00	0
2M V(III) 0.20M MEM 0.56M MEP	2.00	0.20	0.56	0.19	6.1	1.2	0	16.0	0.2	0.9	2.80	0.1	0
2M V(III) 0.57M MEM 0.18M MEP	2.00	0.57	0.18	0.19	6.2	1.2	0	16.0	0.2	2.6	0.9	0.3	0

Table B.7 Bromine / Bromide solutions for Linear Voltammetry

	Concentrations (M)					Volumes (ml)					
Solutions for Linear Voltammetry	**HBr**	**HCl**	**MEM**	**MEP**	**Br_2**	**8.84 M HBr**	**Br_2**	**MEM**	**MEP**	**7.6 M HBr + 1.46 M HCl**	**H_2O**
6.2 M HBr 0.2 M Br_2	6.2	0	0.2	0	0.2	14	0.2	0	0	0	4.8
6.2 M HBr 1 M Br_2	6.2	0	1	0	1	14	1	0	0	0	4
6.2 M HBr 1.2 M HCl 0.2 M Br_2	6.2	1.2	0.2	0	0.2	0	0.2	0	0	16.3	3.5
6.2 M HBr 1.2 M HCl 1 M Br_2	6.2	1.2	1	0	1	0	1	0	0	16.3	2.7
6.2 M HBr 1.2 M HCl 0.2 M Br_2 0.19 M MEM 0.56 M MEP	6.2	1.2	0.19	0.56	0.2	0	0.2	0.9	2.9	16.1	0

Appendix C Graphs of CV, i_p vs $v^{1/2}$ and $\ln(i_p)$ vs (E_p-E^o) for simulated negative electrolytes

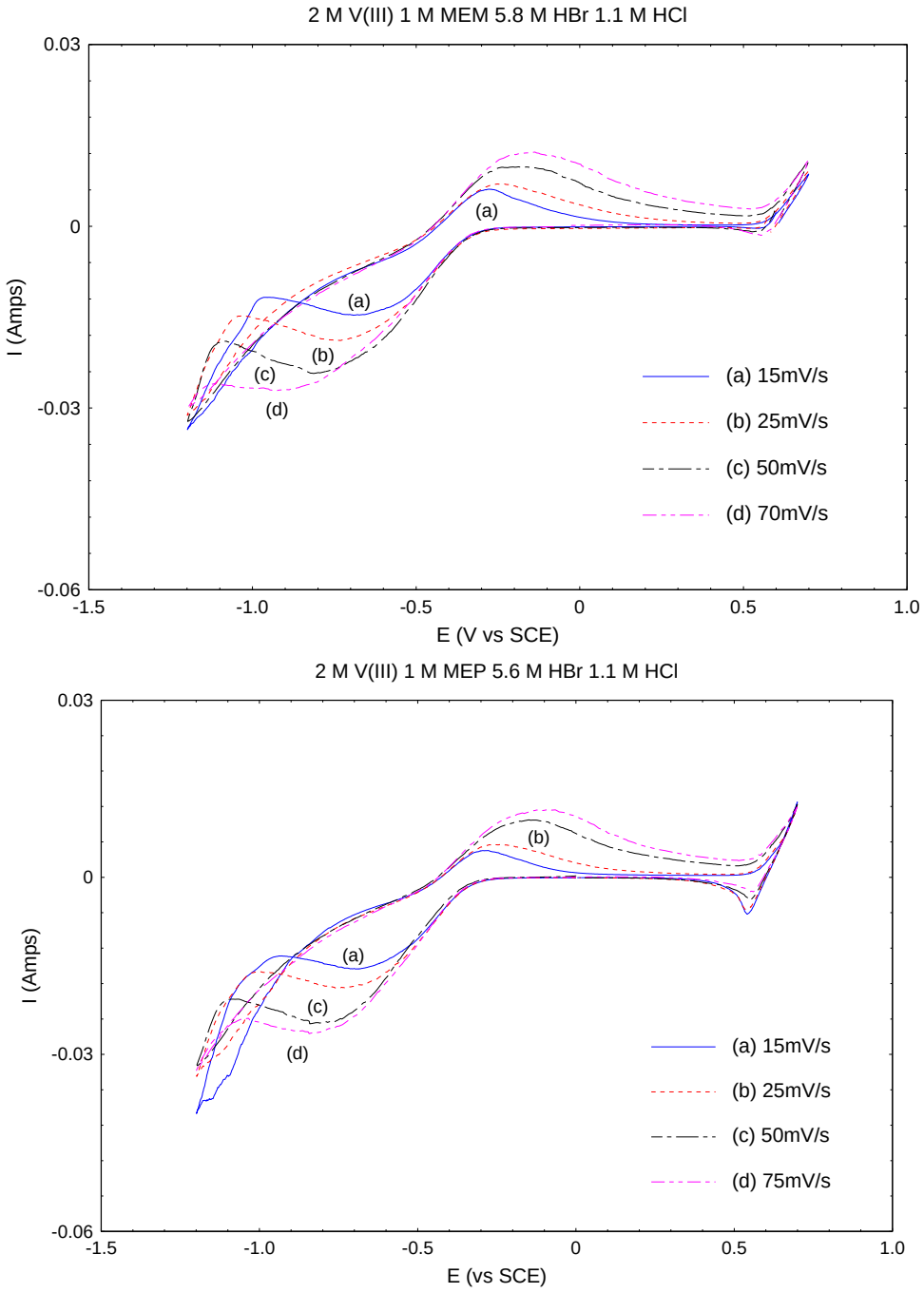

Figure C.1 CV for (top) 2 M V(III) 1 M MEM 5.8 M HBr 1.1 M HCl (bottom) 2 M V(III) 1 M MEP 5.6 M HBr 1.1 M HCl

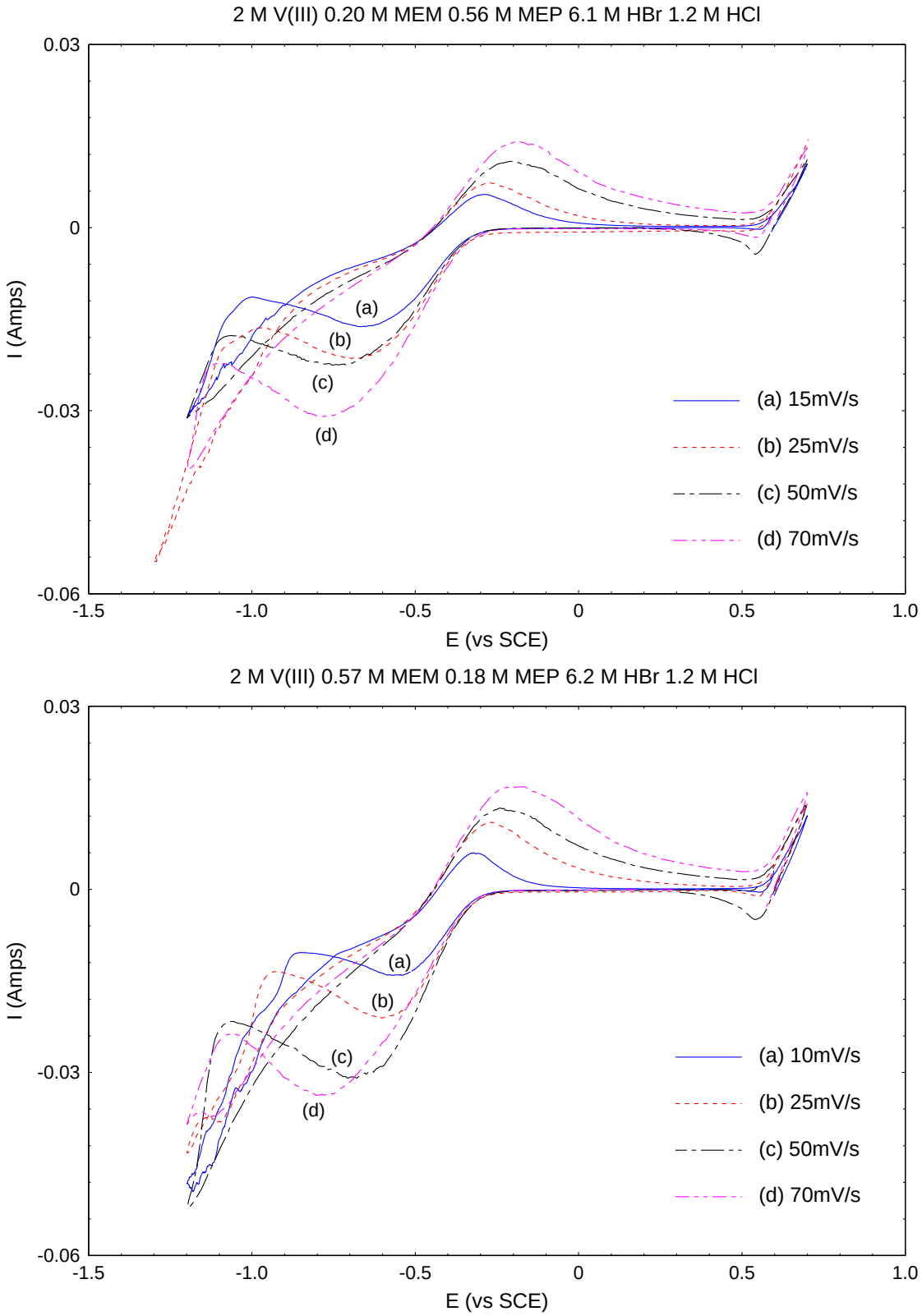

Figure C.2 CV for (top) 2 M V(III) 0.20 M MEM 0.56 M MEP 6.1 M HBr 1.2 M HCl (bottom) 2 M V(III) 0.57 M MEM 0.18 M MEP 6.2 M HBr 1.2 M HCl

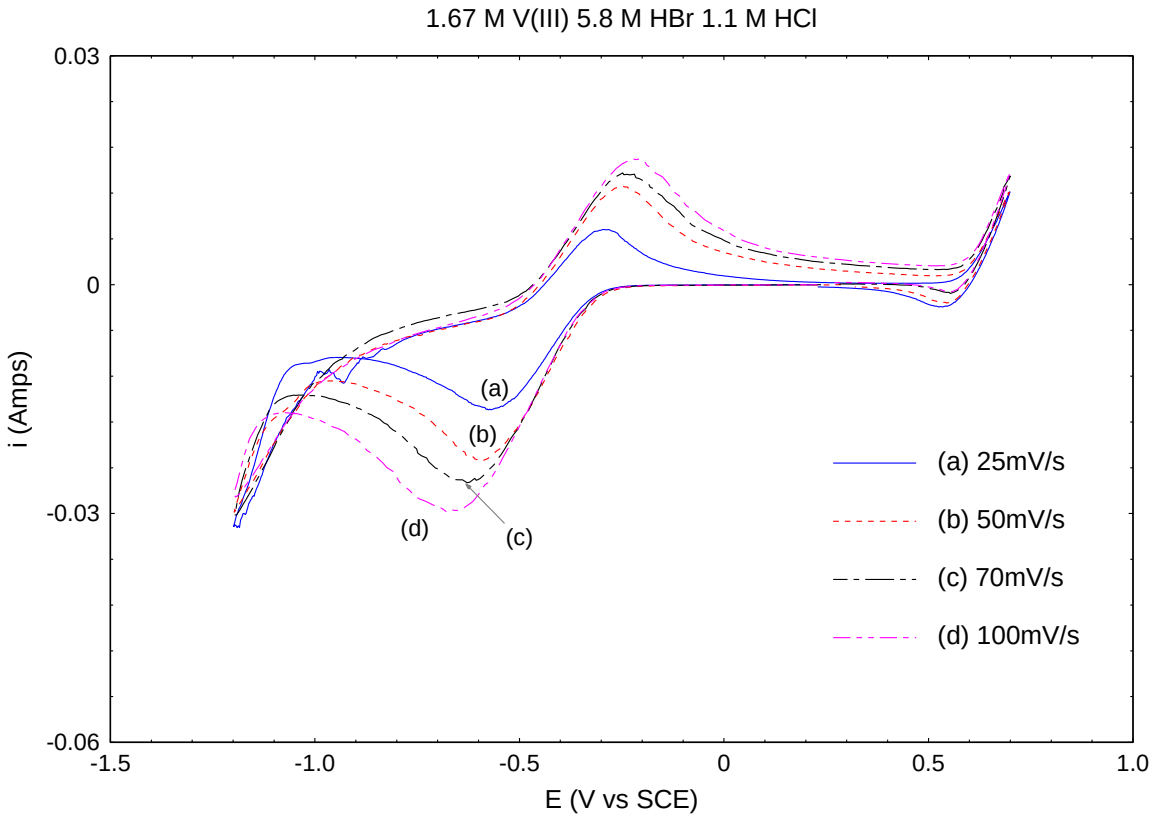

Figure C.3 CV for 1.67 M V(III) 5.8 M HBr 1.1 M HCl

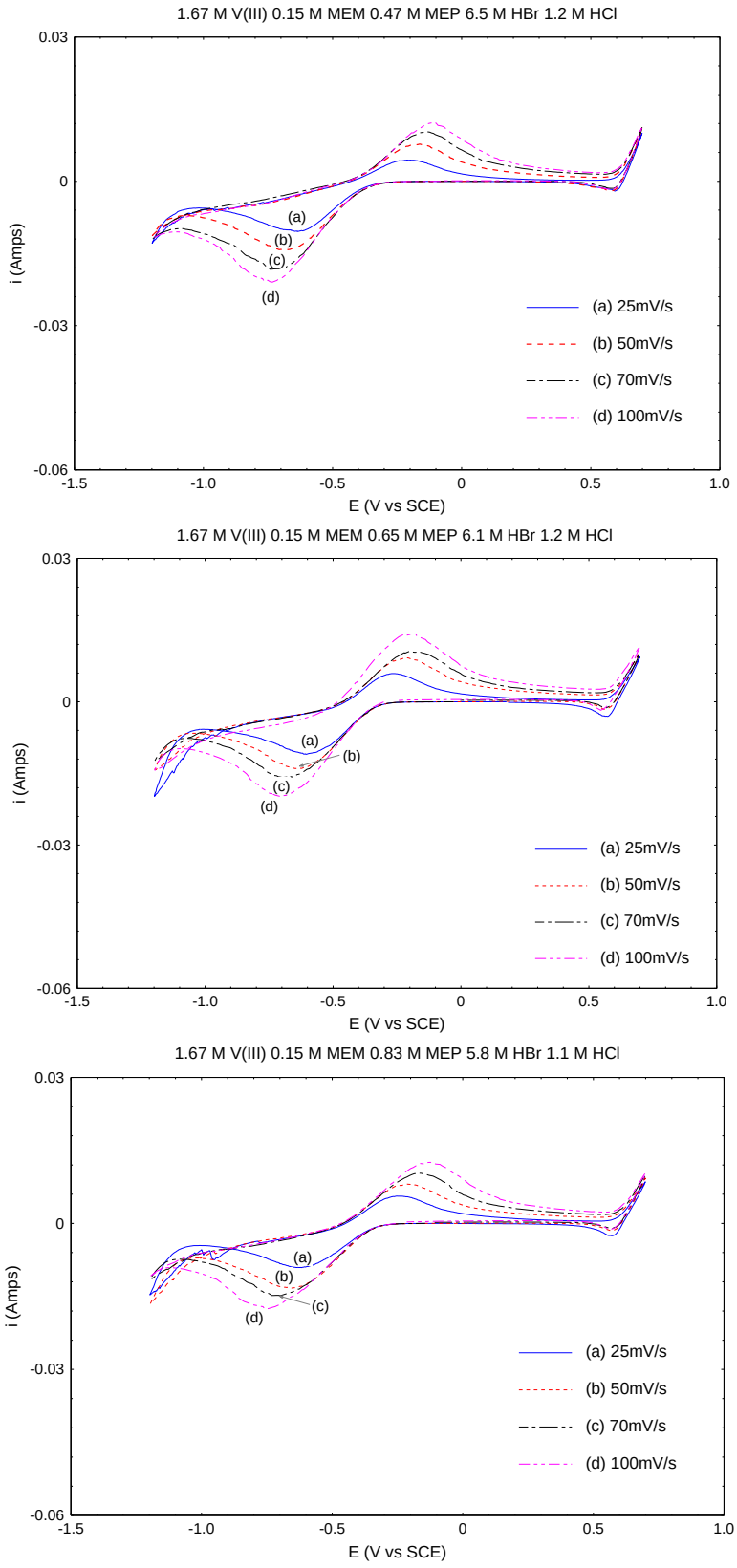

Figure C.4 CV (top) 1.67 M V(III) 0.15 M MEM 0.47 M MEP 6.5 M HBr 1.2 M HCl (mid) 1.67 M V(III) 0.15 M MEM 0.65 M MEP 6.1 M HBr 1.2 M HCl (bottom) 1.67 M V(III) 0.15 M MEM 0.83 M MEP 5.8 M HBr 1.1 M HCl

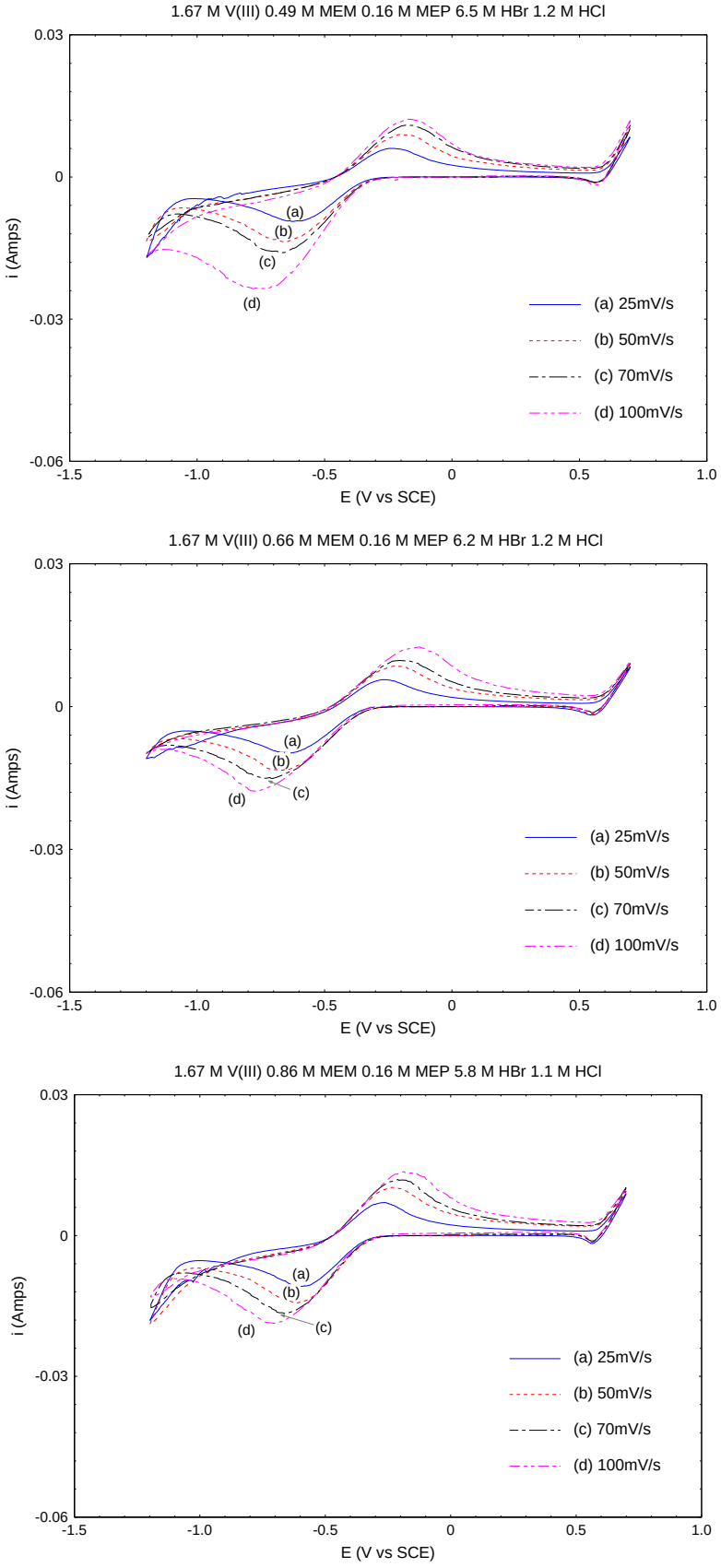

Figure C.5 CV (top) 1.67 M V(III) 0.49 M MEM 0.16 M MEP 6.5 M HBr 1.2 M HCl (mid) 1.67 M V(III) 0.66 M MEM 0.16 M MEP 6.2 M HBr 1.2 M HCl (bottom) 1.67 M V(III) 0.86 M MEM 0.16 M MEP 5.8 M HBr 1.1 M HCl

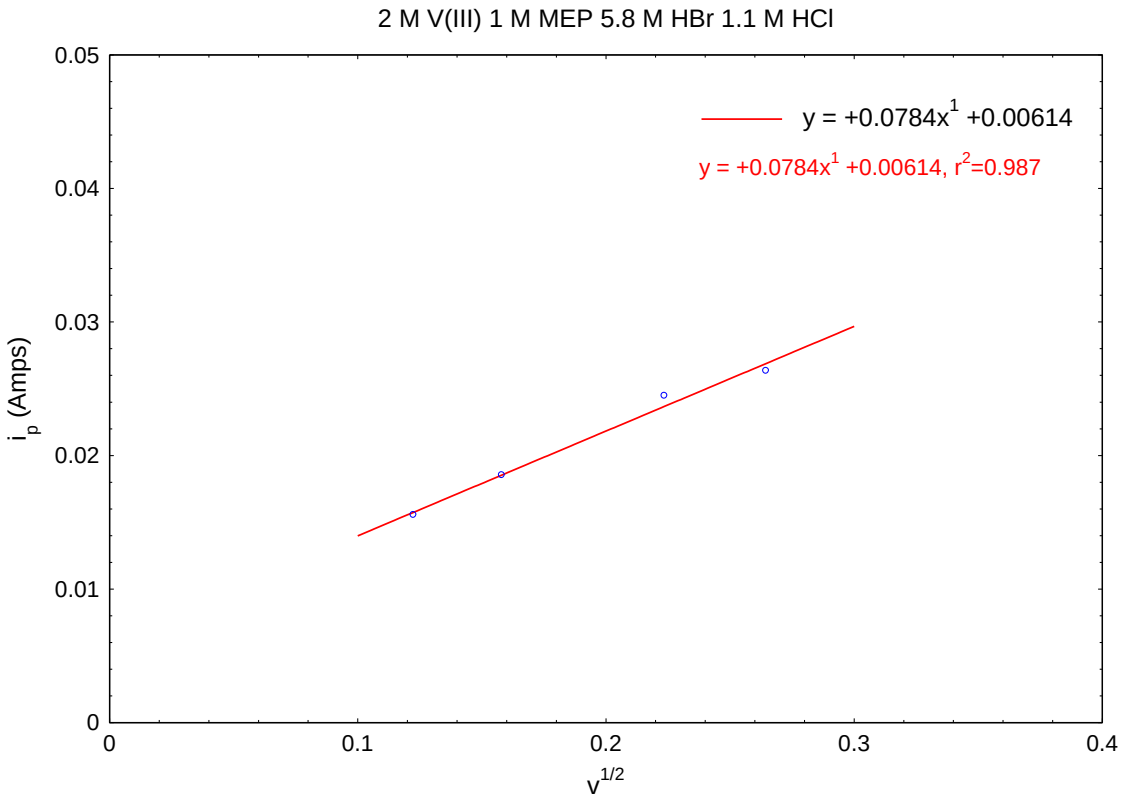

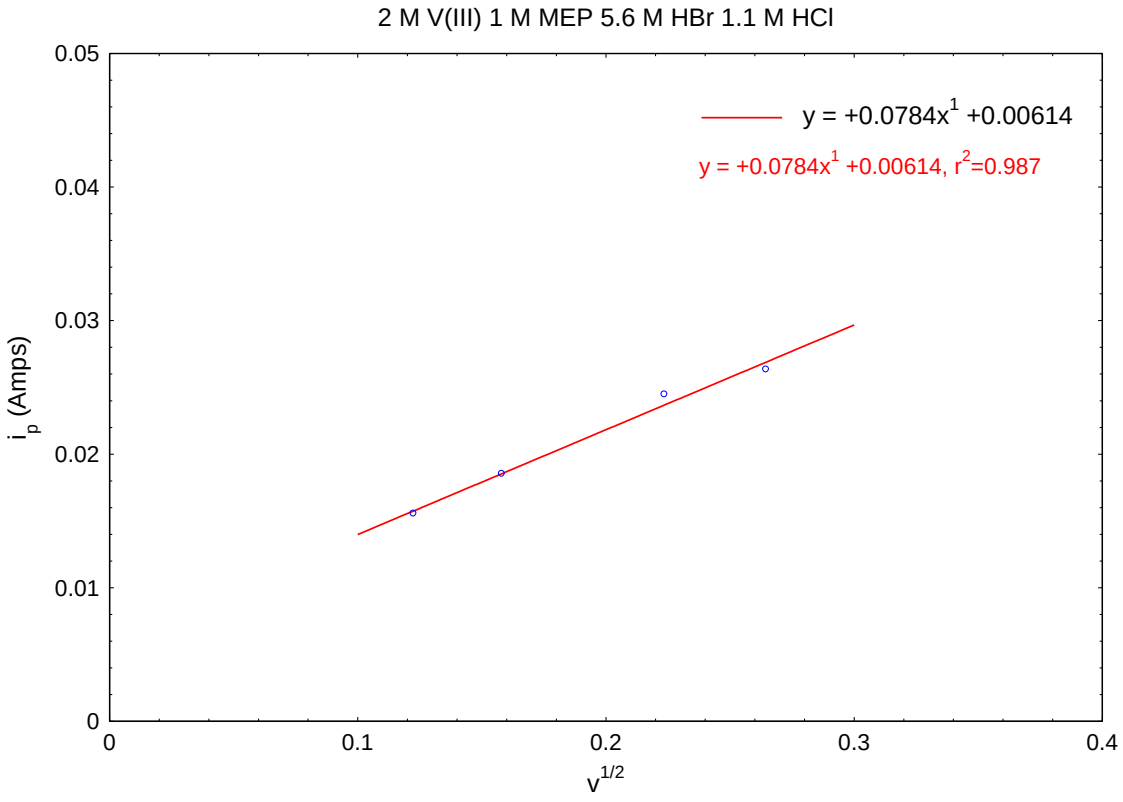

Figure C.6 Peak current (ip) against square root of scan rate ($v^{1/2}$) (top) 2 M V(III) 1 M MEM 5.8 M HBr 1.1 M HCl (bottom) 2 M V(III) 1 M MEP 5.6 M HBr 1.1 M HCl

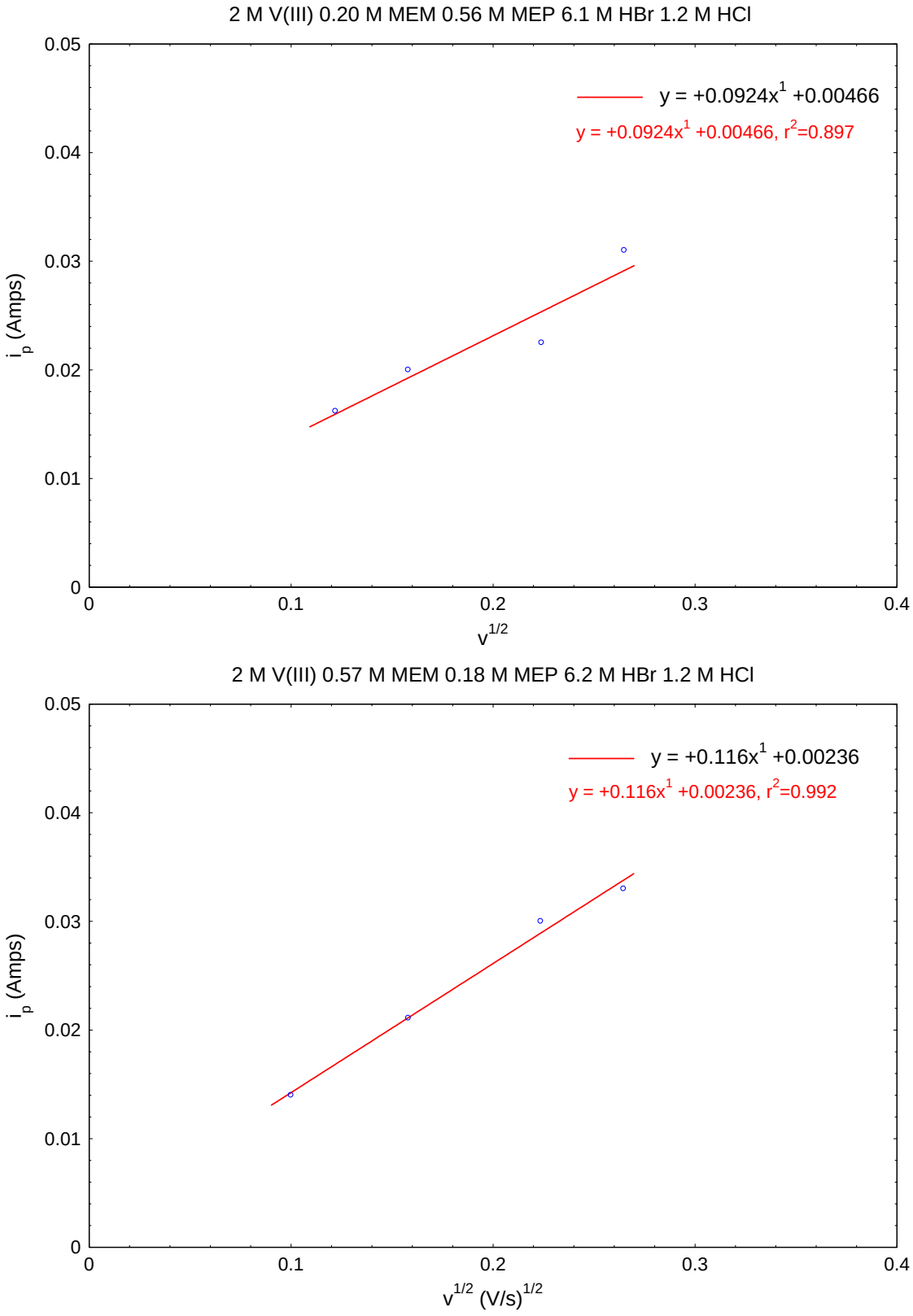

Figure C.7 Peak current (ip) against square root of scan rate ($v^{1/2}$) (top) 2 M V(III) 0.20 M MEM 0.56 M MEP 6.1 M HBr 1.2 M HCl (bottom) 2 M V(III) 0.57 M MEM 0.18 M MEP 6.2 M HBr 1.2 M HCl

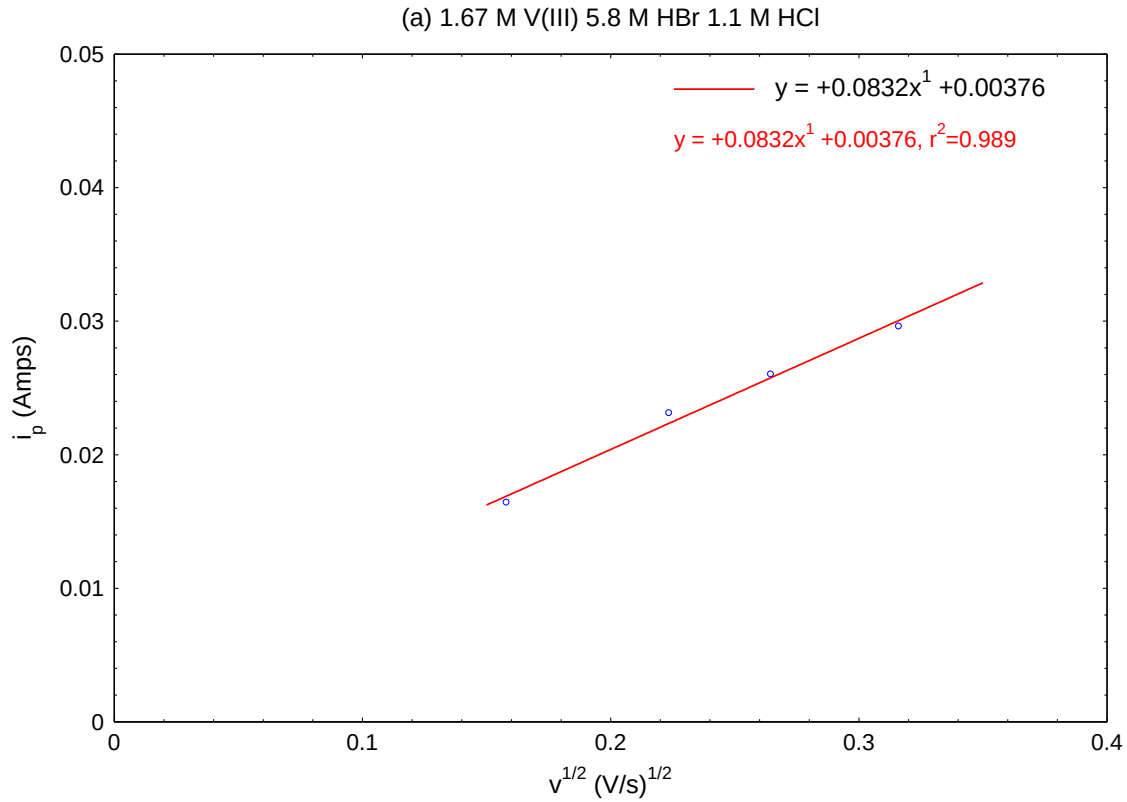

Figure C.8 Peak current (i_p) against square root of scan rate ($v^{1/2}$)

(a) 1.67 M V(III) 5.8 M HBr 1.1 M HCl

(b) 1.67 M V(III) 0.15 M MEM 0.47 M MEP 6.5 M HBr 1.2 M HCl

(c) 1.67 M V(III) 0.15 M MEM 0.65 M MEP 6.1 M HBr 1.2 M HCl

(d) 1.67 M V(III) 0.15 M MEM 0.83 M MEP 5.8 M HBr 1.1 M HCl

(e) 1.67 M V(III) 0.49 M MEM 0.16 M MEP 6.5 M HBr 1.2 M HCl

(f) 1.67 M V(III) 0.66 M MEM 0.16 M MEP 6.2 M HBr 1.2 M HCl

(g) 1.67 M V(III) 0.86 M MEM 0.16 M MEP 5.8 M HBr 1.1 M HCl

(b) 1.67 M V(III) 0.15 M MEM 0.47 M MEP 6.5 M HBr 1.1 M HCl

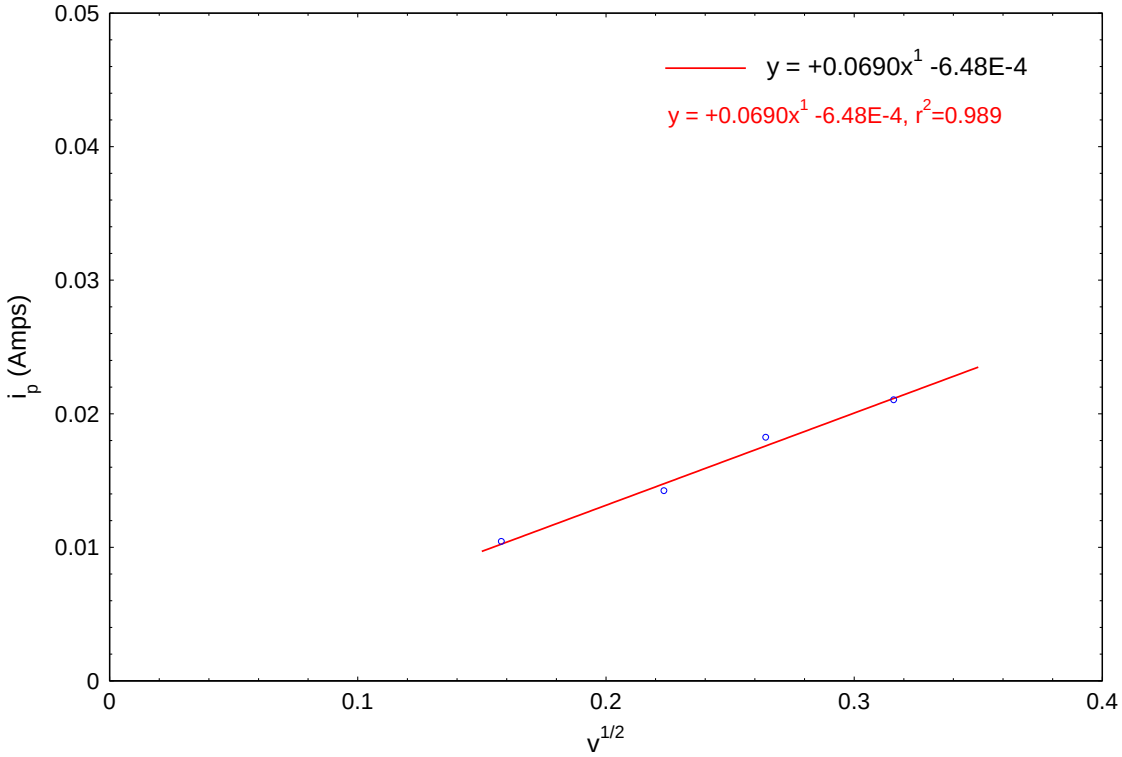

(c) 1.67 M V(III) 0.15 M MEM 0.65 M MEP 6.1 M HBr 1.2 M HCl

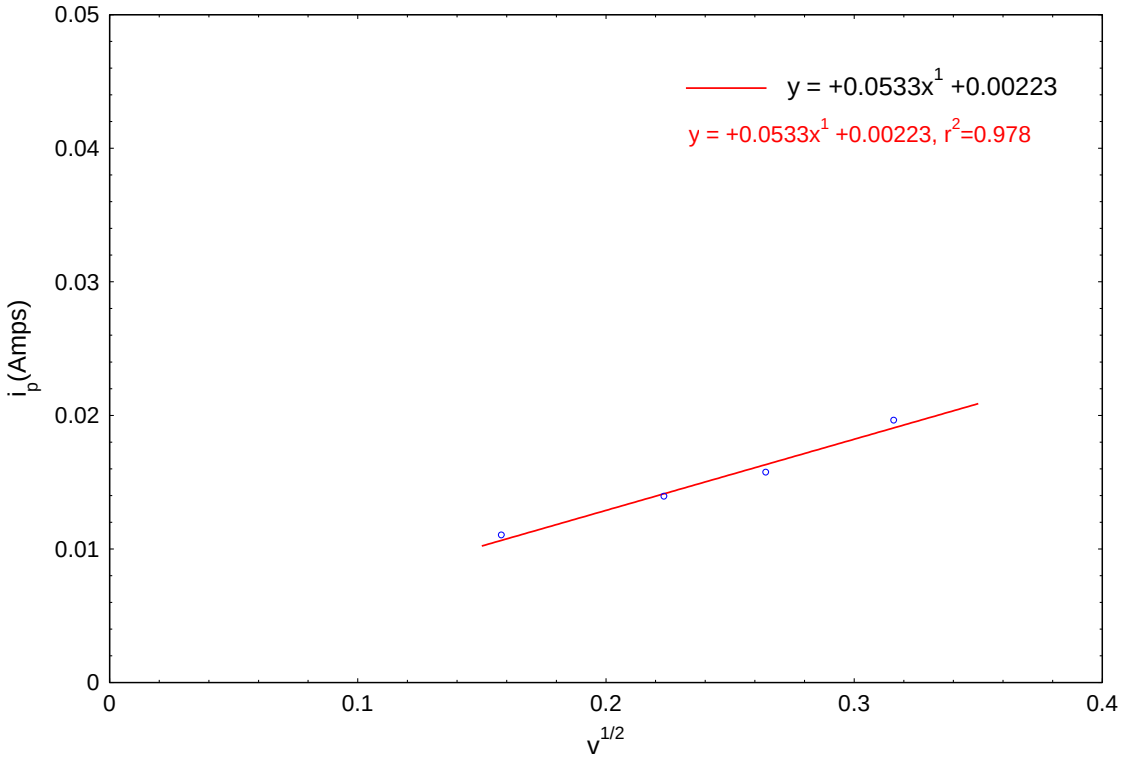

(d) 1.67 M V(III) 0.15 M MEM 0.83 M MEP 5.8 M HBr 1.1 M HCl

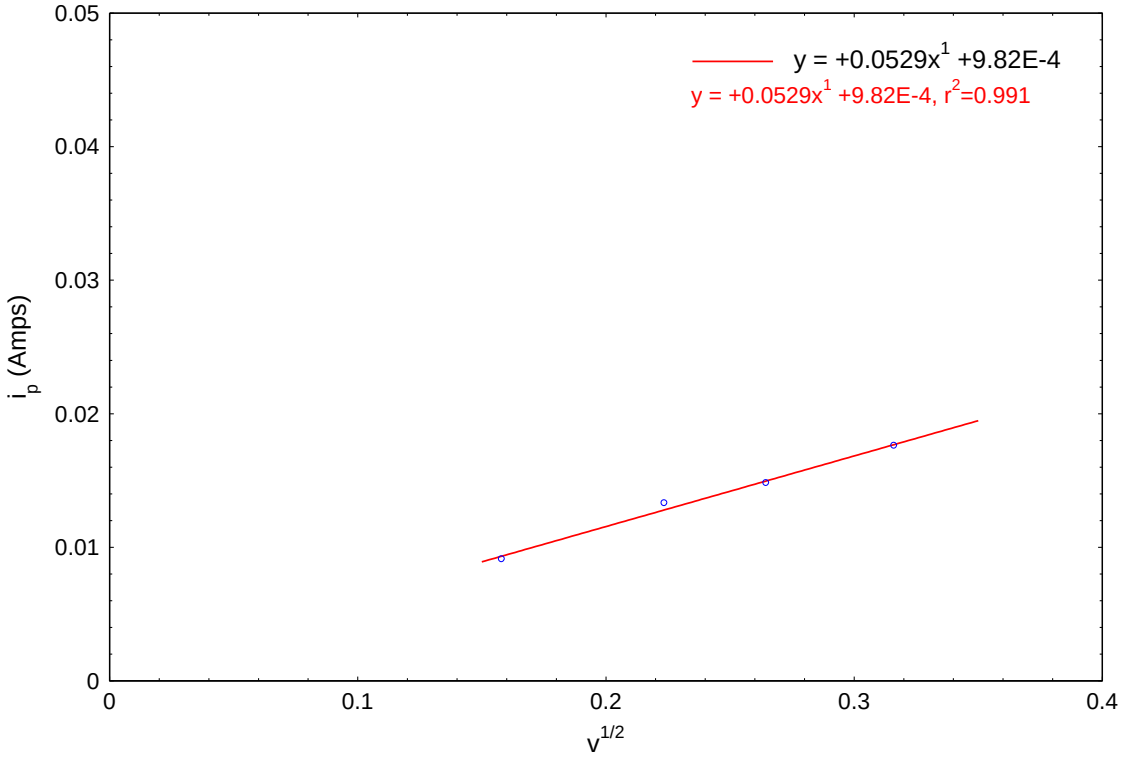

(e) 1.67 M V(III) 0.49 M MEM 0.16 M MEP 6.5 M HBr 1.2 M HCl

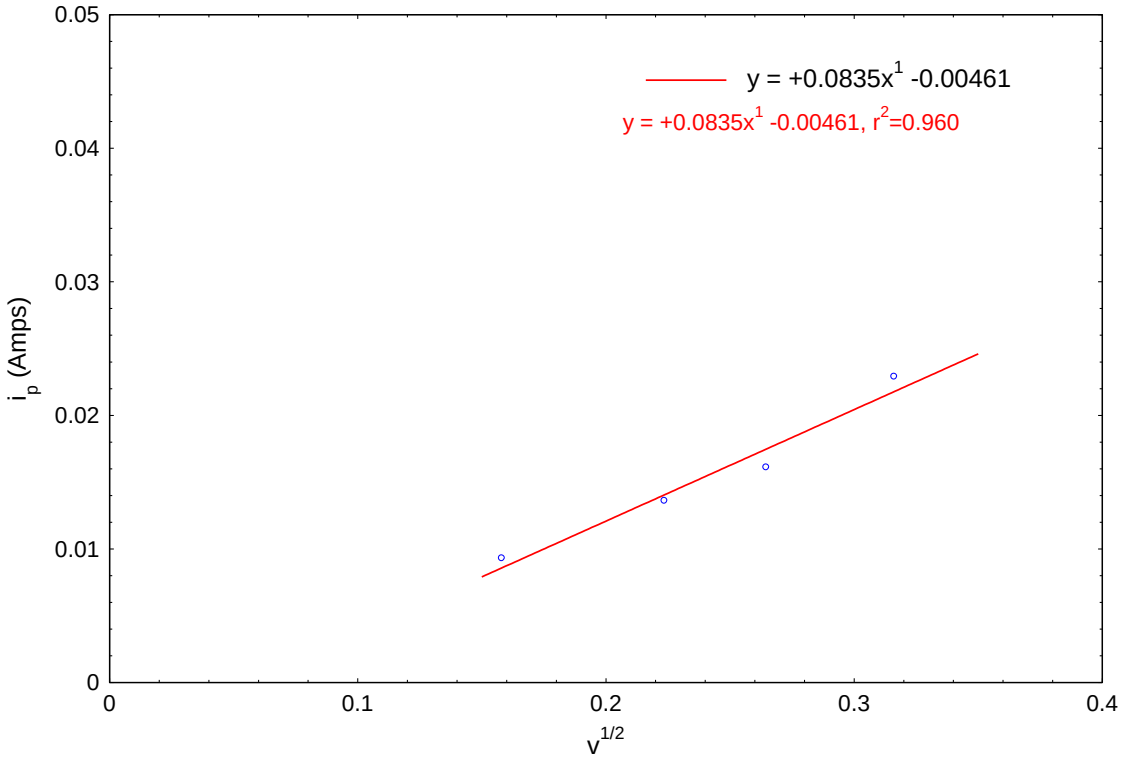

(f) 1.67 M V(III) 0.66 M MEM 0.16 M MEP 6.2 M HBr 1.2 M HCl

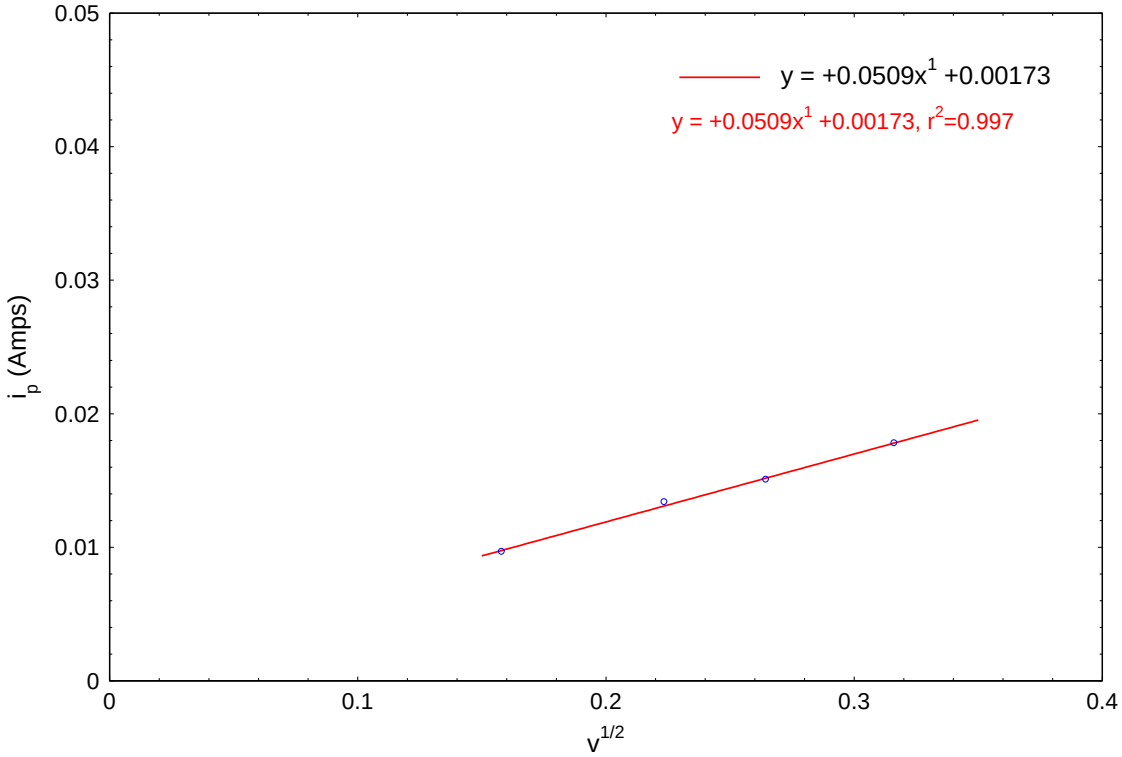

(g) 1.67 M V(III) 0.86 M MEM 0.16 M MEP 5.8 M HBr 1.1 M HCl

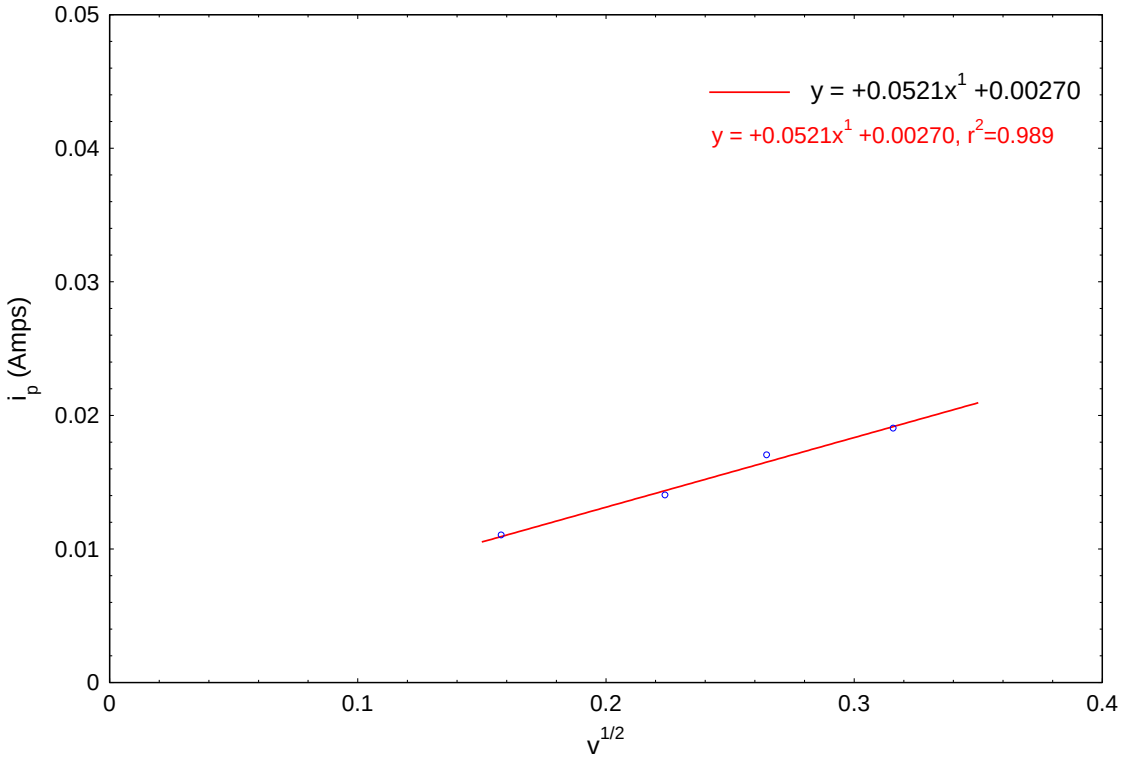

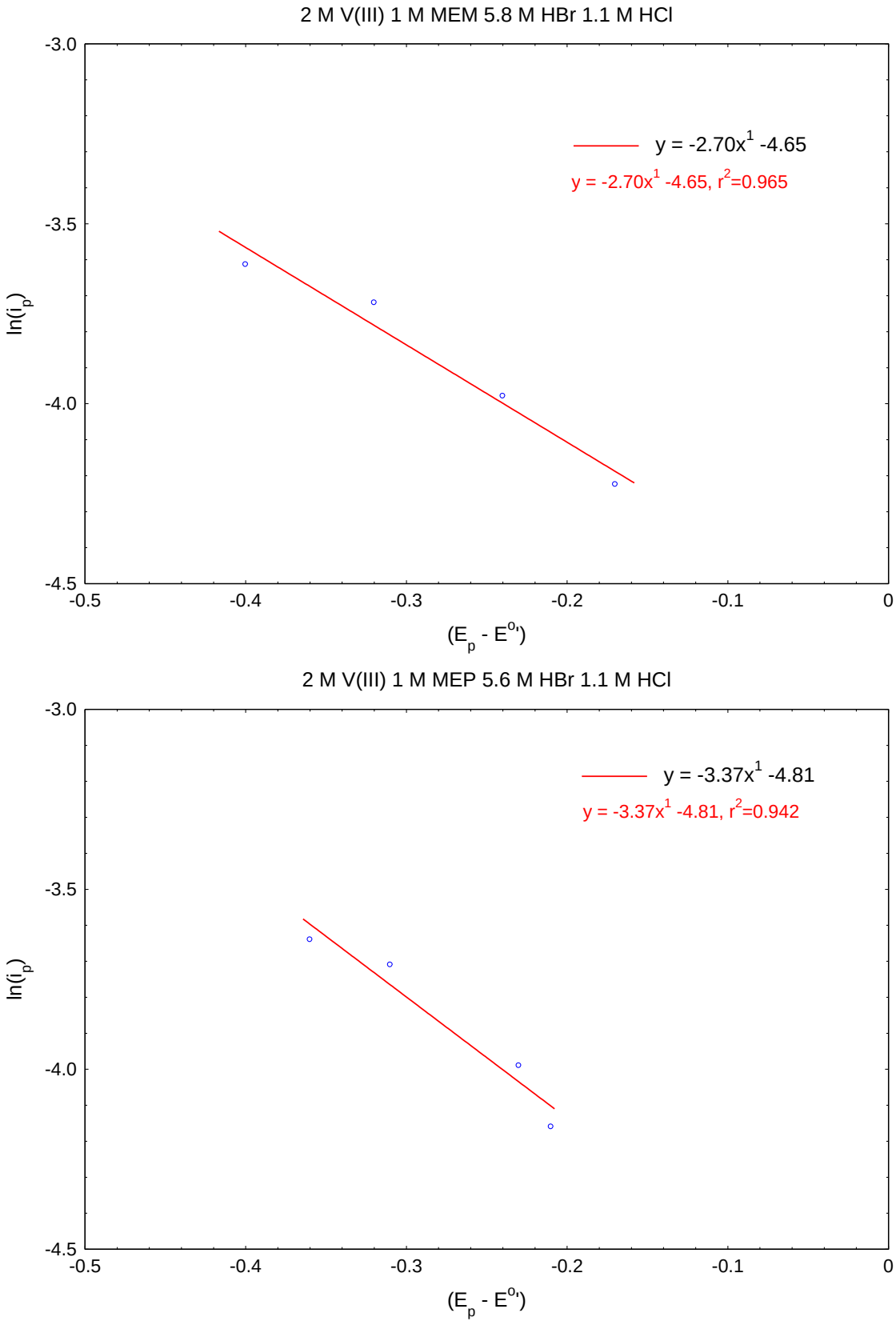

Figure C.9 $\ln(i_p)$ against vs (E_p – $E^{o'}$) from cyclic voltammogram of (top) 2 M V(III) 1 M MEM 5.8 M HBr 1.1 M HCl (bottom) 2 M V(III) 1 M MEP 5.6 M HBr 1.1 M HCl

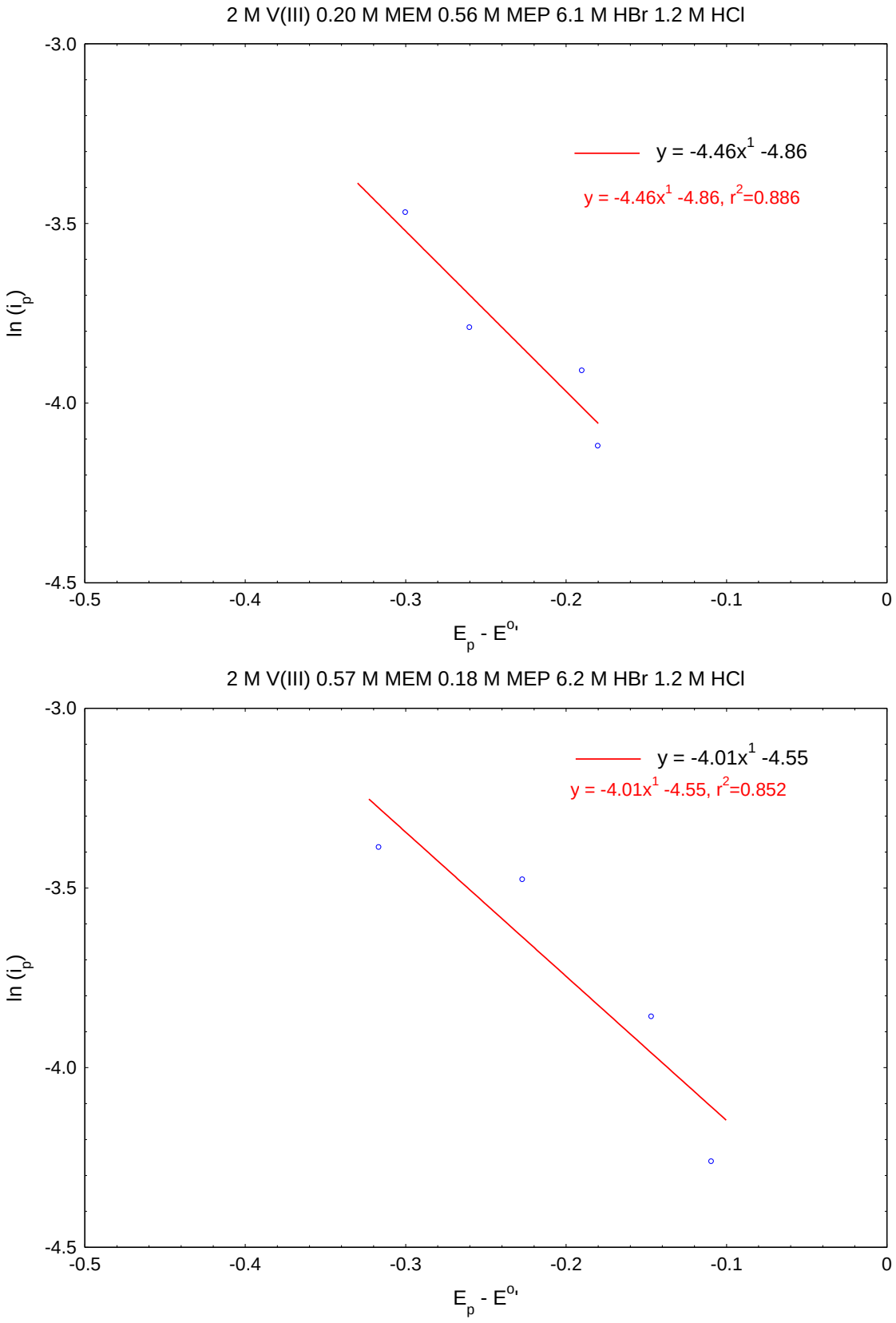

Figure C.10 ln(i_p) against vs (E_p – $E^{o'}$) from cyclic voltammogram of (top) 2 M V(III) 0.20 M MEM 0.56 M MEP 6.1 M HBr 1.2 M HCl (bottom) 2 M V(III) 0.57 M MEM 0.18 M MEP 6.2 M HBr 1.2 M HCl

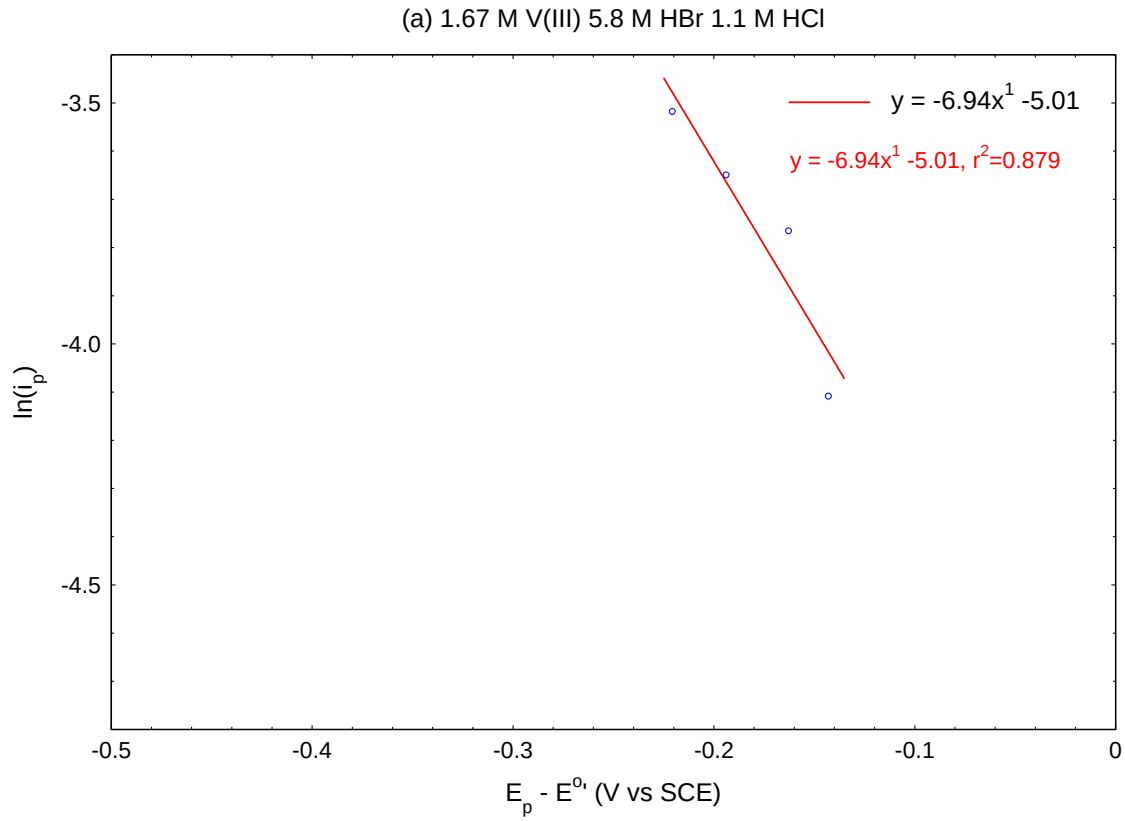

Figure C.11 ln(ip) against vs (Ep – Eo')

(a) 1.67 M V(III) 5.8 M HBr 1.1 M HCl

(b) 1.67 M V(III) 0.15 M MEM 0.47 M MEP 6.5 M HBr 1.2 M HCl

(c) 1.67 M V(III) 0.15 M MEM 0.65 M MEP 6.1 M HBr 1.2 M HCl

(d) 1.67 M V(III) 0.15 M MEM 0.83 M MEP 5.8 M HBr 1.1 M HCl

(e) 1.67 M V(III) 0.49 M MEM 0.16 M MEP 6.5 M HBr 1.2 M HCl

(f) 1.67 M V(III) 0.66 M MEM 0.16 M MEP 6.2 M HBr 1.2 M HCl

(g) 1.67 M V(III) 0.86 M MEM 0.16 M MEP 5.8 M HBr 1.1 M HCl

(b) 1.67 M V(III) 0.15 M MEM 0.47 M MEP 6.5 M HBr 1.2 M HCl

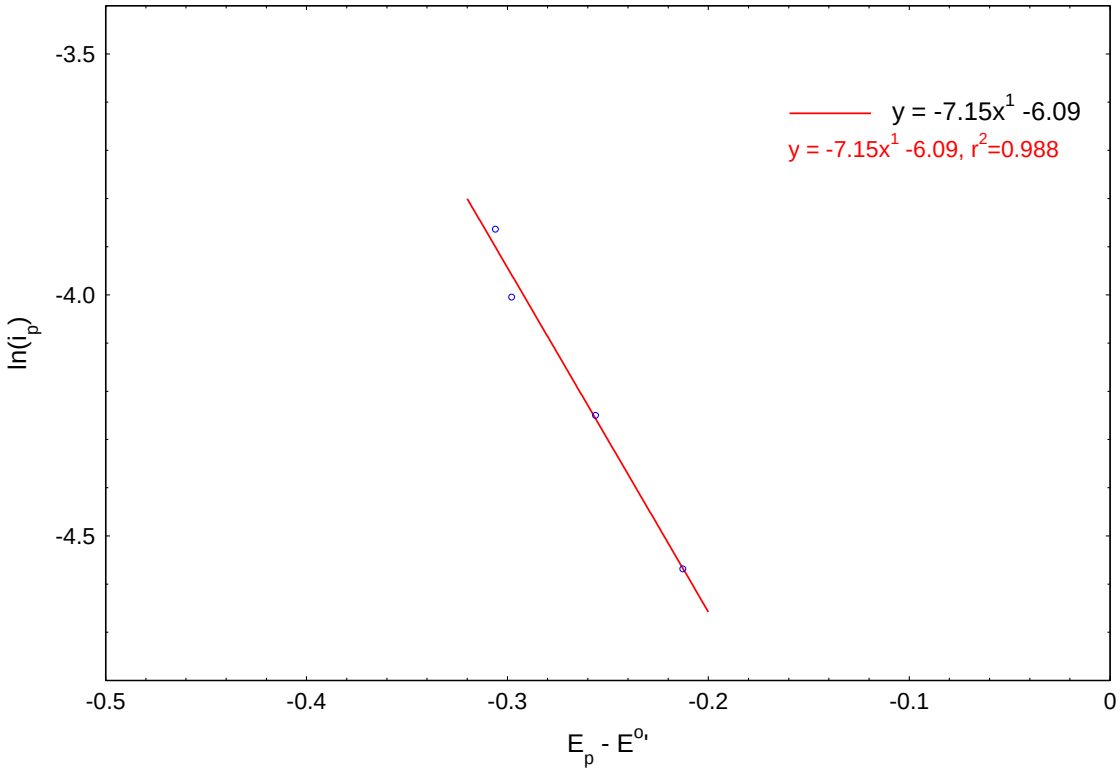

(c) 1.67 M V(III) 0.15 M MEM 0.65 M MEP 6.1 M HBr 1.2 M HCl

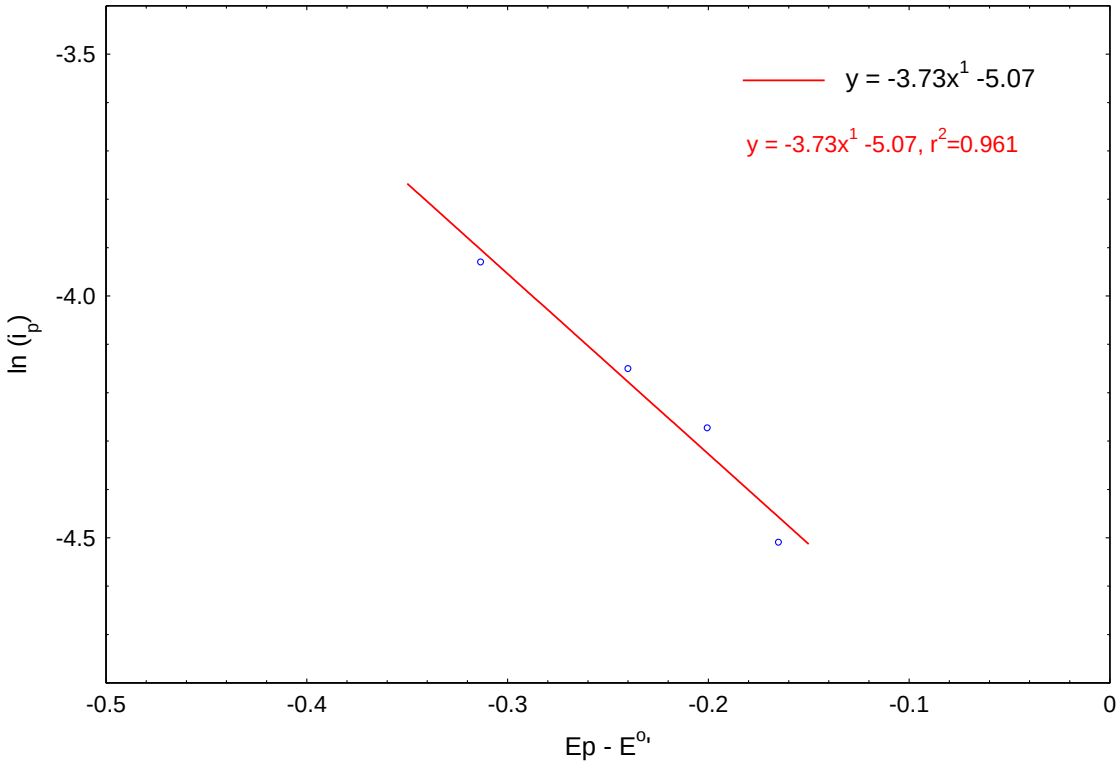

(d) 1.67 M V(III) 0.15 M MEM 0.83 M MEP 5.8 M HBr 1.1 M HCl

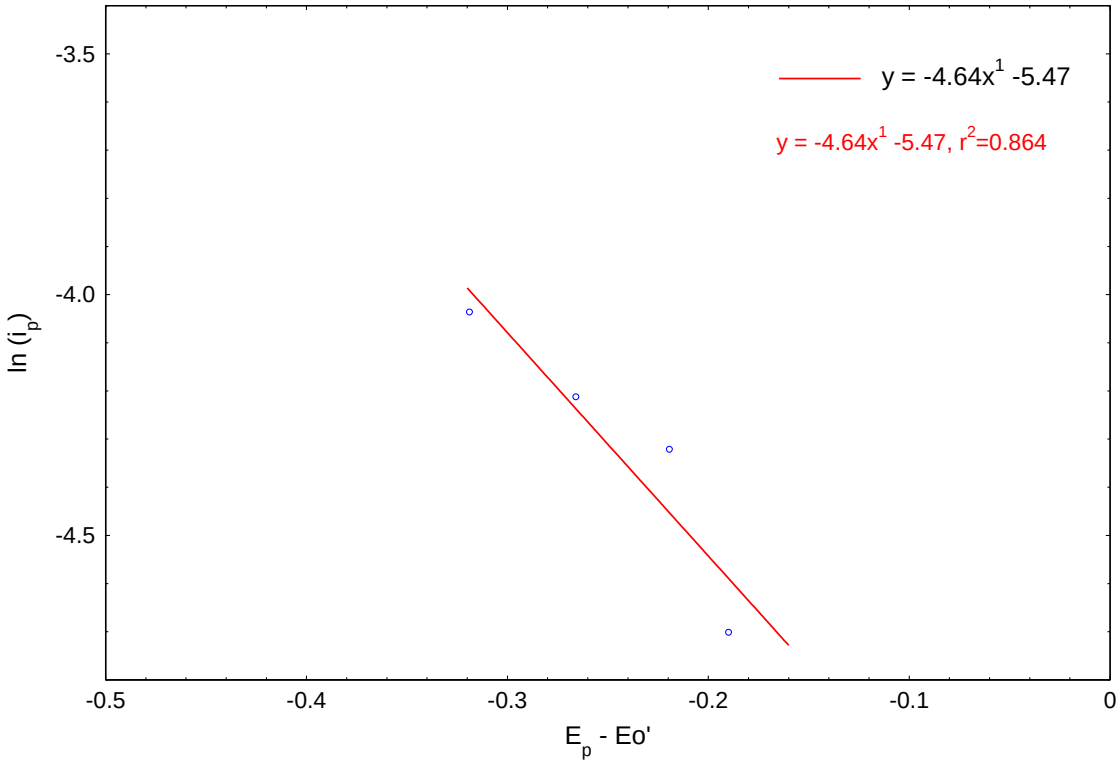

(e) 1.67 M V(III) 0.49 M MEM 0.16 M MEP 6.5 M HBr 1.2 M HCl

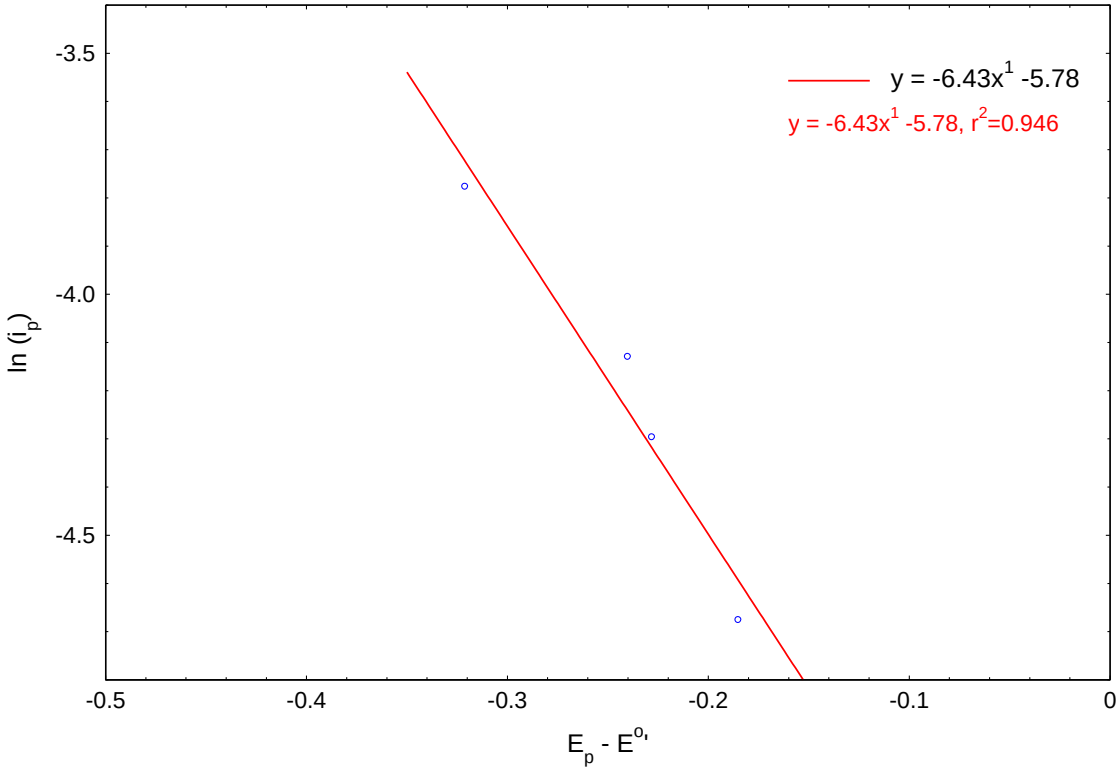

(f) 1.67 M V(III) 0.66 M MEM 0.16 M MEP 6.2 M HBr 1.2 M HCl

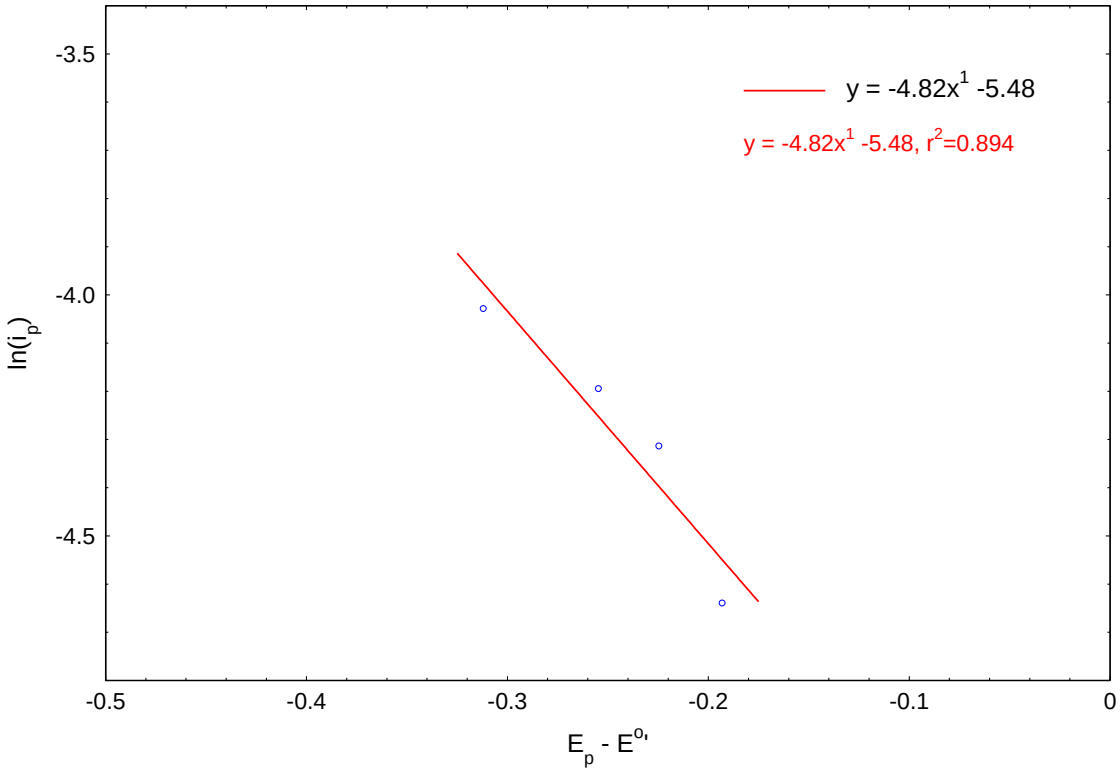

(g) 1.67 M V(III) 0.86 M MEM 0.16 M MEP 5.8 M HBr 1.1 M HCl

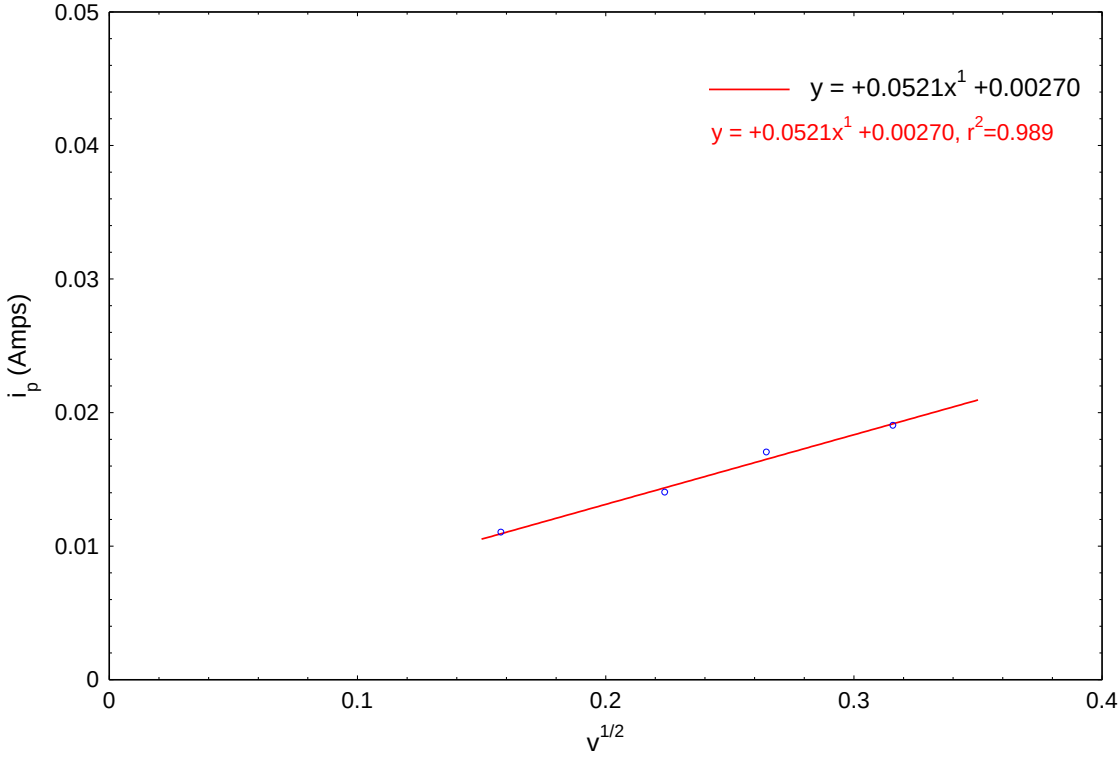

Appendix D Graphs of linear sweep voltammograms and Tafel plot of simulated positive electrolytes

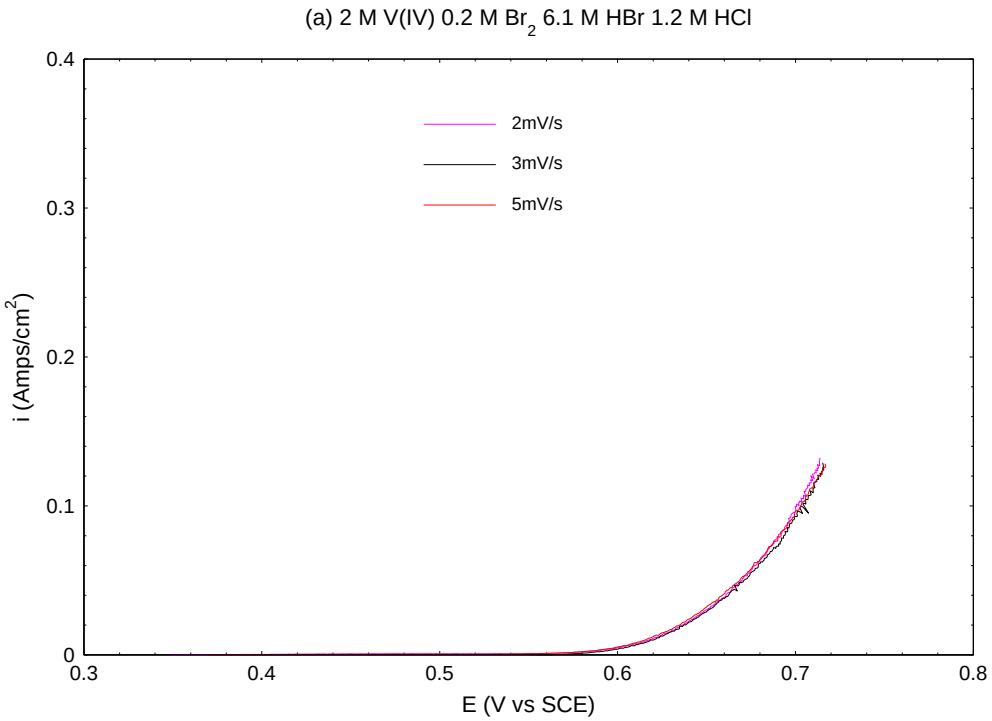

Figure D.1 Linear sweep voltammograms of (a) 2 M V(IV) 0.2 M Br_2 6.1 M HBr 1.2 M HCl (b) 2 M V(IV) 0.2 M Br_2 0.36 M MEM 0.38 M MEP 6.2 M HBr 1.2 M HCl (c) 2 M V(IV) 0.2 M Br_2 0.24 M MEM 0.51 M MEP 6.1 M HBr 1.2 M HCl (d) 2 M V(IV) 0.2 M Br_2 0.19 M MEM 0.56 M MEP 6.1 M HBr 1.2 M HCl (e) 2 M V(IV) 0.2 M Br_2 0.51 M MEM 0.24 M MEP 6.2 M HBr 1.2 M HCl (f) 2 M V(IV) 0.2 M Br_2 0.56 M MEM 0.18 M MEP 6.2 M HBr 1.2 M HCl

(b) 2 M V(IV) 0.2 M Br_2 0.36 M MEM 0.38 M MEP 6.2 M HBr 1.2 M HCl

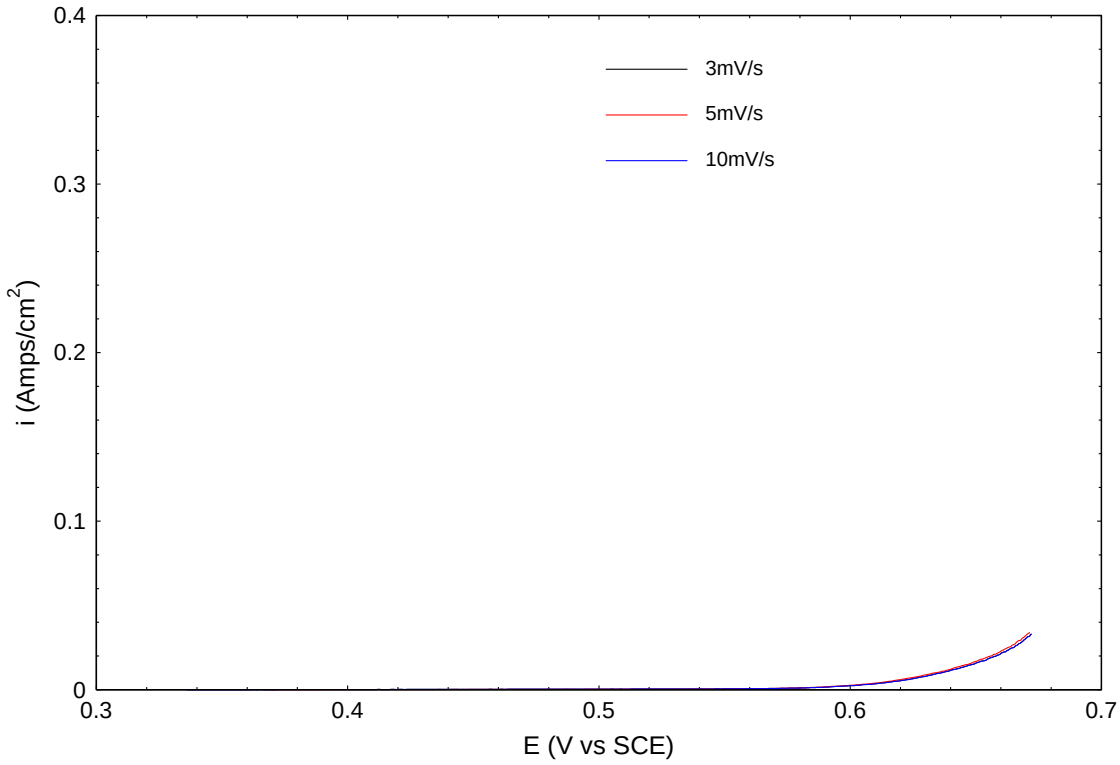

(c) 2 M V(IV) 0.2 M Br_2 0.24 M MEM 0.51 M MEP 6.1 M HBr 1.2 M HCl

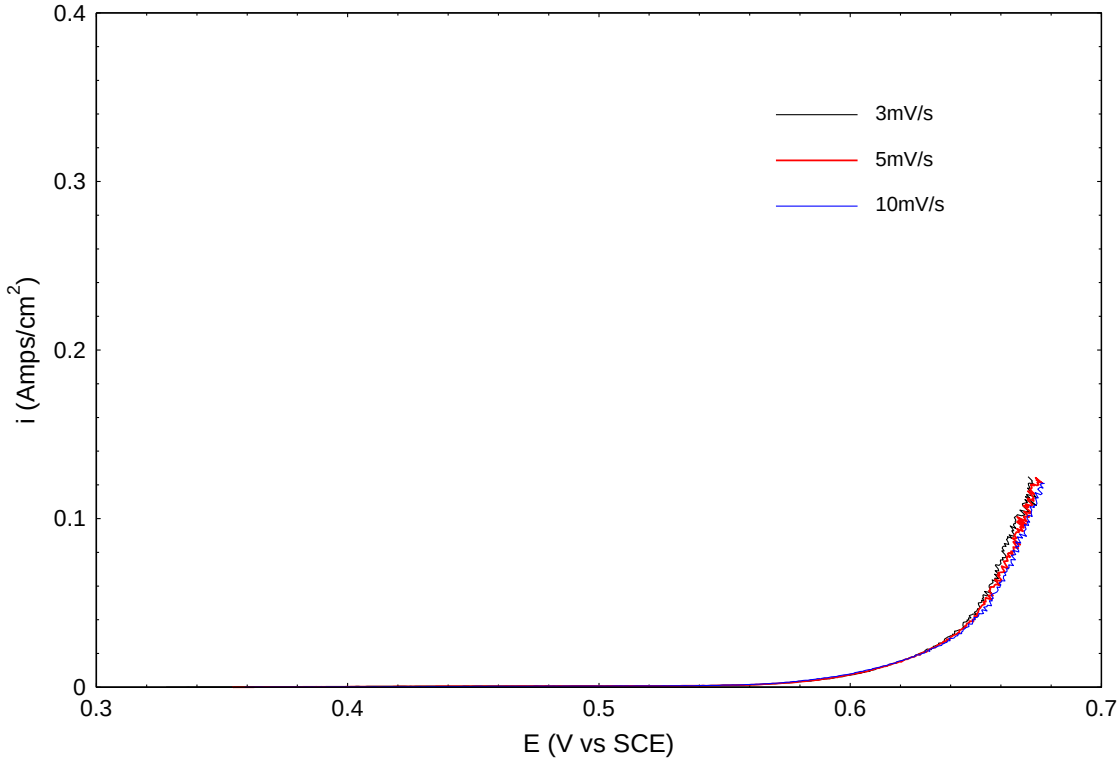

(d) 2 M V(IV) 0.2 M Br_2 0.19 M MEM 0.56 M MEP 6.1 M HBr 1.2 M HCl

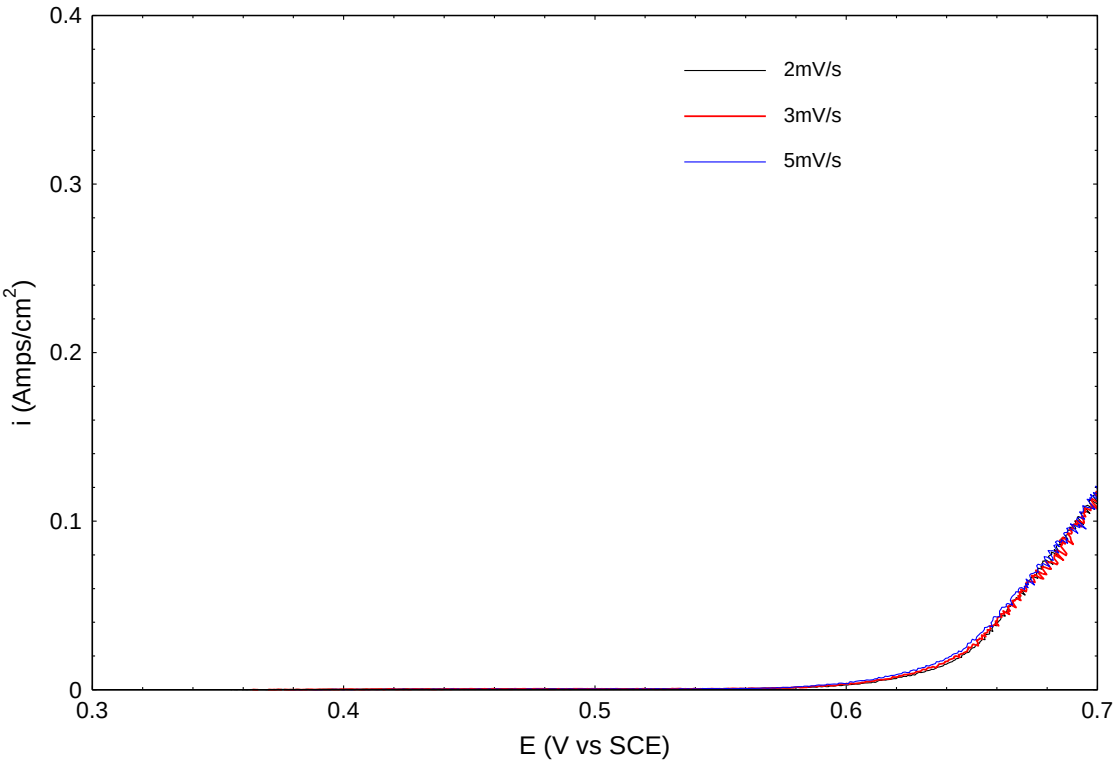

(e) 2 M V(IV) 0.2 M Br_2 0.51 M MEM 0.24 M MEP 6.2 M HBr 1.2 M HBr

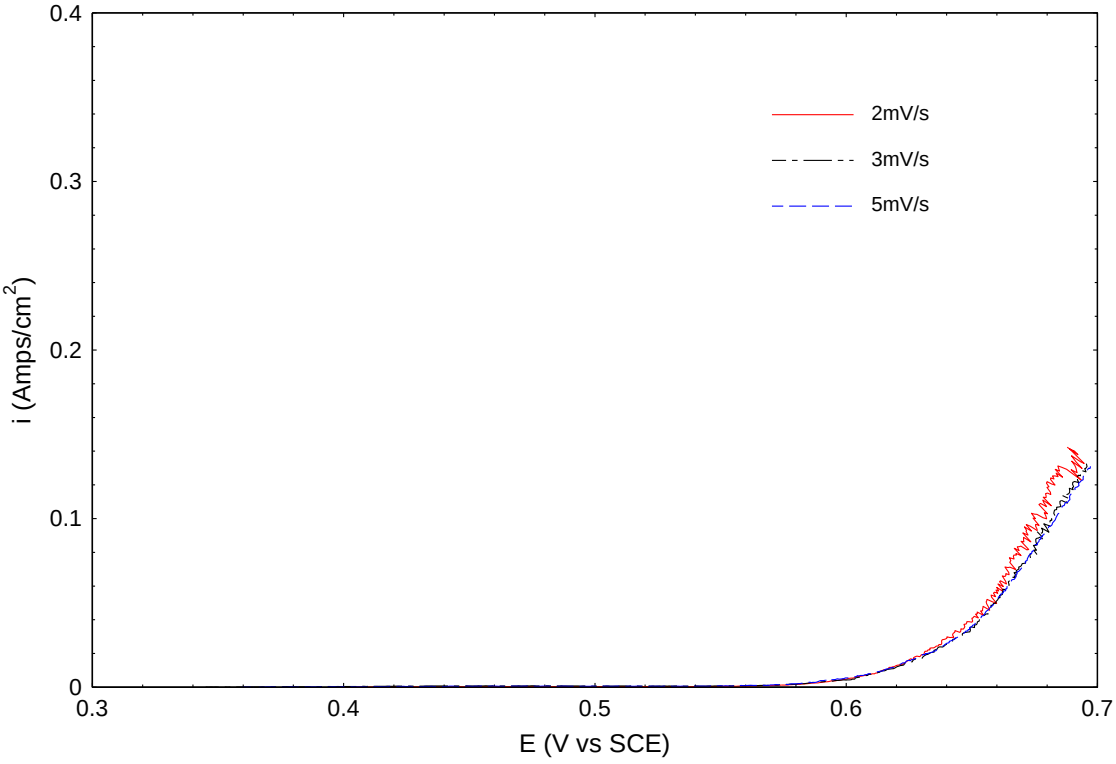

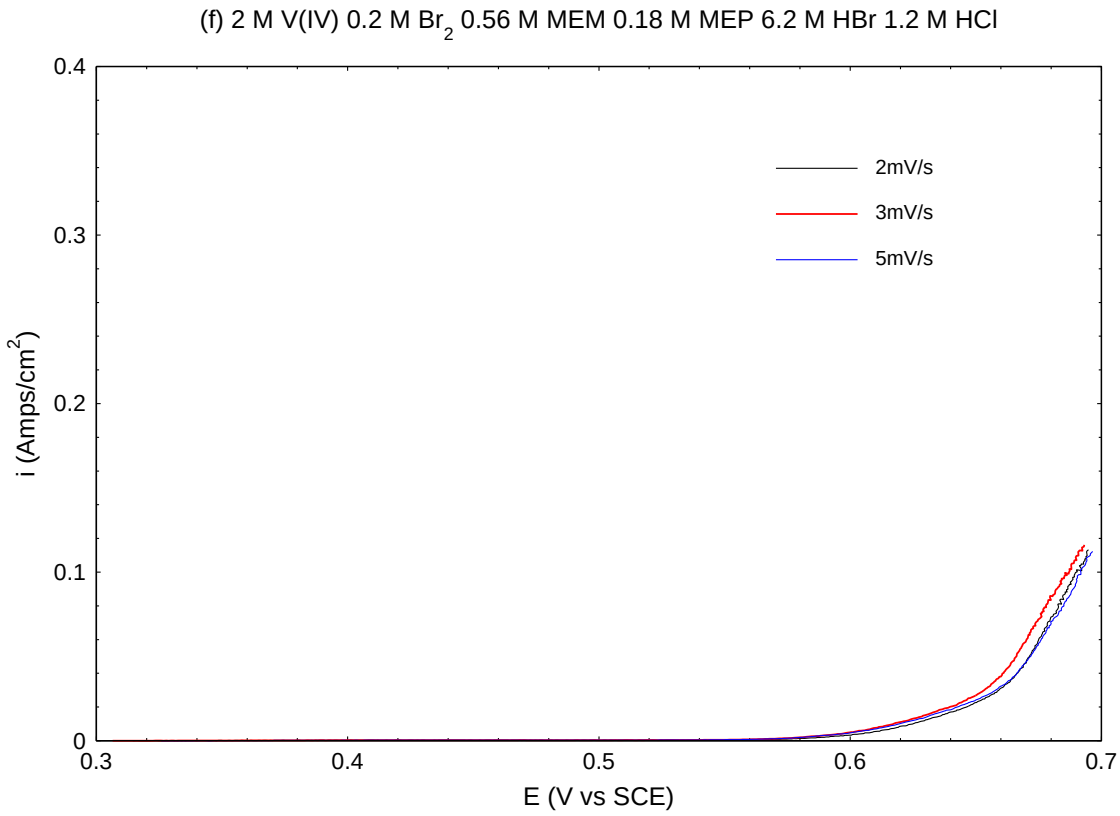
(f) 2 M V(IV) 0.2 M Br2 0.56 M MEM 0.18 M MEP 6.2 M HBr 1.2 M HCl
2mV/s
3mV/s
5mV/s
i (Amps/cm2)
E (V vs SCE)
0.4
0.3
0.2
0.1
0
0.3
0.4
0.5
0.6
0.7

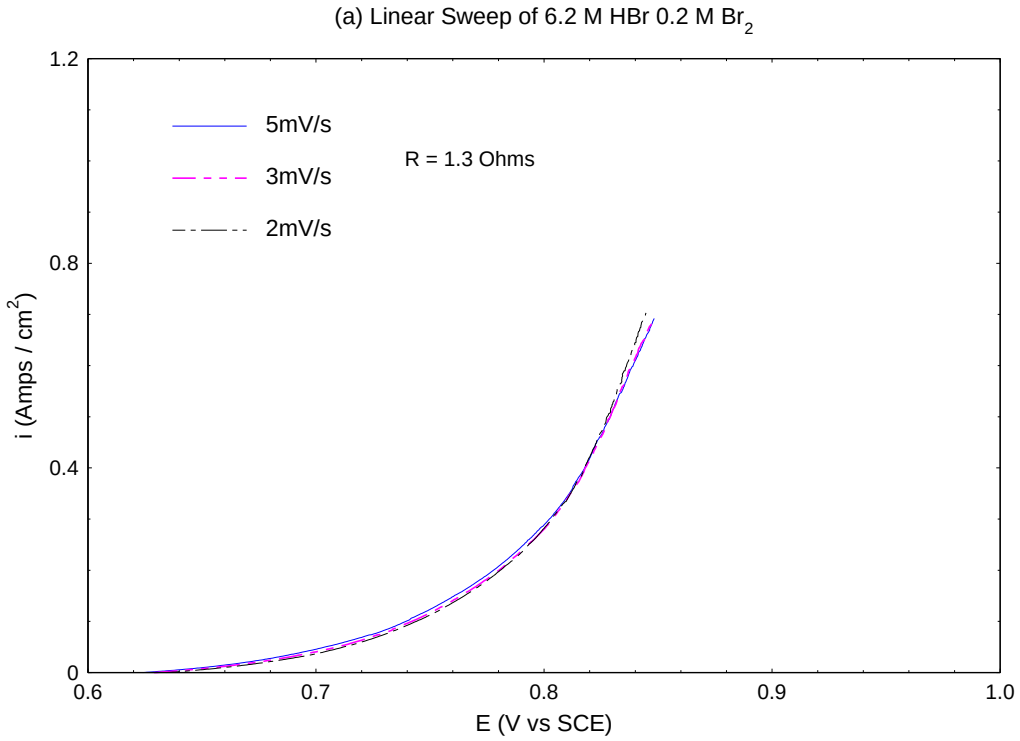

Figure D.2 Linear sweep voltammograms of (a) 6.2 M HBr 0.2 M Br_2 (b) 6.2 M HBr 1 M Br_2 (c) 6.2 M HBr 1.2 M HCl 0.2 M Br_2 (d) 6.2 M HBr 1.2 M HCl 1 M Br_2 (e) 6.2 M HBr 1.2 M HCl 0.2 M Br_2 0.19 M MEM 0.56 M MEP

(b) Linear Sweep Voltammogram 6.2M HBr 1M Br_2

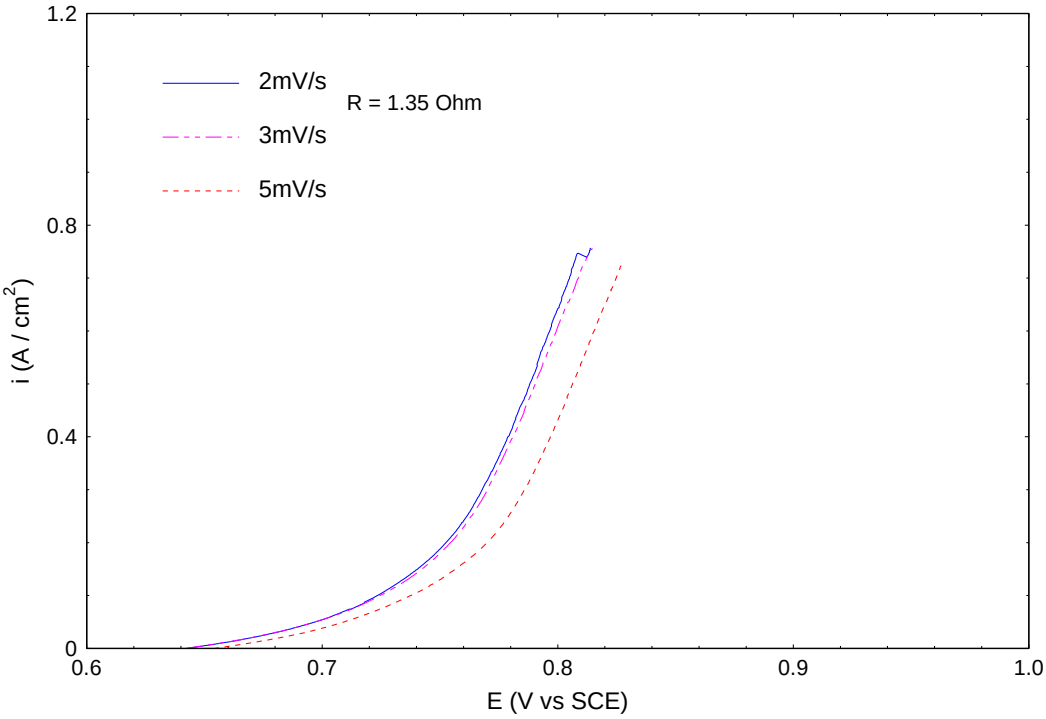

(c) Linear sweep voltammogram of 6.2 M HBr 1.2 M HCl 0.2 M Br_2

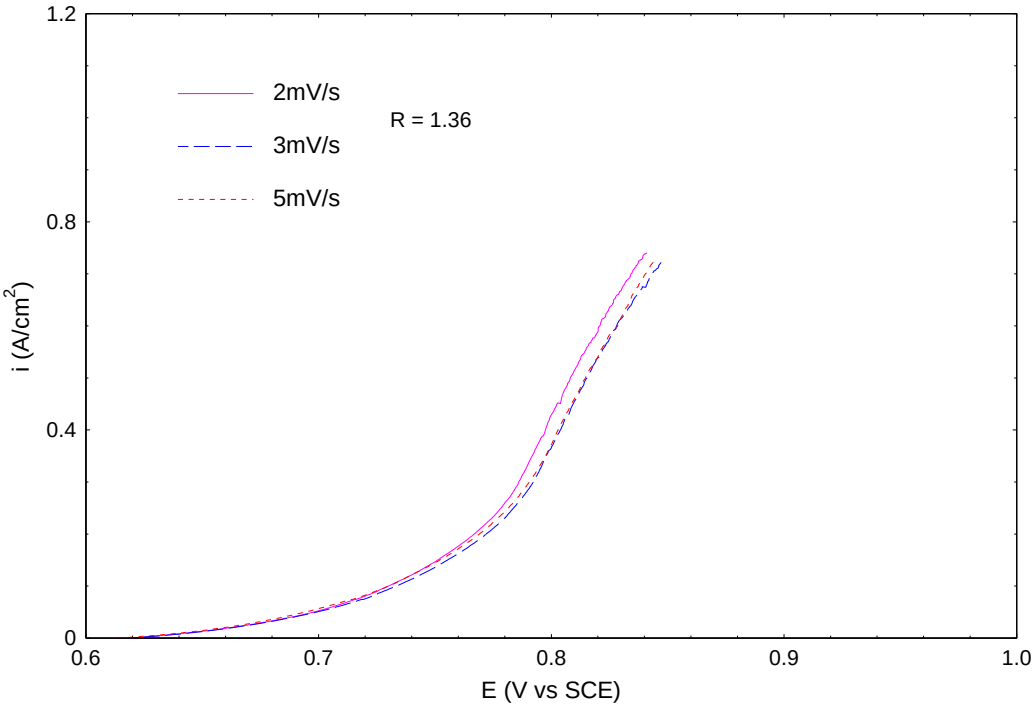

(d) Linear sweep voltammogram of 6.2 M HBr 1.2 M HCl 1 M Br_2

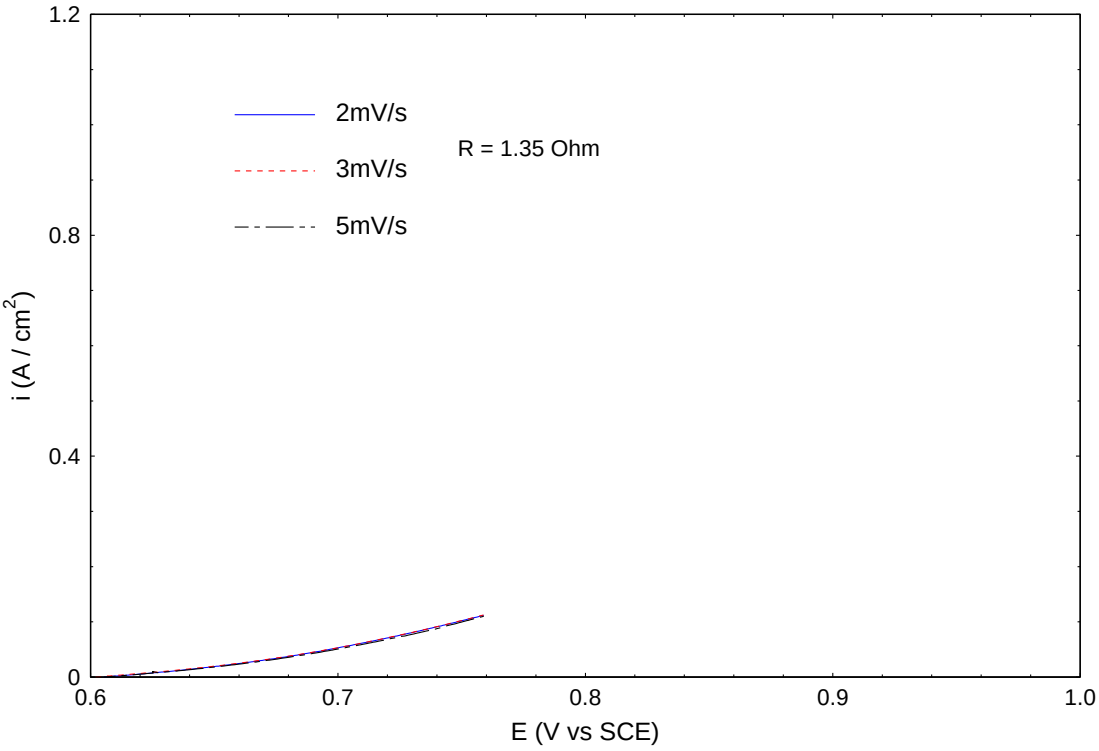

(e) Linear Voltammogram of 6.2 M HBr 1.2 M HCl 0.2 M Br_2 0.19 M MEM 0.56 M MEP

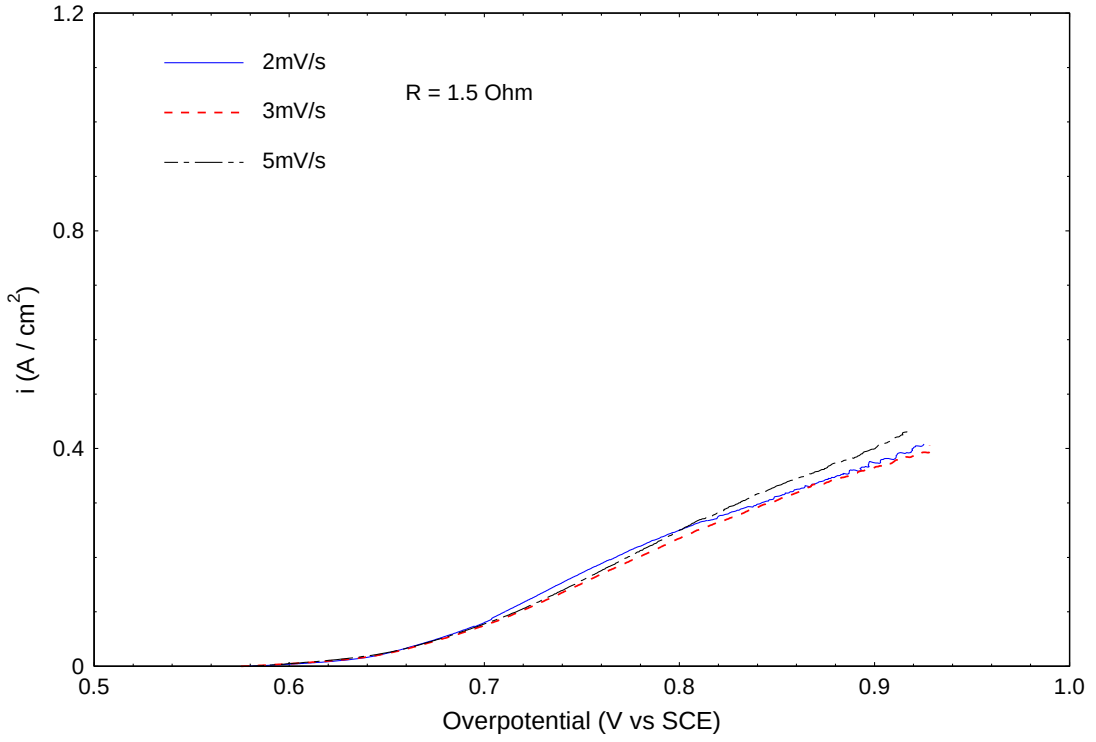

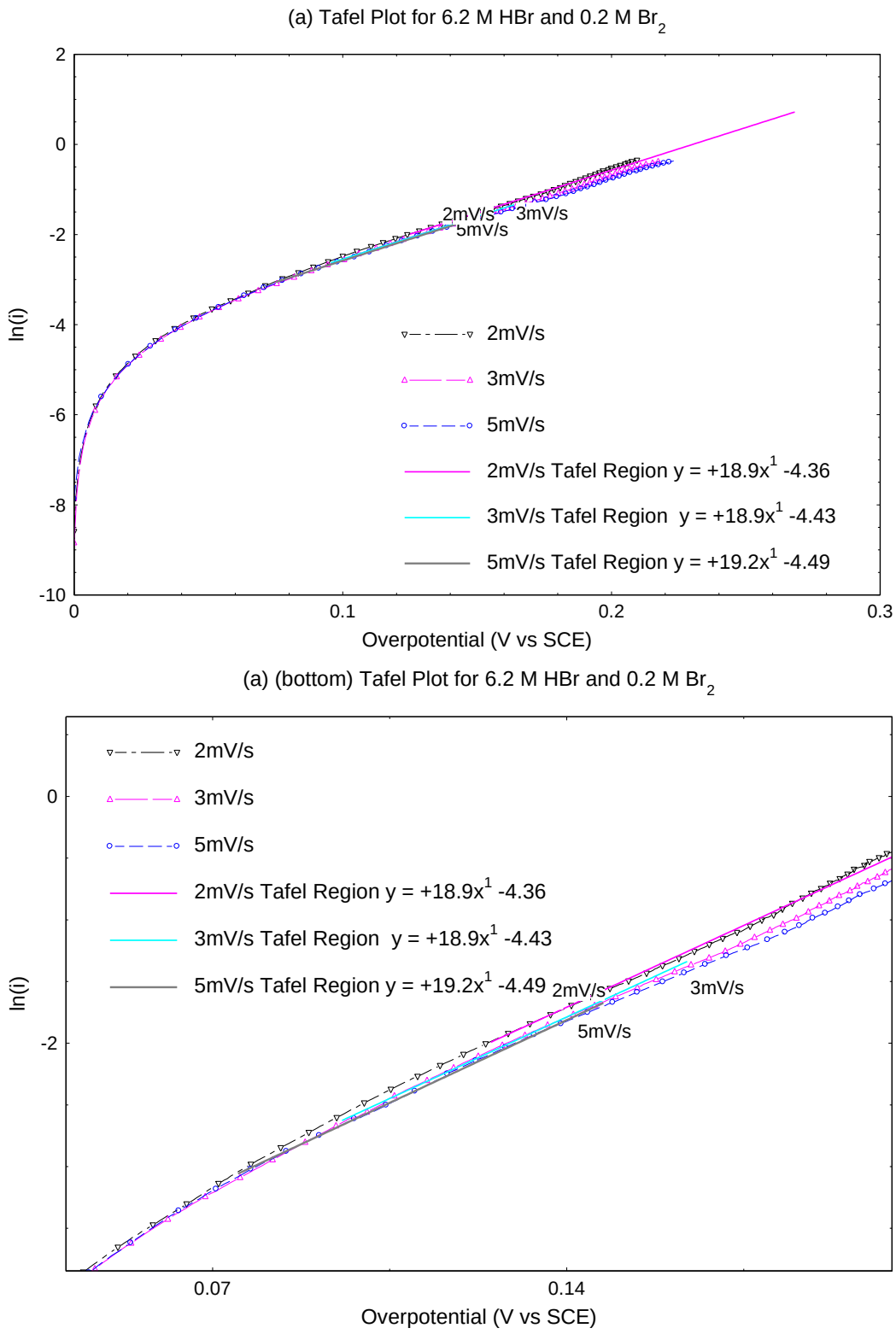

Figure D.3 Tafel plots of (a) 6.2 M HBr 0.2 M Br_2 (b) 6.2 M HBr 1 M Br_2 (c) 6.2 M HBr 1.2 M HCl 0.2 M Br_2 (d) 6.2 M HBr 1.2 M HCl 1 M Br_2 (e) 6.2 M HBr 1.2 M HCl 0.2 M Br_2 0.19 M MEM 0.56 M MEP; for each sample (top) original (bottom) expansion of linear region

b) Tafel Plot of 6.2 M HBr 1 M Br_2

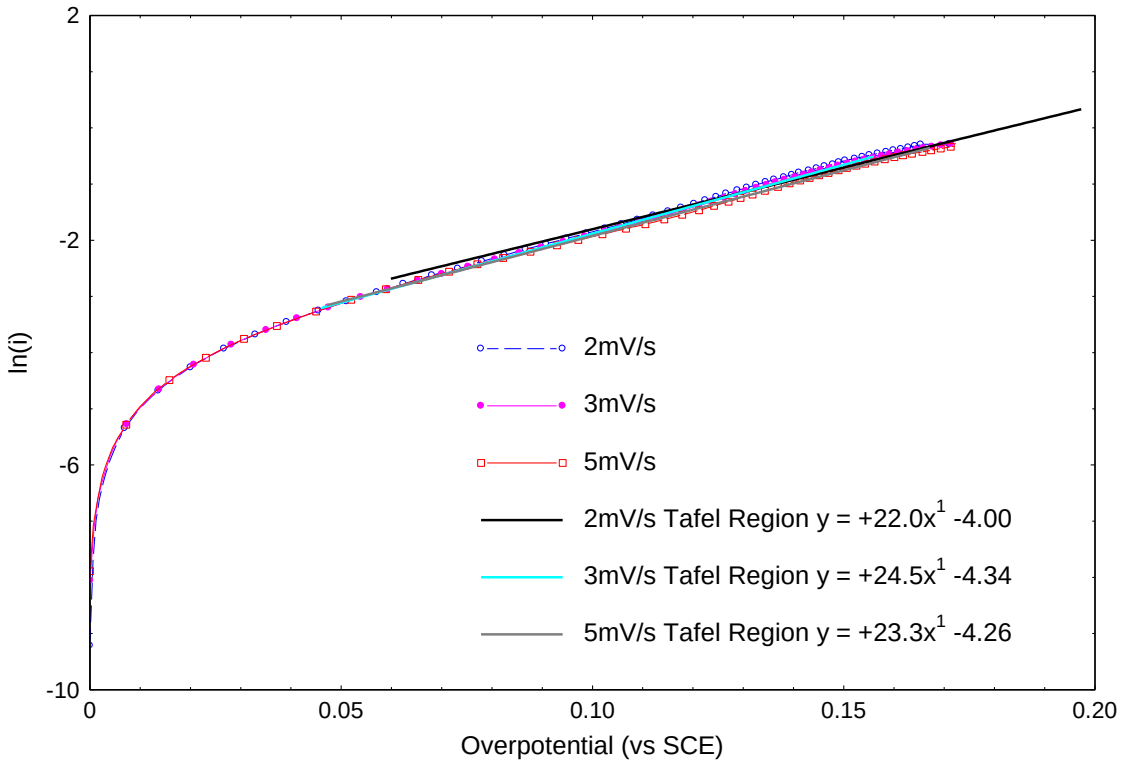

b) (bottom) Tafel Plot of 6.2 M HBr 1 M Br_2

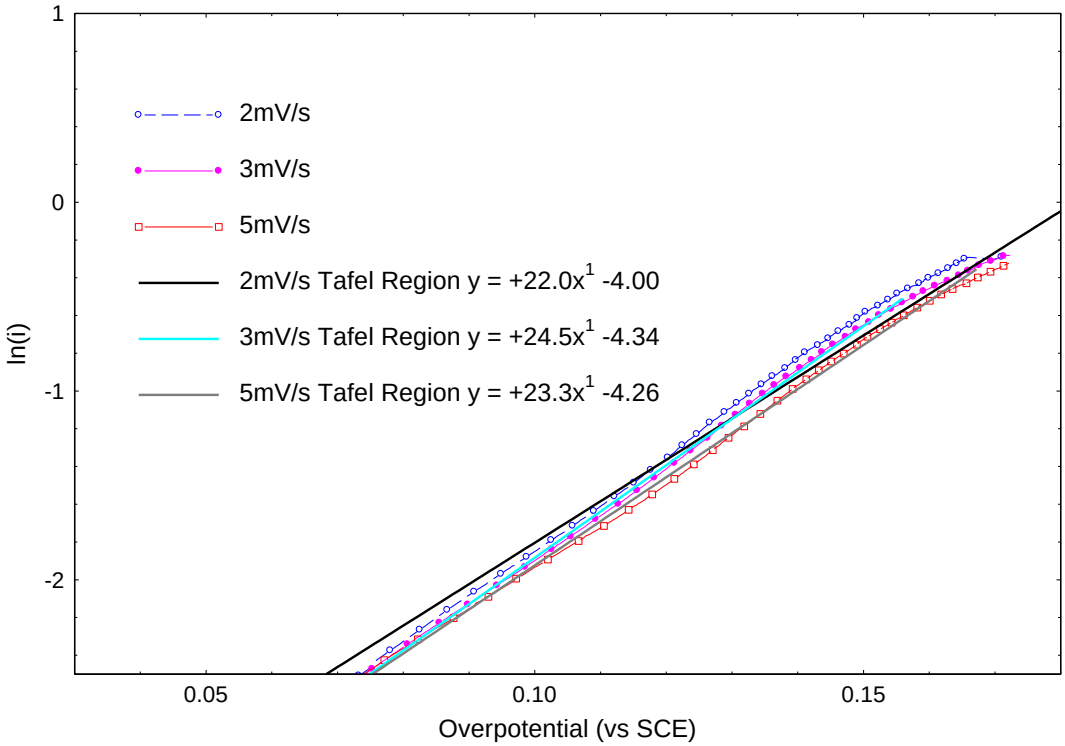

c) Tafel Plot of 6.2 M HBr 1.2 M HCl 0.2 M Br_2 at different scan rates

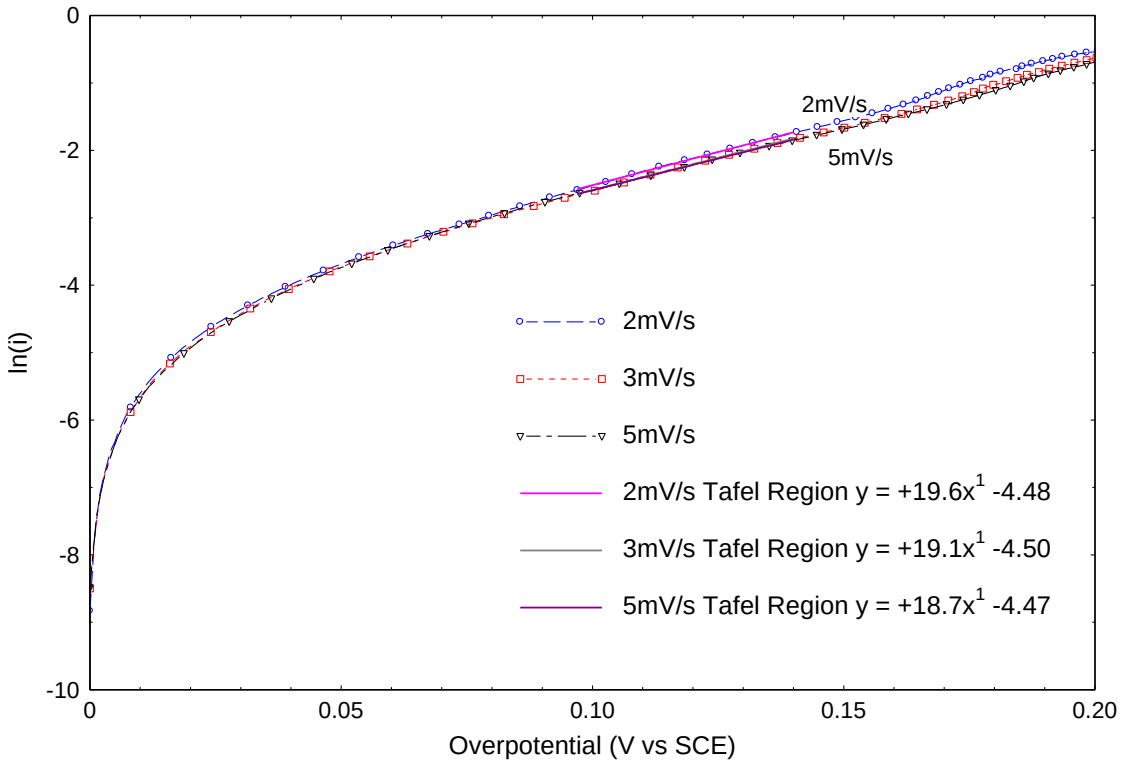

c) (bottom) Tafel Plot of 6.2 M HBr 1.2 M HCl 0.2 M Br_2 at different scan rates

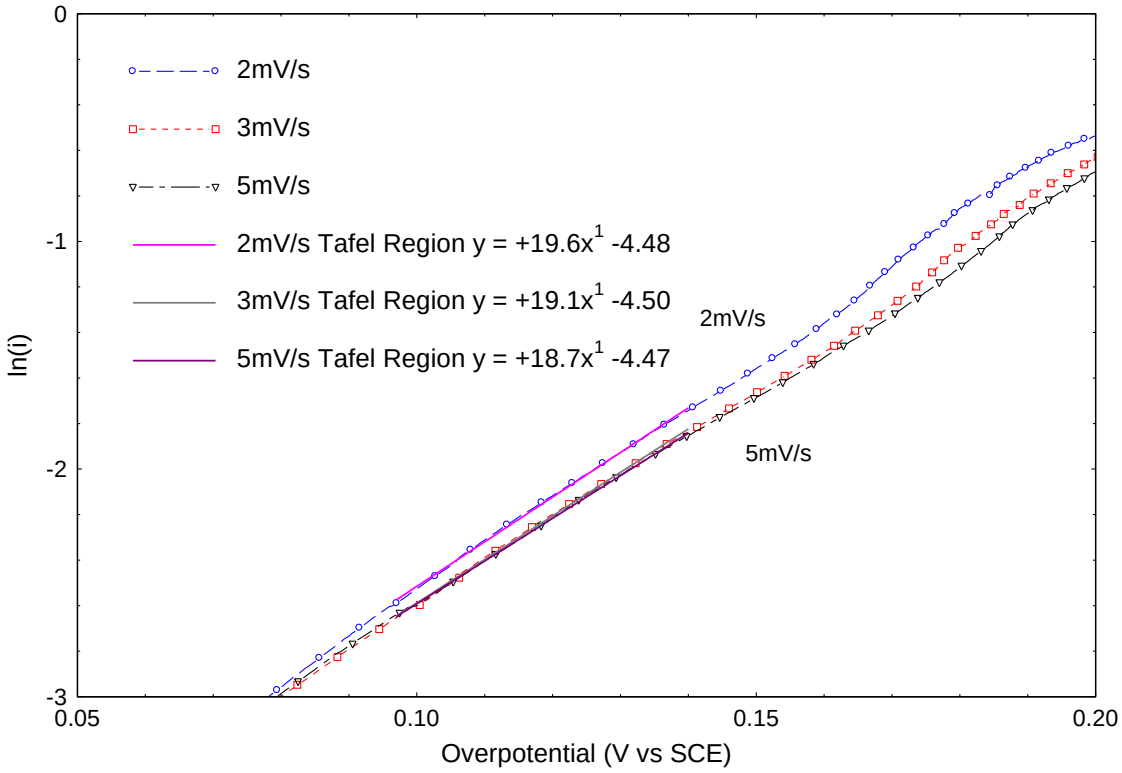

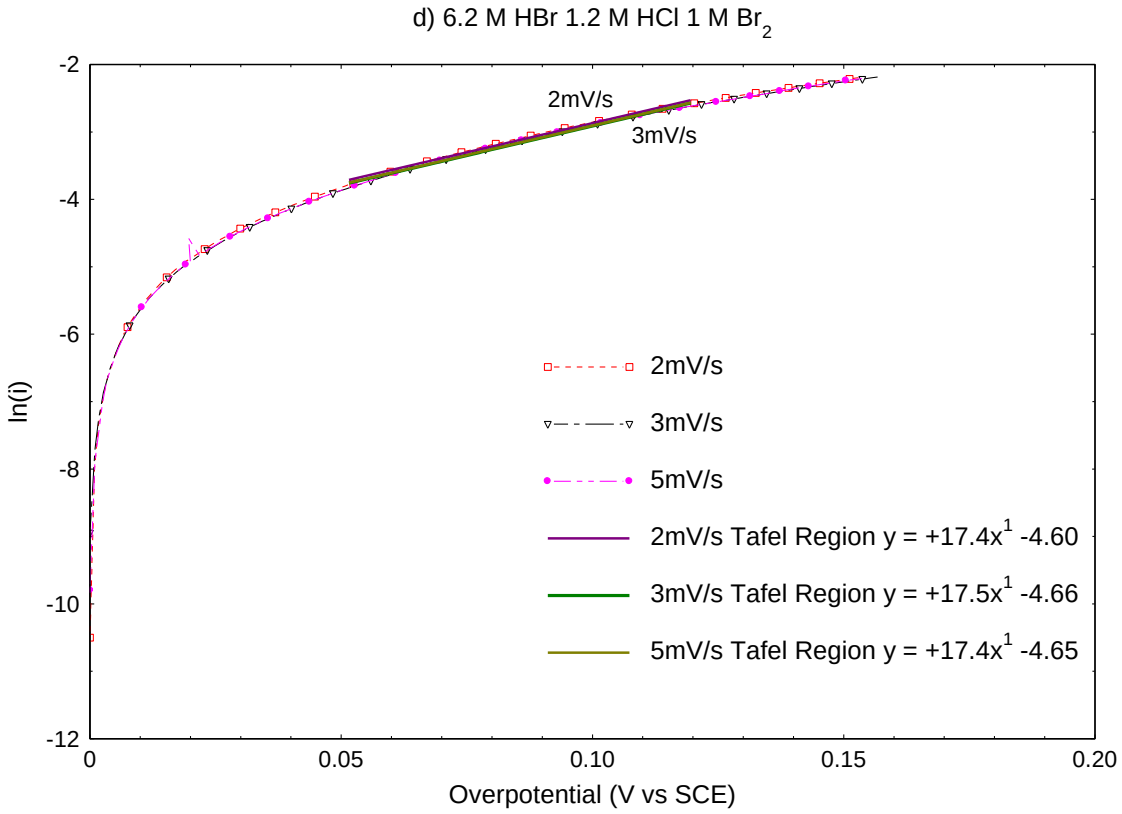
d) 6.2 M HBr 1.2 M HCl 1 M Br2
ln(i)
Overpotential (V vs SCE)
2mV/s
3mV/s
5mV/s
2mV/s Tafel Region y = +17.4x1 -4.60
3mV/s Tafel Region y = +17.5x1 -4.66
5mV/s Tafel Region y = +17.4x1 -4.65

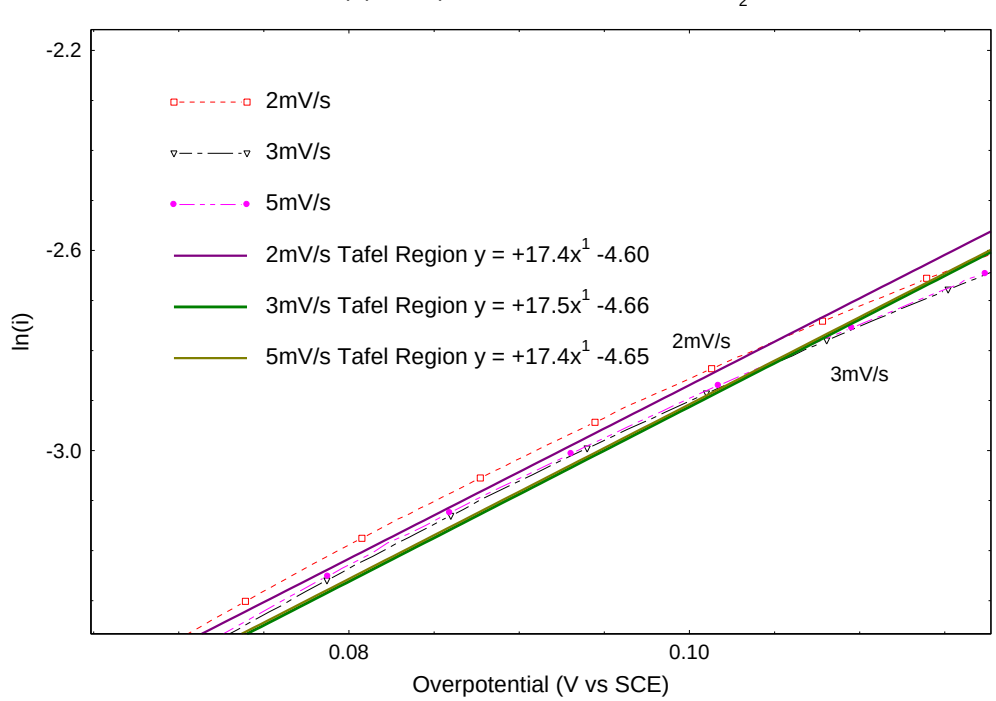
d) (bottom) 6.2 M HBr 1.2 M HCl 1 M Br2
ln(i)
Overpotential (V vs SCE)
2mV/s
3mV/s
5mV/s
2mV/s Tafel Region y = +17.4x1 -4.60
3mV/s Tafel Region y = +17.5x1 -4.66
5mV/s Tafel Region y = +17.4x1 -4.65

e) Tafel Plot of 6.2 M HBr 1.2 M HCl 0.2 M Br_2 0.19 M MEM 0.56 M MEP

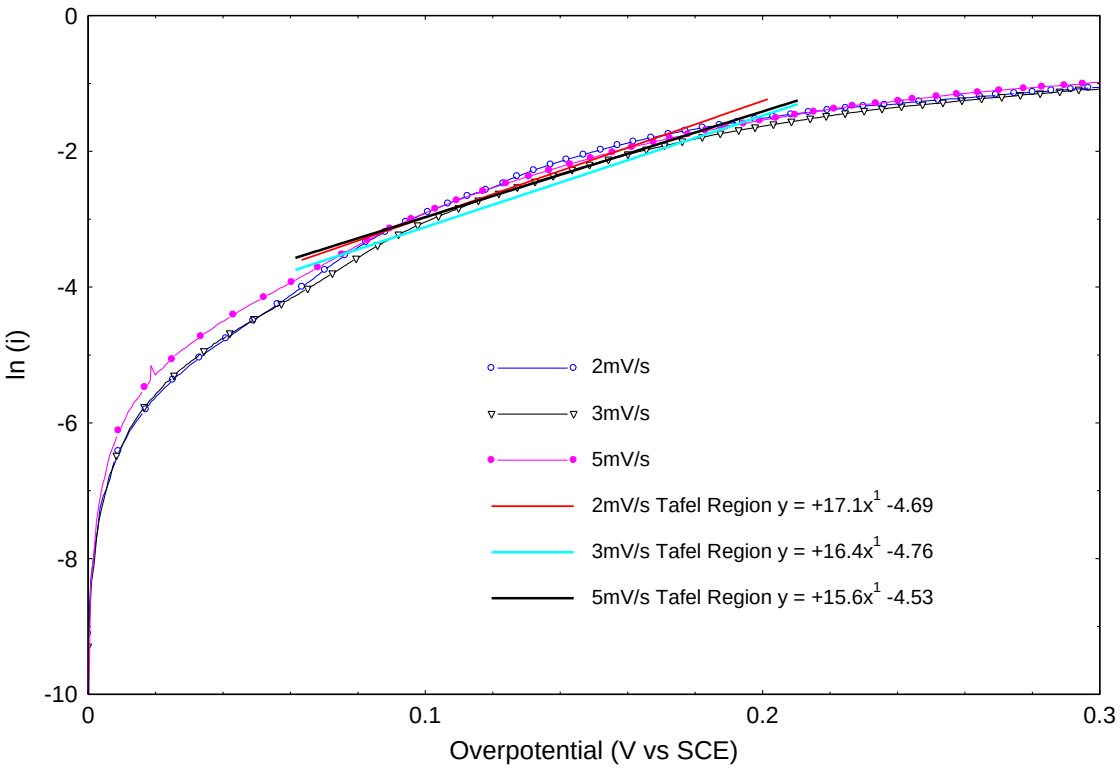

e) (bottom) Tafel Plot of 6.2 M HBr 1.2 M HCl 0.2 M Br_2 0.19 M MEM 0.56 M MEP

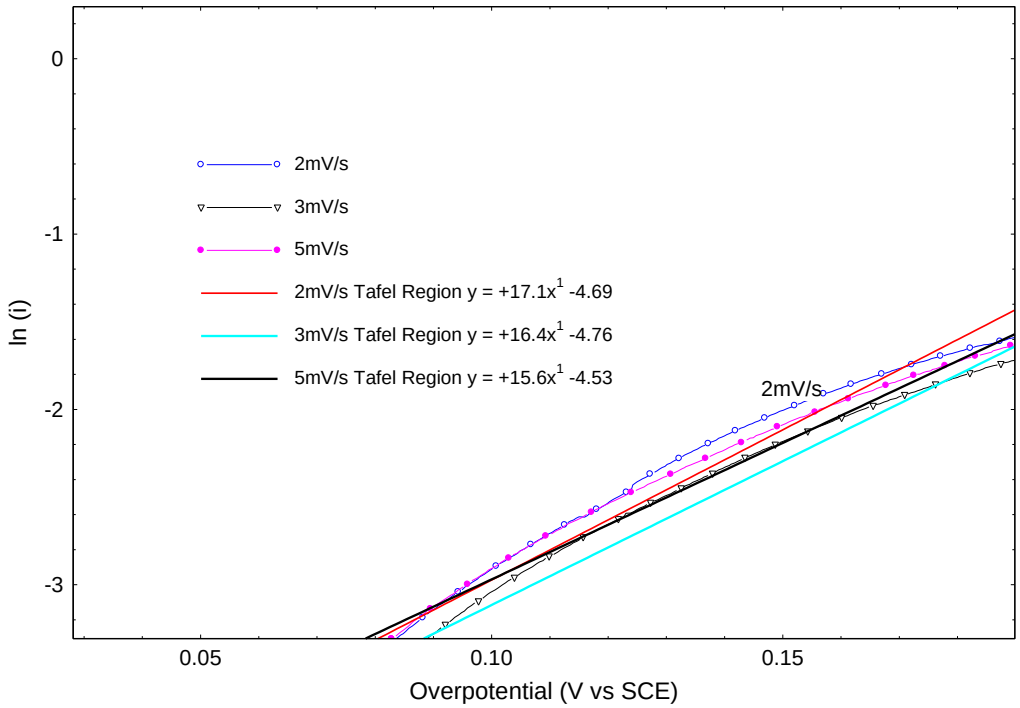

Table D.1 Kinetic parameters of bromine / bromide couple from Tafel plots of Figure D.3 (a) – (e)

Sample	R (ohms)	Scan Rate mV/s	Slope	Intercept βnF/RT	io	β
		2	18.9	-4.36	0.013	0.49
		3	18.90	-4.43	0.012	0.49
6.2 M HBr 0.2 M Br_2	1.3	5	19.20	-4.49	0.011	0.49
		2	22.00	-4.00	0.018	0.56
		3	24.50	-4.34	0.013	0.63
6.2 M HBr 1 M Br_2	1.35	5	23.30	-4.26	0.014	0.60
		2	19.60	-4.48	0.011	0.50
		3	19.10	-4.50	0.011	0.49
6.2 M HBr 1.2 M HCl 0.2 M Br_2	1.36	5	18.70	-4.47	0.011	0.48
		2	17.40	-4.60	0.010	0.45
		3	17.50	-4.66	0.009	0.45
6.2 M HBr 1.2 M HCl 1 M Br_2	1.35	5	17.40	-4.65	0.010	0.45
		2	17.10	-4.69	0.009	0.44
6.2 M HBr 1.2 M HCl 0.2 M Br_2		3	16.40	-4.76	0.009	0.42
0.19 M MEM 0.56 M MEP	1.5	5	15.60	-4.53	0.011	0.40

Appendix E Bromine / Bromide theoretical OCP calculations

The theoretical equilibrium potential or OCP is calculated using the equation (Equation E.) derived by Bell and Pring [1], where E^o = 1.065 V (vs NHE). With the corresponding equilibrium constants K and K_1, $[Br_2]_{eq}$ and $[Cl^-]_{eq}$ is determined from Rxn E. and Rxn repectively.

Rxn E.1 $$Br_2 + Br^- \overset{K}{\Leftrightarrow} Br_3^-$$

Rxn E.2 $$Br_2 + Cl^- \overset{K_1}{\Leftrightarrow} Br_2Cl^-$$

Rxn E.3 $$Br_2 + 2Cl^- \overset{K_2}{\Leftrightarrow} Br_2Cl^- + Br^-$$

Rxn E.4 $$Br_2 + Cl^- \overset{K_3}{\Leftrightarrow} BrCl + Br^- \qquad neglected \quad if \quad \frac{[Br^-]}{[Cl^-]} > 0.03$$

Rxn E.5 $$Br_2 + 2e \Leftrightarrow 2Br^- \qquad E^o = 1.065V\,(vsNHE)$$

Equation E.1 $$E = E^o + \frac{RT}{nF}\ln\frac{[Br_2]_{eq}}{\left(1 + K[Br^-] + K_1[Cl^-] + \frac{K_2[Cl^-]^2}{[Br^-]}\right)[Br^-]^2}$$

$$K = \frac{[Br_3^-]}{[Br_2][Br^-]},\quad K_1 = \frac{[Br_2Cl^-]}{[Br_2][Cl^-]},\quad K_2 = \frac{[BrCl_2^-][Br^-]}{[Br_2][Cl^-]^2},\quad K_3 = \frac{[BrCl_2][Br^-]}{[Br_2][Cl^-]}$$

K = 16 M^{-1} , K_1 = 1.14 M^{-1}, K_2 = 7.2 x 10^{-3} M^{-1}

K_3 = 2.4 x 10^{-5} M^{-1} solutions $[Br^-]/[Cl^-] > 0.03$ the formation of BrCl can be neglected

Table E.1 Sample concentration of Br_2/Br^- solutions at equilibrium

Sample	Initial concentration (M)				Equilibrium concentration (M)			
	$[Br_2]$	$[Br^-]$	$[Br_3^-]$	$[Cl^-]$	$[Br_2]_{eq}$	$[Br^-]_{eq}$	$[Br_3^-]_{eq}$	$[Cl^-]_{eq}$
6.2M HBr 0.2M Br_2	0.2	6.2	0	0	0.002	6.002	0.198	0.000
6.2M HBr 1M Br_2	1	6.2	0	0	0.012	5.212	0.988	0.000
6.2M HBr 1.2M HCl 0.2M Br_2	0.2	6.2	0	1.2	0.002	6.002	0.198	0.002
6.2M HBr 1.2M HCl 1M Br_2	1	6.2	0	1.2	0.012	5.212	0.988	0.012
6.2M HBr 1.2M HCl 0.2M Br_2 0.19M MEM 0.56M MEP	0.2	6.868	0	1.2	0.0006*	6.670	0.198	0.002

* assumed 30% of the aqueous bromine remained in aqueous phase after equilibrium

Table E.2 Calculated theoretical open circuit potential using Equation E. where E^o = 1.065 V (vs NHE) with $[Br^-]$, $[Cl^-]$ and $[Br_2]_{eq}$ from Table E.

Sample	Theoretical OCP
	E_{th} vs SCE
6.2M HBr 0.2M Br_2	0.63921
6.2M HBr 1M Br_2	0.66221
6.2M HBr 1.2M HCl 0.2M Br_2	0.63904
6.2M HBr 1.2M HCl 1M Br_2	0.66204
6.2M HBr 1.2M HCl 0.2M Br_2 0.19M MEM 0.56M MEP	0.6197

Appendix F Theoretical Calculations on V/Br Redox Cell

A vanadium bromine redox flow cell with 2M $V^{3.5+}$ (7.6M HBr+1.46M HCl) 50ml electrolyte in each half cell, the theoretical charging time and the concentration of each species can be found. For 2M $V^{3.5+}$ that contains 50% mol V^{3+} and 50% mol V^{4+} would have 0.05mol V^{3+} and 0.05mol V^{4+} in 50ml of 2M $V^{3.5+}$ .Now calculate the theoretical charging time of each half cell with the Faraday's Law when constant current 1A is applied: As $mole_T = \frac{It_T}{nF}$ or $t_T = \frac{nFmole_T}{I}$

Table F.1 Theoretical calculations of V/Br redox cell in each half-cell

In the negative half cell	In the positive half cell
$VO^{2+} + e \rightarrow 2V^{3+}$ t_T = (1) (96487) (0.05)/(1A) = 4824.15s = 1.34hr	$V^{3+} \rightarrow VO^{2+} + e$ t_T = (1) (96483) (0.05)/(1A) = 4824.15s = 1.34hr
$V^{3+} + e \rightarrow V^{2+}$ Mole of V3+ = 0.05 + 0.05 (which were converted from VO^{2+}) t_T = (1) (96487) (0.1)/(1A) = 9648.3s =2.68hr	$3Br^- \rightarrow Br_3^- + 2e$ Or $2Br^- \rightarrow Br_2 + 2e$ The time is limited by the negative half cell, is 2.68hr (ie. 9648.3s) Now the amount of Br_3^- / Br_2 produced can be found If we assume all Br^- followed the second equation and formed bromine. Using the same calculation as theoretical time. Mole = (1) (9648.3)/2(96487) = 0.05 mole Maximum [Br_2] = 1M
Total 1st cycle charging time = 4.02hr	

Appendix G Procedures for Cell efficiency calculation using excel file with built-in macro

File Name: Graphing.xls

A) Create “New Folder” (eg ABC) to store exported TXT files and processing files

B) Export TXT file from cell testing file eg ABC.cel

1. Open ABC.cel files
2. move the mouse in the data region (on the right side of the screen)
3. right click uncheck ‘Data Pucker’
4. and in Time unit choose ‘second’
5. keep ‘Process independent’ to be checked
6. Press ‘Convert to TXT files..’
7. Browse to save the txt files in a folder named “ABC” as created previously
8. uncheck all 3 options “include channel info” , “include process info”, “include unit info”
9. click “OK”

C) Open Excel File: Graphing

1. Press “Enable Macro”
2. clear content from A1:E1
3. Press “Bulk File Name” in “CEMP Graphing” tool bar
4. When the Open window comes up choose and open the TXT file that has been exported
5. in cell B1 type “1000”
6. in cell C1 type “4”
7. Press “Process Bulk” in “CEMP Graphing” tool bar

D) Open ABC folder
Cell Efficiency would be in a text file named: ABC.TXT_Table

E) Convert cell efficiency to excel file

Appendix H Cell Performance of V/Br Redox Cell

H.1 Static Cell testing for MEM and MEP concentration comparison

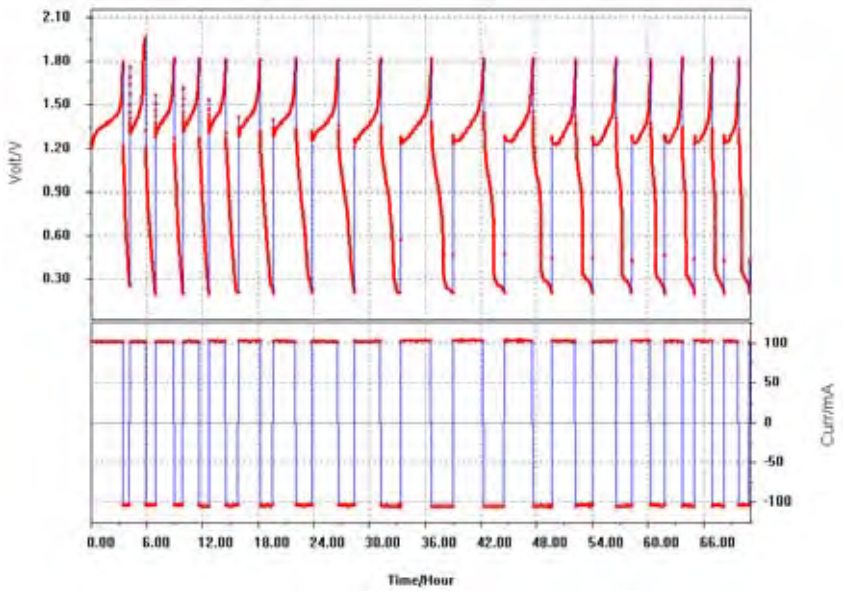

Figure H.1 Charge / discharge cycles of 2 M $V^{3.7+}$, 0.19 M MEP, 0.56 M MEM, 6.1 M HBr, 1.2 M HCl with ChiNafion membrane at room temperature 25°C (21JULSA2.cel)

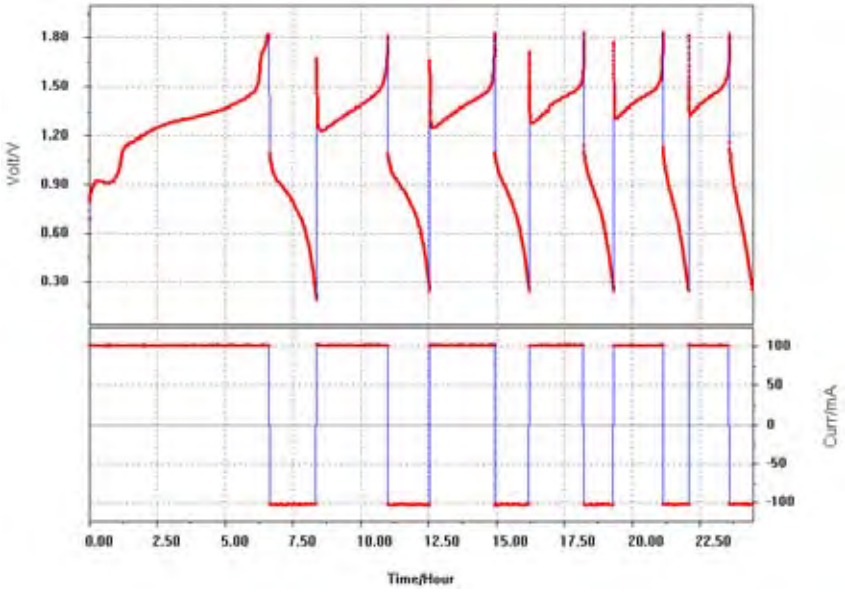

Figure H.2 Charge / discharge cycles of 2 M $V^{3.7+}$, 0.19 M MEP, 0.56 M MEM, 6.1 M HBr, 1.2 M HCl with ChiNafion membrane at room temperature 25°C (20JULSA1.cel)

Table H.1 Coulombic, voltaic and energy efficiency of each cycles obtained by 2M $V^{3.7+}$ 0.56M MEM 0.19M MEP and 2M $V^{3.7+}$ 0.19M MEM 0.56M MEP static cell built with ChiNafion charge-discharge at 4 mA cm^{-2}

21JULSA2	2M V3.7+ 0.56M MEM 0.19M MEP			20JULSA1	2M V3.7+ 0.19M MEM 0.56M MEP		
Cycle No.	C. Eff (%)	V. Eff (%)	E. Eff (%)	Cycle No.	C. Eff (%)	V. Eff (%)	E. Eff (%)
1	21.67	48.15	10.43	1	25.88	58.71	15.20
2	60.49	40.92	24.75	2	57.79	55.53	32.09
3	45.75	44.63	20.41	3	52.18	53.94	28.15
4	57.48	45.48	26.14	4	54.11	51.79	28.03
5	72.54	40.19	29.15	5	51.91	49.28	25.58
6	61.91	43.10	26.69	6	55.22	45.98	25.39
7	68.83	47.17	32.47				
8	62.80	53.83	33.81	Average	54.24	51.31	27.85
9	78.06	47.80	37.32				
10	70.28	46.22	32.48				
11	66.81	44.61	29.81				
12	66.07	45.65	30.16				
13	68.78	43.90	30.19				
14	67.39	42.57	28.69				
15	70.89	39.54	28.03				
16	72.49	36.82	26.69				
17	70.41	36.51	25.71				
18	72.63	35.21	25.57				
Average 5 cycles	59.63	42.86	25.43				
Average 17cycles	66.68	43.19	28.71				

H.2 QBr addition and temperature effect on VF11 static cell (10, 20, 40mAcm^{-2})

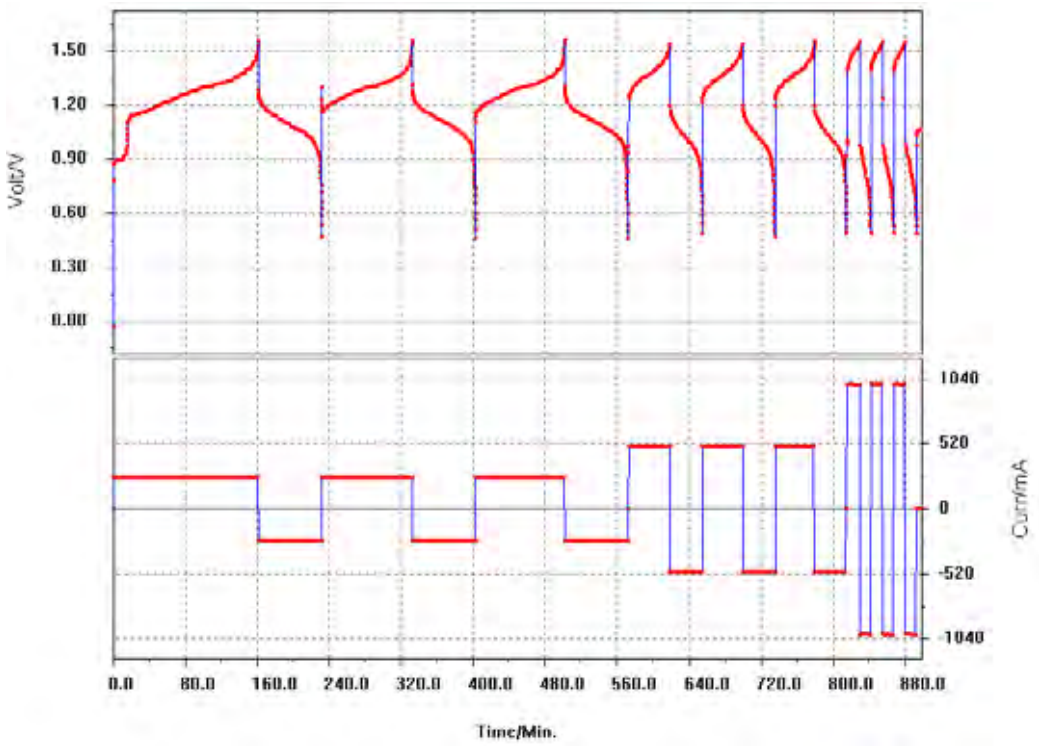

Figure H.3 Cell potential of 2 M $V^{3.7+}$, 7.6 M HBr, 1.46 M HCl (7ml in each half-cells) with VF11 membrane at 10^{o}C (T10_0324.cel)

Table H.2 Cell efficiencies of 2 M V3.7+, 7.6 M HBr, 1.46 M HCl with VF11 membrane at 10oC (T10_0324.cel)

T10_0324.cel cycle no.	Current (mA)	C. Eff (%)	V. Eff (%)	E. Eff (%)
1	250	43.74	87.38	38.22
2	250	70.03	84.82	59.41
3	250	71.19	84.53	60.17
4	500	79.05	72.97	57.69
5	500	80.01	73.38	58.71
6	500	79.99	73.06	58.44
7	1000	83.49	54.34	45.37
8	1000	87.77	54.36	47.71
9	1000	87.89	54.64	48.02
	Current (mA)	Avg. C. Eff (%)	Avg. V. Eff (%)	Avg. E. Eff (%)
2M $V^{3.7+}$ 10^{o}C Average	250	70.61	84.68	59.79
	500	80.00	73.22	58.57
	1000	87.83	54.50	47.86

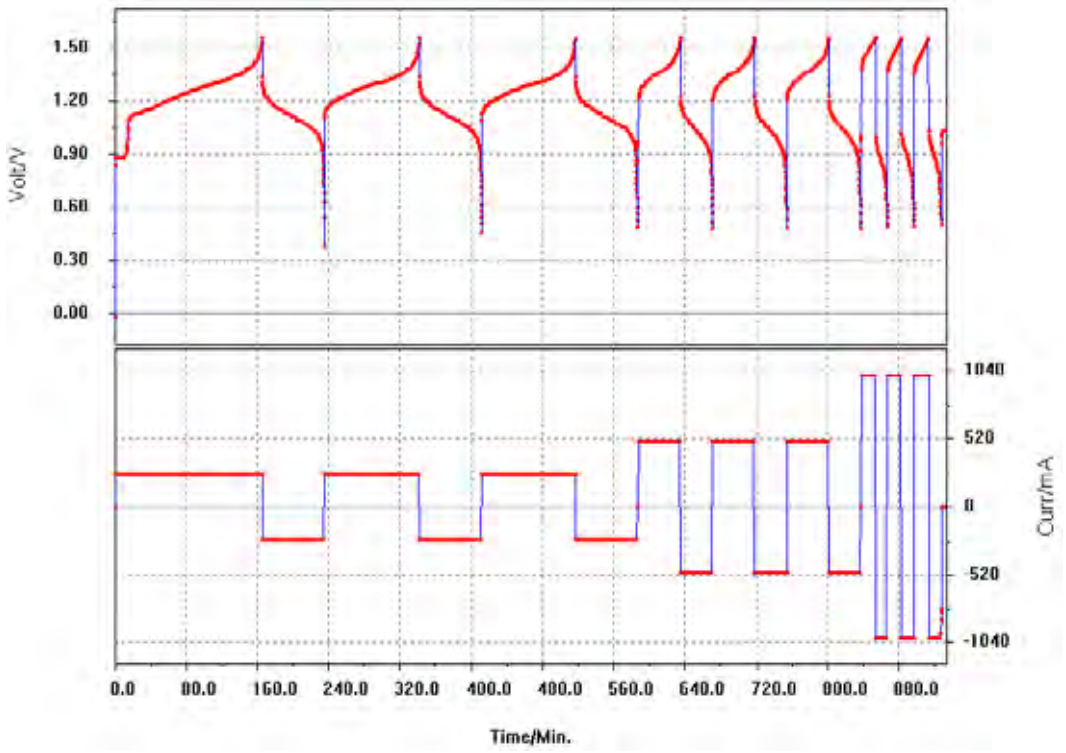

Figure H.4 Cell potential of 2 M $V^{3.7+}$, 7.6 M HBr, 1.46 M HCl (7ml in each half-cells) with VF11 membrane at 15°C (T15_0327.cel)

Table H.3 Cell efficiencies of 2 M $V^{3.7+}$, 7.6 M HBr, 1.46 M HCl with VF11 membrane at 15°C (T15_0327.cel)

T15_0327.cel cycle no.	Current (mA)	C. Eff (%)	V. Eff (%)	E. Eff (%)
1	250	42.18	89.62	37.81
2	250	65.69	85.33	56.05
3	250	66.74	85.34	56.96
4	500	76.77	74.46	57.16
5	500	77.15	74.38	57.39
6	500	77.24	74.18	57.30
7	1000	82.12	56.24	46.18
8	1000	84.05	57.81	48.59
9	1000	85.96	57.96	49.82
	Current (mA)	Avg. C. Eff (%)	Avg. V. Eff (%)	Avg. E. Eff (%)
2M V3.7+ 15oC Average	250	66.21	85.34	56.50
	500	77.20	74.28	57.34
	1000	85.00	57.88	49.20

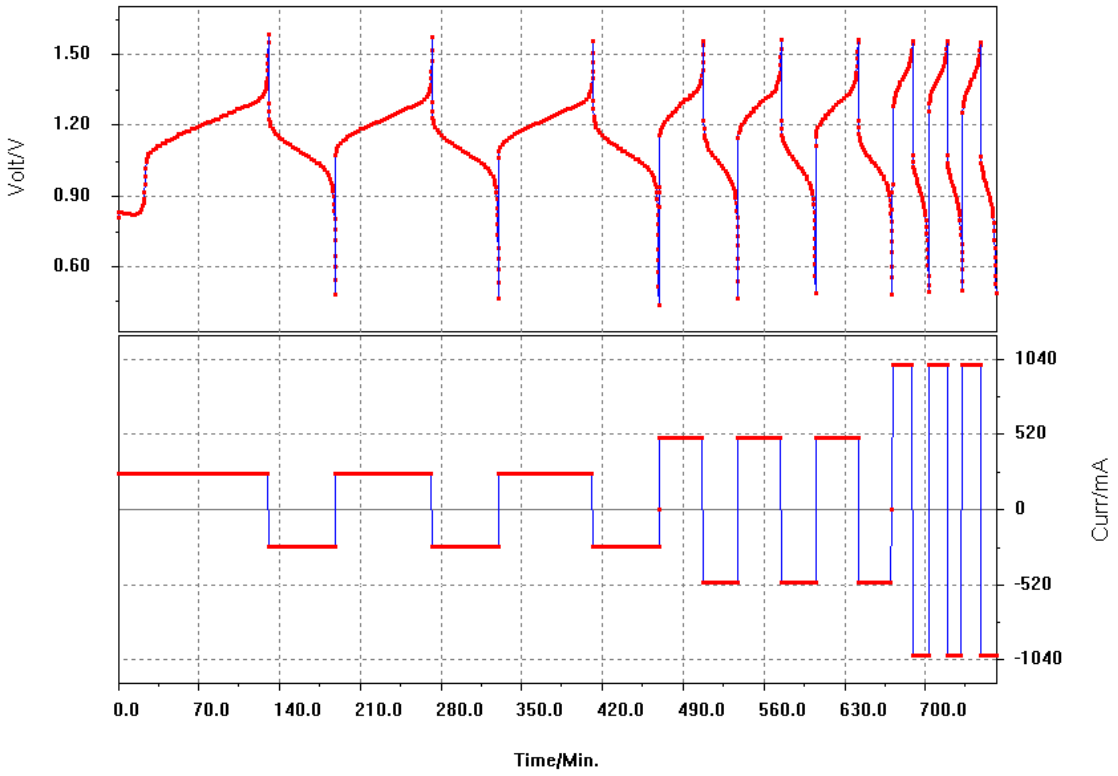

Figure H.5 Cell potential of 2 M $V^{3.7+}$, 7.6 M HBr, 1.46 M HCl (7ml in each half-cells) with VF11 membrane at 25°C (T25_0329.cel)

Table H.4 Cell efficiencies of 2 M $V^{3.7+}$, 7.6 M HBr, 1.46 M HCl with VF11 membrane at 25°C (T25_0329.cel)

T25_0329.cel cycle no.	Current (mA)	C. Eff (%)	V. Eff (%)	E. Eff (%)
1	250	44.68	94.28	42.12
2	250	68.55	87.84	60.21
3	250	68.99	87.95	60.68
4	500	78.95	78.95	62.33
5	500	79.76	79.04	63.04
6	500	79.79	79.07	63.09
7	1000	82.91	63.46	52.61
8	1000	84.79	63.87	54.15
9	1000	85.16	63.99	54.49
	Current (mA)	Avg. C. Eff (%)	Avg. V. Eff (%)	Avg. E. Eff (%)
2M $V^{3.7+}$ 25°C Average	250	68.77	87.89	60.45
	500	79.77	79.06	63.07
	1000	84.97	63.93	54.32

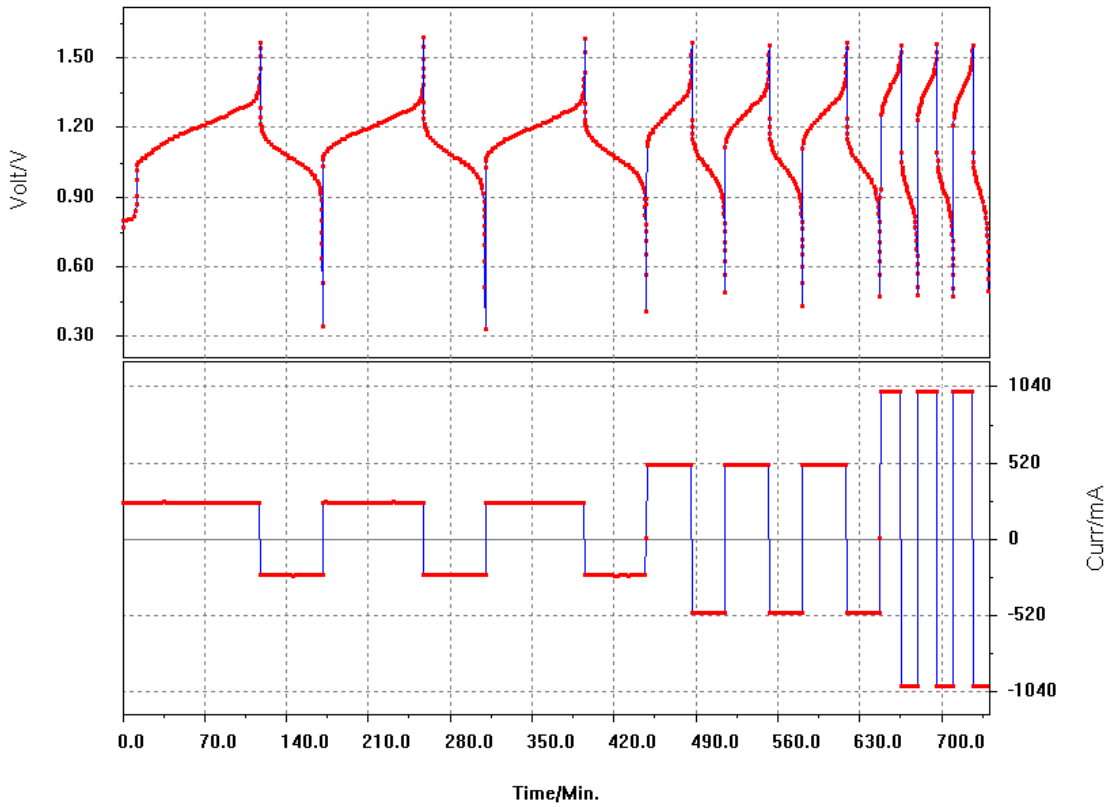

Figure H.6 Cell potential of 2M $V^{3.7+}$ 7.6 M HBr 1.46 M HCl (7ml in each half-cells) with VF11 membrane at 35°C (T35_0330.cel)

Table H.5 Cell efficiencies of 2M $V^{3.7+}$ 7.6 M HBr 1.46 M HCl with VF11 membrane at 35°C (T35_0330.cel)

T35_0330.cel cycle no.	Current (mA)	C. Eff (%)	V. Eff (%)	E. Eff (%)
1	250	44.98	91.63	41.22
2	250	60.98	88.58	54.02
3	250	61.69	88.78	54.77
4	500	75.01	80.09	60.07
5	500	75.89	79.90	60.63
6	500	75.76	79.87	60.51
7	1000	81.21	64.36	52.26
8	1000	82.74	64.92	53.71
9	1000	82.51	65.07	53.69
	Current (mA)	Avg. C. Eff (%)	Avg. V. Eff (%)	Avg. E. Eff (%)
2M $V^{3.7+}$ 35°C Average	250	61.34	88.68	54.40
	500	75.82	79.88	60.57
	1000	82.62	65.00	53.70

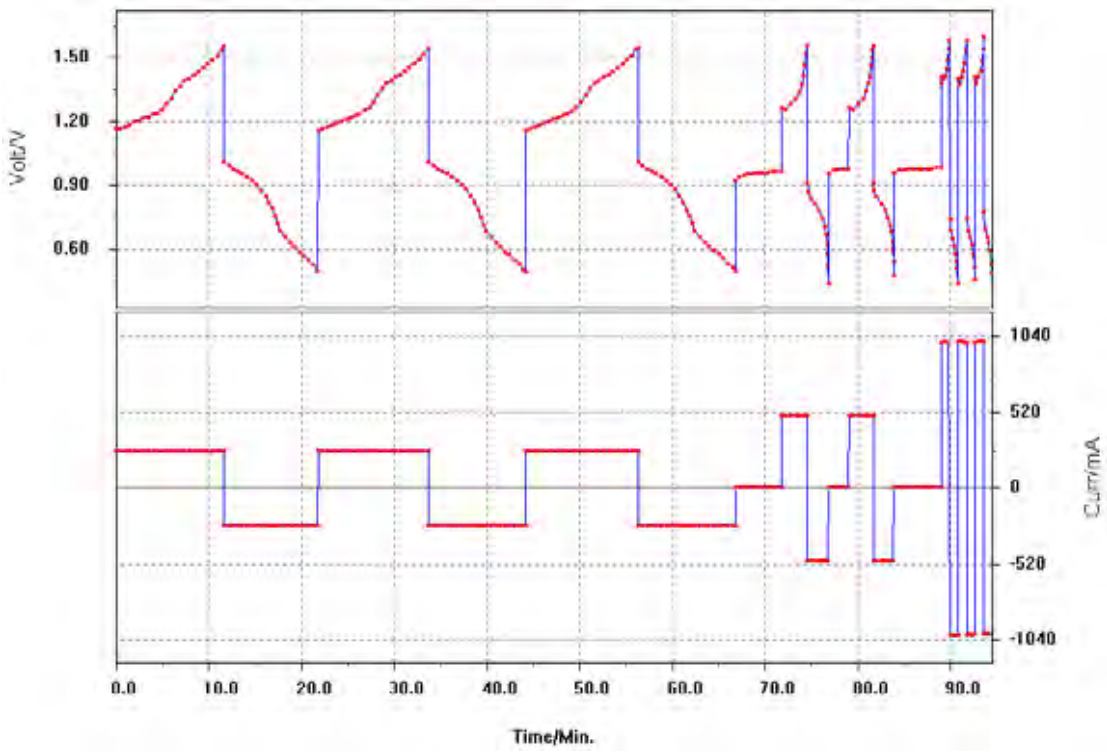

Figure H.7 Charge / discharge cycles of 2 M V3.7+, 0.19 M MEM, 0.56 M MEP, 6.1 M HBr, 1.2 M HCl (7ml in each half-cells) with VF11 membrane at 10°C (T10A0317.cel)

Table H.6 Cell efficiencies of 2 M $V^{3.7+}$, 0.19 M MEM, 0.56 M MEP, 6.1 M HBr, 1.2 M HCl with VF11 membrane at 10°C (T10A317.cel)

T10A0317.cel cycle no.	Current (mA)	C. Eff (%)	V. Eff (%)	E. Eff (%)
1	250	87.50	58.58	51.26
2	250	87.15	58.51	50.99
3	250	85.86	58.53	50.26
4	500	83.20	57.63	47.94
5	500	89.68	58.16	52.15
6	1000	94.67	43.10	40.81
7	1000	92.84	43.67	40.54
8	1000	91.18	44.15	40.26
T10A0317.cel	Current (mA)	Avg. C. Eff (%)	Avg. V. Eff (%)	Avg. E. Eff (%)
2M $V^{3.7+}$ 0.19M MEM 0.56M MEP 10°C Average	250	86.51	58.52	50.62
	500	86.44	57.89	50.05
	1000	92.01	43.91	40.40

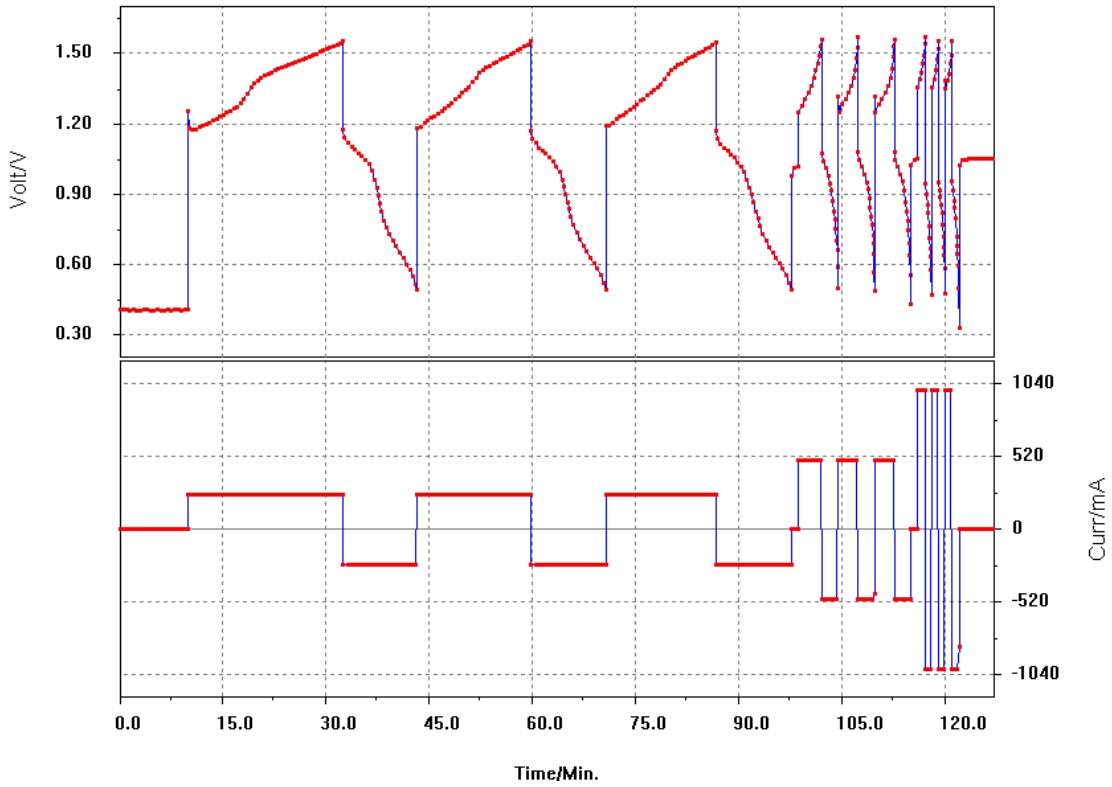

Figure H.8 Charge / discharge cycles of 2 M $V^{3.7+}$, 0.19 M MEM, 0.56 M MEP, 6.1 M HBr, 1.2 M HCl (7ml in each half-cells) with VF11 membrane at 15°C (T15_0321.cel)

Table H.7 Cell efficiencies of 2M $V^{3.7+}$ 0.19M MEM 0.56M MEP 6.1 M HBr 1.2 M HCl with VF11 membrane at 15°C (T15_0321.cel)

T15_0321.cel cycle no.	Current (mA)	C. Eff (%)	V. Eff (%)	E. Eff (%)
1	250	47.61	55.78	26.56
2	250	67.36	62.05	41.80
3	250	69.24	62.05	42.96
4	500	67.06	55.04	36.91
5	500	81.63	67.43	55.04
6	500	84.19	67.44	56.78
7	1000	86.84	32.84	28.52
8	1000	93.33	55.65	51.93
9	1000	99.44	53.99	53.69
	Current (mA)	Avg. C. Eff (%)	Avg. V. Eff (%)	Avg. E. Eff (%)
2M V3.7+ 0.19M MEM 0.56M MEP 15oC Average	250	68.30	62.05	42.38
	500	82.91	67.43	55.91
	1000	96.38	54.82	52.81

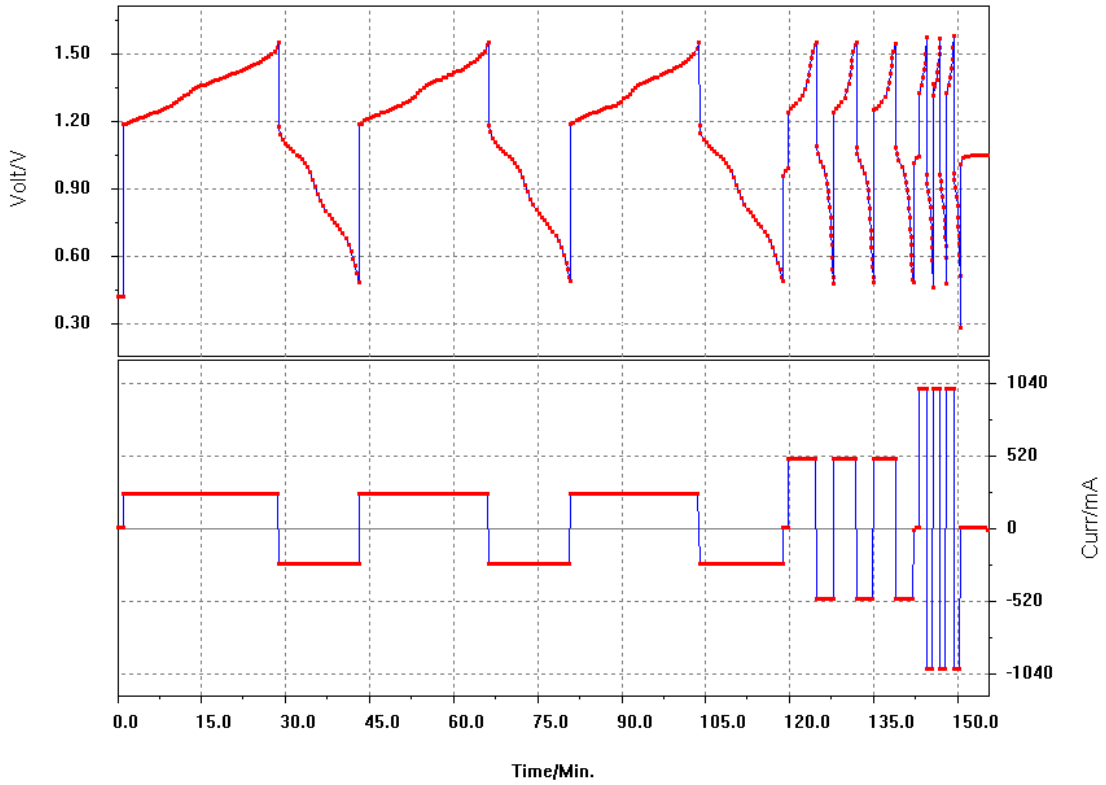

Figure H.9 Charge / discharge cycles of 2 M $V^{3.7+}$, 0.19 M MEM, 0.56 M MEP, 6.1 M HBr, 1.2 M HCl with (7ml in each half-cells) VF11 membrane at 25°C (T25_0322.cel)

Table H.8 Cell efficiencies of 2 M $V^{3.7+}$, 0.19 M MEM, 0.56 M MEP, 6.1 M HBr, 1.2 M HCl with VF11 membrane at 25oC (T25_0322.cel)

T25_0322.cel cycle no.	Current (mA)	C. Eff (%)	V. Eff (%)	E. Eff (%)
1	250	51.72	64.91	33.57
2	250	63.51	64.98	41.27
3	250	64.53	65.11	42.01
4	500	56.45	66.93	37.78
5	500	74.09	66.75	49.46
6	500	78.57	66.33	52.12
7	1000	85.00	57.66	49.01
8	1000	89.47	57.81	51.72
9	1000	94.74	56.52	53.54
	Current (mA)	Avg. C. Eff (%)	Avg. V. Eff (%)	Avg. E. Eff (%)
2M $V^{3.7+}$ 0.19M MEM 0.56M MEP 25°C Average	250	64.02	65.04	41.64
	500	76.33	66.54	50.79
	1000	92.11	57.16	52.63

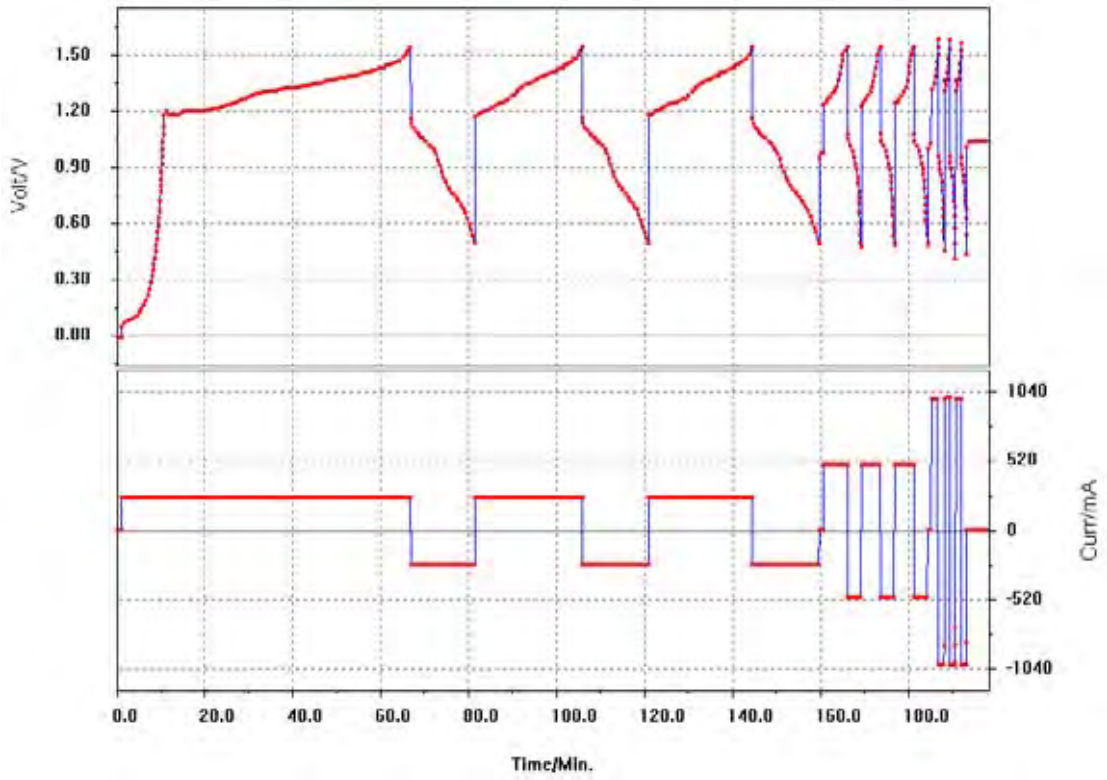

Figure H.10 Charge / discharge cycles of 2 M $V^{3.7+}$, 0.19 M MEM, 0.56 M MEP, 6.1 M HBr, 1.2 M HCl (7ml in each half-cell) with VF11 membrane at 35°C (T35A0323.cel)

Table H.9 Cell efficiencies of 2 M $V^{3.7+}$, 0.19 M MEM, 0.56 M MEP, 6.1 M HBr, 1.2 M HCl with VF11 membrane at 35°C (T35A0323.cel)

T35A0323.cel cycle no.	Current (mA)	C. Eff (%)	V. Eff (%)	E. Eff (%)
1	250	22.12	74.26	16.43
2	250	61.92	64.72	40.08
3	250	64.25	64.85	41.67
4	500	56.85	65.74	37.37
5	500	74.13	65.74	48.73
6	500	78.08	65.66	51.27
7	1000	86.62	57.54	49.84
8	1000	92.24	57.36	52.91
9	1000	90.57	57.68	52.24
	Current (mA)	Avg. C. Eff (%)	Avg. V. Eff (%)	Avg. E. Eff (%)
2M $V^{3.7+}$ 0.19M MEM 0.56M MEP 35°C Average	250	63.09	64.79	40.87
	500	76.11	65.70	50.00
	1000	91.41	57.52	52.58

H.3 Cycling Cell testing for VF11

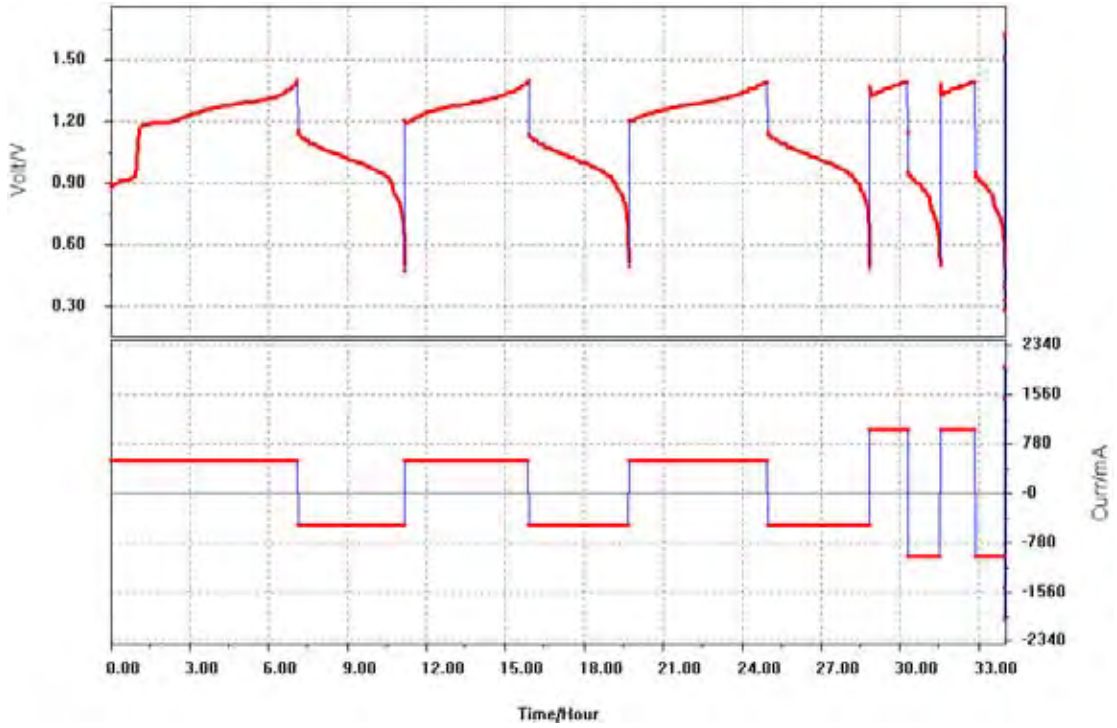

Figure H.11 Charge / discharge cycles of 2 M $V^{3.7+}$, 7.6 M HBr, 1.46 M HCl using VF11 membrane at 10°C (T10_1206.cel; 40ml electrolytes, 3mm flow frame)

Table H.10 Cell efficiencies of 2M $V^{3.7+}$, 7.6 M HBr, 1.46 M HCl using VF11 membrane at 10°C

T10_1206.cel cycle no.	Current (mA)	C. Eff (%)	V. Eff (%)	E. Eff (%)
1	500	56.77	82.12	46.62
2	500	80.65	77.18	62.24
3	500	73.65	77.62	57.16
4	1000	82.87	61.15	50.68
5	1000	84.35	60.41	50.96
6	1000	100.05	26.35	26.36
CY060929.cel	Current Density ($mAcm^{-2}$)	Avg. C. Eff (%)	Avg. V. Eff (%)	Avg. E. Eff (%)
Average cycle 2-3	20	77.15	77.40	59.70
2nd cycle	40	84.35	60.41	50.96

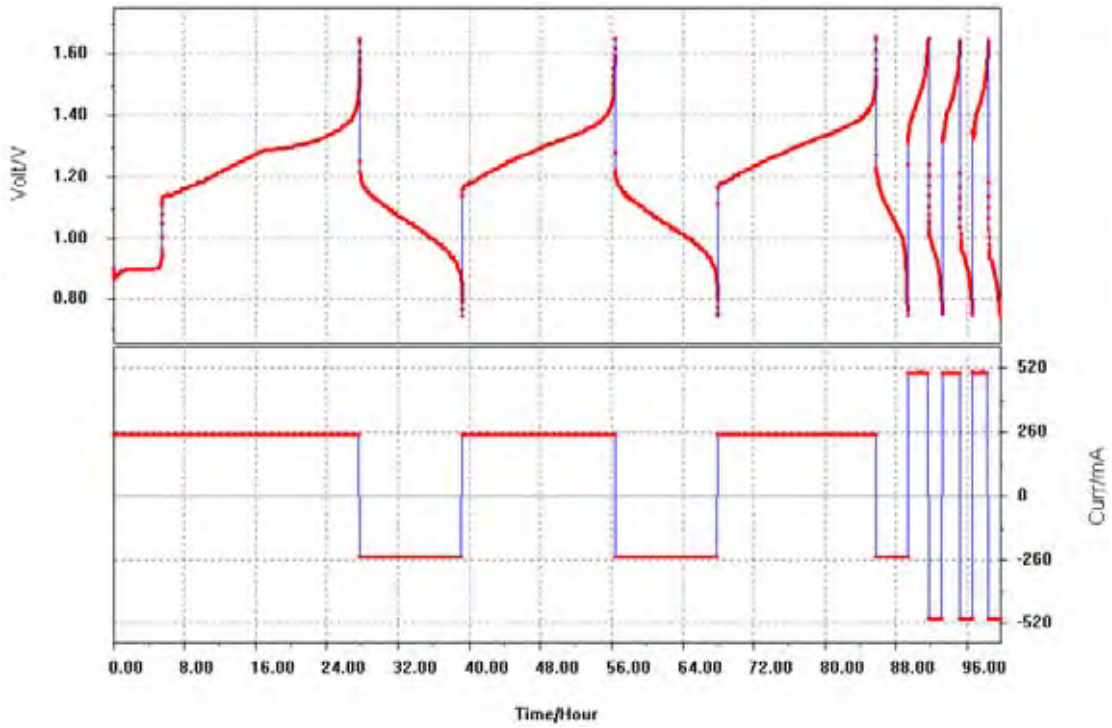

Figure H.12 Charge / discharge cycles of 2 M $V^{3.7+}$, 0.19 M MEM, 0.56 M MEP 6.1 M HBr, 1.2 M HCl using VF11 membrane at 10^{o}C (T10_0314.cel, Stoped flowing after 3cycle of 500mA)

Table H.11 Cell efficiencies of 2 M $V^{3.7+}$, 0.19 M MEM, 0.56 M MEP 6.1 M HBr, 1.2 M HCl using VF11 membrane at 10^{o}C

T15_0301.cel cycle no.	Current (mA)	C. Eff (%)	V. Eff (%)	E. Eff (%)
1	250	41.56	87.42	36.34
2	250	67.51	81.04	54.71
3	250	20.03	82.43	16.51
4	500	68.62	64.00	43.92
5	500	70.90	61.96	43.93
6	500	70.75	60.59	42.87
	Current Density ($mAcm^{-2}$)	Avg. C. Eff (%)	Avg. V. Eff (%)	Avg. E. Eff (%)
2nd cycle	10	67.51	81.04	54.71
Average cycle 5-6	20	70.83	61.27	43.40

H.4 Static Cell testing for membrane selection

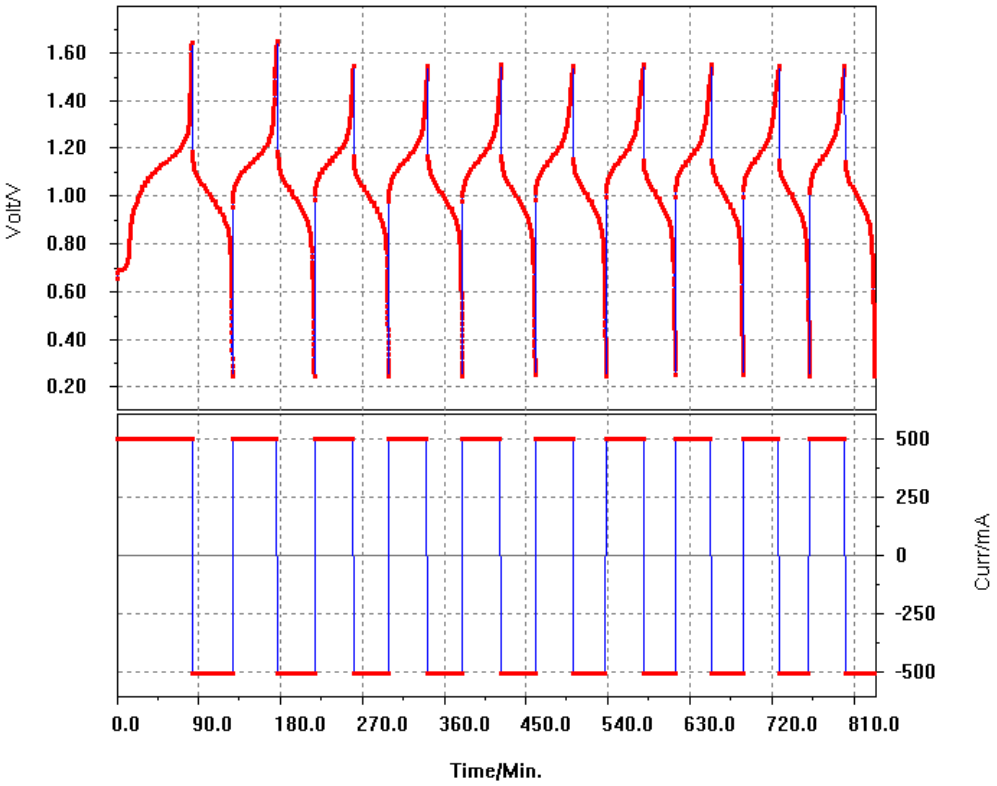

Figure H.13 Charge / discharge respond of 2 M $V^{3.7+}$, 7.6 M HBr, 1.46 M HCl (8ml in each half-cells) static cell with ChiNafion membrane using frame with 3 mm thickness (6aprsa.cel)

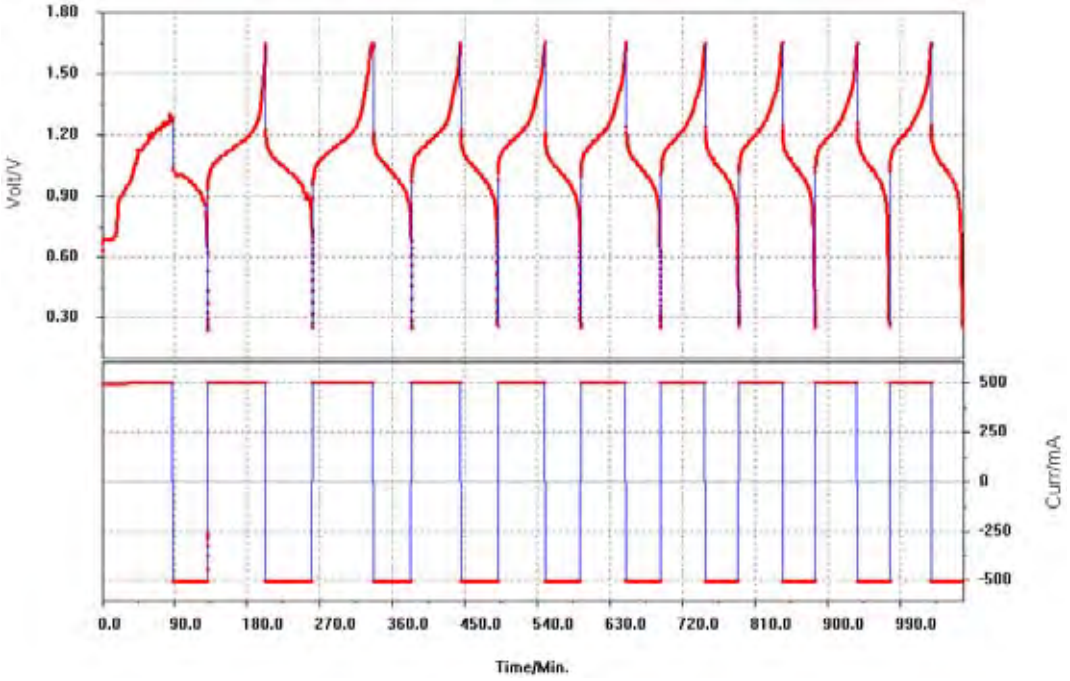

Figure H.14 Charge / discharge respond of 2 M $V^{3.7+}$, 7.6 M HBr, 1.46 M HCl (11ml in each half-cell) static cell with VF11 membrane using frame with 3 mm thickness (11apr.cel)

Table H.12 Coulombic, voltaic and energy efficiency of each cycles obtained by 2 M $V^{3.7+}$, 7.6 M HBr, 1.46 M HCl static cell built with ChiNafion and VF11 membranes

ChiNafion 6aprsa.cel	t_{TH} (min)			VF11 11apr.cel	t_{TH} (min)		
1st cycle	87.5			1st cycle	120.3		
Cycles 2-10	51.5			Cycles 2-10	70.8		
Cycle No.	C. Eff (%)	V. Eff (%)	E. Eff (%)	Cycle No.	C. Eff (%)	V. Eff (%)	E. Eff (%)
1	53.11	92.30	49.02	1	49.21	92.23	45.39
2	78.91	80.85	63.79	2	81.59	85.72	69.94
3	89.80	81.64	73.31	3	62.64	81.73	51.20
4	87.32	81.13	70.84	4	75.46	80.56	60.79
5	86.04	80.31	69.10	5	75.78	78.49	59.48
6	86.07	79.22	68.18	6	75.83	79.09	59.97
7	85.90	78.52	67.45	7	76.28	78.15	59.61
8	86.12	77.99	67.17	8	76.43	77.80	59.47
9	85.46	77.47	66.20	9	77.09	77.43	59.70
10	85.54	76.94	65.81	10	77.04	77.06	59.37
	C. Eff (%)	V. Eff (%)	E. Eff (%)		C. Eff (%)	V. Eff (%)	E. Eff (%)
Average of cycle 3 - 10	86.5	79.2	68.5	Average of cycle 2 - 10	75.4	79.6	60.0

t_{TH} – theoretical cell charging time, C. Eff – Coulombic efficiency, V. Eff – Voltaic efficiency, E. Eff – Energy efficiency

H.5 Flow cell with ChiNafion membrane that monitor each half cell OCP

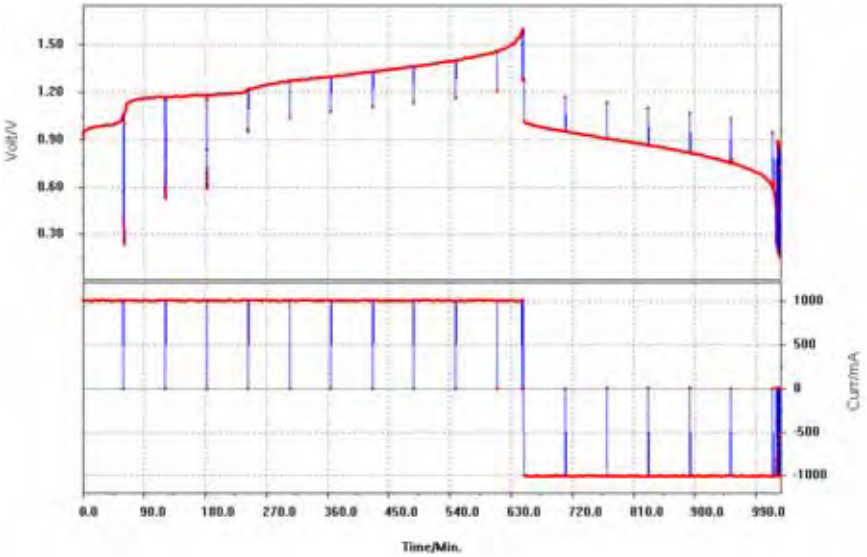

Figure H.15 First charge / discharge cycle of 2M $V^{3.7+}$, 7.6 M HBr, 1.46 M HCl (100ml in each half-cells) using ChiNafion membrane at 25°C for OCP measurements (18maycyc.cel)

Table H.13 Half cell OCP measurements from 18maycyc.cel

OCP pt	Time (min)	+ve half cell OCP (V vs SCE)	-ve half cell OCP (V vs SCE)	cell OCP (V vs SCE)
0	0	0.32	0.28	0
1	61	0.41	0.15	0.234
2	122	0.66	0.11	0.526
3	183	0.67	0.06	0.59
4	244	0.69	-0.29	0.955
5	305	0.70	-0.36	1.037
6	366	0.71	-0.39	1.075
7	427	0.72	-0.41	1.105
8	488	0.73	-0.43	1.132
9	549	0.74	-0.45	1.164
10	610	0.75	-0.48	1.208
11	647	0.76	-0.55	1.277
12	648	0.76	-0.55	1.277
13	710	0.73	-0.46	1.177
14	771	0.72	-0.44	1.137
15	832	0.71	-0.42	1.104
16	893	0.7	-0.4	1.072
17	954	0.69	-0.37	1.033
18	1015	0.68	-0.3	0.949
19	1021	0.67	-0.24	0.893
20	1022	0.67	-0.23	0.887
21	1023	0.67	-0.22	0.88
22	1024	0.67	-0.22	0.874

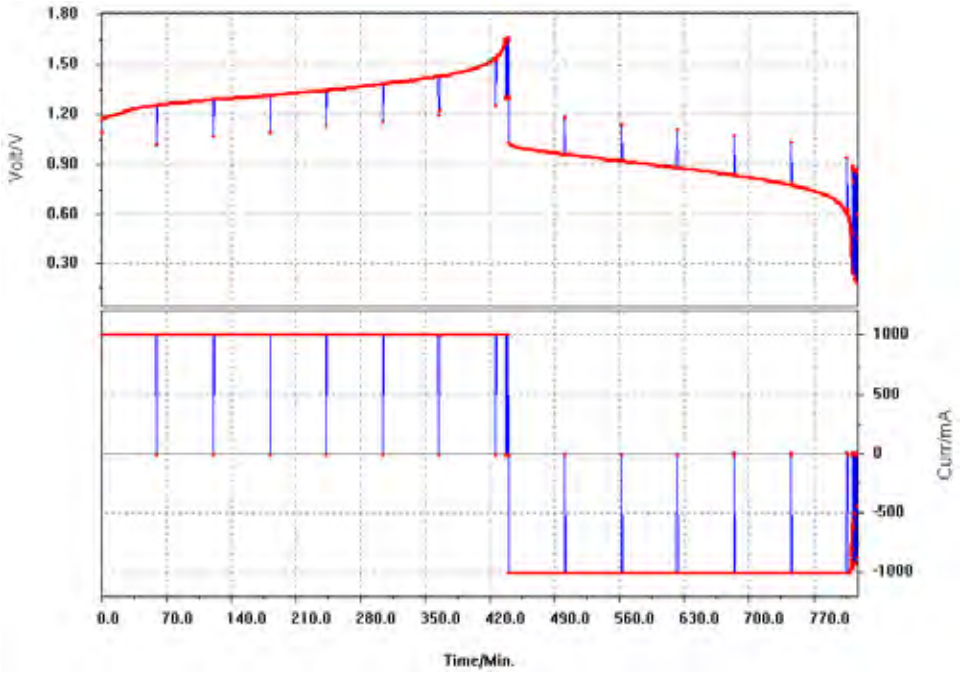

Figure H.16 Second charge / discharge cycle of 2 M $V^{3.7+}$, 7.6 M HBr, 1.46 M HCl using ChiNafion membrane at 25°C for OCP measurements (24maycyc.cel; 4.5mm flowframe; 100ml in each reservoir; C.Eff: 85% V.$Eff_{50\%SOC}$: 65% E.Eff: 56%)

Table H.14 Half cell OCP measurements from 18maycyc.cel

OCP pt	Time (min)	+ve half cell OCP (V vs SCE)	-ve half cell OCP (V vs SCE)	cell OCP (V vs SCE)
0	0	0.66	0.27	0
1	61	0.69	-0.34	1.014
2	122	0.7	-0.37	1.058
3	183	0.71	-0.4	1.089
4	244	0.72	-0.42	1.119
5	305	0.73	-0.44	1.148
6	366	0.74	-0.46	1.182
7	427	0.75	-0.52	1.248
8	437	0.75	-0.56	1.287
9	439	0.75	-0.56	1.288
10	440	0.75	-0.56	1.288
11	441	0.75	-0.56	1.29
12	502	0.73	-0.46	1.176
13	563	0.72	-0.43	1.138
14	624	0.71	-0.41	1.104
15	685	0.7	-0.39	1.071
16	746	0.68	-0.36	1.032
17	807	0.67	-0.28	0.942
18	812	0.67	-0.24	0.89
19	814	0.67	-0.23	0.882
20	815	0.67	-0.22	0.876
21	816	0.67	-0.22	0.873
22	817	0.67	-0.22	0.868

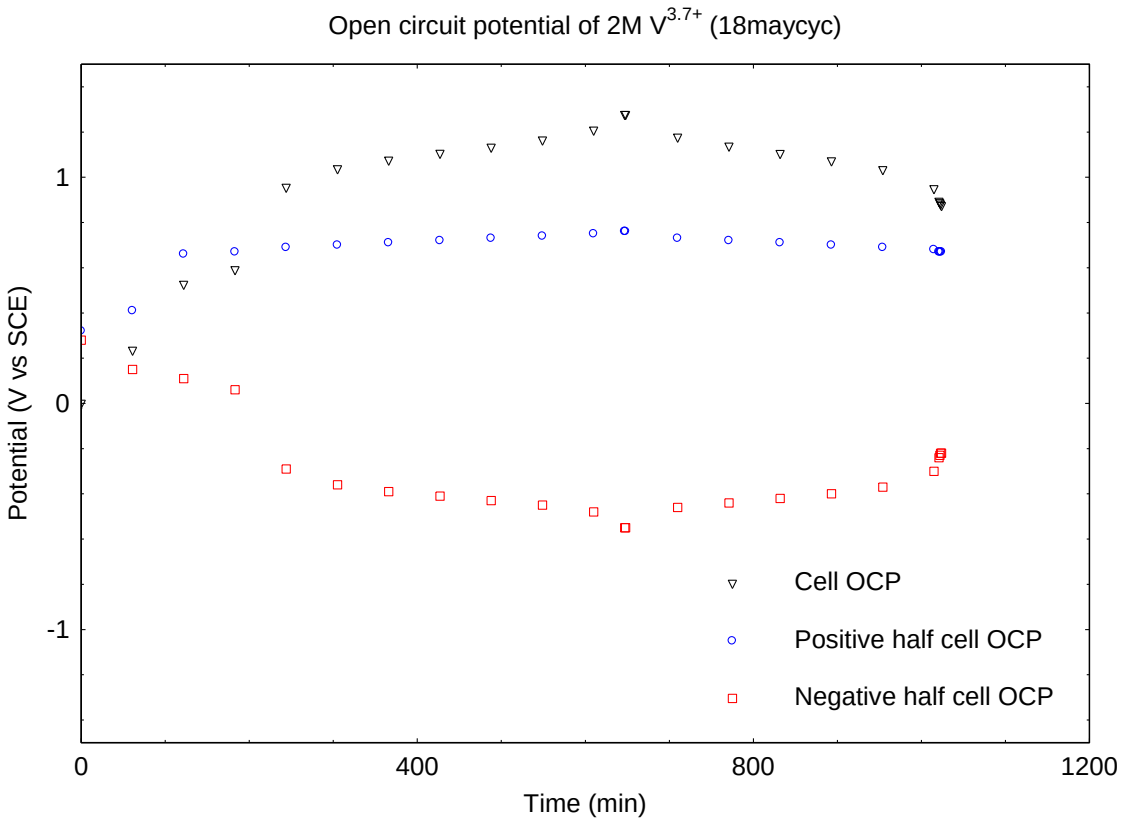

Figure H.17 Measurements of positive, negative and overall open circuit potential (OCP) of 2 M $V^{3.7+}$, 7.6 M HBr, 1.46 M HCl during charge/discharge of flow cell at 25°C (18maycyc.cel)

H.6 Flow Cell with ChiNafion membrane

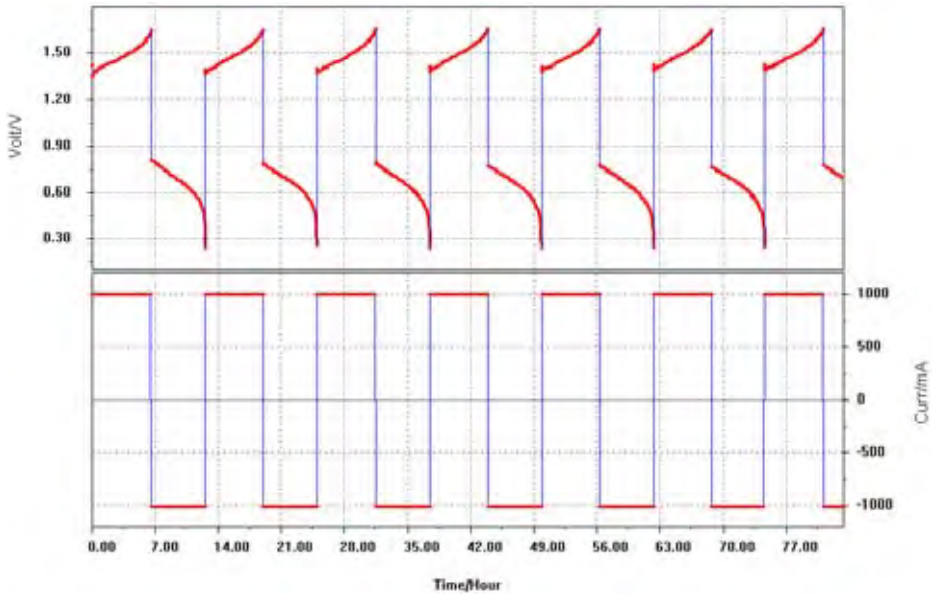

Figure H.18 Charge / discharge cycles of 2 M $V^{3.7+}$, 7.6 M HBr, 1.46 M HCl using ChiNafion membrane at 25°C (30maycyc.cel, 100ml electrolyte, 4.5mm flowframe)

Table H.15 Cell efficiencies of 2 M $V^{3.7+}$, 7.6 M HBr, 1.46 M HCl using ChiNafion membrane at 25°C (30maycyc.cel)

30maycyc.cel cycle no.	Current (mA)	C. Eff (%)	V. Eff (%)	E. Eff (%)
1	1000	89.43	45.26	40.47
2	1000	91.33	44.15	40.32
3	1000	91.03	43.93	39.99
4	1000	91.41	43.10	39.40
5	1000	91.29	42.97	39.23
6	1000	91.56	42.59	38.99
30maycyc.cel	Current Density ($mAcm^{-2}$)	Avg. C. Eff (%)	Avg. V. Eff (%)	Avg. E. Eff (%)
2M $V^{3.7+}$	40	91.32	43.35	39.59

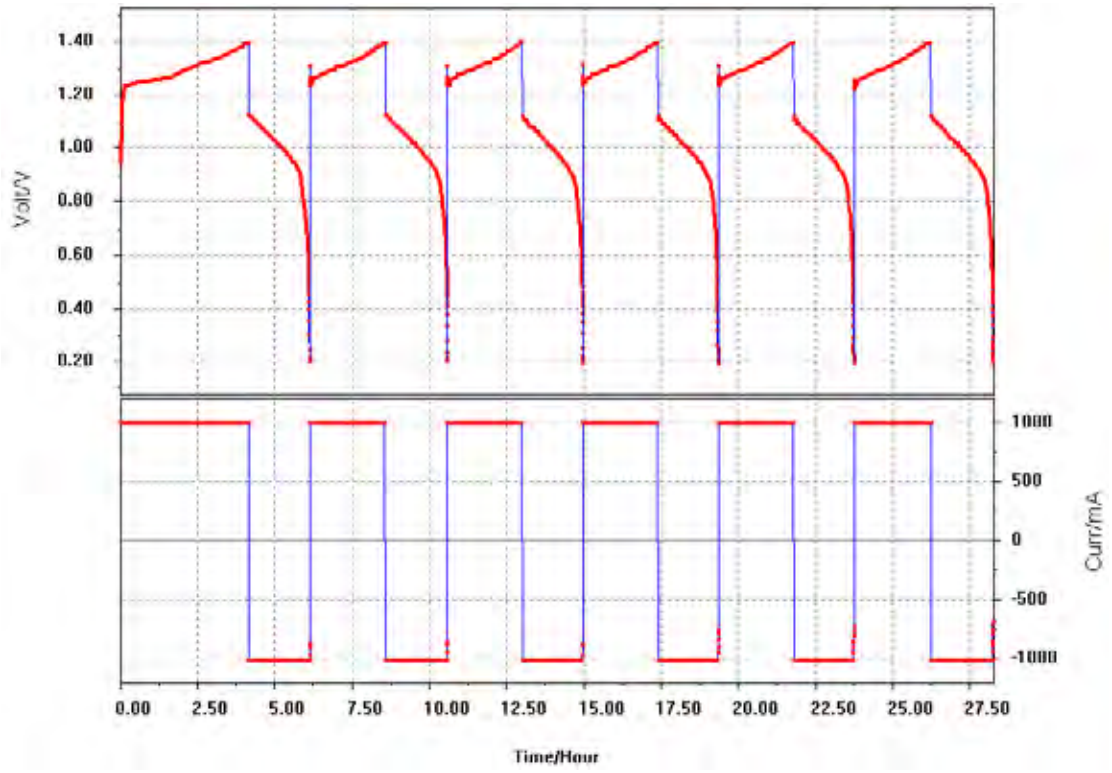

Figure H.19 Charge / discharge cycles of 2 M $V^{3.7+}$, 7.6 M HBr, 1.46 M HCl (100ml in each half-cell) using ChiNafion membrane and 3mm flowframe at 25°C (CY061204.cel)

Table H.16 Cell efficiencies of 2 M $V^{3.7+}$, 7.6 M HBr, 1.46 M HCl using ChiNafion membrane at 25°C (CY061204.cel)

T15_0301.cel cycle no.	Current (mA)	C. Eff (%)	V. Eff (%)	E. Eff (%)
1	1000	46.8	75.7	35.4
2	1000	79.9	74.1	59.2
3	1000	80.2	73.7	59.1
4	1000	80.3	73.3	58.9
5	1000	79.9	73.4	58.6
6	1000	79.1	73.4	58.0
	Current Density ($mAcm^{-2}$)	Avg. C. Eff (%)	Avg. V. Eff (%)	Avg. E. Eff (%)
Average	40	79.9	73.6	58.8

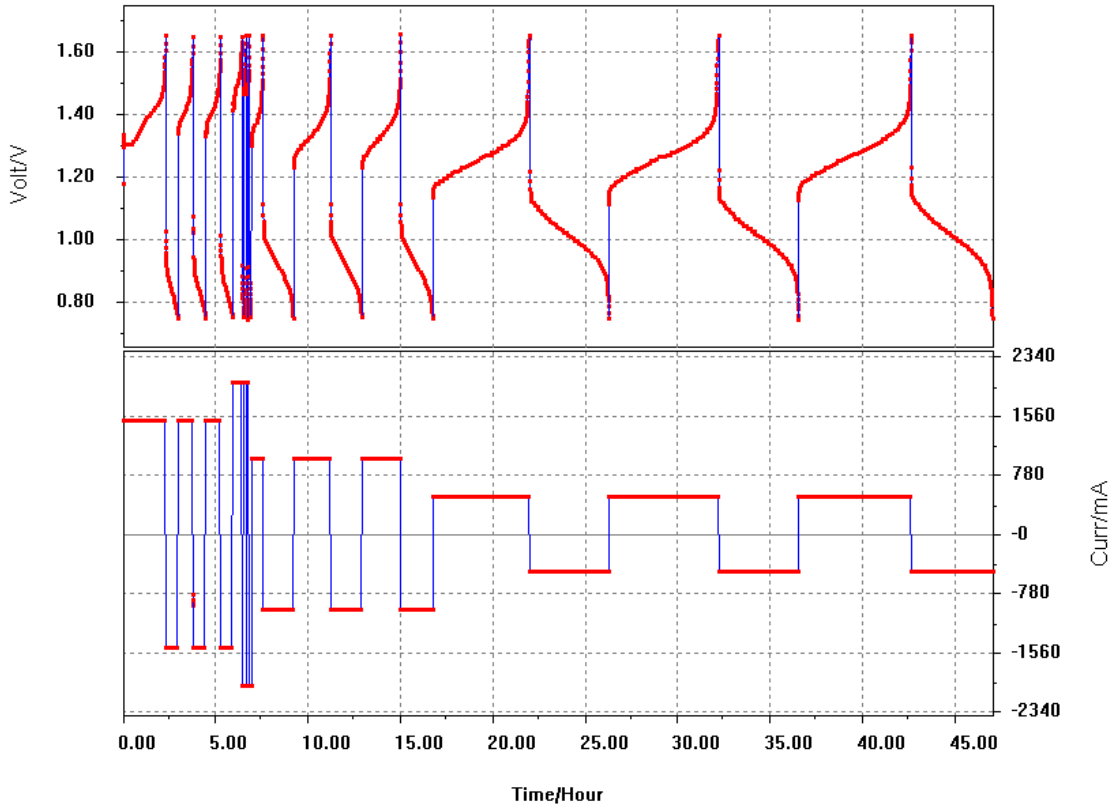

Figure H.20 Charge / discharge cycles of 2 M $V^{3.7+}$, 7.6 M HBr, 1.46 M HCl using ChiNafion membrane at 10°C (T10_0221.cel, 40ml, Electrolyte Temperature: -ve: outlet 14°C, reservoir 11°C)

Table H.17 Cell efficiencies of 2 M $V^{3.7+}$, 7.6 M HBr, 1.46 M HCl using ChiNafion membrane at 10°C (T10_0221.cel)

T10_0221.cel cycle no.	Current (mA)	C. Eff (%)	V. Eff (%)	E. Eff (%)
1	1500	29.49	61.07	18.01
2	1500	85.48	61.10	52.23
3	1500	83.91	58.63	49.19
4	2000	18.29	54.19	9.91
5	2000	81.15	53.49	43.41
6	2000	75.79	53.57	40.60
7	1000	250.80	65.75	164.90
8	1000	85.64	68.31	58.49
9	1000	82.71	68.49	56.65
10	500	80.64	79.60	64.19
11	500	72.70	79.44	57.76
12	500	72.20	79.17	57.16
	Current (mA)	Avg. C. Eff (%)	Avg. V. Eff (%)	Avg. E. Eff (%)
2M V3.7+ 10°C Average	500	72.45	79.31	57.46
	1000	84.17	68.40	57.57
	1500	84.69	59.86	50.71
	2000	78.47	53.53	42.00

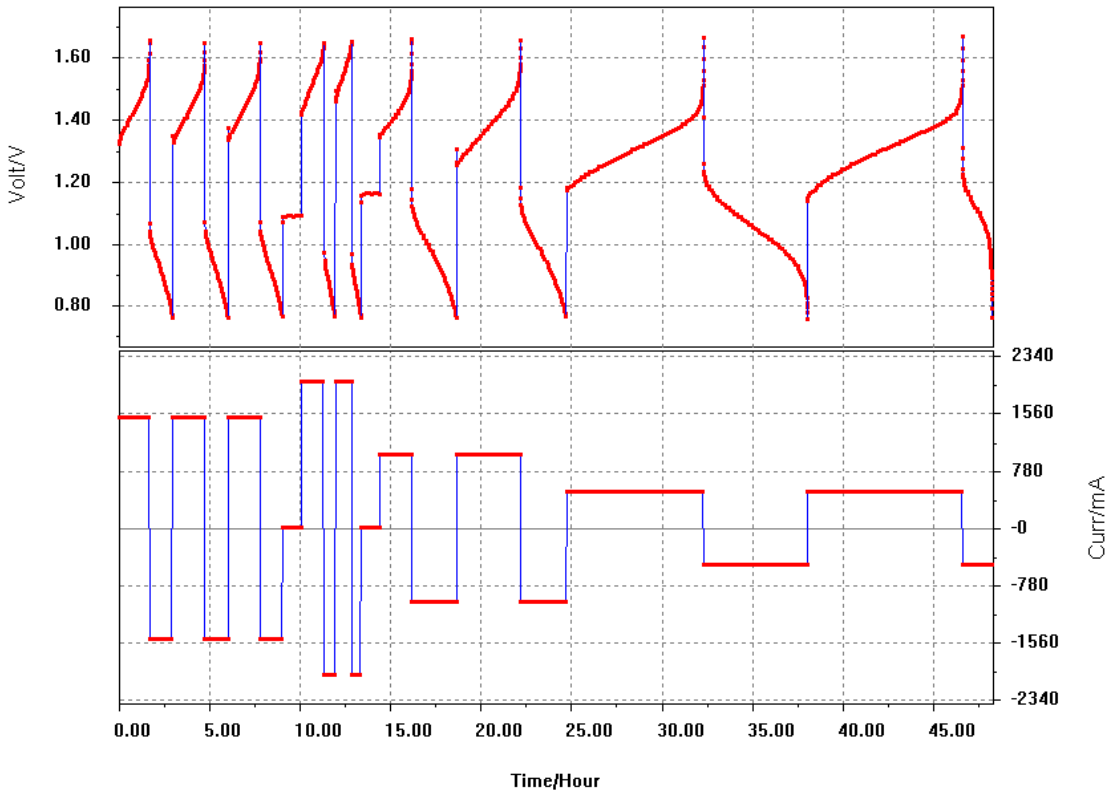

Figure H.21 Charge / discharge cycles of 2 M $V^{3.7+}$, 7.6 M HBr, 1.46 M HCl using ChiNafion membrane at 10°C (T10_0131.cel, 40ml)

Table H.18 Cell efficiencies of 2 M $V^{3.7+}$, 7.6 M HBr, 1.46 M HCl using ChiNafion membrane at 10°C (T10_0131.cel)

T10_0131.cel cycle no.	Current (mA)	C. Eff (%)	V. Eff (%)	E. Eff (%)
1	1500	76.55	63.45	48.57
2	1500	72.70	63.27	46.00
3	1500	71.98	62.94	45.30
4	2000	45.51	36.49	16.61
5	2000	57.92	54.85	31.77
6	1000	137.57	63.67	46.28
7	1000	72.14	69.06	49.82
8	500	75.74	80.04	60.62
9	500	19.45	16.33	83.99
	Current Density ($mAcm^{-2}$)	Avg. C. Eff (%)	Avg. V. Eff (%)	Avg. E. Eff (%)
2M V3.7+ 10°C Average	20*	19.45	16.33	83.99
	40*	72.14	69.06	49.82
	60	72.34	63.10	45.65
	80*	57.92	54.85	31.77

* 2nd cycle

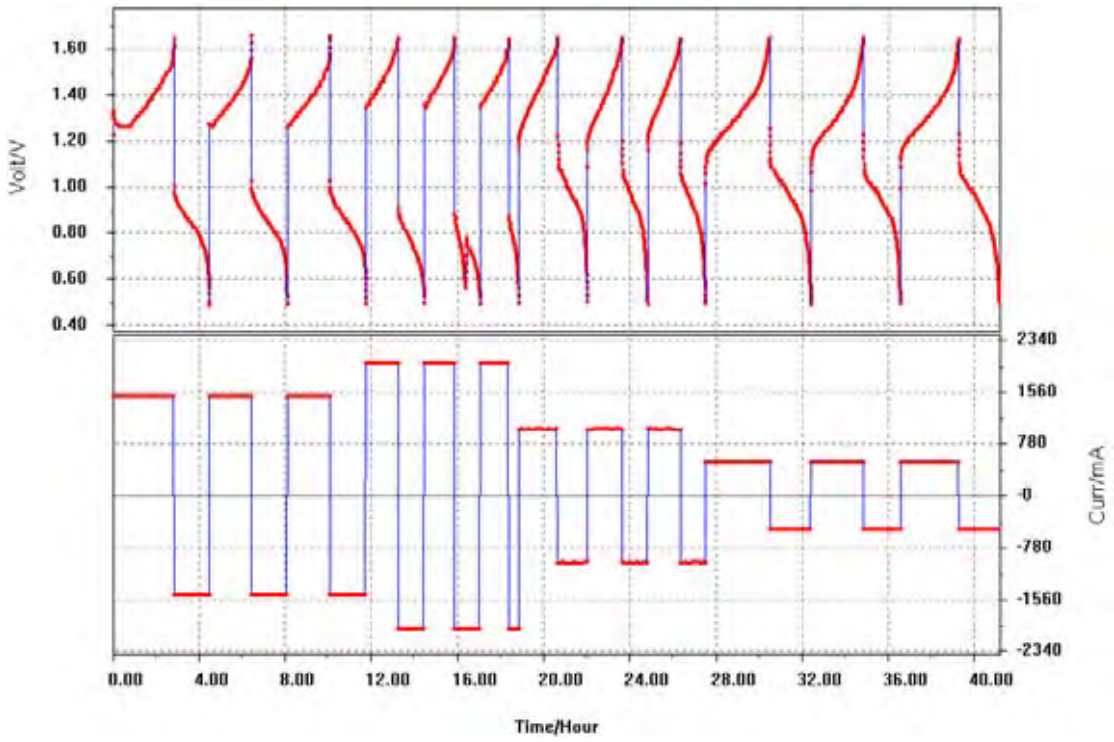

Figure H.22 Charge / discharge cycles of 2 M $V^{3.7+}$, 7.6 M HBr, 1.46 M HCl using ChiNafion membrane at 15°C (T15_0301.cel, 40ml)

Table H.19 Cell efficiencies of 2 M $V^{3.7+}$, 7.6 M HBr, 1.46 M HCl using ChiNafion membrane at 15°C (T15_0301.cel)

T15_0301.cel cycle no.	Current (mA)	C. Eff (%)	V. Eff (%)	E. Eff (%)
1	1500	57.22	60.68	34.72
2	1500	85.04	60.75	51.66
3	1500	83.94	60.46	50.75
4	2000	83.53	51.12	42.70
5	2000	85.42	48.44	41.38
6	2000	32.82	51.49	16.90
7	1000	74.61	66.41	49.55
8	1000	72.17	64.52	46.56
9	1000	75.77	63.21	47.89
10	500	65.60	70.68	46.36
11	500	70.57	69.02	48.70
12	500	68.92	67.96	46.83
	Current Density ($mAcm^{-2}$)	Avg. C. Eff (%)	Avg. V. Eff (%)	Avg. E. Eff (%)
2 M $V^{3.7+}$ 15°C Average	20	69.74	68.49	47.77
	40	73.97	63.86	47.23
	60	84.49	60.60	51.20
	80	84.47	49.78	42.04

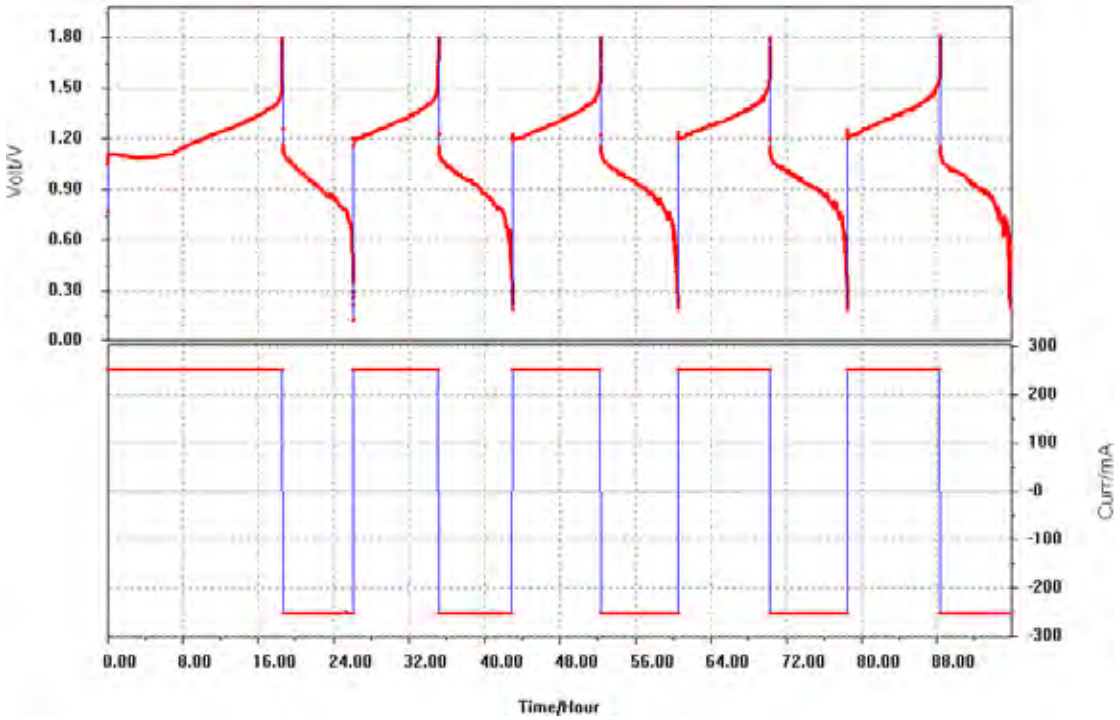

Figure H.23 Charge / discharge cycles of 2 M $V^{3.7+}$, 0.19 M MEM, 0.56 M MEP, 6.1 M HBr, 1.2 M HCl using ChiNafion membrane at 25°C (CY060929.cel; 50ml electrolytes; (+ve) 27°C (-ve) 26°C)

Table H.20 Cell efficiencies of 2 M $V^{3.7+}$, 0.19 M MEM, 0.56 M MEP, 6.1 M HBr, 1.2 M HCl using ChiNafion membrane at 25°C (CY060929.cel)

CY060929.cel cycle no.	Current (mA)	C. Eff (%)	V. Eff (%)	E. Eff (%)
1	250	40.49	75.52	30.58
2	250	86.97	68.50	59.57
3	250	86.77	68.45	59.40
4	250	83.20	68.68	57.14
5	250	75.24	66.80	50.26
CY060929.cel	Current Density ($mAcm^{-2}$)	Avg. C. Eff (%)	Avg. V. Eff (%)	Avg. E. Eff (%)
Average cycle 2-4	10	85.64	68.54	58.70

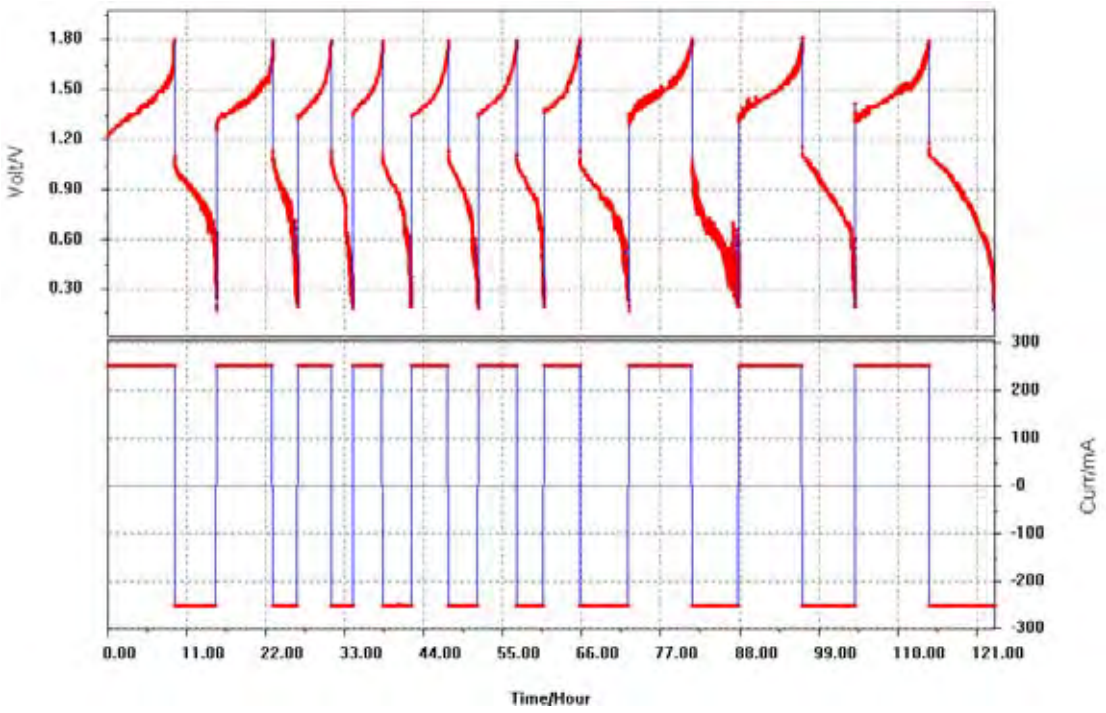

Figure H.24 Charge / discharge cycles of 2 M $V^{3.7+}$, 0.19 M MEM, 0.56 M MEP, 6.1 M HBr, 1.2 M HCl (50ml each half-cells) using ChiNafion membrane at 25°C (CY060930.cel) continued from CY060929.cel

Table H.21 Cell efficiencies of 2 M $V^{3.7+}$, 0.19 M MEM, 0.56 M MEP, 6.1 M HBr, 1.2 M HCl using ChiNafion membrane at 25°C (CY060930.cel)

CY060930.cel cycle no.	Current (mA)	C. Eff (%)	V. Eff (%)	E. Eff (%)
1	250	63.29	60.93	38.56
2	250	44.33	54.71	24.25
3	250	68.30	53.19	36.33
4	250	96.78	54.67	52.90
5	250	81.26	56.33	45.78
6	250	69.51	57.76	40.15
7	250	136.64	54.41	74.34
8	250	74.02	41.31	30.58
9	250	82.15	57.72	47.42
10	250	87.74	57.07	50.08
CY060930.cel	Current Density (mAcm-2)	Avg. C. Eff (%)	Avg. V. Eff (%)	Avg. E. Eff (%)
Average cycle 3-6,8-10	10	80.0	54.0	43.3

[1] R. P. Bell and M. Pring, Journal of the Chemical Society A: Inorganic, Physical, Theoretical (1966) 1607